GE Nuclear Energy

26A6642AL
Revision 1
January 2006

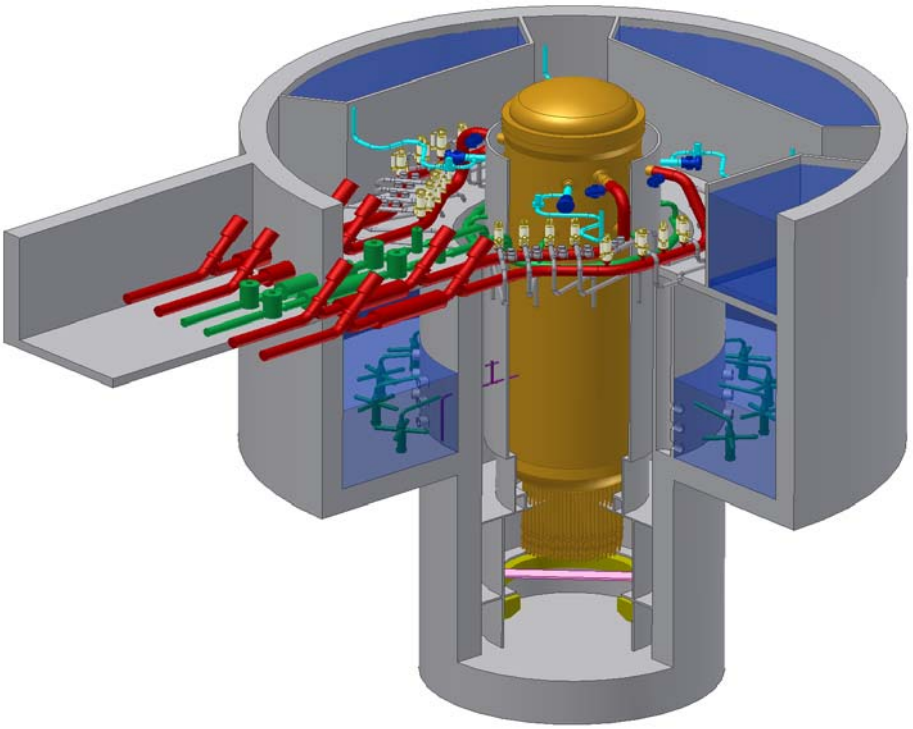

ESBWR Design Control Document

Tier 2

Chapter 3

Design of Structures, Components, Equipment, and Systems

Appendices 3A-3F

Contents

List of Tables

List of Illustrations

Global Abbreviations And Acronyms List

Term	Definition
10 CFR	Title 10, Code of Federal Regulations
A/D	Analog-to-Digital
AASHTO	American Association of Highway and Transportation Officials
AB	Auxiliary Boiler
ABS	Auxiliary Boiler System
ABWR	Advanced Boiling Water Reactor
ac / AC	Alternating Current
AC	Air Conditioning
ACF	Automatic Control Function
ACI	American Concrete Institute
ACS	Atmospheric Control System
AD	Administration Building
ADS	Automatic Depressurization System
AEC	Atomic Energy Commission
AFIP	Automated Fixed In-Core Probe
AGMA	American Gear Manufacturer's Association
AHS	Auxiliary Heat Sink
AISC	American Institute of Steel Construction
AISI	American Iron and Steel Institute
AL	Analytical Limit
ALARA	As Low As Reasonably Achievable
ALWR	Advanced Light Water Reactor
ANS	American Nuclear Society
ANSI	American National Standards Institute
AOO	Anticipated Operational Occurrence
AOV	Air Operated Valve
AP	Annulus Pressurization
API	American Petroleum Institute
APLHGR	Average Planar Linear Heat Generation Rate
APRM	Average Power Range Monitor
APR	Automatic Power Regulator
APRS	Automatic Power Regulator System
ARI	Alternate Rod Insertion
ARMS	Area Radiation Monitoring System
ARS	Amplified Response Spectrum
ASA	American Standards Association
ASD	Adjustable Speed Drive
ASHRAE	American Society of Heating, Refrigerating, and Air Conditioning Engineers
ASME	American Society of Mechanical Engineers

Term	Definition
AST	Alternate Source Term
ASTM	American Society of Testing Methods
AT	Unit Auxiliary Transformer
ATLM	Automated Thermal Limit Monitor
ATWS	Anticipated Transients Without Scram
AV	Allowable Value
AWS	American Welding Society
AWWA	American Water Works Association
B&PV	Boiler and Pressure Vessel
BAF	Bottom of Active Fuel
BE	Best Estimate
BHP	Brake Horse Power
BOP	Balance of Plant
BPU	Bypass Unit
BPWS	Banked Position Withdrawal Sequence
BRE	Battery Room Exhaust
BRL	Background Radiation Level
BTP	NRC Branch Technical Position
BTU	British Thermal Unit
BWR	Boiling Water Reactor
BWROG	Boiling Water Reactor Owners Group
CAV	Cumulative absolute velocity
C&FS	Condensate and Feedwater System
C&I	Control and Instrumentation
C/C	Cooling and Cleanup
C-I	Class one (I)
C-II	Class two (II)
CB	Control Building
CBHVAC	Control Building HVAC
CCI	Core-Concrete Interaction
CDF	Core Damage Frequency
CFR	Code of Federal Regulations
CH	Pool Chugging
CIRC	Circulating Water System
CIS	Containment Inerting System
CIV	Combined Intermediate Valve
CLAVS	Clean Area Ventilation Subsystem of Reactor Building HVAC
CM	Cold Machine Shop
CMS	Containment Monitoring System
CMU	Control Room Multiplexing Unit

Term	Definition
CO	Condensation Oscillation
COL	Combined Operating License
COLR	Core Operating Limits Report
CONAVS	Controlled Area Ventilation Subsystem of Reactor Building HVAC
CPR	Critical Power Ratio
CPS	Condensate Purification System
CPU	Central Processing Unit
CR	Control Rod
CRD	Control Rod Drive
CRDA	Control Rod Drop Accident
CRDH	Control Rod Drive Housing
CRDHS	Control Rod Drive Hydraulic System
CRGT	Control Rod Guide Tube
CRHA	Control Room Habitability Area
CRT	Cathode Ray Tube
CS&TS	Condensate Storage and Transfer System
CSDM	Cold Shutdown Margin
CS / CST	Condensate Storage Tank
CT	Compact Tension
CTVCF	Constant Voltage Constant Frequency
CUF	Cumulative usage factor
CWS	Chilled Water System
D-RAP	Design Reliability Assurance Program
DAC	Design Acceptance Criteria
DAW	Dry Active Waste
DBA	Design Basis Accident
dc / DC	Direct Current
DCS	Drywell Cooling System
DCIS	Distributed Control and Information System
DEGB	Double Ended Guillotine Break
DEPSS	Drywell Equipment and Pipe Support Structure
DF	Decontamination Factor
D/F	Diaphragm Floor
DG	Diesel-Generator
DHR	Decay Heat Removal
DM&C	Digital Measurement and Control
DOF	Degree of freedom
DOI	Dedicated Operators Interface
DOT	Department of Transportation
dPT	Differential Pressure Transmitter

Term	Definition
DPS	Diverse Protection System
DPV	Depressurization Valve
DR&T	Design Review and Testing
DTM	Digital Trip Module
DW	Drywell
EB	Electrical Building
EBAS	Emergency Breathing Air System
EBHV	Electrical Building HVAC
ECCS	Emergency Core Cooling System
E-DCIS	Essential DCIS (Distributed Control and Information System)
EDO	Environmental Qualification Document
EFDS	Equipment and Floor Drainage System
EFPY	Effective full power years
EHC	Electrohydraulic Control (Pressure Regulator)
ENS	Emergency Notification System
EOC	Emergency Operations Center
EOC	End of Cycle
EOF	Emergency Operations Facility
EOP	Emergency Operating Procedures
EPDS	Electric Power Distribution System
EPFM	Elastic Plastic Fracture Mechanics
EPG	Emergency Procedure Guidelines
EPRI	Electric Power Research Institute
EQ	Environmental Qualification
ERICP	Emergency Rod Insertion Control Panel
ERIP	Emergency Rod Insertion Panel
ESBWR	Economic Simplified Boiling Water Reactor
ESF	Engineered Safety Feature
ESP	Early Site Permit
ETS	Emergency Trip System
FAC	Flow-Accelerated Corrosion
FAPCS	Fuel and Auxiliary Pools Cooling System
FATT	Fracture Appearance Transition Temperature
FB	Fuel Building
FBHV	Fuel Building HVAC
FCI	Fuel-Coolant Interaction
FCM	File Control Module
FCS	Flammability Control System
FCU	Fan Cooling Unit
FDDI	Fiber Distributed Data Interface

Term	Definition
FFT	Fast Fourier Transform
FFWTR	Final Feedwater Temperature Reduction
FHA	Fire Hazards Analysis
FIV	Flow-Induced Vibration
FMCRD	Fine Motion Control Rod Drive
FMEA	Failure Modes and Effects Analysis
FPS	Fire Protection System
FO	Diesel Fuel Oil Storage Tank
FOAKE	First-of-a-Kind Engineering
FPE	Fire Pump Enclosure
FTDC	Fault-Tolerant Digital Controller
FTS	Fuel Transfer System
FW	Feedwater
FWCS	Feedwater Control System
FWS	Fire Water Storage Tank
GCS	Generator Cooling System
GDC	General Design Criteria
GDCS	Gravity-Driven Cooling System
GE	General Electric Company
GE-NE	GE Nuclear Energy
GEN	Main Generator System
GETAB	General Electric Thermal Analysis Basis
GL	Generic Letter
GM	Geiger-Mueller Counter
GM-B	Beta-Sensitive GM Detector
GMAW	Gas Metal Arc Welding
GSIC	Gamma-Sensitive Ion Chamber
GSOS	Generator Sealing Oil System
GTAW	Gas Tungsten Arc Welding
GWSR	Ganged Withdrawal Sequence Restriction
HAZ	Heat-Affected Zone
HCU	Hydraulic Control Unit
HCW	High Conductivity Waste
HDVS	Heater Drain and Vent System
HEI	Heat Exchange Institute
HELB	High Energy Line Break
HEP	Human error probability
HEPA	High Efficiency Particulate Air/Absolute
HFE	Human Factors Engineering
HFF	Hollow Fiber Filter

Term	Definition
HGCS	Hydrogen Gas Cooling System
HIC	High Integrity Container
HID	High Intensity Discharge
HIS	Hydraulic Institute Standards
HM	Hot Machine Shop & Storage
HP	High Pressure
HPNSS	High Pressure Nitrogen Supply System
HPT	High-pressure turbine
HRA	Human Reliability Assessment
HSI	Human-System Interface
HSSS	Hardware/Software System Specification
HVAC	Heating, Ventilation and Air Conditioning
HVL	Horizontal Vent Chugging
HVS	High Velocity Separator
HWCS	Hydrogen Water Chemistry System
HWS	Hot Water System
HX	Heat Exchanger
I&C	Instrumentation and Control
I/O	Input/Output
IAS	Instrument Air System
IASCC	Irradiation Assisted Stress Corrosion Cracking
IBC	International Building Code
IC	Isolation Condenser
ICD	Interface Control Diagram
ICS	Isolation Condenser System
IE	Inspection and Enforcement
IEB	Inspection and Enforcement Bulletin
IED	Instrument and Electrical Diagram
IEEE	Institute of Electrical and Electronic Engineers
IGSCC	Intergranular Stress Corrosion Cracking
IIS	Iron Injection System
ILRT	Integrated Leak Rate Test
IOP	Integrated Operating Procedure
IMC	Induction Motor Controller
IMCC	Induction Motor Controller Cabinet
IRM	Intermediate Range Monitor
ISA	Instrument Society of America
ISI	In-Service Inspection
ISLT	In-Service Leak Test
ISM	Independent Support Motion

Term	Definition
ISMA	Independent Support Motion Response Spectrum Analysis
ISO	International Standards Organization
ITA	Inspections, Tests or Analyses
ITAAC	Inspections, Tests, Analyses and Acceptance Criteria
ITA	Initial Test Program
J-R	Curve representing J-integral Resistance
LAPP	Loss of Alternate Preferred Power
LB	Lower Bound
LBB	Leak Before Break
LCO	Local Condensation Oscillation
LCW	Low Conductivity Waste
LD	Logic Diagram
LDA	Lay down Area
LD&IS	Leak Detection and Isolation System
LERF	Large early release frequency
LEFM	Linear Elastic Fracture Mechanics
LFCV	Low Flow Control Valve
LHGR	Linear Heat Generation Rate
LLRT	Local Leak Rate Test
LMU	Local Multiplexer Unit
LO	Dirty/Clean Lube Oil Storage Tank
LOCA	Loss-of-Coolant-Accident
LOFW	Loss-of-feedwater
LOOP	Loss of Offsite Power
LOPP	Loss of Preferred Power
LP	Low Pressure
LPCI	Low Pressure Coolant Injection
LPCRD	Locking Piston Control Rod Drive
LPMS	Loose Parts Monitoring System
LPRM	Local Power Range Monitor
LPSP	Low Power Setpoint
LWMS	Liquid Waste Management System
MAAP	Modular Accident Analysis Program
MAPLHGR	Maximum Average Planar Linear Head Generation Rate
MAPRAT	Maximum Average Planar Ratio
MBB	Motor Built-In Brake
MCC	Motor Control Center
MCES	Main Condenser Evacuation System
MCPR	Minimum Critical Power Ratio
MCR	Main Control Room

Term	Definition
MCRP	Main Control Room Panel
MELB	Moderate Energy Line Break
MLHGR	Maximum Linear Heat Generation Rate
MMI	Man-Machine Interface
MMIS	Man-Machine Interface Systems
MOV	Motor-Operated Valve
MPC	Maximum Permissible Concentration
MPL	Master Parts List
MS	Main Steam
MSIV	Main Steam Isolation Valve
MSL	Main Steamline
MSLB	Main Steamline Break
MSLBA	Main Steamline Break Accident
MSR	Moisture Separator Reheater
MSV	Mean Square Voltage
MT	Main Transformer
MTTR	Mean Time To Repair
MWS	Makeup Water System
NBR	Nuclear Boiler Rated
NBS	Nuclear Boiler System
NCIG	Nuclear Construction Issues Group
NDE	Nondestructive Examination
NE-DCIS	Non-Essential Distributed Control and Information System
NDRC	National Defense Research Committee
NDT	Nil Ductility Temperature
NFPA	National Fire Protection Association
NIST	National Institute of Standard Technology
NMS	Neutron Monitoring System
NOV	Nitrogen Operated Valve
NPHS	Normal Power Heat Sink
NPSH	Net Positive Suction Head
NRC	Nuclear Regulatory Commission
NRHX	Non-Regenerative Heat Exchanger
NS	Non-seismic
NSSS	Nuclear Steam Supply System
NT	Nitrogen Storage Tank
NTSP	Nominal Trip Setpoint
O&M	Operation and Maintenance
O-RAP	Operational Reliability Assurance Program
OBCV	Overboard Control Valve

Term	Definition
OBE	Operating Basis Earthquake
OGS	Offgas System
OHLHS	Overhead Heavy Load Handling System
OIS	Oxygen Injection System
OLMCPR	Operating Limit Minimum Critical Power Ratio
OLU	Output Logic Unit
OOS	Out-of-Service
ORNL	Oak Ridge National Laboratory
OSC	Operational Support Center
OSHA	Occupational Safety and Health Administration
OSI	Open Systems Interconnect
P&ID	Piping and Instrumentation Diagram
PA/PL	Page/Party-Line
PABX	Private Automatic Branch (Telephone) Exchange
PAM	Post Accident Monitoring
PAR	Passive Autocatalytic Recombiner
PAS	Plant Automation System
PASS	Post Accident Sampling Subsystem of Containment Monitoring System
PAW	Platinum Arc welding
PCC	Passive Containment Cooling
PCCS	Passive Containment Cooling System
PCT	Peak cladding temperature
PCV	Primary Containment Vessel
PFD	Process Flow Diagram
PGA	Peak Ground Acceleration
PGCS	Power Generation and Control Subsystem of Plant Automation System
PH	Pump House
PL	Parking Lot
PM	Preventive Maintenance
PMCS	Performance Monitoring and Control Subsystem of NE-DCIS
PMF	Probable Maximum Flood
PMP	Probable Maximum Precipitation
PQCL	Product Quality Check List
PRA	Probabilistic Risk Assessment
PRMS	Process Radiation Monitoring System
PRNM	Power Range Neutron Monitoring
PS	Plant Stack
PSD	Power Spectra Density
PSS	Process Sampling System
PSWS	Plant Service Water System

Term	Definition
PT	Pressure Transmitter
PWR	Pressurized Water Reactor
QA	Quality Assurance
RACS	Rod Action Control Subsystem
RAM	Reliability, Availability and Maintainability
RAPI	Rod Action and Position Information
RAT	Reserve Auxiliary Transformer
RB	Reactor Building
RBC	Rod Brake Controller
RBCC	Rod Brake Controller Cabinet
RBCWS	Reactor Building Chilled Water Subsystem
RBFB	Reactor Building/Fuel Building
RBHV	Reactor Building HVAC
RBS	Rod Block Setpoint
RBV	Reactor Building Vibration
RC&IS	Rod Control and Information System
RCC	Remote Communication Cabinet
RCCV	Reinforced Concrete Containment Vessel
RCCWS	Reactor Component Cooling Water System
RCPB	Reactor Coolant Pressure Boundary
RCS	Reactor Coolant System
RDA	Rod Drop Accident
RDC	Resolver-to-Digital Converter
REPAVS	Refueling and Pool Area Ventilation Subsystem of Fuel Building HVAC
RFP	Reactor Feed Pump
RG	Regulatory Guide
RHR	Residual Heat Removal (function)
RHX	Regenerative Heat Exchanger
RMS	Root Mean Square
RMS	Radiation Monitoring Subsystem
RMU	Remote Multiplexer Unit
RO	Reverse Osmosis
ROM	Read-only Memory
RPS	Reactor Protection System
RPV	Reactor Pressure Vessel
RRPS	Reference Rod Pull Sequence
RSM	Rod Server Module
RSPC	Rod Server Processing Channel
RSS	Remote Shutdown System
RSSM	Reed Switch Sensor Module

Term	Definition
RSW	Reactor Shield Wall
RTIF	Reactor Trip and Isolation Function(s)
RT_{NDT}	Reference Temperature of Nil-Ductility Transition
RTP	Reactor Thermal Power
RW	Radwaste Building
RWCU	Reactor Water Cleanup
RWE	Rod Withdrawal Error
RWM	Rod Worth Minimizer
SA	Severe Accident
SAM	Seismic Anchor Movement
SAR	Safety Analysis Report
SB	Service Building
S/C	Digital Gamma-Sensitive GM Detector
S/D	Scintillation Detector
S/DRSRO	Single/Dual Rod Sequence Restriction Override
S/N	Signal-to-Noise
S/P	Suppression Pool
SAS	Service Air System
SAW	Submerged Arc Welding
SB&PC	Steam Bypass and Pressure Control System
SBO	Station Blackout
SBWR	Simplified Boiling Water Reactor
SCEW	System Component Evaluation Work
SCRRI	Selected Control Rod Run-in
SDC	Shutdown Cooling
SDM	Shutdown Margin
SDS	System Design Specification
SEOA	Sealed Emergency Operating Area
SER	Safety Evaluation Report
SF	Service Water Building
SFP	Spent Fuel Pool
SIL	Service Information Letter
SIT	Structural Integrity Test
SIU	Signal Interface Unit
SJAE	Steam Jet Air Ejector
SLC	Standby Liquid Control
SLCS	Standby Liquid Control system
SLMCPR	Safety Limit Minimum Critical Power Ratio
SMAW	Shielded Metal Arc Welding
SMU	SSLC Multiplexing Unit

Term	Definition
SOV	Solenoid Operated Valve
SP	Suppression Pool
SPC	Suppression Pool Cooling
SPDS	Safety Parameter Display System
SPTMS	Suppression Pool Temperature Monitoring Subsystem of Containment Monitoring System
SR	Surveillance Requirement
SRM	Source Range Monitor
SRNM	Startup Range Neutron Monitor
SRO	Senior Reactor Operator
SRP	Standard Review Plan
SRS	Software Requirements Specification
SRSRO	Single Rod Sequence Restriction Override
SRSS	Square Root of the Sum of the Squares
SRV	Safety Relief Valve Discharge
SRVDL	Safety relief valve discharge line
SSAR	Standard Safety Analysis Report
SSC(s)	Structure, System and Component(s)
SSE	Safe Shutdown Earthquake
SSLC	Safety System Logic and Control
SSPC	Steel Structures Painting Council
ST	Spare Transformer
STP	Sewage Treatment Plant
STRAP	Scram Time Recording and Analysis Panel
STRP	Scram Time Recording Panel
SV	Safety Valve
SWH	Static water head
SWMS	Solid Waste Management System
SY	Switch Yard
TAF	Top of Active Fuel
TASS	Turbine Auxiliary Steam System
TB	Turbine Building
TBCE	Turbine Building Compartment Exhaust
TBE	Turbine Building Exhaust
TBLOE	Turbine Building Lube Oil Area Exhaust
TBS	Turbine Bypass System
TBHV	Turbine Building HVAC
TBV	Turbine Bypass Valve
TC	Training Center
TCCWS	Turbine Component Cooling Water System
TCS	Turbine Control System

Term	Definition
TCV	Turbine Control Valve
TDH	Total Developed Head
TEMA	Tubular Exchanger Manufacturers' Association
TFSP	Turbine first stage pressure
TG	Turbine Generator
TGSS	Turbine Gland Seal System
THA	Time-history Accelerograph
TLOS	Turbine Lubricating Oil System
TLU	Trip Logic Unit
TMI	Three Mile Island
TMSS	Turbine Main Steam System
TRM	Technical Requirements Manual
TS	Technical Specification(s)
TSC	Technical Support Center
TSI	Turbine Supervisory Instrument
TSV	Turbine Stop Valve
UBC	Uniform Building Code
UHS	Ultimate Heat Sink
UL	Underwriter's Laboratories Inc.
UPS	Uninterruptible Power Supply
USE	Upper Shelf Energy
USM	Uniform Support Motion
USMA	Uniform Support Motion response spectrum analysis
USNRC	United States Nuclear Regulatory Commission
USS	United States Standard
UV	Ultraviolet
V&V	Verification and Validation
Vac / VAC	Volts Alternating Current
Vdc / VDC	Volts Direct Current
VDU	Video Display Unit
VW	Vent Wall
VWO	Valves Wide Open
WD	Wash Down Bays
WH	Warehouse
WS	Water Storage
WT	Water Treatment
WW	Wetwell
XMFR	Transformer
ZPA	Zero Period Acceleration

3A. SEISMIC SOIL-STRUCTURE INTERACTION ANALYSIS

3A.1 INTRODUCTION

This appendix presents soil-structure interaction (SSI) analysis performed for two site conditions, generic site and North Anna ESP site-specific, adopted to establish seismic design loads for the Reactor Building (RB), Fuel Building (FB) and Control Building (CB) of the ESBWR standard plant under safe shutdown earthquake (SSE) excitation. The RB and FB are integrated and founded on a common basemat. They are termed RBFB hereafter. The SSE design ground motion at the foundation level for both site conditions is described in Subsection 3.7.1. The SSI analysis results are presented here in the form of site-enveloped seismic responses at key locations in the RBFB and CB. The structural adequacy calculations for the RB, FB and CB are shown in Appendix 3G.

For a standard plant design, the analysis must be performed over a range of site parameters. The site parameters considered and their ranges together form the generic site conditions. The generic site conditions are selected to provide an adequate seismic design margin for the standard plant located at any site with site parameters within the range of parameters considered in this study. In addition, the North Anna ESP site-specific condition is also considered in this study. When actual sites for these facilities are selected, site-specific geotechnical data will be developed and submitted to the NRC demonstrating compatibility with the site enveloping parameters considered in the standard design.

This appendix details the basis for selecting the site conditions and analysis cases, and the method of the seismic soil-structure interaction analysis. Descriptions of the input motion and damping values, the structural model, and the soil model are included. The parametric study SSI results as well as the enveloping seismic responses are also presented.

To demonstrate the seismic adequacy of the standard ESBWR design, a total of 7 SSI cases are analyzed using the sway-rocking stick model for the SSE condition. The enveloped results reported in this appendix form the design SSE loads.

3A.2 ESBWR STANDARD PLANT SITE PLAN

The typical site plan of the ESBWR standard plant is shown in Figure 1.1-1. The plan orientations are identified by 0°–180° (NS) and 90°–270° (EW) directions. The RBFB complex and the CB are rectangular in plan with dimensions and embedment depths shown in Table 3A.2-1.

In modeling the building, the 0°–180° (NS) and 90°–270° (EW) directions are designated as X- and Y-axes, respectively. The Z-axis is in the vertical direction.

Table 3A.2-1

Standard ESBWR Building Dimensions

	RBFB Complex Dimensions (m)	CB Dimension (m)
0°–180° (NS) width	70.0	30.3
90°–270° (EW) width	49.0	23.8
Embedment depth	20.15	15.05

3A.3 SITE CONDITIONS

This section describes the generic site conditions and the North Anna ESP site-specific conditions used in the SSI analysis.

3A.3.1 Generic Site Conditions

Design philosophy of the standard plant stipulates that the design should be applicable to as many practical sites as possible suitable for nuclear plant construction. To implement this philosophy, the effects of a wide range of subsurface conditions are considered in the seismic design. To evaluate these effects, a series of seismic soil-structure interaction (SSI) analyses in various subsurface conditions are performed. However, performing SSI analysis for combinations of all possible site properties and conditions where a nuclear power plant may be sited would be a formidable task. The purpose of this section is to define a limited number of bracketing subsurface conditions selected according to experience gained from previous generic SSI studies. Three subsurface conditions are finally selected to encompass a wide range of applicable site properties and conditions. They are classified as soft, medium and hard sites. The soft site is intended to cover a spectrum of soft soil conditions. The medium site is for medium stiff soil and soft rock conditions, and the hard site for competent rock conditions. For hard sites a fixed-base case is also considered to account for very stiff sites. These sites are considered to be uniform half-space with final enveloping properties provided in Table 3A.3-1 for SSI analysis.

3A.3.2 North Anna ESP Site Conditions

As described in Subsection 3.7.1, the North Anna ESP site-specific conditions are also considered for the ESBWR design. North Anna is a rock site. The foundation properties considered in the SSI analysis are presented in Table 3A.3-2.

Table 3A.3-1

Generic Site Properties for SSI Analysis (1), (2)

	Soft	Medium	Hard	Fixed Base
Shear wave velocity (m/s)	300	800	1700	>1700
Mass density (kg/m^3)	2000	2200	2500	NA
Poisson's ratio	0.478	0.40	0.35	NA
Material damping (%)	5	4	3	NA

(1) The shear wave velocity and material damping specified above are used as strain compatible values.

(2) The maximum ground water table is 0.61m (2 ft) below grade. The effect of ground water on SSI analysis is considered in the selected values for the Poisson's ratio, resulting in the P-wave velocity no less than the minimum P-wave velocity of water (1460 m/sec).

Table 3A.3-2

North Anna Site-specific Properties for SSI Analysis

	RBFB Complex			Control Building		
	(BE)	(UB)	(LB)	(BE)	(UB)	(LB)
Low strain shear modulus (kg/m^2)	G 6.70E+08	1.5G 1.00E+09	G/1.5 4.47E+08	G 4.97E+08	1.5G 7.46E+08	G/1.5 3.31E+08
Shear wave velocity (m/s)	1589	1946	1297	1369	1677	1118
Mass density (kg/m^3)	2606	2606	2606	2606	2606	2606
Poisson's ratio	0.33	0.33	0.33	0.33	0.33	0.33
Material damping (%)	2	2	2	2	2	2

Note: The rock properties are provided for three conditions, G, 1.5G, & G/1.5, which are considered as best-estimate (BE), upper bound (UB) and lower bound (LB) cases.

3A.4 INPUT MOTION AND DAMPING VALUES

3A.4.1 Input Motion

The time-history method is used in performing the seismic soil-structure interaction analysis. Earthquake input motions in the form of synthetic acceleration time histories are generated as described in Subsection 3.7.1.1 for three orthogonal components designated as H_1, H_2, and V. The H_1 and H_2 are the two horizontal components mutually perpendicular to each other. In the SSI analyses, H_1 and H_2 components are used in the horizontal X-(0°) and Y-(90°) directions, respectively. The V component is used in the vertical Z-direction.

Depending on the soil characteristics at the site and subject to availability of appropriate recorded ground-motion data, the control motion is defined on the soil surface at the top of finished grade or on an outcrop or a hypothetical outcrop at a location on the top of the competent material in accordance with the NRC Standard Review Plan (SRP) 3.7.1. For the generic sites defined in Section 3A.3.1, the design response spectra are conservatively applied at the level of foundation in the free field. The input motion for North Anna ESP site is also defined at the foundation level.

Vertically propagating plane seismic shear waves for the horizontal components and compression waves for the vertical component are assumed to generate the input motion.

3A.4.2 Damping Values

The structural components damping values used in the seismic analysis are in accordance with those specified in Regulatory Guide 1.61. These values for the SSE are summarized in Table 3.7-1.

3A.5 SOIL-STRUCTURE INTERACTION ANALYSIS METHOD

The seismic analysis is performed using the sway-rocking soil-structure interaction model.

The analysis model is a lumped mass-beam model with soil springs. The structural models are described in Subsection 3.7.2, and in Subsection 3A.7 in more detail.

To account for soil-structure interaction effect, sway-rocking base soil springs are attached to the structural model. The base spring is evaluated from vibration admittance theory, based on three-dimensional wave propagation theory for uniform half space soil. Though the spring values consist of frequency dependent real and imaginary parts, they are simplified and replaced with frequency independent soil spring Kc, and damping coefficient Cc, respectively, for the time history analysis solved in time domain. The calculated Kc and Cc values are tabulated in Tables 3A.5-1 and 3A.5-2 for the RBFB complex and the CB, respectively.

The effect of lateral soil/backfill on embedded foundations is conservatively accounted for by applying the control motion directly at the foundation level. Dynamic lateral soil pressures are calculated separately and considered in the design of external walls, using the elastic solution procedures in Section 3.5.3.2 of ASCE 4-98.

Because the three component ground motion time histories are statistically independent as described in Subsections 3.7.1.1.2 and 3.7.1.1.3, they are input simultaneously in the response analysis using the time history method of analysis solved by direct integration. The numerical integration time step is 0.002 sec. for the generic site cases and 0.001 sec. for the North Anna site cases. Structural responses in terms of accelerations, forces, and moments are computed directly. Floor response spectra are obtained from the calculated response acceleration time histories (Subsection 3.7.2.5).

Table 3A.5-1

Soil Spring and Damping Coefficient for RBFB complex

			Generic Site			North Anna Site		
			Soft	Medium	Hard	BE	UB	LB
			300 m/s	800 m/s	1700 m/s	1589 m/s	1946 m/s	1297 m/s
Soil Spring Kc	X-dir	MN/m	2.910E+04	2.178E+05	1.087E+06	9.676E+05	1.451E+06	6.447E+05
	Y-dir	MN/m	3.085E+04	2.281E+05	1.131E+06	1.001E+06	1.501E+06	6.670E+05
	Z-dir	MN/m	4.366E+04	2.972E+05	1.408E+06	1.245E+06	1.868E+06	8.297E+05
	X-X Rot.	MN•m/rad	2.466E+07	1.678E+08	7.950E+08	6.871E+08	1.030E+09	4.578E+08
	Y-Y Rot.	MN•m/rad	4.280E+07	2.913E+08	1.379E+09	1.145E+09	1.717E+09	7.627E+08
	Z-Z Rot.	MN•m/rad	9.804E+15	9.804E+15	9.804E+15	9.804E+15	9.804E+15	9.804E+15
Damping coefficient Cc	X-dir	MN•sec/m	1.708E+03	4.837E+03	1.143E+04	1.083E+04	1.324E+04	8.870E+03
	Y-dir	MN•sec/m	1.910E+03	5.294E+03	1.236E+04	1.159E+04	1.416E+04	9.484E+03
	Z-dir	MN•sec/m	3.852E+03	9.740E+03	2.114E+04	2.011E+04	2.437E+04	1.663E+04
	X-X Rot.	MN•m•sec/rad	2.512E+05	4.378E+05	4.626E+05	4.631E+05	4.235E+05	4.877E+05
	Y-Y Rot.	MN•m•sec/rad	8.432E+05	1.590E+06	1.694E+06	1.567E+06	1.444E+06	1.643E+06
	Z-Z Rot.	MN•m•sec/rad	0.0	0.0	0.0	0.0	0.0	0.0

Table 3A.5-2

Soil Spring and Damping Coefficient for CB

			Generic Site			North Anna Site		
			Soft	Medium	Hard	BE	UB	LB
			300 m/s	800 m/s	1700 m/s	1369 m/s	1677 m/s	1118 m/s
Soil Spring Kc	X-dir	MN/m	1.322E+04	9.876E+04	4.925E+05	3.297E+05	4.948E+05	2.199E+05
	Y-dir	MN/m	1.372E+04	1.017E+05	5.049E+05	3.375E+05	5.064E+05	2.250E+05
	Z-dir	MN/m	1.963E+04	1.336E+05	6.329E+05	4.157E+05	6.237E+05	2.773E+05
	X-X Rot.	MN•m/rad	2.508E+06	1.707E+07	8.085E+07	5.311E+07	7.969E+07	3.542E+07
	Y-Y Rot.	MN•m/rad	3.543E+06	2.411E+07	1.142E+08	7.501E+07	1.125E+08	5.003E+07
	Z-Z Rot.	MN•m/rad	9.804E+15	9.804E+15	9.804E+15	9.804E+15	9.804E+15	9.804E+15
Damping coefficient Cc	X-dir	MN•sec/m	3.515E+02	9.961E+02	2.349E+03	1.975E+03	2.412E+03	1.620E+03
	Y-dir	MN•sec/m	3.796E+02	1.058E+03	2.470E+03	2.071E+03	2.527E+03	1.698E+03
	Z-dir	MN•sec/m	7.794E+02	1.986E+03	4.307E+03	3.561E+03	4.314E+03	2.940E+03
	X-X Rot.	MN•m•sec/rad	1.421E+04	2.775E+04	3.073E+04	3.330E+04	3.163E+04	3.364E+04
	Y-Y Rot.	MN•m•sec/rad	2.720E+04	5.542E+04	6.489E+04	6.916E+04	6.670E+04	6.872E+04
	Z-Z Rot.	MN•m•sec/rad	0.0	0.0	0.0	0.0	0.0	0.0

3A.6 SOIL-STRUCTURE INTERACTION ANALYSIS CASES

To establish design envelopes of seismic responses of the RBFB complex, SSI analyses are performed for a total of 7 cases, as summarized in Table 3A.6-1. Similarly, SSI analyses are performed for the CB.

The enveloping results are obtained from the responses of all SSI cases to cover a wide range of site conditions.

Table 3A.6-1

Seismic SSI Analysis Cases

Case No.	Soil Properties							Input Wave (SSE)					
	Generic Site				North Anna ESP Site			RG 1.60			North Anna		
	Soft	Medium	Hard	Fixed Base	Best estimate	Upper bound	Lower bound	H1	H2	V	H1	H2	V
1	√							√	√	√			
2		√						√	√	√			
3			√					√	√	√			
4				√				√	√	√			
5					√						√	√	√
6						√					√	√	√
7							√				√	√	√

3A.7 ANALYSIS MODELS

The analysis model is a three-dimensional lumped mass-beam model that considers shear, bending, torsion and axial deformations. The structural elements of the reactor building outside containment and the fuel building are reduced to one set of stick models. The containment and the containment internal structures including the reactor pressure vessel are modeled as separate interconnected sticks. The control building is modeled with a single stick.

3A.7.1 Method of Dynamic Structural Model Development

Evaluation of stiffness for the seismic model is done according to the following assumptions.

- Exterior walls and those inner walls that are continuous up from the basemat and have 500 mm or more in thickness are treated as seismic walls.
- Those openings that have 2.0 m^2 or larger area are explicitly considered in the stiffness evaluation.

Effective Shear Area (Sx, Sy):

As effective shear area, seismic walls parallel to each of two earthquake directions are considered. When openings exist in a wall, equivalent shear area is calculated so that shear displacements of two walls, with and without openings, are equal.

Moment of Inertia (Iyy, Ixx):

Moment of inertia of seismic walls is calculated according to the following procedures.

- Moment of inertia in each direction is calculated around a horizontal axis that goes through the centroid.
- When openings exist in a wall, equivalent moment of inertia is calculated so that angles of rotation of two walls, with and without openings, are equal.
- The effective flange length is taken to be eight times the flange wall thickness, and it is limited to one-half of the flange wall length.

Torsional Constant (Izz):

Torsional constant of seismic walls is calculated around the vertical axis that goes through the center of rigidity.

Vertical Axial Area (Sa):

Vertical axial area of each element is equal to summation of effective shear areas that are evaluated in two directions for the horizontal analysis. However, the overlap area at the corner of box walls is subtracted from the summation.

The locations (X_c and Y_c) of centroid of axial area for various sections determined in Step (4) above define the locations of center of rigidity of the equivalent beam stick model in the vertical direction.

Because the stick model has different center-of-rigidity locations in the horizontal and the vertical directions, the lumped mass-beam model comprises two stick models. One stick consists of elements with axial areas located at the centers of rigidity for axial area, and another stick consists of elements with all other remaining sectional properties (i.e., excluding axial area)

located at the centers of rigidity for shear and torsional deformations. Both sticks are connected at common centers of mass at various floor elevations.

As described above, the RBFB complex is represented by several stick models. These stick models are interconnected by horizontal links representing the floor diaphragm at respective elevations. These links are modeled as rigid springs for floor in-plane translational displacement and having no stiffness for all other deformations.

The vertical floor frequencies are obtained at major floor locations by independent modal analysis of the respective floor finite element model. These frequencies are included in the stick model by a series of vertical single degree-of-freedom oscillators at the corresponding floor elevations.

To obtain the mass properties for the stick model, the dead load, 25% of the respective live load and an additional 50 psf load for piping and cable trays, etc. were used to compute the lumped mass properties following the steps described below.

(1) Depending on whether the floor has a regular or an irregular layout, hand calculations or floor finite element models are used to obtain the total mass (M_x, $M_{y,}$ M_z), the mass moments of inertia (M_{xx}, M_{yy}, M_{zz}) and the center of mass of each floor. Similar calculations are performed for the tributary areas of the walls above and below the floors.

(2) These properties are subsequently reduced to one center of mass with its associated properties at each floor elevation. The water masses in the pools are also included in this calculation.

(3) The bending mass moment of inertia at various floor elevations are also added to each floor mass.

Based on the methodology described above, the lumped mass-beam stick model for SSI is developed as described in Section 3A.7.2.

3A.7.2 Lumped Mass-Beam Stick Model for SSI Analysis

The lumped mass-beam stick models for the RBFB complex in the XZ- and YZ-planes are shown in Figures 3A.7-1. Similarly, the stick models corresponding to the RCCV and pedestal wall are shown in Figures 3A.7-2 and 3A.7-3. The overall integrated building model is shown in Figure 3A.7-4. As shown in the figure, the building model is also coupled to the vent wall (VW), the reactor shield wall (RSW) and the reactor pressure vessel (RPV). They are symmetric in both horizontal directions.

The stick models are interconnected at floor elevations by horizontal links. These links are rigid for floor in-plane displacements and have no stiffness for out-of-plane displacement and rotations.

The lumped mass-beam stick models for the CB in the XZ- and YZ-planes are shown in Figures 3A.7-5.

To account for soil-structure interaction effect, sway-rocking base soil springs are attached to this structural model, as described in Section 3A.5. Natural frequencies of the seismic model at all site conditions are shown in Tables 3A.7-1 through 3A.7-7 for the RBFB model and Tables 3A.7-8 through 3A.7-14 for the CB model.

Table 3A.7-1

Eigenvalue Analysis Results for RBFB model at Soft Site

Mode No.	Frequency (HZ)	Period (sec)	Participation Factor					
			X dir.	Y dir.	Z dir.	X rot.	Y rot.	Z rot.
1	1.19	0.84	0.02	1.56	-0.01	-1038	17	-38
2	1.40	0.71	1.44	-0.02	0.10	7	811	5
3	2.09	0.48	-0.23	0.01	2.34	2	220	0
4	2.78	0.36	-0.31	-0.20	-1.42	-373	942	1
5	2.89	0.35	0.02	0.63	-0.01	1314	-79	15
6	3.11	0.32	-0.46	0.03	-0.10	71	1809	8
7	3.81	0.26	-0.09	0.09	0.01	-120	-277	124
8	3.81	0.26	-0.07	-0.11	0.01	148	-201	-160
9	5.23	0.19	0.11	0.01	-0.09	24	-1005	-51
10	5.25	0.19	-0.06	0.01	-0.22	29	597	114
11	5.94	0.17	0.00	-0.05	0.00	1335	190	-12815
12	5.99	0.17	-0.11	0.00	-0.01	40	693	-153
13	5.99	0.17	-0.01	-0.08	0.00	-1874	-166	12660
14	6.76	0.15	-0.04	0.01	-0.12	60	347	-191
15	8.71	0.11	-0.01	-0.10	0.01	-548	79	302
16	9.53	0.10	-0.03	0.01	-0.04	13	4849	74
17	9.97	0.10	0.14	0.00	-0.05	-429	6204	95
18	10.27	0.10	-0.03	0.02	0.01	-5570	-1198	-2635
19	10.41	0.10	-0.06	-0.01	0.03	385	-3528	110
20	10.83	0.09	-0.11	0.00	-0.03	-103	-1451	-185

Note: The participation factors are calculated for mode vectors normalized by the maximum mode displacement.

Table 3A.7-2

Eigenvalue Analysis Results for RBFB model at Medium Site

Mode No.	Frequency (HZ)	Period (sec)	Participation Factor					
			X dir.	Y dir.	Z dir.	X rot.	Y rot.	Z rot.
1	2.58	0.39	0.01	1.68	0.02	-1173	14	-250
2	2.72	0.37	1.22	-0.22	1.48	120	1087	56
3	2.93	0.34	1.88	0.00	0.06	-3	1321	33
4	3.81	0.26	0.00	-0.29	-0.03	1024	-24	-49
5	3.81	0.26	-0.80	0.01	-0.19	-12	-1348	-36
6	4.93	0.20	-0.58	-0.17	5.96	-204	726	100
7	5.22	0.19	-0.97	-0.03	-0.08	-24	1490	-61
8	5.47	0.18	0.99	0.15	-5.04	206	-1696	-56
9	5.96	0.17	0.18	4.14	0.70	10031	129	-27285
10	5.98	0.17	1.87	-0.23	1.20	27	-4231	-2709
11	6.00	0.17	-0.12	0.87	-0.06	-2869	-335	30291
12	6.21	0.16	-0.05	-4.67	-0.43	-6804	174	-3195
13	6.50	0.15	2.78	-0.08	0.93	-141	-6411	69
14	6.77	0.15	-2.38	0.14	-2.14	267	5607	-207
15	9.77	0.10	-0.06	-0.70	0.03	-652	23	662
16	10.26	0.10	-1.23	0.27	0.01	1099	1143	43
17	10.30	0.10	-0.23	-0.27	-0.19	-2979	3197	-843
18	10.33	0.10	0.45	-0.01	-0.21	991	3266	591
19	10.91	0.09	-1.25	0.00	0.32	227	-7710	-233
20	11.19	0.09	0.10	-0.01	0.37	164	-5553	-53

Note: The participation factors are calculated for mode vectors normalized by the maximum mode displacement.

Table 3A.7-3

Eigenvalue Analysis Results for RBFB model at Hard Site

Mode No.	Frequency (HZ)	Period (sec)	Participation Factor					
			X dir.	Y dir.	Z dir.	X rot.	Y rot.	Z rot.
1	2.73	0.37	0.15	0.05	1.16	-56	252	-4
2	3.51	0.28	-0.03	3.70	0.07	-2570	-6	-1432
3	3.81	0.26	9.86	0.09	0.43	-112	6169	379
4	3.81	0.26	0.01	-2.61	-0.08	2538	-10	1157
5	3.93	0.25	-8.77	-0.06	-0.44	98	-6101	-394
6	5.20	0.19	-0.04	-0.14	1.95	-92	28	289
7	5.22	0.19	-0.71	0.00	-0.26	16	312	-133
8	5.98	0.17	0.15	0.63	-0.15	2714	69	-12791
9	5.99	0.17	0.60	-0.04	-0.13	-26	-1069	-178
10	6.05	0.17	-0.10	0.29	0.08	-1739	-152	13192
11	6.75	0.15	0.09	-0.30	2.32	-247	-104	-732
12	7.62	0.13	0.20	1.23	-0.45	1639	-438	904
13	8.05	0.12	-1.11	0.30	1.34	423	2411	200
14	8.82	0.11	0.63	0.07	2.21	91	-1101	-33
15	10.30	0.10	0.13	0.55	-0.34	-2312	352	-1390
16	10.36	0.10	0.02	0.02	-0.95	418	3408	291
17	10.62	0.09	1.57	0.12	-0.20	113	-3763	-138
18	11.22	0.09	-0.03	-0.69	0.00	320	-11	842
19	11.25	0.09	0.11	0.00	0.08	17	-1518	-41
20	11.64	0.09	-0.15	-2.92	-0.10	-2148	-28	2104

Note: The participation factors are calculated for mode vectors normalized by the maximum mode displacement.

Table 3A.7-4

Eigenvalue Analysis Results for RBFB model in Fixed-base Case

Mode No.	Frequency (HZ)	Period (sec)	Participation Factor					
			X dir.	Y dir.	Z dir.	X rot.	Y rot.	Z rot.
1	2.74	0.37	0.10	0.03	1.09	-45	191	-3
2	3.81	0.26	-0.16	7.02	0.15	-4075	-53	-3906
3	3.81	0.26	2.41	0.07	0.05	-42	943	63
4	3.94	0.25	0.11	-5.96	-0.16	4051	36	3613
5	4.36	0.23	1.66	0.03	0.07	-33	1090	107
6	5.21	0.19	-0.07	-0.16	1.63	-65	9	381
7	5.22	0.19	-0.82	0.00	-0.30	26	95	-186
8	5.98	0.17	0.12	0.50	-0.09	1955	55	-8551
9	5.99	0.17	0.49	-0.04	-0.07	-15	-829	-143
10	6.09	0.16	-0.08	0.26	0.06	-1236	-109	8979
11	6.75	0.15	0.15	-0.19	1.37	-86	-188	-697
12	8.02	0.12	0.15	1.33	-0.21	1889	-348	1273
13	8.58	0.12	1.47	-0.21	-0.71	-302	-3477	-237
14	10.24	0.10	0.65	0.19	4.42	-457	1077	-298
15	10.32	0.10	-0.10	0.38	-1.37	-1965	-845	-1088
16	10.52	0.10	-0.47	0.00	-4.23	35	1763	100
17	10.67	0.09	1.09	0.06	-1.52	55	-3554	-121
18	11.23	0.09	-0.01	-0.27	-0.01	408	-17	504
19	11.25	0.09	0.08	0.00	0.04	20	-1324	-39
20	11.89	0.08	0.87	0.23	2.13	-824	539	-576

Note: The participation factors are calculated for mode vectors normalized by the maximum mode displacement.

Table 3A.7-5

Eigenvalue Analysis Results for RBFB model at Best-estimate North Anna Site

Mode No.	Frequency (HZ)	Period (sec)	Participation Factor					
			X dir.	Y dir.	Z dir.	X rot.	Y rot.	Z rot.
1	2.73	0.37	0.17	0.05	1.17	-59	266	-5
2	3.46	0.29	-0.03	3.23	0.05	-2255	-4	-1182
3	3.81	0.26	20.00	0.13	0.96	-207	13513	793
4	3.81	0.26	0.00	-2.13	-0.07	2222	-13	909
5	3.86	0.26	-18.91	-0.11	-0.98	193	-13444	-806
6	5.19	0.19	-0.04	-0.14	2.00	-95	30	280
7	5.22	0.19	-0.71	0.00	-0.25	14	337	-128
8	5.98	0.17	0.15	0.65	-0.16	2852	68	-13591
9	5.99	0.17	0.63	-0.05	-0.15	-43	-1112	-100
10	6.05	0.17	-0.10	0.29	0.09	-1838	-162	13995
11	6.75	0.15	0.06	-0.33	2.56	-285	-61	-751
12	7.57	0.13	0.22	1.19	-0.52	1578	-474	848
13	7.95	0.13	-1.04	0.35	1.49	489	2248	218
14	8.65	0.12	0.68	0.06	1.94	89	-1247	-30
15	10.30	0.10	0.15	0.57	-0.31	-2328	389	-1421
16	10.36	0.10	0.02	0.02	-0.86	445	3490	304
17	10.62	0.09	1.62	0.14	-0.17	131	-3774	-139
18	11.21	0.09	-0.03	-0.85	-0.01	221	-9	954
19	11.25	0.09	0.12	0.00	0.08	18	-1571	-42
20	11.55	0.09	-0.12	-3.08	-0.06	-2317	-5	2117

Note: The participation factors are calculated for mode vectors normalized by the maximum mode displacement.

Table 3A.7-6

Eigenvalue Analysis Results for RBFB model at Upper-bound North Anna Site

Mode No.	Frequency (HZ)	Period (sec)	Participation Factor					
			X dir.	Y dir.	Z dir.	X rot.	Y rot.	Z rot.
1	2.73	0.37	0.14	0.04	1.14	-53	238	-4
2	3.60	0.28	-0.05	4.98	0.10	-3452	-13	-2113
3	3.81	0.26	5.88	0.07	0.23	-76	3407	215
4	3.81	0.26	0.02	-3.89	-0.11	3419	-4	1835
5	4.01	0.25	-4.79	-0.04	-0.24	61	-3338	-232
6	5.20	0.19	-0.04	-0.14	1.86	-86	23	306
7	5.22	0.19	-0.73	0.00	-0.27	18	261	-143
8	5.98	0.17	0.14	0.59	-0.13	2516	68	-11713
9	5.99	0.17	0.58	-0.04	-0.11	-23	-1004	-163
10	6.06	0.17	-0.09	0.28	0.07	-1612	-143	12114
11	6.75	0.15	0.12	-0.26	1.98	-191	-154	-705
12	7.72	0.13	0.18	1.28	-0.36	1720	-397	997
13	8.21	0.12	1.21	-0.25	-1.09	-346	-2659	-188
14	9.18	0.11	0.46	0.06	2.25	63	-683	-36
15	10.30	0.10	0.11	0.52	-0.42	-2292	256	-1339
16	10.36	0.10	-0.01	0.02	-1.23	359	3329	263
17	10.64	0.09	1.48	0.10	-0.24	88	-3868	-140
18	11.22	0.09	-0.02	-0.50	0.00	412	-12	706
19	11.25	0.09	0.10	0.00	0.07	17	-1480	-41
20	11.79	0.08	0.49	2.25	0.52	1383	252	-1850

Note: The participation factors are calculated for mode vectors normalized by the maximum mode displacement.

Table 3A.7-7

Eigenvalue Analysis Results for RBFB model at Lower-bound North Anna Site

Mode No.	Frequency (HZ)	Period (sec)	Participation Factor					
			X dir.	Y dir.	Z dir.	X rot.	Y rot.	Z rot.
1	2.73	0.37	0.22	0.06	1.21	-71	316	-7
2	3.27	0.31	-0.01	2.34	0.03	-1645	1	-705
3	3.65	0.27	7.62	0.02	0.41	-56	5494	271
4	3.81	0.26	0.00	-1.23	-0.05	1615	-18	436
5	3.81	0.26	-6.52	0.00	-0.43	41	-5428	-281
6	5.19	0.19	-0.06	-0.14	2.30	-111	47	250
7	5.22	0.19	-0.71	-0.01	-0.23	10	452	-112
8	5.98	0.17	0.18	0.75	-0.23	3437	69	-16769
9	5.99	0.17	0.72	-0.05	-0.23	-45	-1315	-156
10	6.03	0.17	-0.11	0.32	0.12	-2216	-191	17187
11	6.74	0.15	-0.24	-0.59	4.53	-607	491	-970
12	7.28	0.14	0.56	1.18	-1.73	1553	-1162	794
13	7.49	0.13	-0.39	0.60	1.06	818	824	336
14	8.11	0.12	1.03	0.03	1.29	55	-2053	-34
15	10.29	0.10	0.19	0.70	-0.24	-2309	525	-1566
16	10.35	0.10	0.04	0.02	-0.61	540	3789	352
17	10.58	0.09	1.82	0.23	-0.13	254	-3484	-150
18	11.10	0.09	-0.04	-1.80	-0.01	-1061	5	1283
19	11.25	0.09	0.17	0.00	0.10	25	-1719	-41
20	11.27	0.09	-0.02	-1.84	-0.01	-2242	13	801

Note: The participation factors are calculated for mode vectors normalized by the maximum mode displacement.

Table 3A.7-8

Eigenvalue Analysis Results for CB model at Soft Site

Mode No.	Frequency (HZ)	Period (sec)	Participation Factor					
			X dir.	Y dir.	Z dir.	X rot.	Y rot.	Z rot.
1	3.22	0.31	0.01	1.22	0.00	-306	4	-1
2	3.41	0.29	1.18	-0.01	0.00	3	368	1
3	5.19	0.19	0.00	0.00	1.37	-1	0	0
4	7.24	0.14	0.46	0.02	0.00	19	-755	0
5	7.42	0.13	-0.02	0.56	0.00	592	31	0
6	10.32	0.10	0.00	0.00	-0.37	-8	3	0
7	14.92	0.07	0.00	0.00	-0.19	-3	2	-1
8	16.66	0.06	0.00	0.00	0.00	0	0	25
9	20.80	0.05	0.00	0.00	-0.11	17	-3	2
10	22.65	0.04	-0.02	-0.01	0.00	277	-417	1

Note: The participation factors are calculated for mode vectors normalized by the maximum mode displacement.

Table 3A.7-9

Eigenvalue Analysis Results for CB model at Medium Site

Mode No.	Frequency (HZ)	Period (sec)	Participation Factor					
			X dir.	Y dir.	Z dir.	X rot.	Y rot.	Z rot.
1	6.94	0.14	0.07	1.27	0.01	-299	22	-7
2	7.37	0.14	1.25	-0.07	0.00	15	378	7
3	9.64	0.10	-0.01	-0.01	2.22	-2	3	0
4	13.11	0.08	-0.02	-0.03	3.41	-16	18	0
5	15.43	0.06	0.04	0.05	-2.74	39	-41	0
6	16.66	0.06	0.00	0.00	0.00	0	-3	52
7	17.08	0.06	0.48	0.09	0.01	68	-610	-64
8	17.60	0.06	-0.09	0.58	0.01	444	118	10
9	20.83	0.05	0.00	-0.01	-1.02	-2	1	1
10	25.88	0.04	0.09	0.05	0.00	-254	323	-2

Note: The participation factors are calculated for mode vectors normalized by the maximum mode displacement.

Table 3A.7-10

Eigenvalue Analysis Results for CB model at Hard Site

Mode No.	Frequency (HZ)	Period (sec)	Participation Factor					
			X dir.	Y dir.	Z dir.	X rot.	Y rot.	Z rot.
1	9.29	0.11	0.14	1.24	0.01	-231	39	-15
2	9.85	0.10	1.21	-0.14	0.04	23	300	18
3	9.90	0.10	-0.32	0.00	1.34	-2	-75	-4
4	14.62	0.07	-0.02	-0.02	1.87	-10	13	0
5	16.67	0.06	0.00	0.00	0.00	0	0	-30
6	20.55	0.05	-0.14	-0.14	6.63	-169	232	0
7	22.56	0.04	0.28	0.25	-5.70	320	-532	-3
8	24.13	0.04	0.27	0.09	0.08	116	-517	-7
9	25.30	0.04	-0.10	0.36	0.04	419	203	9
10	27.56	0.04	-0.05	-0.15	-2.92	-111	83	1

Note: The participation factors are calculated for mode vectors normalized by the maximum mode displacement.

Table 3A.7-11

Eigenvalue Analysis Results for CB model in Fixed-base Case

Mode No.	Frequency (HZ)	Period (sec)	Participation Factor					
			X dir.	Y dir.	Z dir.	X rot.	Y rot.	Z rot.
1	9.94	0.10	0.03	0.07	1.20	-14	11	-1
2	10.30	0.10	0.18	1.18	0.00	-175	42	-21
3	10.90	0.09	1.17	-0.18	0.00	22	235	26
4	14.70	0.07	-0.02	-0.02	1.42	-9	11	0
5	16.70	0.06	0.00	0.00	0.00	0	0	-38
6	20.70	0.05	-0.04	-0.04	2.41	-63	84	0
7	25.70	0.04	-0.98	-0.56	1.25	-1000	2540	23
8	26.20	0.04	1.30	0.32	4.27	568	-3380	-44
9	27.00	0.04	-0.21	0.48	0.02	811	551	21
10	29.10	0.03	-0.11	-0.25	-4.42	-335	268	1

Note: The participation factors are calculated for mode vectors normalized by the maximum mode displacement.

Table 3A.7-12

Eigenvalue Analysis Results for CB model at Best-estimate North Anna Site

Mode No.	Frequency (HZ)	Period (sec)	Participation Factor					
			X dir.	Y dir.	Z dir.	X rot.	Y rot.	Z rot.
1	8.85	0.11	0.12	1.25	0.01	-251	36	-13
2	9.40	0.11	1.23	-0.12	0.01	22	326	15
3	9.88	0.10	-0.04	-0.02	1.44	0	-6	0
4	14.56	0.07	-0.02	-0.02	2.22	-11	15	0
5	16.67	0.06	0.00	0.00	0.00	0	0	-27
6	19.92	0.05	-0.19	-0.20	9.40	-212	287	0
7	21.25	0.05	0.30	0.29	-8.64	323	-492	-2
8	23.09	0.04	0.33	0.10	0.05	107	-554	-8
9	24.18	0.04	-0.11	0.44	0.03	441	191	9
10	27.41	0.04	-0.03	-0.08	-1.98	-9	22	1

Note: The participation factors are calculated for mode vectors normalized by the maximum mode displacement.

Table 3A.7-13

Eigenvalue Analysis Results for CB model at Upper-bound North Anna Site

Mode No.	Frequency (HZ)	Period (sec)	Participation Factor					
			X dir.	Y dir.	Z dir.	X rot.	Y rot.	Z rot.
1	9.28	0.11	0.14	1.24	0.01	-232	39	-15
2	9.84	0.10	1.21	-0.14	0.04	23	302	18
3	9.90	0.10	-0.29	0.00	1.34	-2	-69	-4
4	14.62	0.07	-0.02	-0.02	1.88	-10	13	0
5	16.67	0.06	0.00	0.00	0.00	0	0	-30
6	20.54	0.05	-0.14	-0.14	6.77	-172	236	0
7	22.51	0.04	0.28	0.25	-5.85	318	-525	-3
8	24.12	0.04	0.27	0.09	0.08	116	-516	-7
9	25.30	0.04	-0.10	0.36	0.04	420	203	9
10	27.55	0.04	-0.05	-0.15	-2.88	-109	82	1

Note: The participation factors are calculated for mode vectors normalized by the maximum mode displacement.

Table 3A.7-14

Eigenvalue Analysis Results for CB model at Lower-bound North Anna Site

Mode No.	Frequency (HZ)	Period (sec)	Participation Factor					
			X dir.	Y dir.	Z dir.	X rot.	Y rot.	Z rot.
1	8.30	0.12	0.10	1.26	0.01	-272	32	-11
2	8.82	0.11	1.24	-0.11	0.01	20	351	12
3	9.84	0.10	-0.02	-0.01	1.59	-1	-1	0
4	14.43	0.07	-0.02	-0.02	2.91	-14	19	0
5	16.67	0.06	0.00	0.00	0.00	0	0	-24
6	18.10	0.06	-0.06	-0.07	4.08	-60	76	-1
7	20.92	0.05	0.30	0.22	-3.50	207	-432	-5
8	21.51	0.05	0.39	0.10	0.03	90	-564	-10
9	22.42	0.04	-0.11	0.52	0.02	432	164	8
10	27.32	0.04	-0.01	-0.04	-1.33	53	-11	2

Note: The participation factors are calculated for mode vectors normalized by the maximum mode displacement.

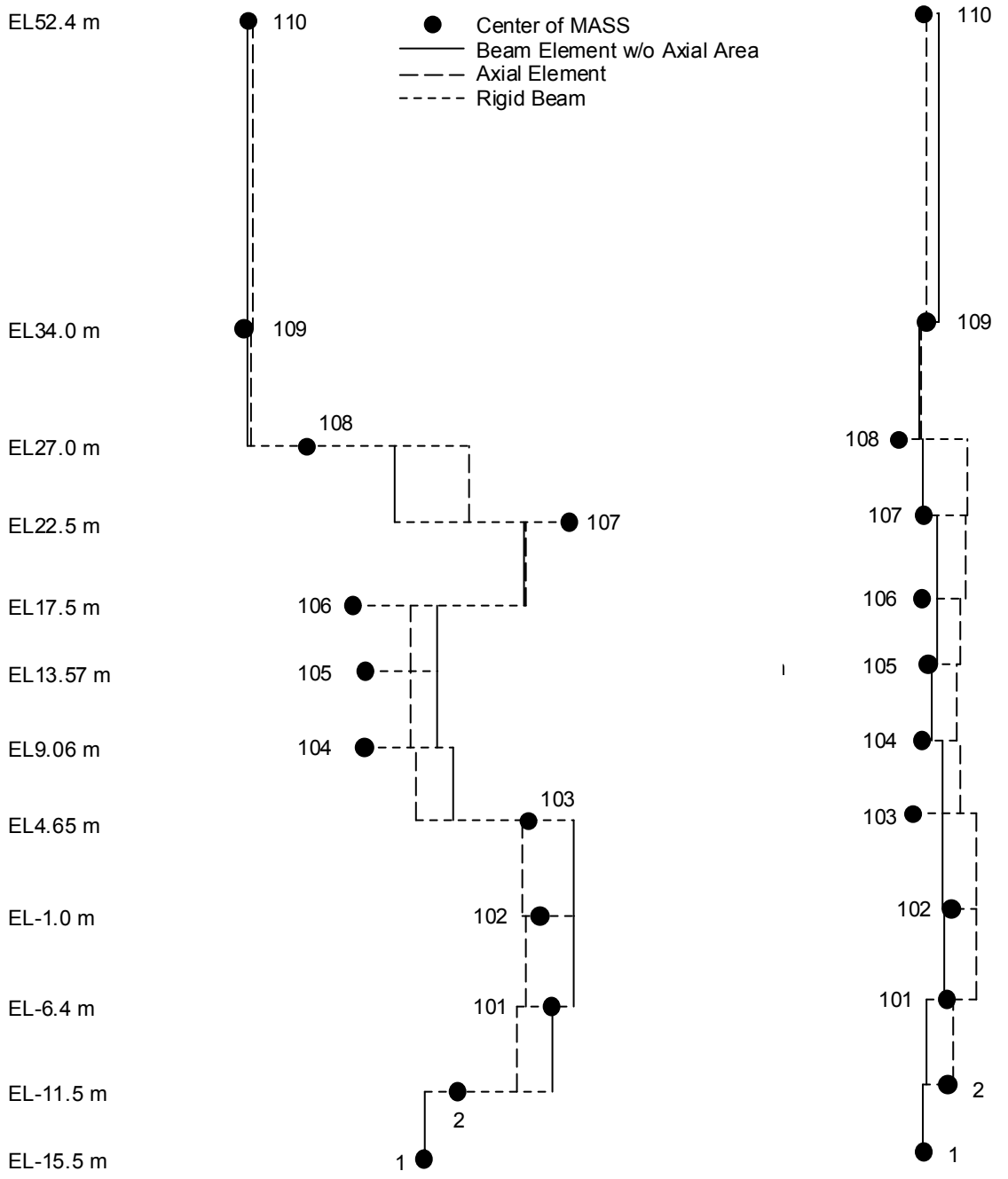

(a) XZ Plane **(b) YZ Plane**

Figure 3A.7-1. RBFB Stick Model

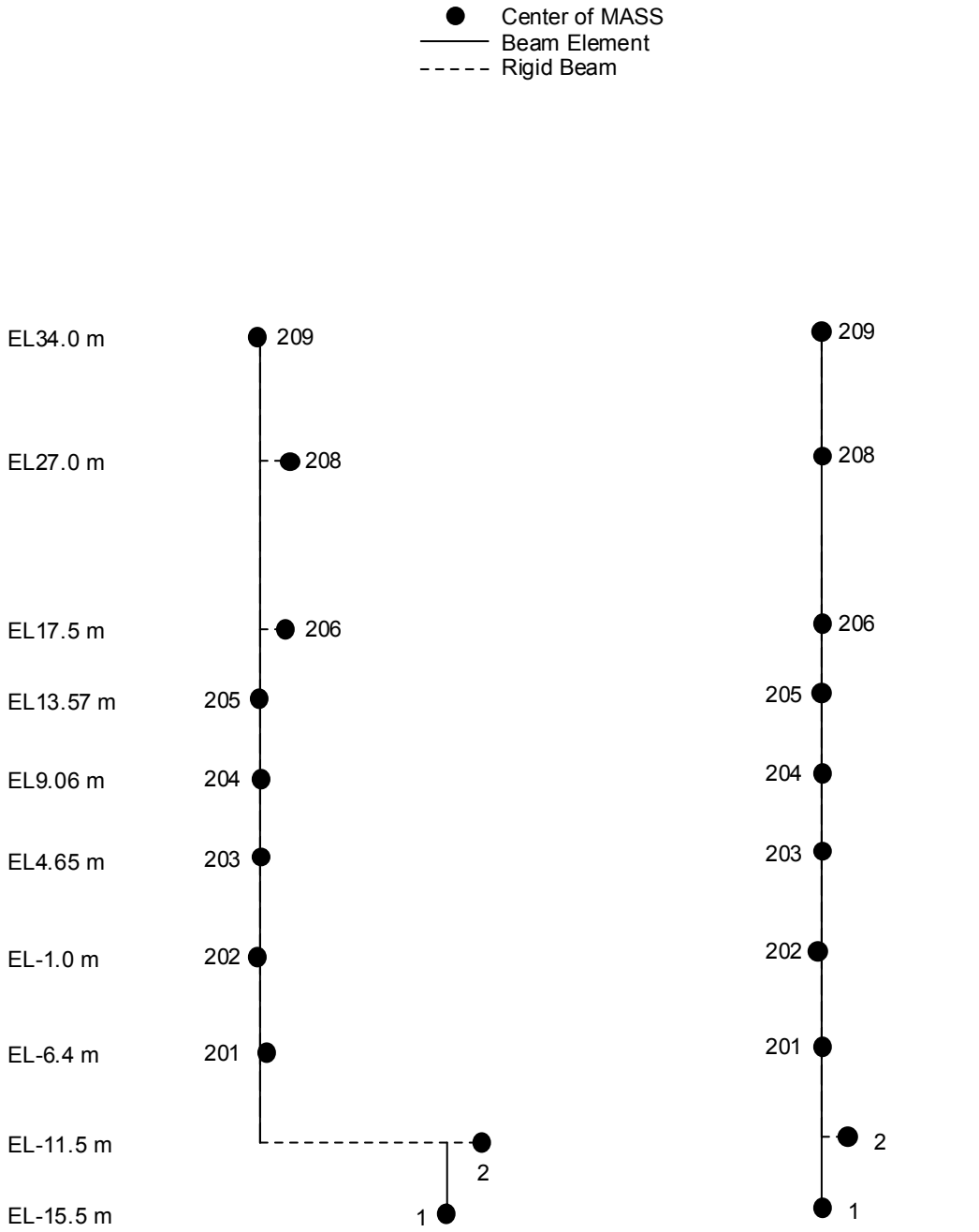

(a) XZ Plane **(b) YZ Plane**

Figure 3A.7-2. RCCV Stick Model

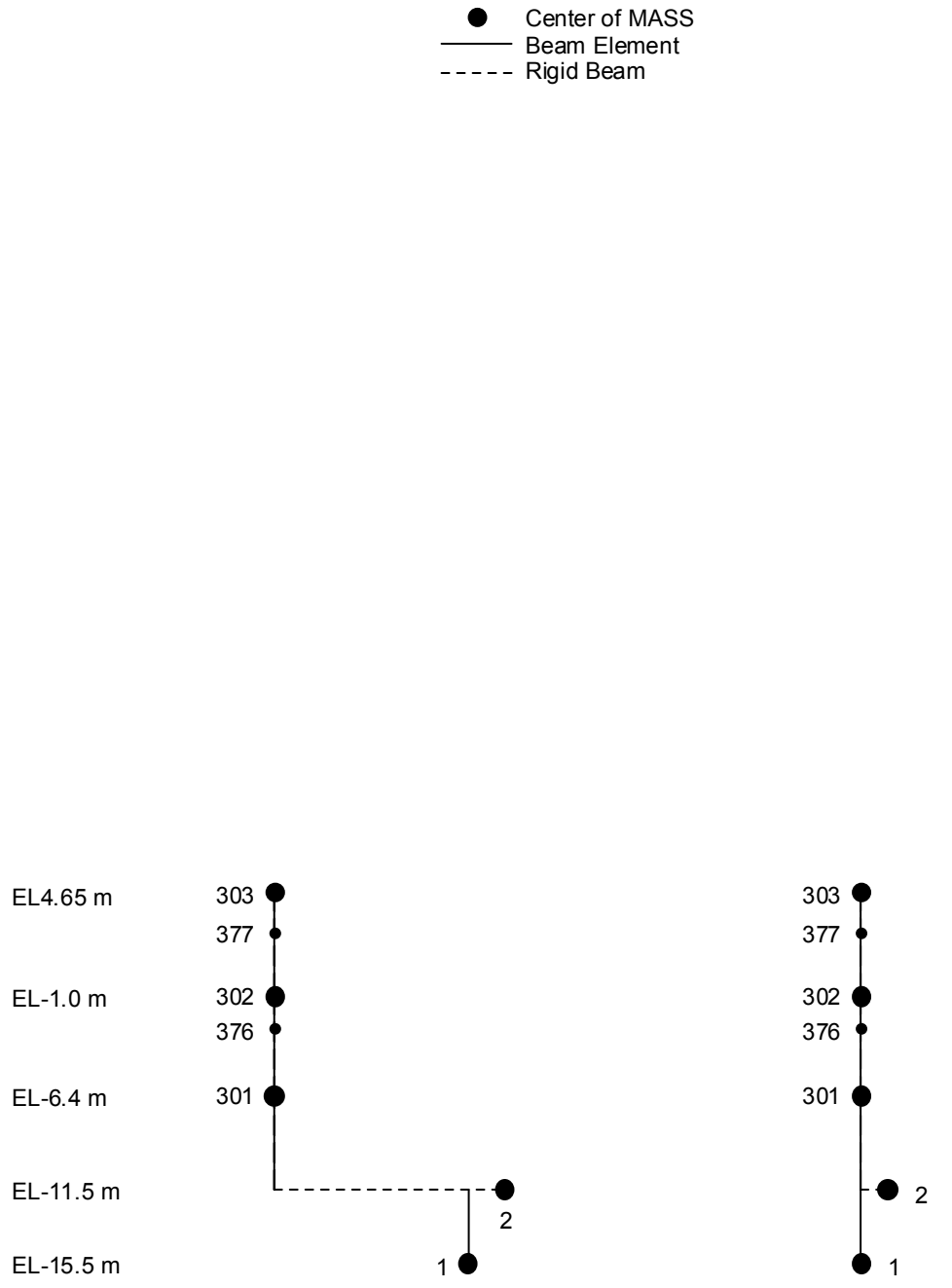

(a) XZ Plane **(b) YZ Plane**

Figure 3A.7-3. Pedestal Stick Model

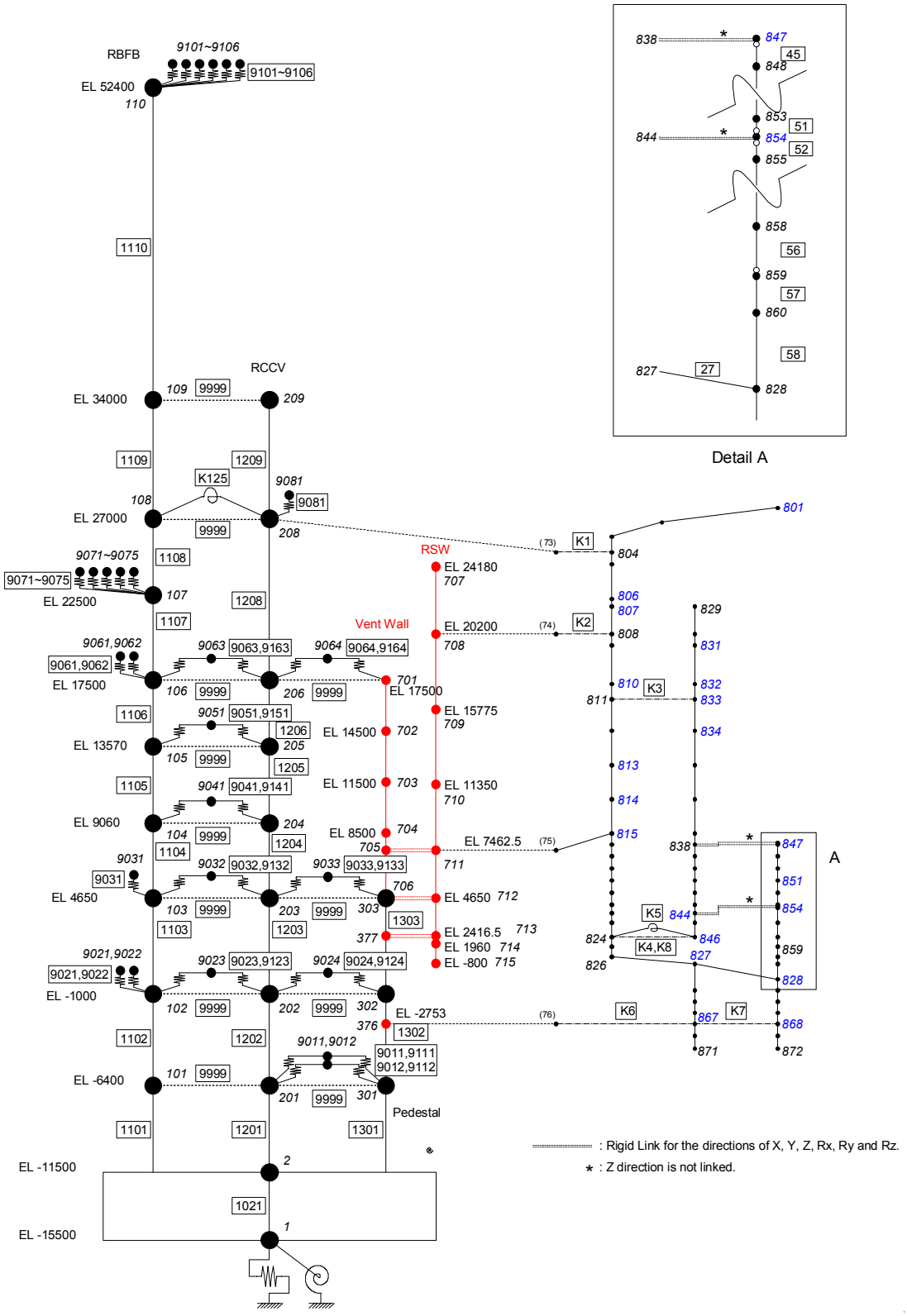

Figure 3A.7-4. ESBWR RBFB Complex Seismic Model

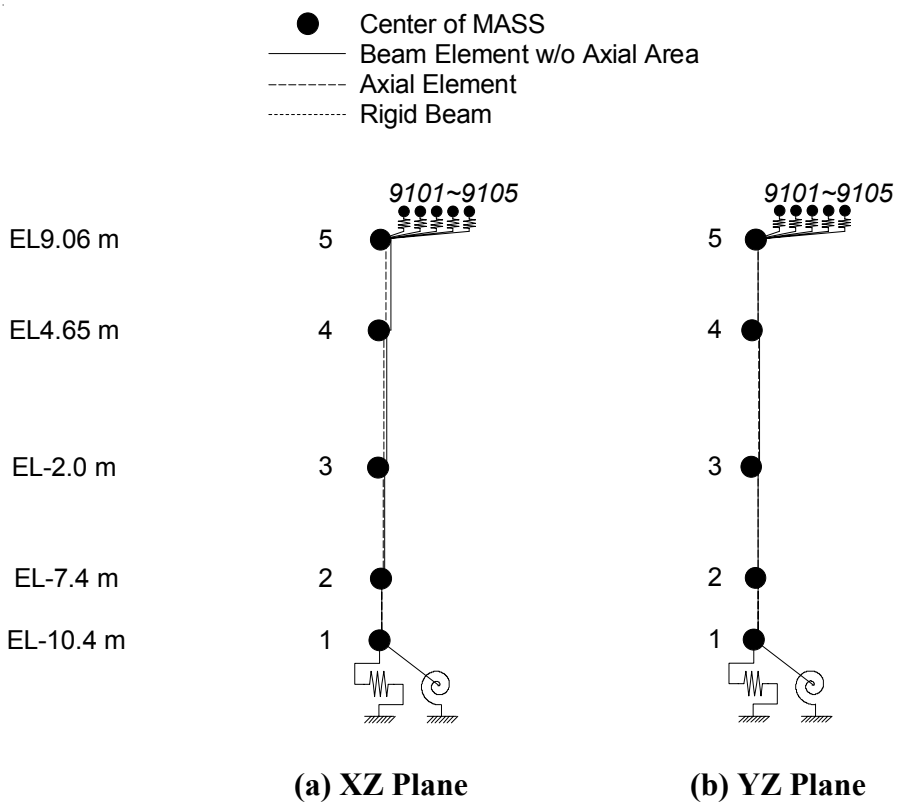

(a) XZ Plane **(b) YZ Plane**

Figure 3A.7-5. ESBWR Control Building Seismic Model

3A.8 ANALYSIS RESULTS

In this section, typical SSI results are presented to show the effect of different soil properties on seismic responses at selected locations in terms of acceleration response spectra and seismic forces. The site-envelope seismic responses are presented in Section 3A.9.

For comparison study, the acceleration response spectra at 5% damping are shown for the following locations:

Location	Node Number
RBFB Refueling Floor	109
RCCV Top Slab	208
Vent Wall Top	701
RSW Top	707
RPV Top	801
RBFB Basemat	2
CB Top	5

The seismic forces are presented at the following locations:

Location	Connecting Nodes
RPV Support	815 – 711
RSW Base	710 – 711
Vent Wall Base	704 – 705
Pedestal Base	301 – 2
RCCV Base	201 – 2
RBFB Base	101 – 2
CB Base	3 –2

The horizontal responses in X-direction are shown in Figures 3A.8-1a through 3A.8-1g. The responses in Y-direction are shown in Figures 3A.8-2a through 3A.8-2g. The vertical responses (Z-direction) are shown in Figure 3A.8-3a through 3A.8-3g. The results of the North Anna cases are the envelopes of the three soil conditions, Best-estimate (BE), Upper-bound (UB), and Lower-bound (LB). Generic site responses are higher at frequencies below 10 Hz, whereas North Anna responses are generally more dominant in the higher frequency range above 10 Hz.

The results in terms of seismic forces are compared in Tables 3A.8-1 and 3A.8-2, respectively for X direction and Y direction. As shown in these tables, the results of generic medium or stiffer sites govern the seismic responses of the RBFB complex structure, except for relatively stiff structures such as the RPV support for which the moment response is controlled by the

North Anna site, due to the high-frequency content in its input ground motion. The results of generic hard rock or North Anna sites govern the seismic responses of the CB structure. The results of all soil cases shown are used to obtain the enveloping results (Section 3A.9).

Table 3A.8-1

Maximum Forces - X Direction

Locations	Response Types	Soil Stiffness				
		SOFT	MEDIUM	HARD	FIX	North Anna
RPV Support	Shear Moment	5 24	13 59	15 89	13 85	9 115
RSW Base	Shear Moment	5 50	12 133	14 164	15 176	10 137
Vent Wall Base	Shear Moment	8 57	16 123	17 134	17 143	11 84
Pedestal Base	Shear Moment	47 711	101 1570	94 1472	91 1467	38 578
RCCV Base	Shear Moment	115 5277	252 10846	235 10611	226 9973	94 3888
RBFB Base	Shear Moment	413 18084	910 32284	848 33902	818 28822	339 10385
CB Base	Shear Moment	62 892	71 1078	70 979	60 842	80 1434

Units: Shear Forces in MN; Moment in MN-m

Table 3A.8-2

Maximum Forces - Y Direction

Locations	Response Types	Soil Stiffness				
		SOFT	MEDIUM	HARD	FIX	North Anna
RPV Support	Shear Moment	6 30	12 54	11 68	11 63	11 106
RSW Base	Shear Moment	6 66	11 122	11 127	10 117	10 123
Vent Wall Base	Shear Moment	10 78	21 166	17 145	16 128	12 77
Pedestal Base	Shear Moment	55 898	122 1970	97 1617	88 1452	40 560
RCCV Base	Shear Moment	137 6909	304 14269	244 11886	221 10895	97 4183
RBFB Base	Shear Moment	475 17620	1032 35490	804 28694	707 25752	342 8776
CB Base	Shear Moment	65 922	70 1003	73 1036	62 832	71 989

Units: Shear Forces in MN; Moment in MN-m

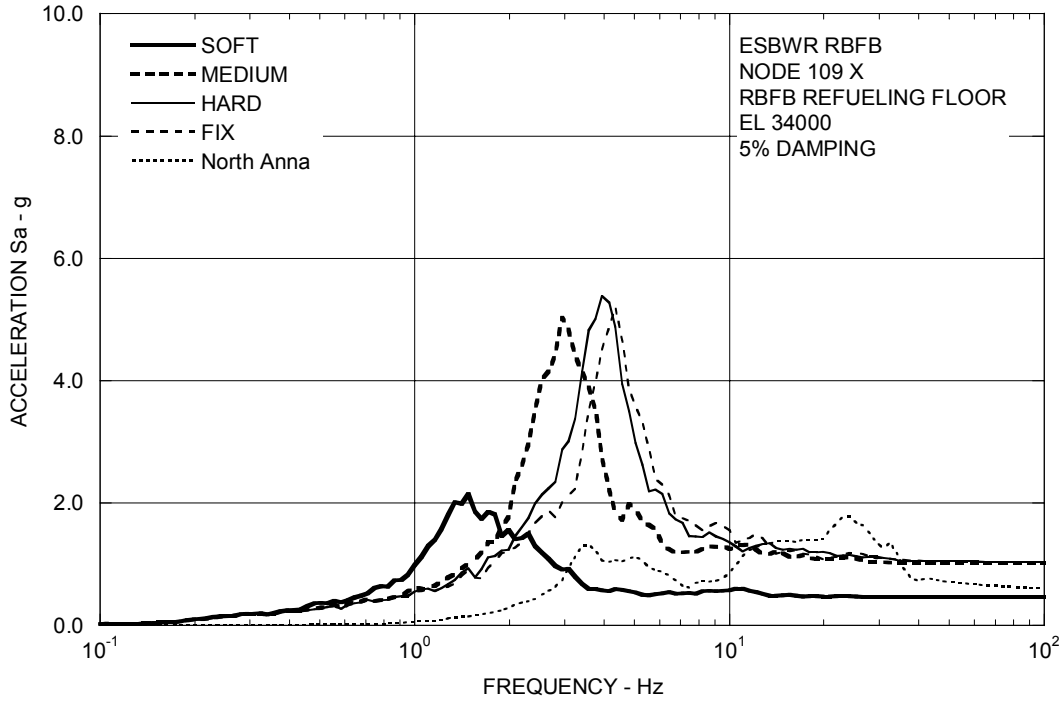

Figure 3A.8-1a. Floor Response Spectra – RBFB Refueling Floor X

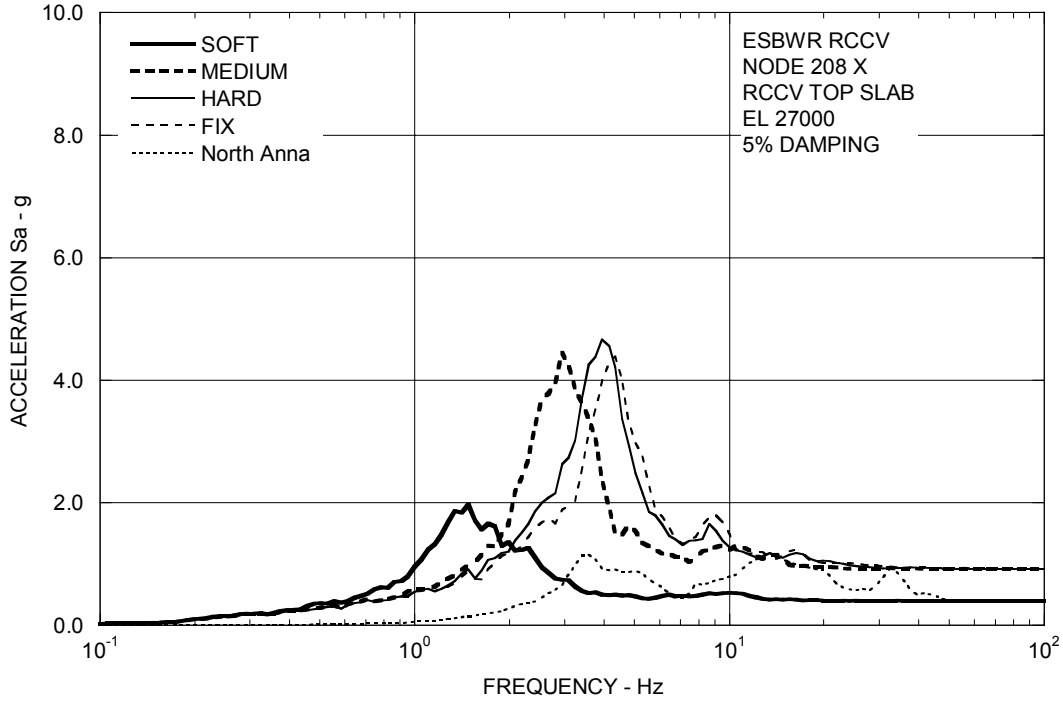

Figure 3A.8-1b. Floor Response Spectra – RCCV Top Slab X

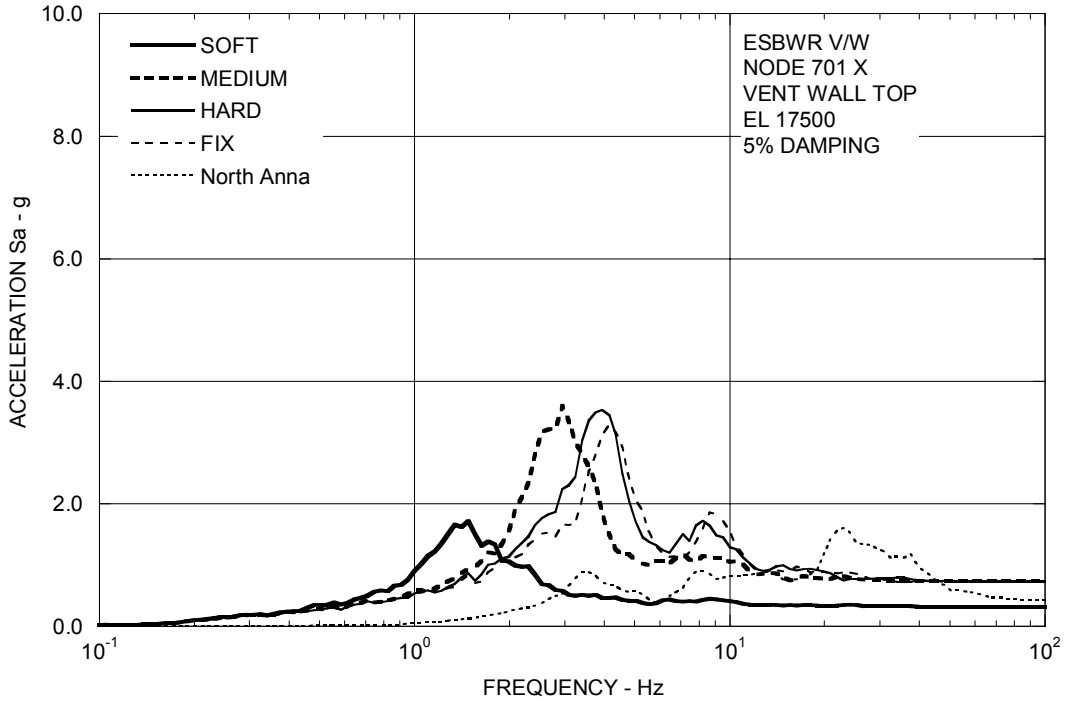

Figure 3A.8-1c. Floor Response Spectra – Vent Wall Top X

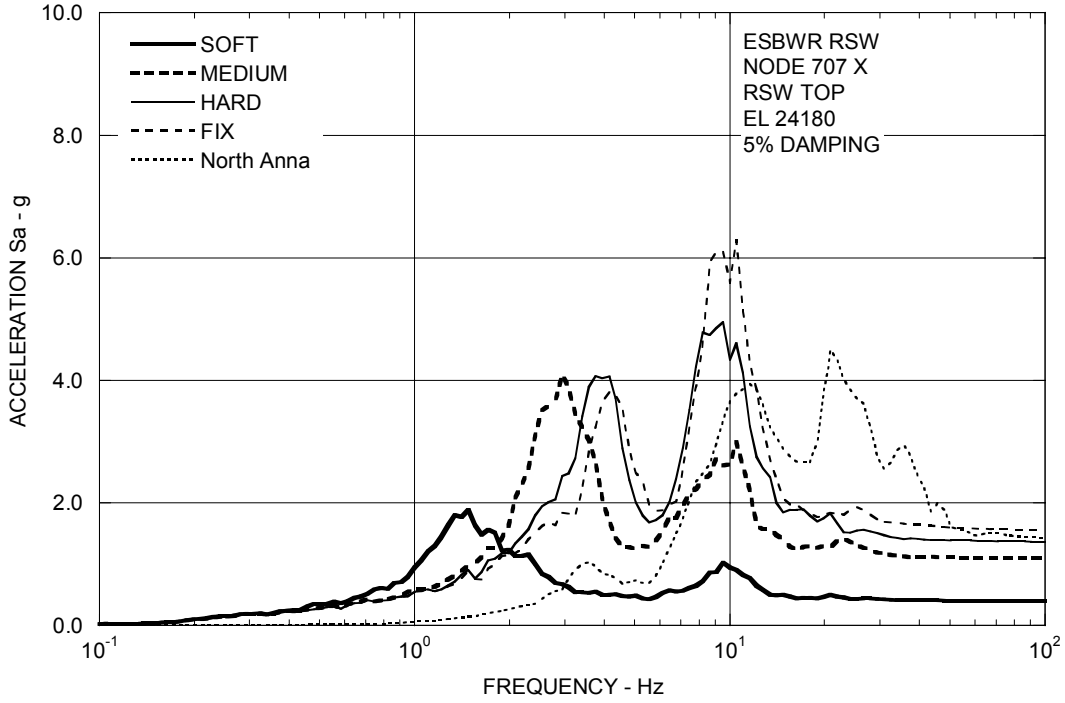

Figure 3A.8-1d. Floor Response Spectra – RSW Top X

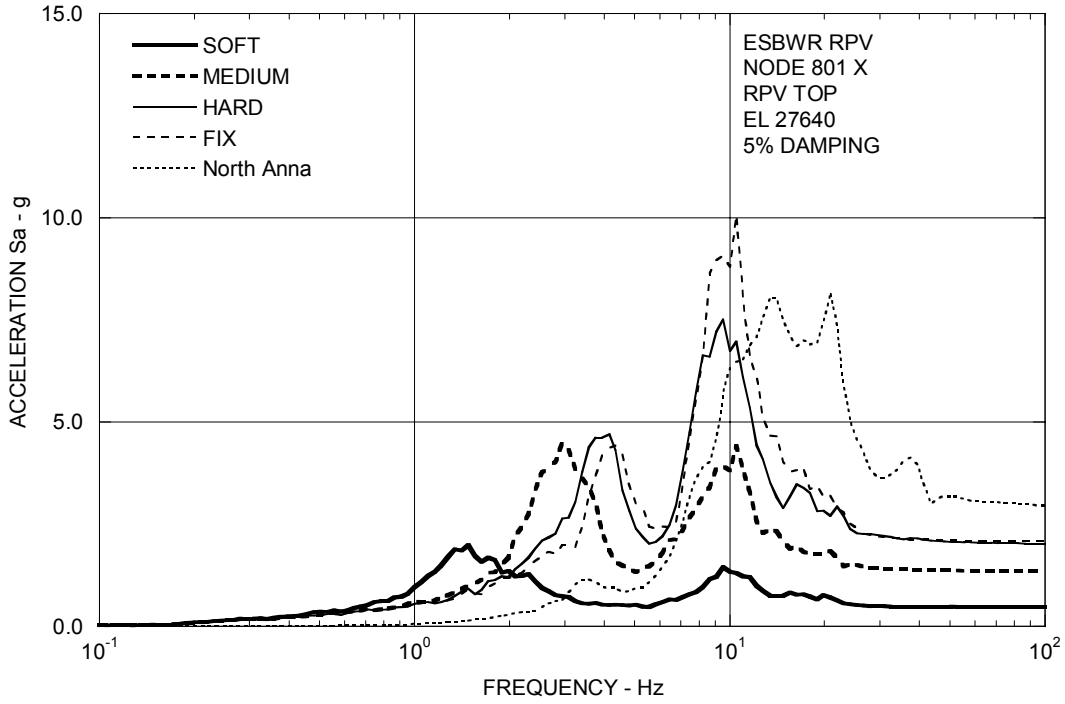

Figure 3A.8-1e. Floor Response Spectra – RPV Top X

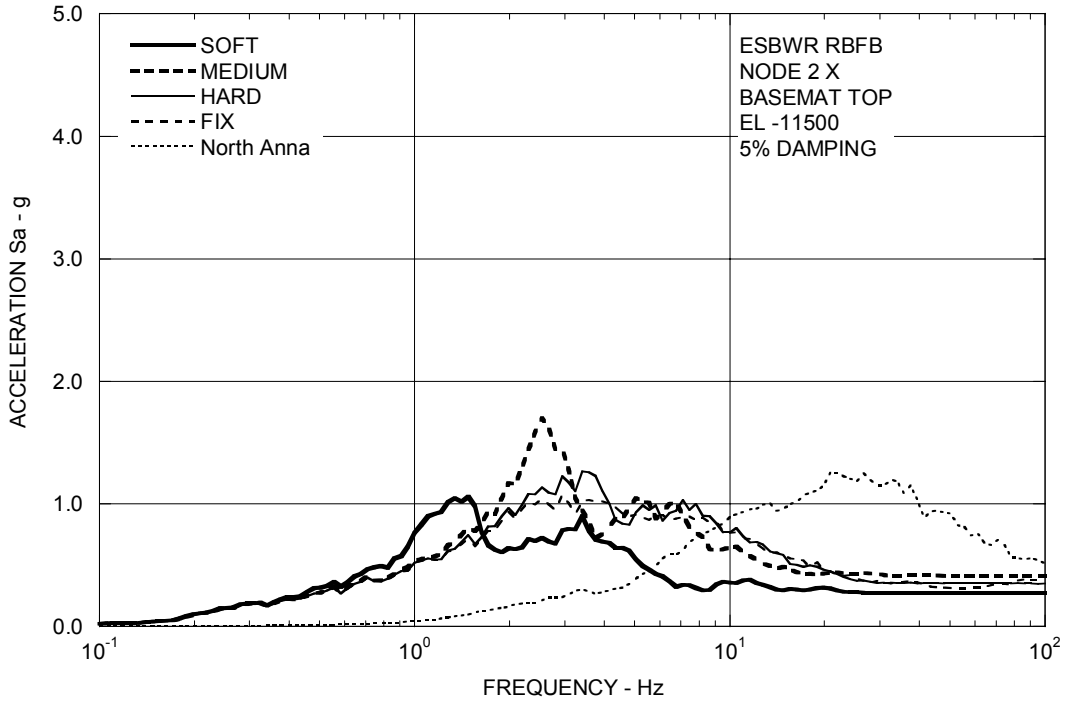

Figure 3A.8-1f. Floor Response Spectra – RBFB Basemat X

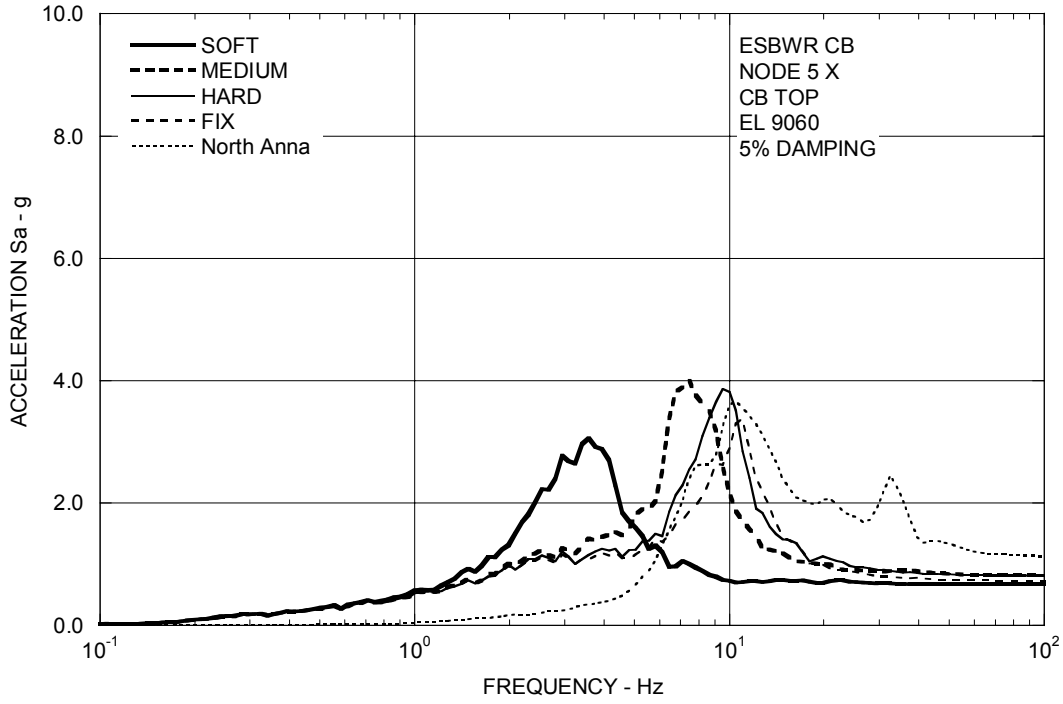

Figure 3A.8-1g. Floor Response Spectra – CB Top X

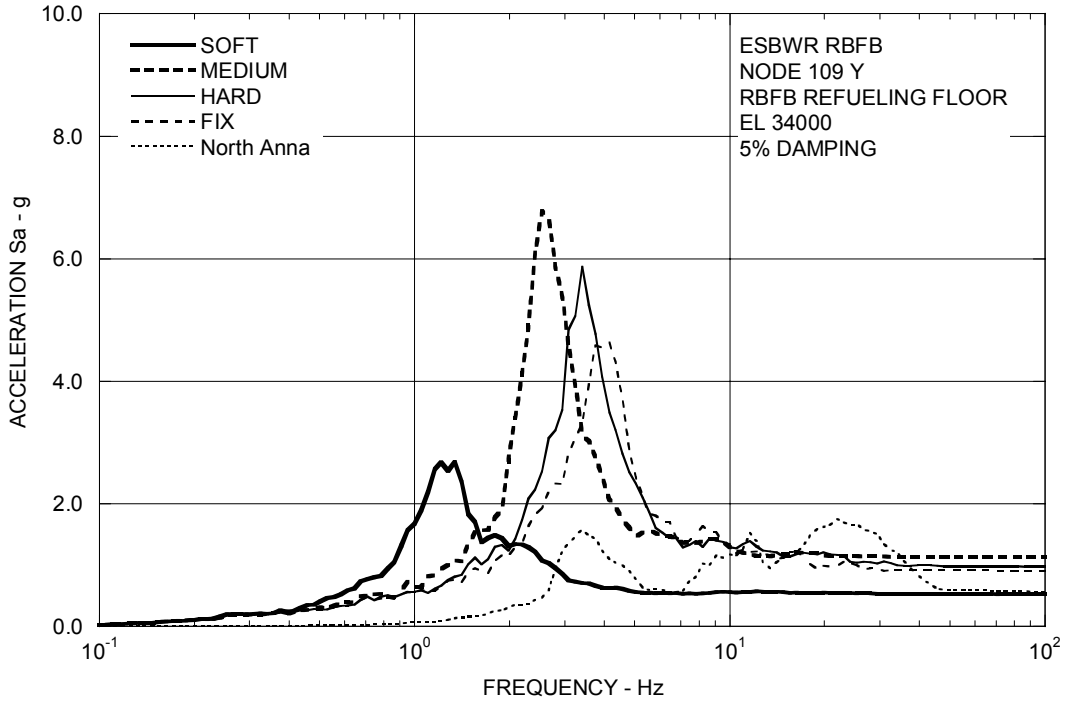

Figure 3A.8-2a. Floor Response Spectra – RBFB Refueling Floor Y

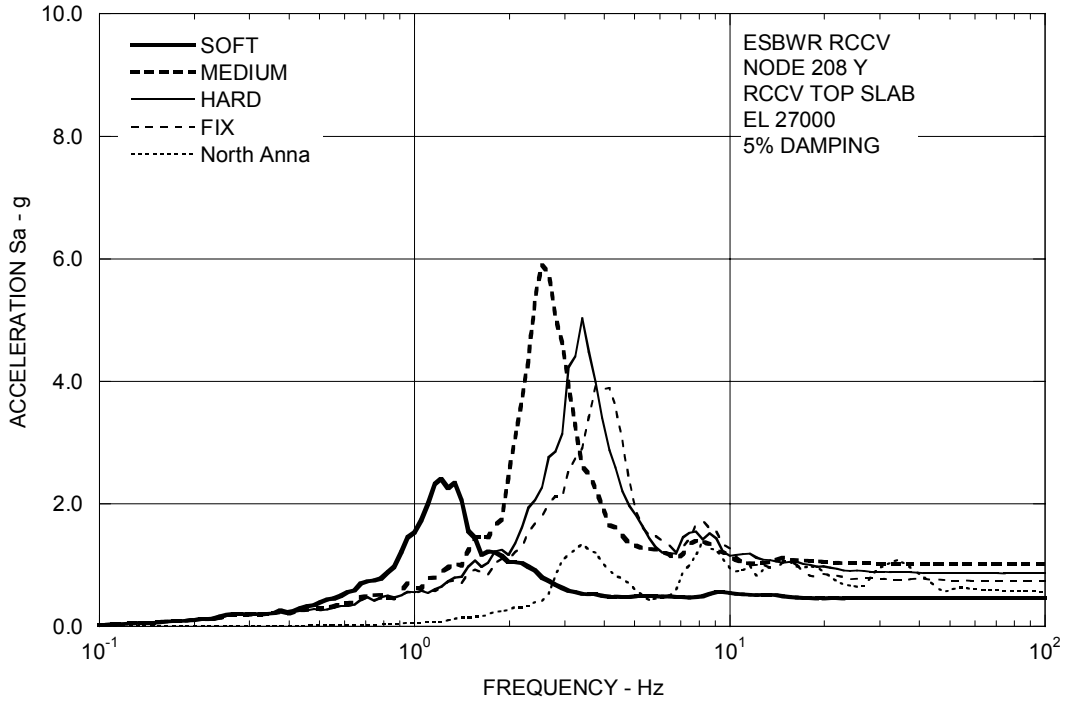

Figure 3A.8-2b. Floor Response Spectra – RCCV Top Slab Y

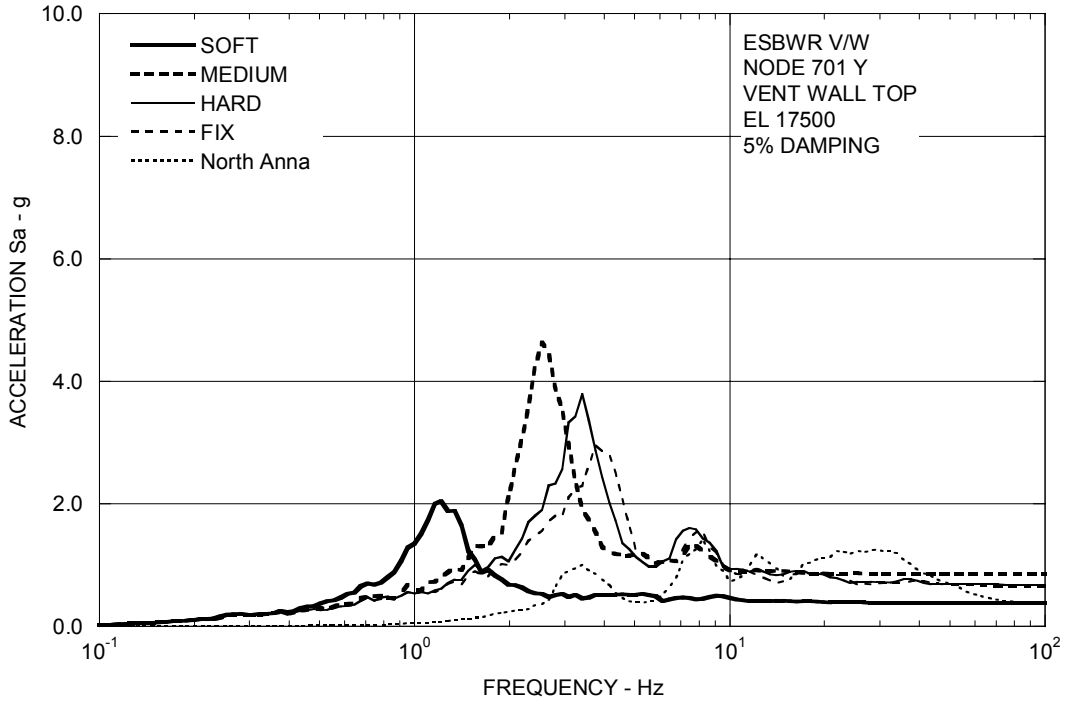

Figure 3A.8-2c. Floor Response Spectra – Vent Wall Top Y

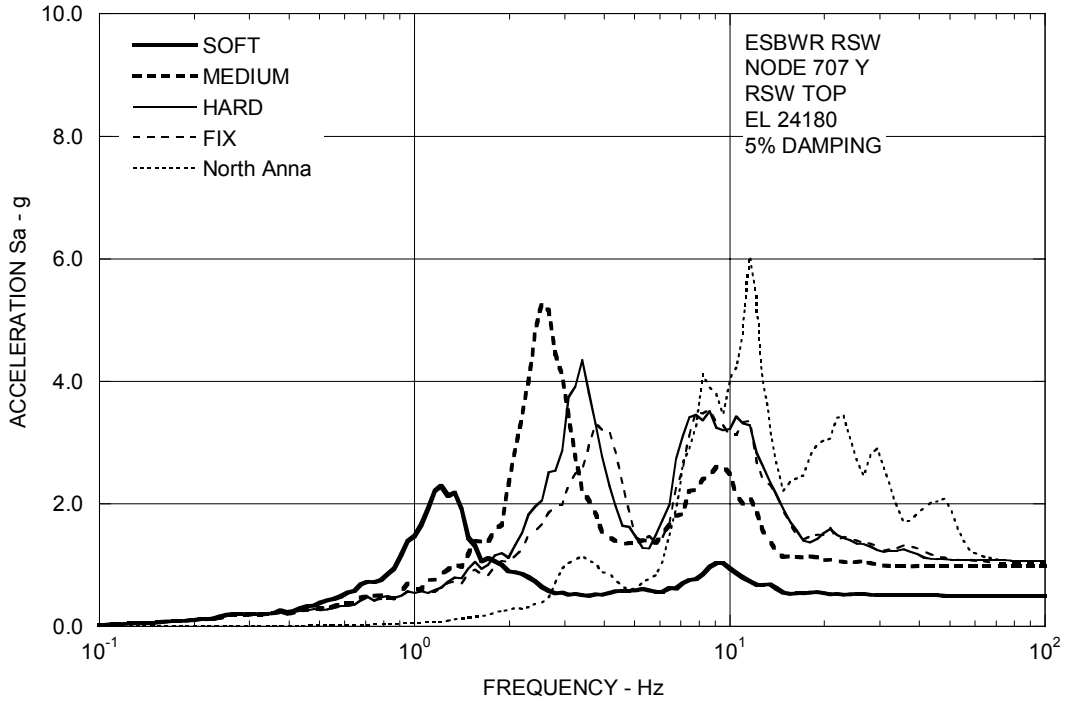

Figure 3A.8-2d. Floor Response Spectra – RSW Top Y

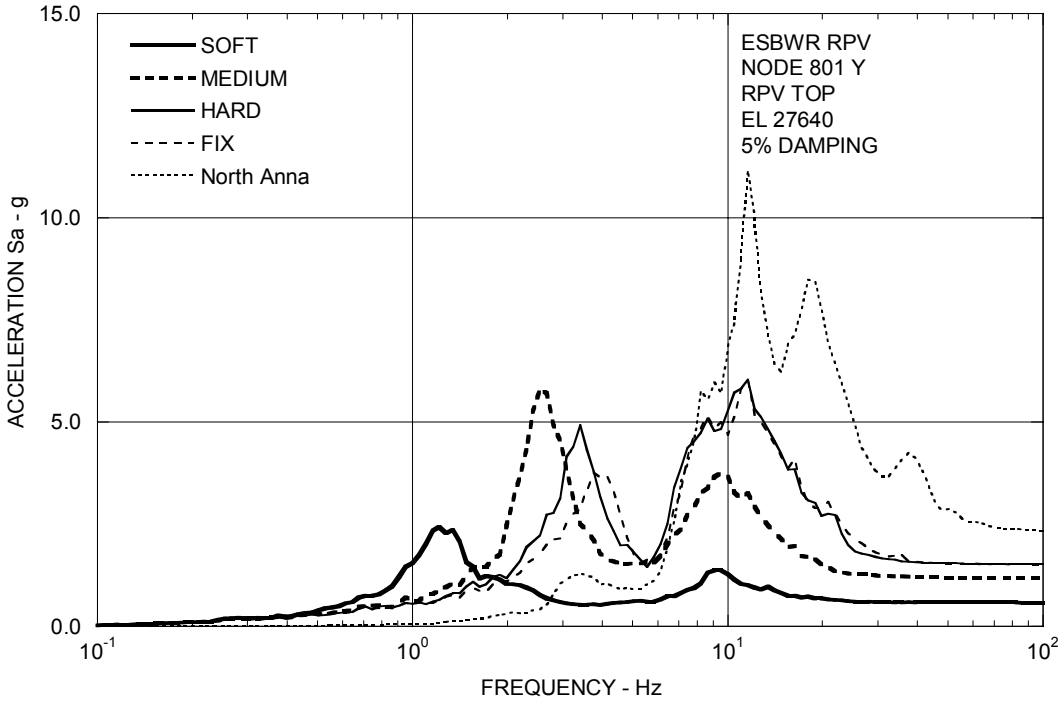

Figure 3A.8-2e. Floor Response Spectra – RPV Top Y

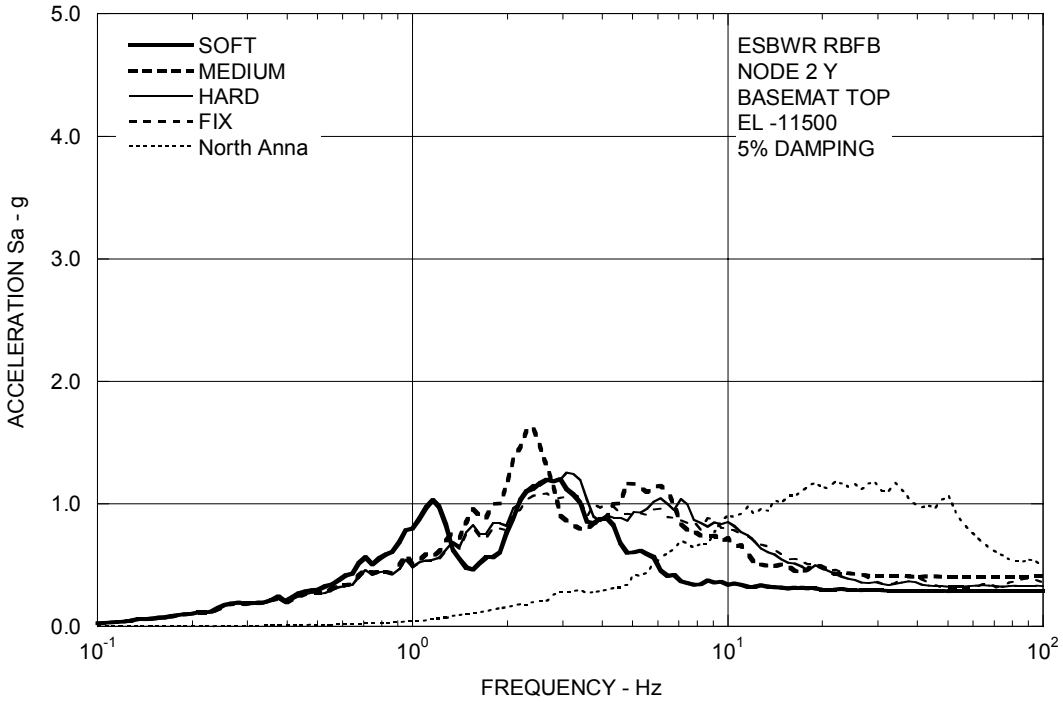

Figure 3A.8-2f. Floor Response Spectra – RBFB Basemat Y

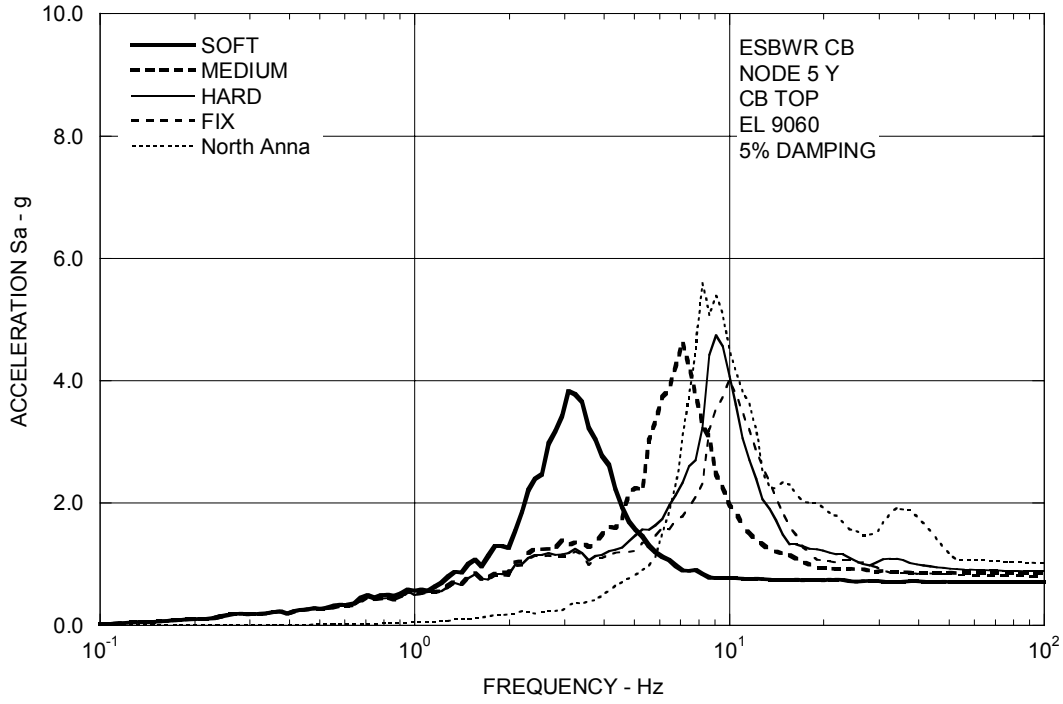

Figure 3A.8-2g. Floor Response Spectra – CB Top Y

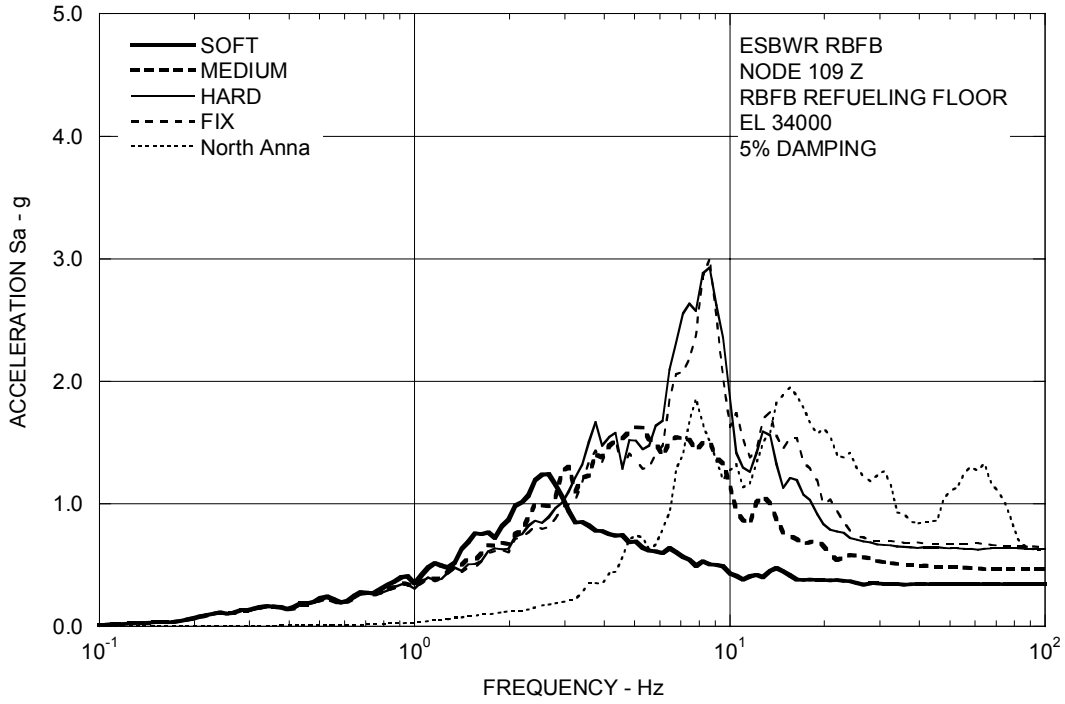

Figure 3A.8-3a. Floor Response Spectra – RBFB Refueling Floor Z

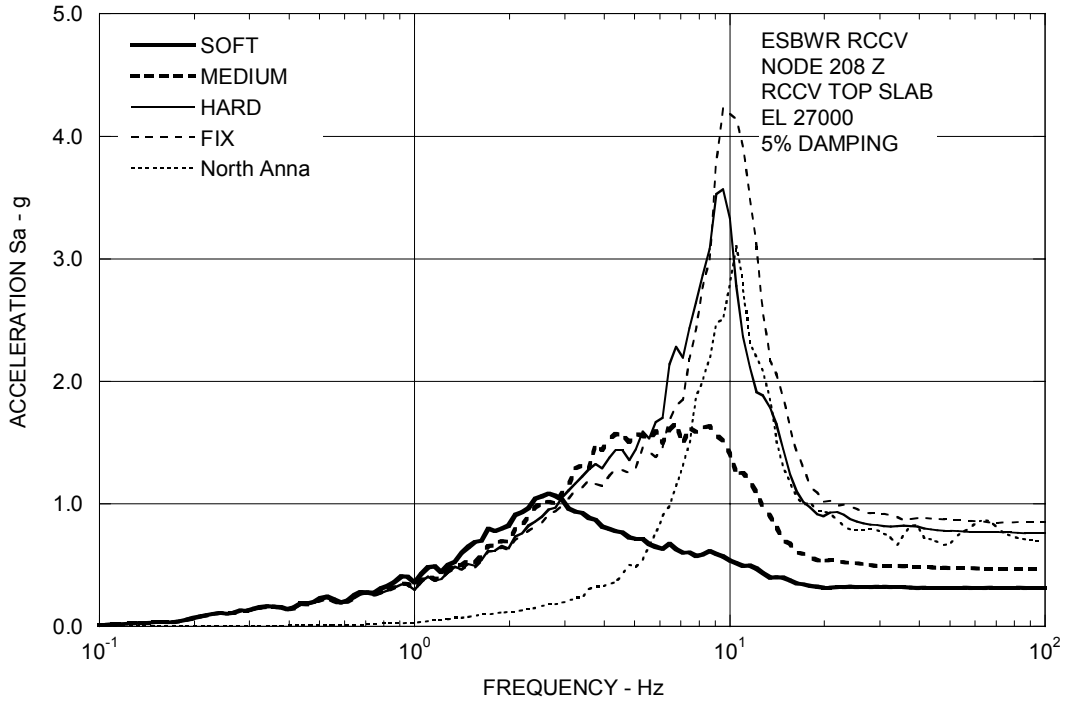

Figure 3A.8-3b. Floor Response Spectra – RCCV Top Slab Z

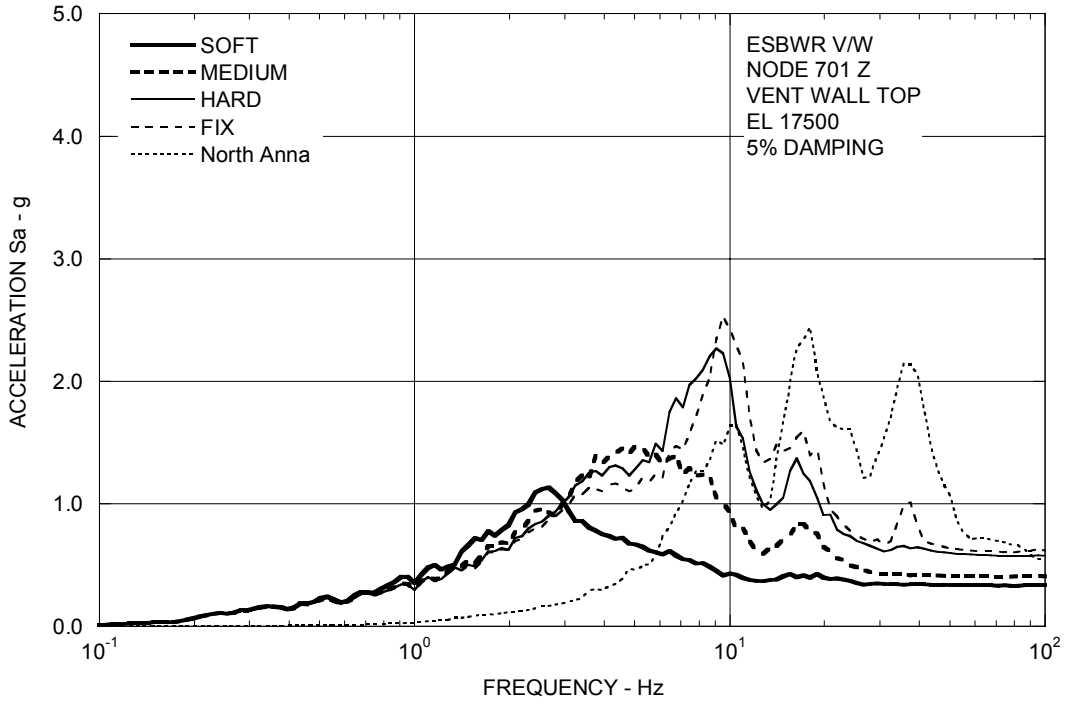

Figure 3A.8-3c. Floor Response Spectra – Vent Wall Top Z

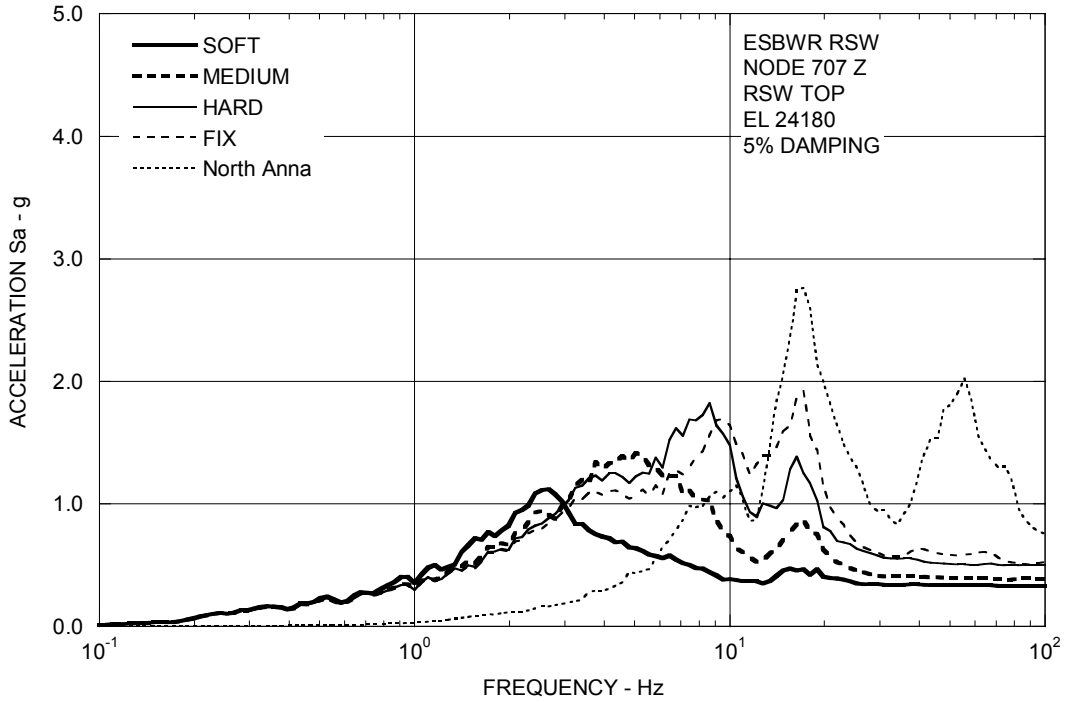

Figure 3A.8-3d. Floor Response Spectra – RSW Top Z

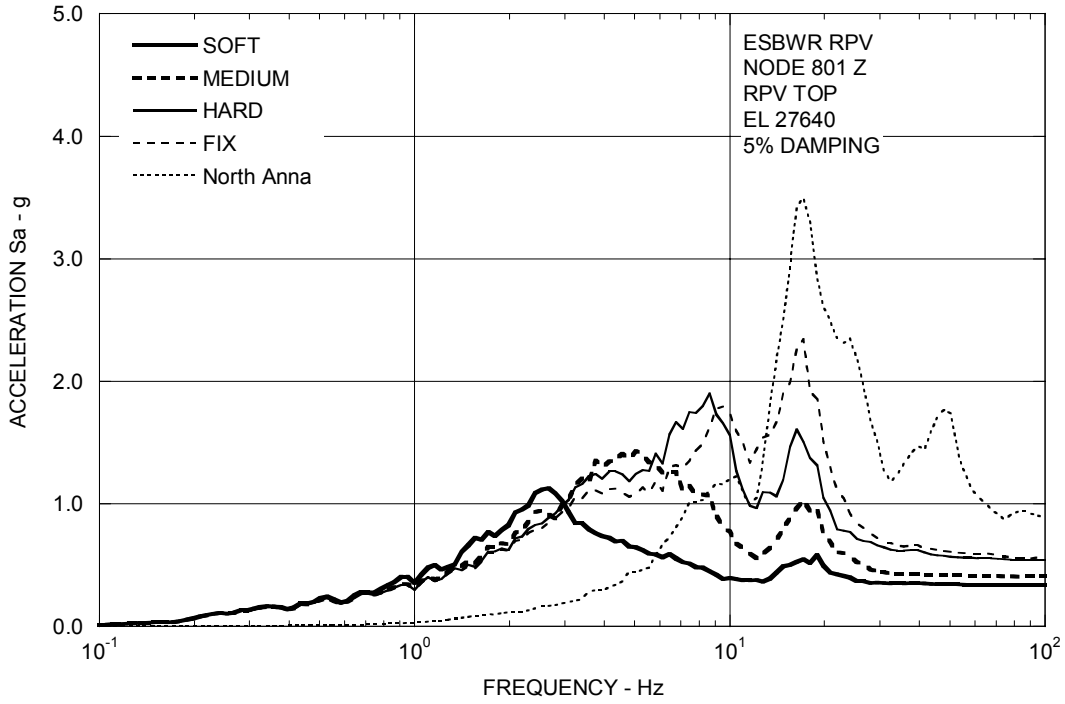

Figure 3A.8-3e. Floor Response Spectra – RPV Top Z

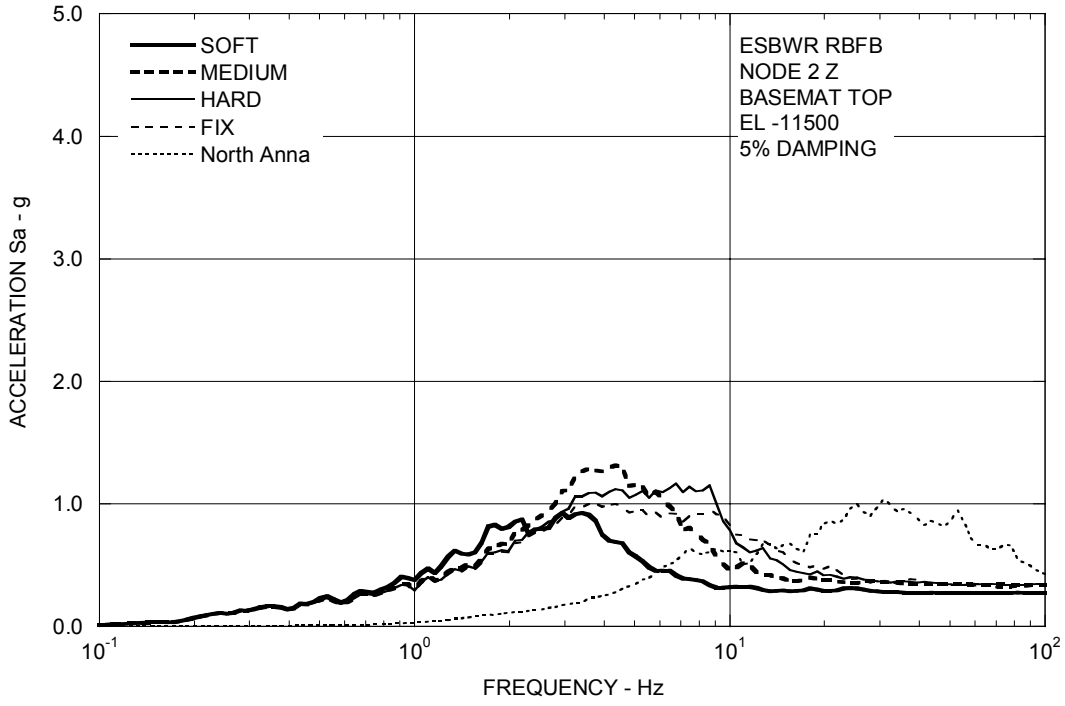

Figure 3A.8-3f. Floor Response Spectra – RBFB Basemat Z

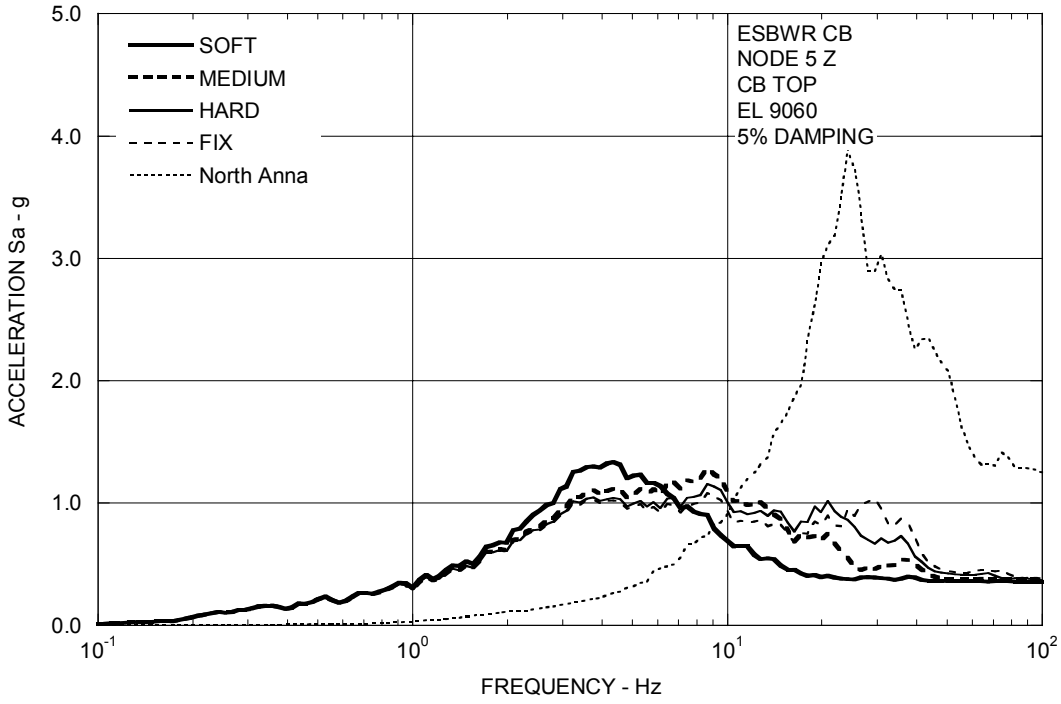

Figure 3A.8-3g. Floor Response Spectra – CB Top Z

3A.9 SITE ENVELOPE SEISMIC RESPONSES

The site-envelope seismic loads are established from the envelopes of all analysis results from SSI cases summarized in Table 3A.6-1. The site-envelope seismic loads obtained are applicable for the design of Seismic Category I (C-I) and II (C-II) structures, systems and components housed in the ESBWR standard plant.

3A.9.1 Enveloping Maximum Structural Loads

The enveloping maximum shear and moment distributions along the RBFB walls, RCCV, vent wall/pedestal, RSW, key RPV/internals, and the CB walls are shown in Tables 3A.9-1 through 3A.9-6. These shears and moments are the envelope of all SSI cases. The torsional moments for building structures are due to geometric eccentricities only. Additional torsion due to an accidental eccentricity of 5% of maximum floor dimension under consideration is added for the design of building structures.

The vertical loads are expressed in terms of enveloping absolute acceleration. The enveloping maximum acceleration values are shown in Tables 3A.9-7 through 3A.9-12. These acceleration values do not include the coupling effect and are only applicable for structural analysis in combination with the seismic loads due to horizontal shakings.

3A.9.2 Enveloping Floor Response Spectra

The site-envelope SSE floor response spectra are obtained according to the following steps:

- For each soil case analyzed, the calculated co-directional floor response spectra in X, Y, and Z directions are combined by the SRSS method to obtain floor response spectra at the building edges considering the coupling effects between vertical and rocking and between lateral and torsion motions.
- Individual site responses are enveloped to form the site-envelope response spectra in each of the 3 directions.
- The reduction factors due to wave incoherence according to ASCE 4-98 are applied to the site-envelope response spectra.
- The envelope spectra are subsequently peak broadened by ±15%.

The site-envelope peak-broadened SSE floor response spectra at critical damping ratios 2, 3, 4, 5, 7, 10, and 20% for the RBFB and CB are shown in Figures 3A.9-1a through 3A.9-1g for the X direction, in Figures 3A.9-2a through 3A.9-2g for the Y direction, and in Figures 3A.9-3a through 3A.9-3g for the vertical direction. For seismic design of equipment and piping, the alternative seismic input can be the individual floor response spectra of each site condition considered in generating the site-envelope spectra.

Table 3A.9-1

Enveloping Seismic Loads: RBFB Stick

EL (m)	Node No.	Elem No.	Shear		Moment		Torsion (MN-m)
			X-Dir. (MN)	Y-Dir. (MN)	X-Dir. (MN-m)	Y-Dir. (MN-m)	
52.40	110				1559	1324	
		1110	147.3	156.8	4151	4080	1091
34.00	109				5686	5404	
		1109	174.9	149.1	6570	6395	1703
27.00	108				8686	7449	
		1108	421.4	401.6	10003	9117	3091
22.50	107				11219	9713	
		1107	477.5	464.7	12847	11807	6081
17.50	106				12866	12396	
		1106	526.5	556.3	14720	14328	5056
13.57	105				15181	14808	
		1105	562.8	601.1	17485	17172	5233
9.06	104				17878	17623	
		1104	603.5	655.7	20280	20104	5959
4.65	103				20908	20722	
		1103	828.9	873.9	24958	24782	11484
-1.00	102				25419	25448	
		1102	860.6	940.2	29381	29508	11582
-6.40	101				29734	30234	
		1101	910.3	1031.7	33902	35490	11660
-11.50	2				45523	52731	
-15.50	1	1021	1355.3	1571.0	50426	59007	11366

Note: Total torsional moments are obtained by the absolute sum of the accidental torsional moments and the values of the geometric torsional moments shown. The accidental torsional moment is the product of the horizontal force component and an eccentricity of 5% of the larger horizontal dimension at various elevations.

Table 3A.9-2

Enveloping Seismic Loads: RCCV Stick

EL (m)	Node No.	Elem No.	Shear		Moment		Torsion (MN-m)
			X-Dir. (MN)	Y-Dir. (MN)	X-Dir. (MN-m)	Y-Dir. (MN-m)	
34.00	209				129	380	
		1209	137.7	188.1	1048	1533	25
27.00	208				1638	2143	
		1208	168.4	247.1	3166	4443	1815
17.50	206				3506	4793	
		1206	230.5	291.6	4354	5845	1976
13.57	205				4532	6033	
		1205	261.8	327.3	5618	7353	2181
9.06	204				5841	7610	
		1204	299.7	366.9	7012	9005	2605
4.65	203				7215	9268	
		1203	210.6	290.1	8195	10640	2885
-1.00	202				8315	10797	
		1202	257.3	331.4	9453	12582	2940
-6.40	201				9560	12719	
-11.50	2	1201	252.2	304.2	10846	14269	1958

Note: Total torsional moments are obtained by the absolute sum of the accidental torsional moments and the values of the geometric torsional moments shown. The accidental torsional moment is the product of the horizontal force component and an eccentricity of 5% of the larger horizontal dimension at various elevations.

Table 3A.9-3

Enveloping Seismic Loads: VW/Pedestal Stick

EL (m)	Node No.	Elem No.	Shear		Moment		Torsion (MN-m)
			X-Dir. (MN)	Y-Dir. (MN)	X-Dir. (MN-m)	Y-Dir. (MN-m)	
17.50	701				63	50	
		701	12.1	12.3	64	49	31
14.50	702				82	61	
		702	14.0	14.3	85	87	32
11.50	703				88	90	
		703	15.5	17.8	127	143	34
8.50	704				126	145	
		704	16.6	20.6	143	166	34
7.4625	705				179	166	
		705	12.5	13.8	212	205	17
4.65	706				454	422	
	303	1303	28.7	45.0	493	522	142
2.4165	377				605	645	
		1377	42.8	66.5	697	872	173
-1.00	302				725	894	
		1302	61.2	81.6	820	1037	147
-2.75	376				820	1037	
		1376	61.4	81.9	1043	1335	147
-6.40	301				1056	1350	
-11.50	2	1301	100.8	121.5	1570	1970	117

Note: Total torsional moments are obtained by the absolute sum of the accidental torsional moments and the values of the geometric torsional moments shown. The accidental torsional moment is the product of the horizontal force component and an eccentricity of 5% of the larger horizontal dimension at various elevations.

Table 3A.9-4

Enveloping Seismic Loads: RSW Stick

EL (m)	Node No.	Elem No.	Shear		Moment		Torsion (MN-m)
			X-Dir. (MN)	Y-Dir. (MN)	X-Dir. (MN-m)	Y-Dir. (MN-m)	
24.18	707				1.2	1.2	
		707	1.8	1.2	7.8	5.5	0.2
20.20	708				11.3	9.3	
		708	10.7	8.4	57.8	44.5	0.8
15.775	709				59.8	46.5	
		709	12.9	9.3	116.7	86.0	1.1
11.35	710				117.2	86.4	
		710	15.1	11.1	175.8	126.6	1.2
7.4625	711				164.4	149.1	
		711	32.2	35.7	251.0	247.8	18.2
4.65	712				95.2	81.7	
		712	12.5	19.5	112.1	124.9	30.4
2.4165	713				2.5	2.0	
		713	0.9	1.0	2.1	1.7	0.1
1.96	714				1.8	1.5	
-0.80	715	714	0.5	0.6	0.4	0.3	0.1

Note: Total torsional moments are obtained by the absolute sum of the accidental torsional moments and the values of the geometric torsional moments shown. The accidental torsional moment is the product of the horizontal force component and an eccentricity of 5% of the larger horizontal dimension at various elevations.

Table 3A.9-5

Enveloping Seismic Loads: RPV Stick

Components	Node No.	Elem No.	Axial (MN)	Shear		Moment	
				X-Dir. (MN)	Y-Dir. (MN)	X-Dir. (MN-m)	Y-Dir. (MN-m)
Shroud	845					11.5	10.7
Bottom	846	844	4.4	5.0	3.4	14.9	12.4
RPV	815					114.9	105.3
Support	711	871	16.5	14.5	12.2	113.6	105.5

Table 3A.9-6

Enveloping Seismic Loads: CB Stick

EL (m)	Node No.	Elem No.	Shear		Moment		Torsion (MN-m)
			X-Dir. (MN)	Y-Dir. (MN)	X-Dir. (MN-m)	Y-Dir. (MN-m)	
9.06	5				174	145	
		5	42.8	35.4	300	232	27.0
4.65	4				446	355	
		4	69.6	57.8	900	616	40.5
-2.00	3				1001	642	
		3	80.1	73.2	1434	1036	38.2
-7.40	2				1476	1048	
-10.40	1	2	82.8	85.6	1697	1305	34.1

Note: Total torsional moments are obtained by the absolute sum of the accidental torsional moments and the values of the geometric torsional moments shown. The accidental torsional moment is the product of the horizontal force component and an eccentricity of 5% of the larger horizontal dimension at various elevations.

Table 3A.9-7

Enveloping Maximum Vertical Acceleration: RBFB

EL (m)	Node No.	Stick Model	Max. Vertical Acceleration (g)
52.40	110	RBFB	0.76
34.00	109	RBFB	0.65
27.00	108	RBFB	0.61
22.50	107	RBFB	0.50
17.50	106	RBFB	0.51
13.57	105	RBFB	0.50
9.06	104	RBFB	0.47
4.65	103	RBFB	0.44
-1.00	102	RBFB	0.43
-6.40	101	RBFB	0.41
-11.50	2	RBFB	0.38
-15.50	1	RBFB	0.34

Note:For structural design use only.

Table 3A.9-8

Enveloping Maximum Vertical Acceleration: RCCV

EL (m)	Node No.	Stick Model	Max. Vertical Acceleration (g)
34.00	209	RCCV	0.84
27.00	208	RCCV	0.84
17.50	206	RCCV	0.71
13.57	205	RCCV	0.66
9.06	204	RCCV	0.57
4.65	203	RCCV	0.52
-1.00	202	RCCV	0.44
-6.40	201	RCCV	0.38

Note: For structural design use only.

Table 3A.9-9

Enveloping Maximum Vertical Acceleration: VW/Pedestal

EL (m)	Node No.	Stick Model	Max. Vertical Acceleration (g)
17.50	701	VW	0.59
14.50	702	VW	0.57
11.50	703	VW	0.53
8.50	704	VW	0.49
7.4625	705	VW	0.50
4.65	706, 303	Pedestal	0.47
2.42	377	Pedestal	0.44
-1.00	302	Pedestal	0.46
-2.75	376	Pedestal	0.43
-6.40	301	Pedestal	0.43

Note:For structural design use only.

Table 3A.9-10

Enveloping Maximum Vertical Acceleration: RSW

EL (m)	Node No.	Stick Model	Max. Vertical Acceleration (g)
24.18	707	RSW	0.67
20.20	708	RSW	0.65
15.775	709	RSW	0.61
11.35	710	RSW	0.56
7.4625	711	RSW	0.50
4.65	712	RSW	0.47
2.4615	713	RSW	0.44
1.96	714	RSW	0.44
-0.80	715	RSW	0.45

Note:For structural design use only.

Table 3A.9-11

Enveloping Maximum Vertical Acceleration: RBFB Flexible Slab Oscillators

EL (m)	Node No.	Stick Model	Max. Vertical Acceleration (g)
52.40	9101	Oscillator	1.20
	9102	Oscillator	1.83
	9103	Oscillator	1.63
	9104	Oscillator	1.72
	9105	Oscillator	1.69
	9106	Oscillator	1.88
27.00	9081	Oscillator	0.94
22.50	9071	Oscillator	1.57
	9072	Oscillator	1.26
	9073	Oscillator	1.39
	9074	Oscillator	0.97
	9075	Oscillator	0.76
17.50	9061	Oscillator	1.08
	9062	Oscillator	0.92
	9063	Oscillator	0.59
	9064	Oscillator	1.17
13.57	9051	Oscillator	0.55
9.06	9041	Oscillator	0.52
4.65	9031	Oscillator	0.87
	9032	Oscillator	0.54
	9033	Oscillator	0.52
-1.00	9021	Oscillator	0.73
	9022	Oscillator	1.05
	9023	Oscillator	0.67
	9024	Oscillator	0.53
-6.40	9011	Oscillator	0.57
	9012	Oscillator	0.66

Note:For structural design use only.

Table 3A.9-12

Enveloping Maximum Acceleration: CB

EL (m)	Node No.	Stick Model	Max. Vertical Acceleration (g)
9.06	5	CB	1.11
4.65	4	CB	0.92
-2.00	3	CB	0.62
-7.40	2	CB	0.47
-10.40	1	CB	0.47
9.06	9101	Oscillator	1.01
	9102	Oscillator	1.51
	9103	Oscillator	2.89
	9104	Oscillator	2.93
	9105	Oscillator	2.62

Note:For structural design use only.

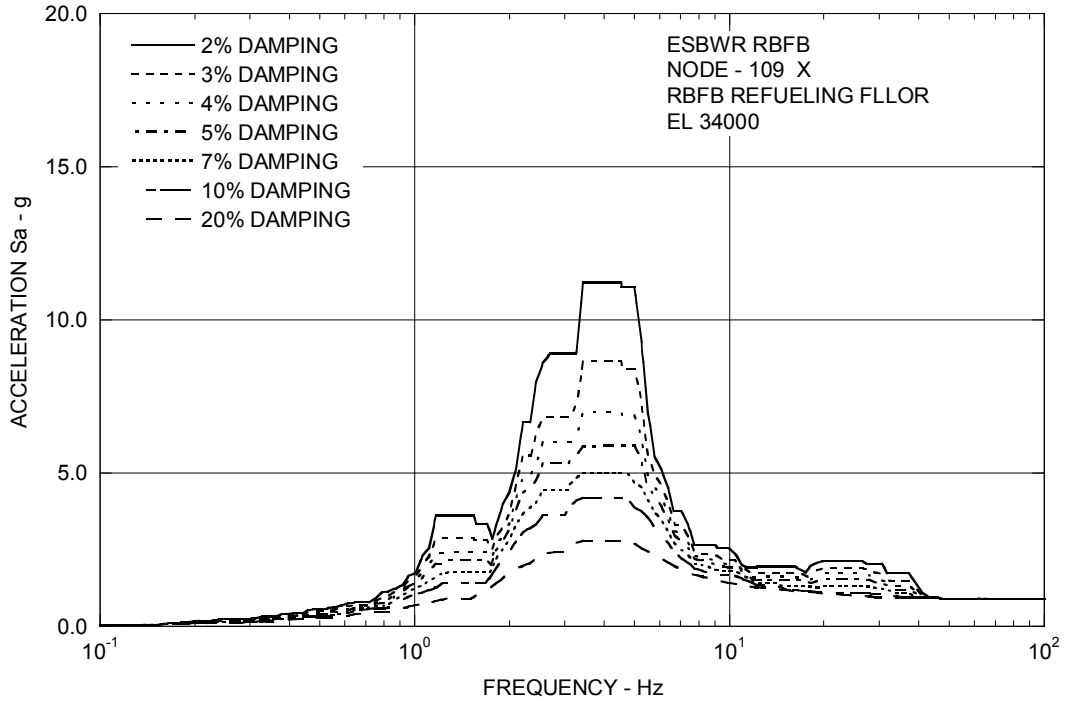

Figure 3A.9-1a. Enveloping Floor Response Spectra – RBFB Refueling Floor X

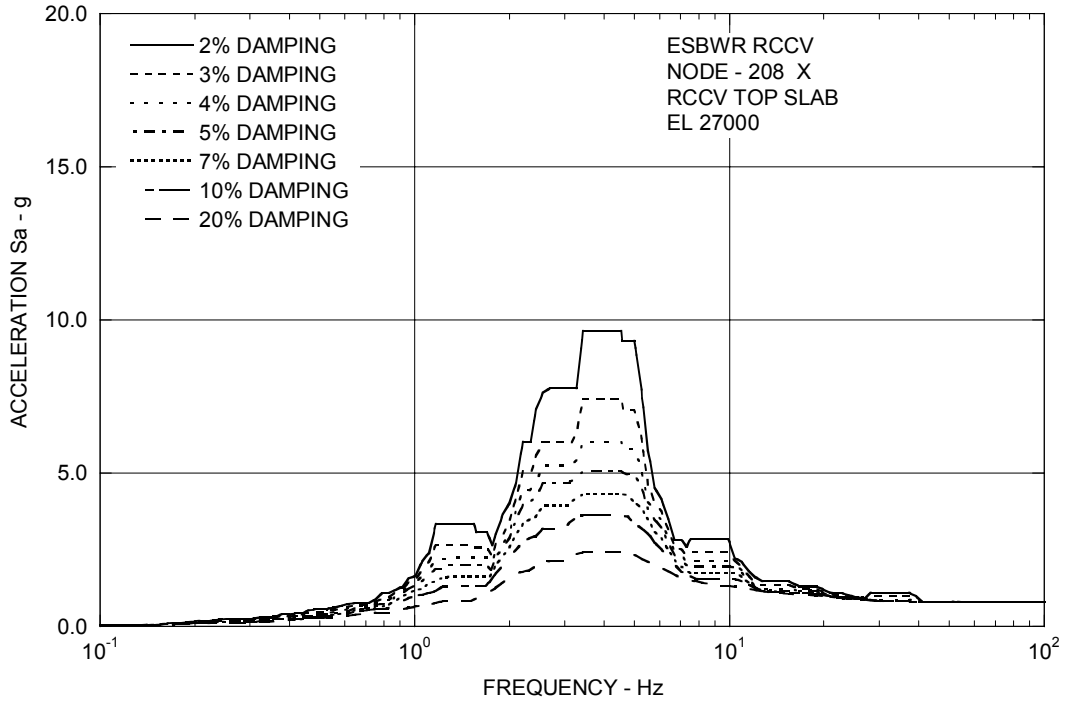

Figure 3A.9-1b. Enveloping Floor Response Spectra – RCCV Top Slab X

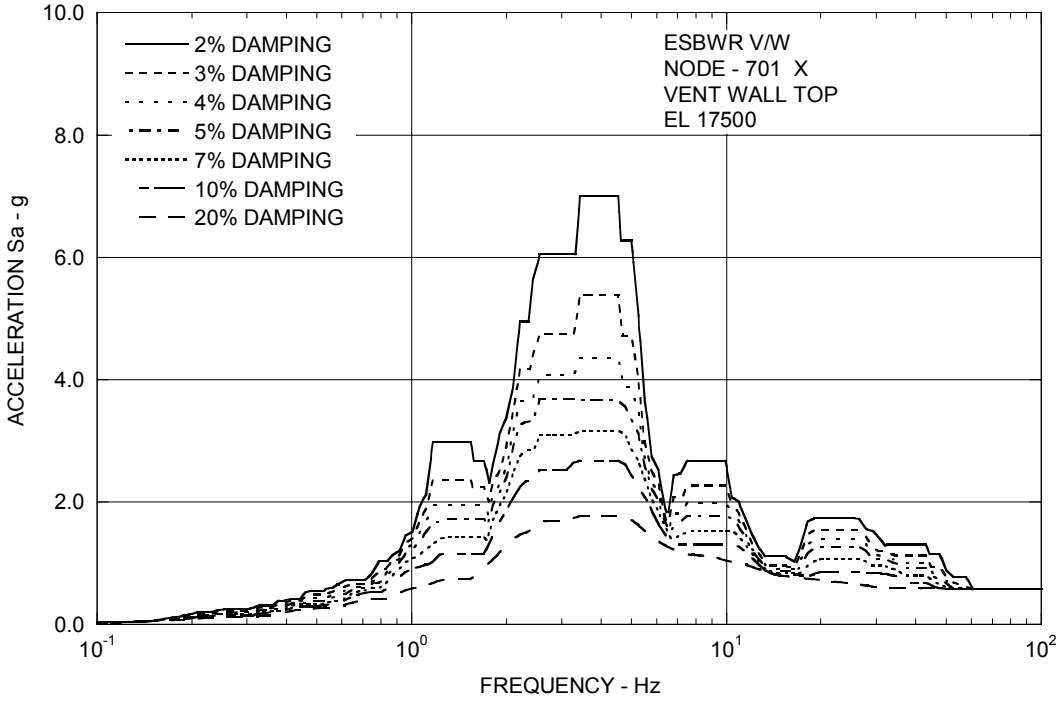

Figure 3A.9-1c. Enveloping Floor Response Spectra – Vent Wall Top X

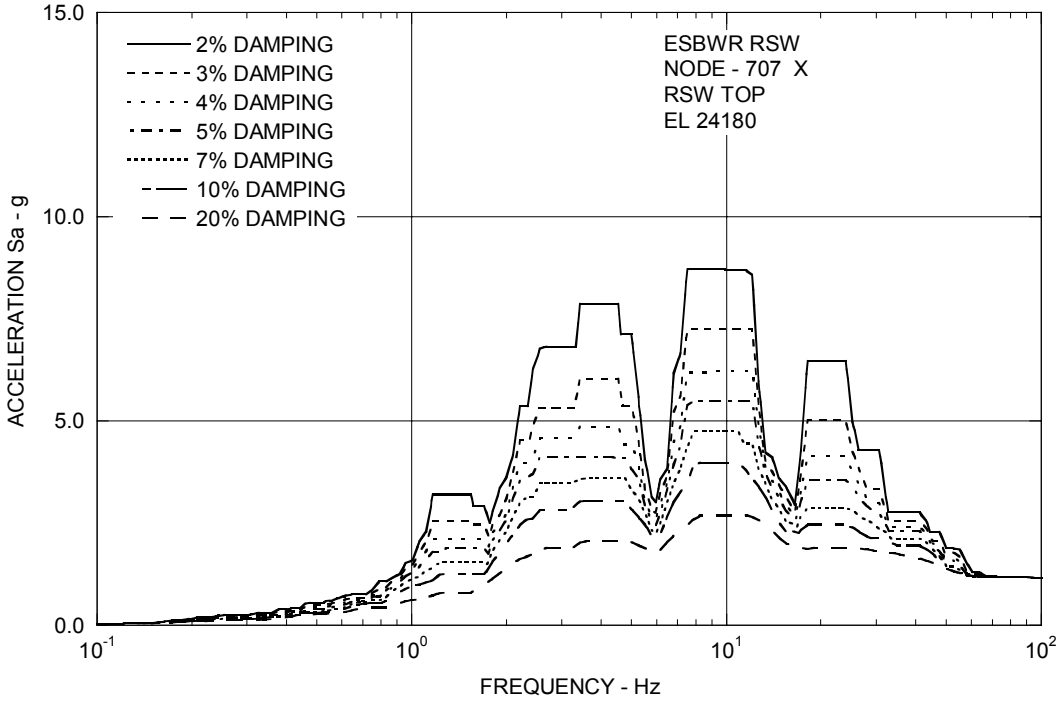

Figure 3A.9-1d. Enveloping Floor Response Spectra – RSW Top X

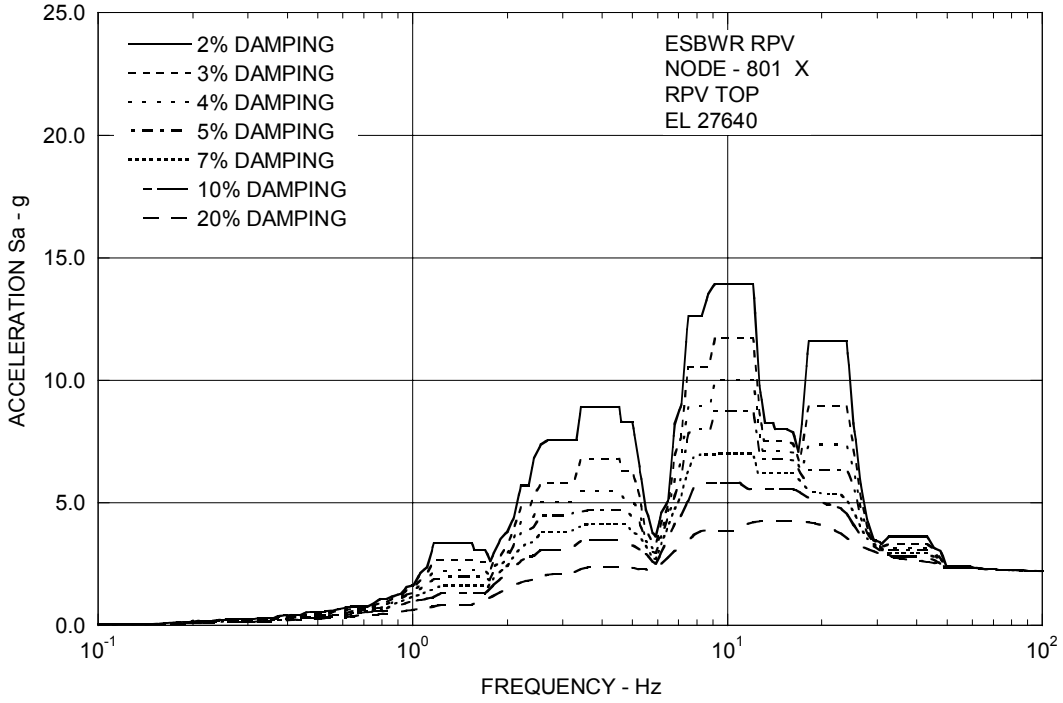

Figure 3A.9-1e. Enveloping Floor Response Spectra – RPV Top X

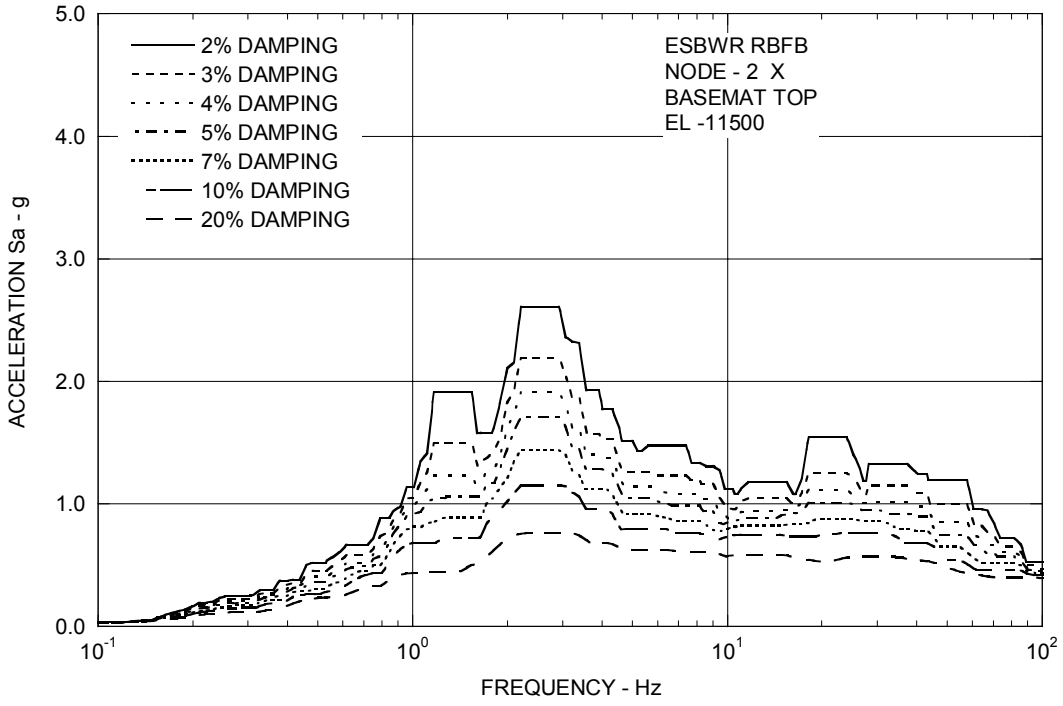

Figure 3A.9-1f. Enveloping Floor Response Spectra – RBFB Basemat X

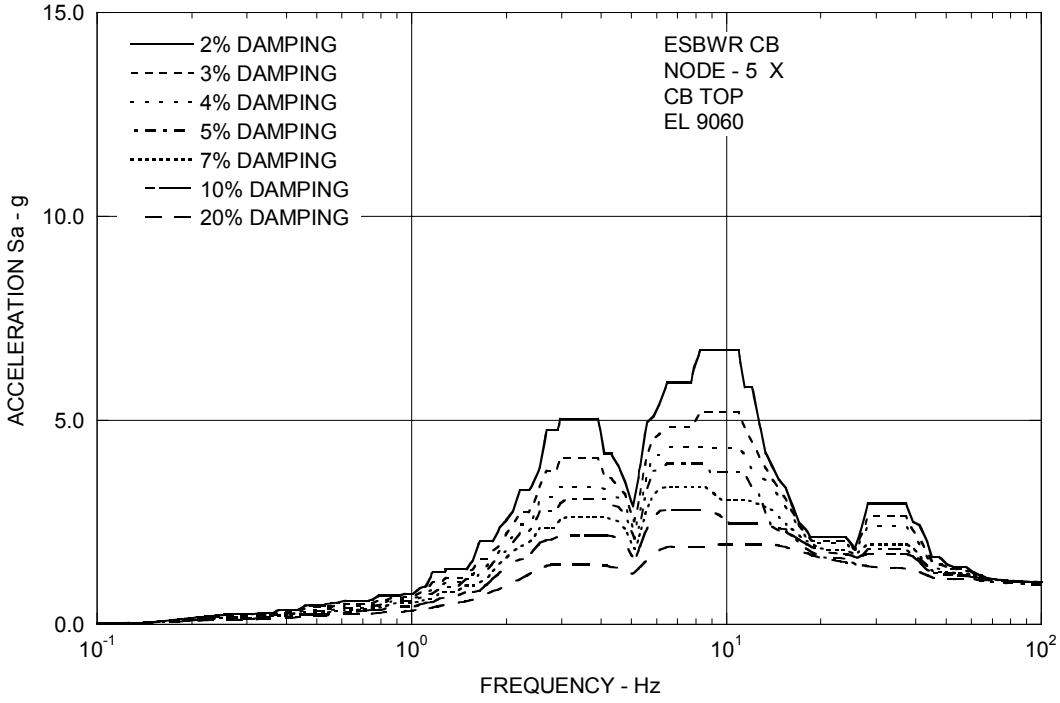

Figure 3A.9-1g. Enveloping Floor Response Spectra – CB Top X

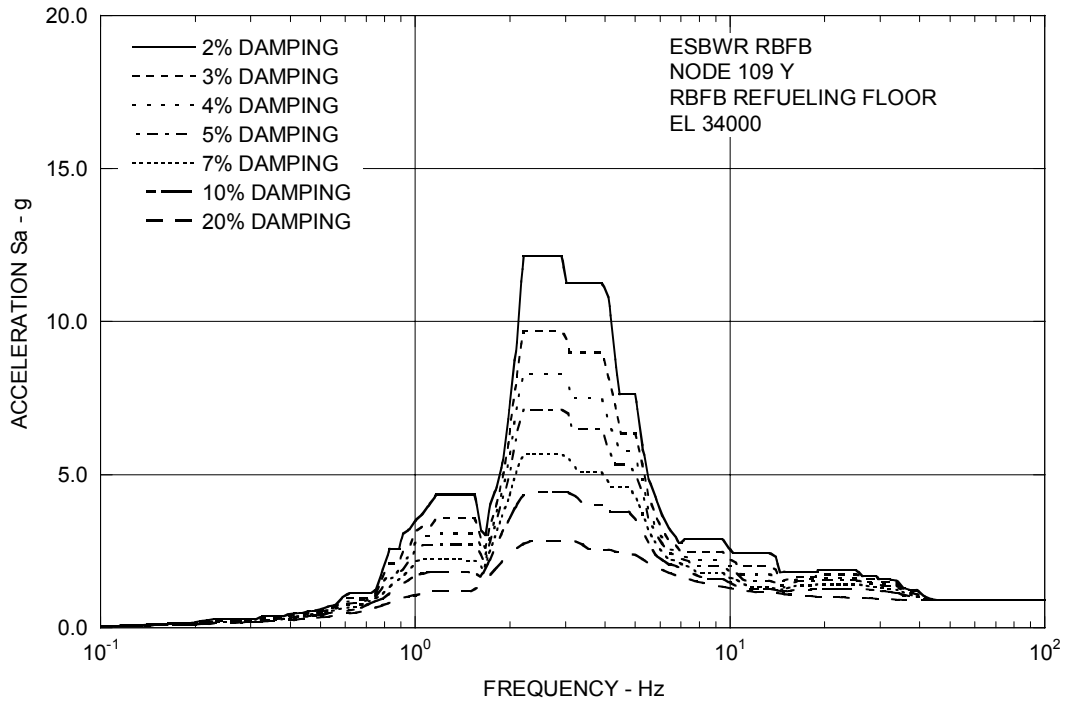

Figure 3A.9-2a. Enveloping Floor Response Spectra – RBFB Refueling Floor Y

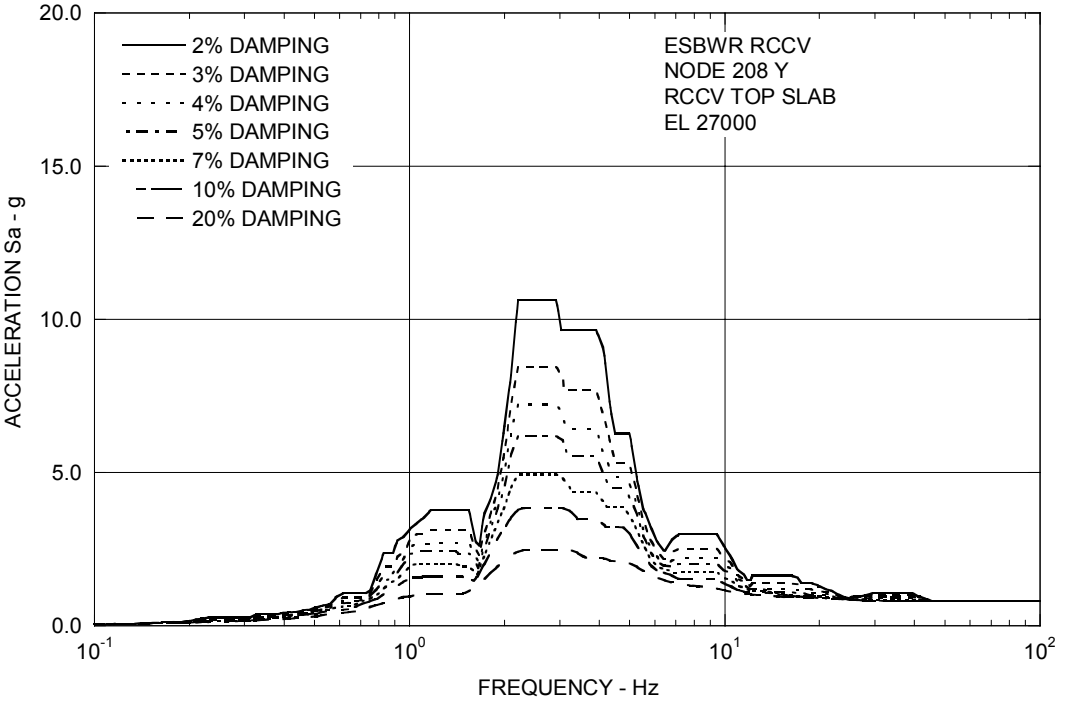

Figure 3A.9-2b. Enveloping Floor Response Spectra – RCCV Top Slab Y

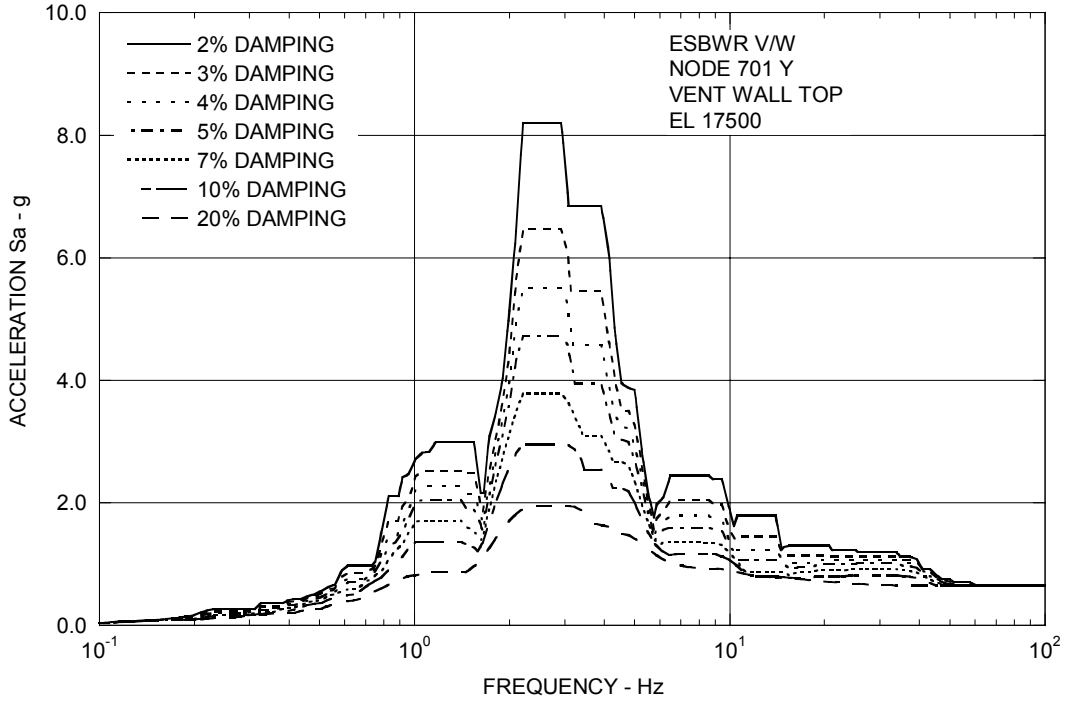

Figure 3A.9-2c. Enveloping Floor Response Spectra – Vent Wall Top Y

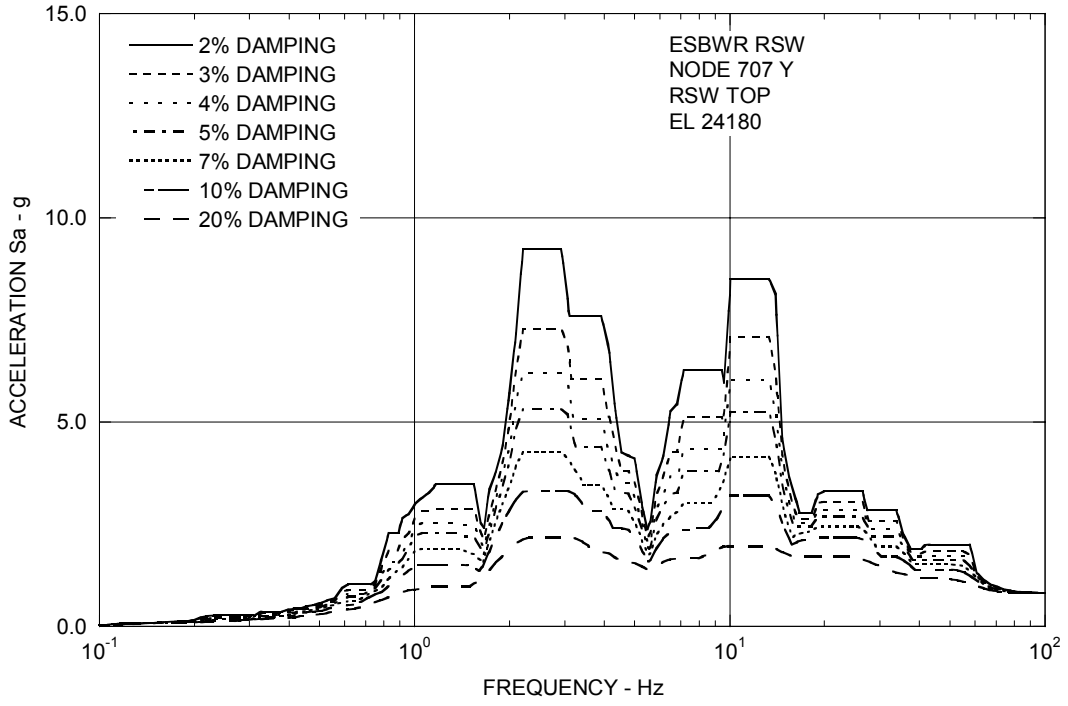

Figure 3A.9-2d. Enveloping Floor Response Spectra – RSW Top Y

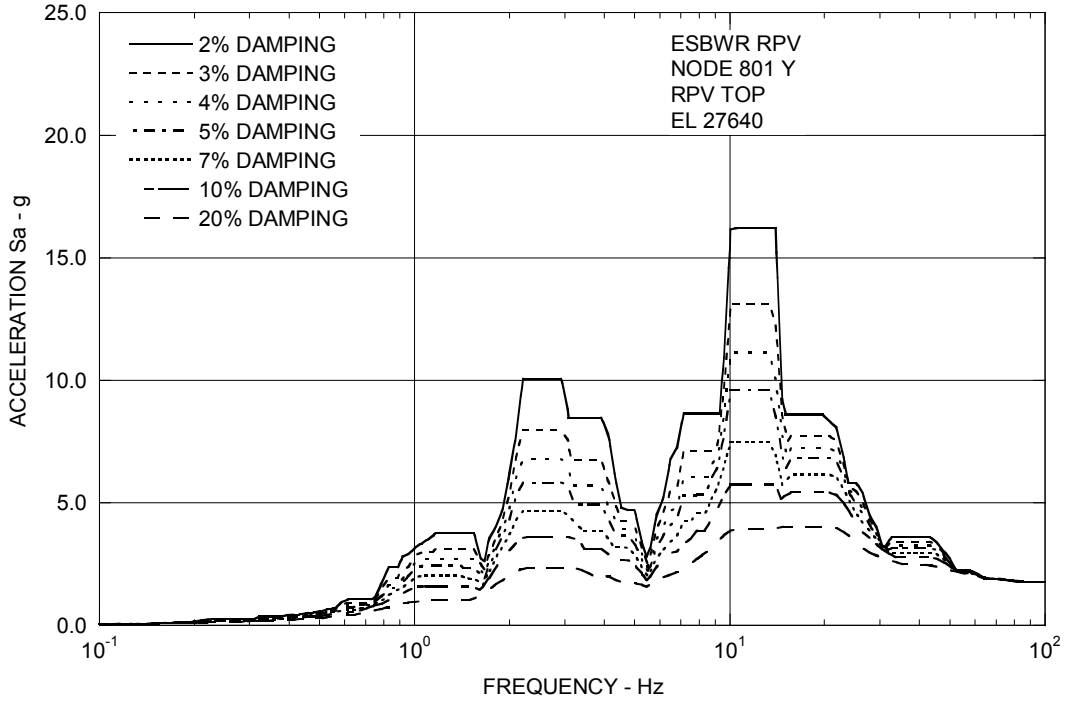

Figure 3A.9-2e. Enveloping Floor Response Spectra – RPV Top Y

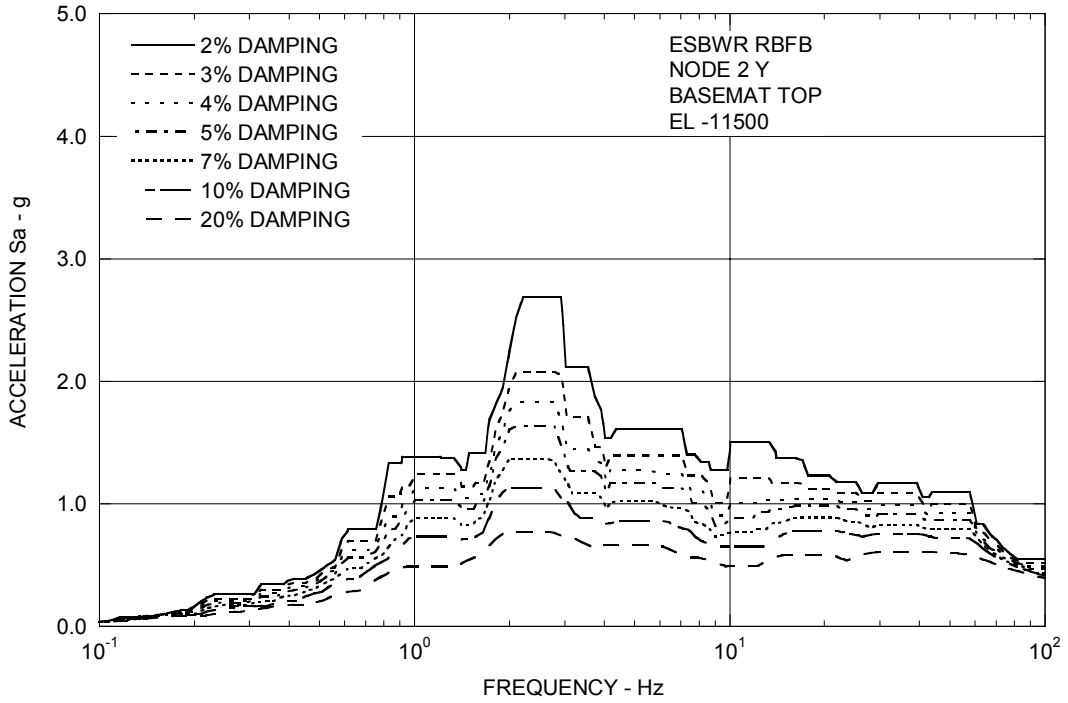

Figure 3A.9-2f. Enveloping Floor Response Spectra – RBFB Basemat Y

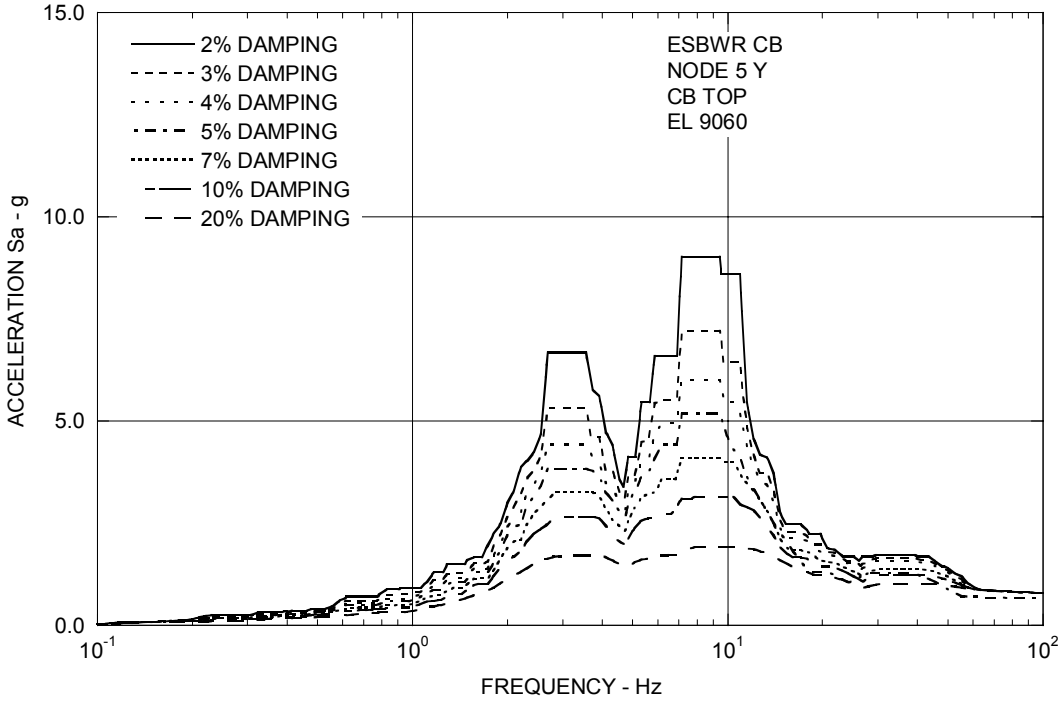

Figure 3A.9-2g. Enveloping Floor Response Spectra – CB Top Y

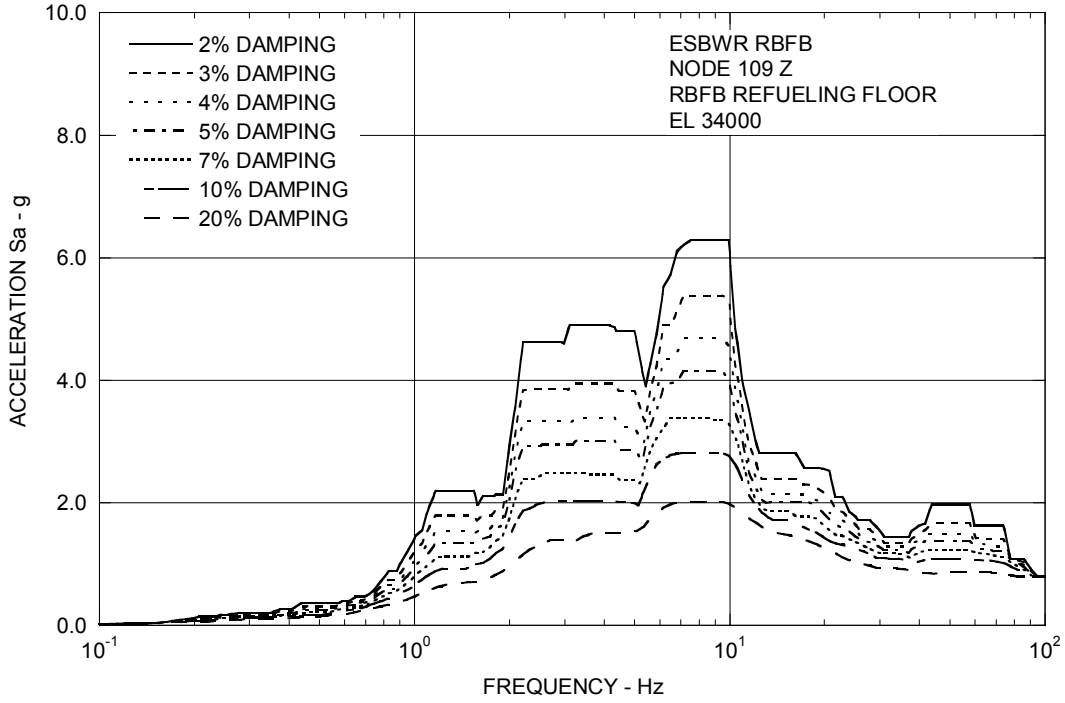

Figure 3A.9-3a. Enveloping Floor Response Spectra – RBFB Refueling Floor Z

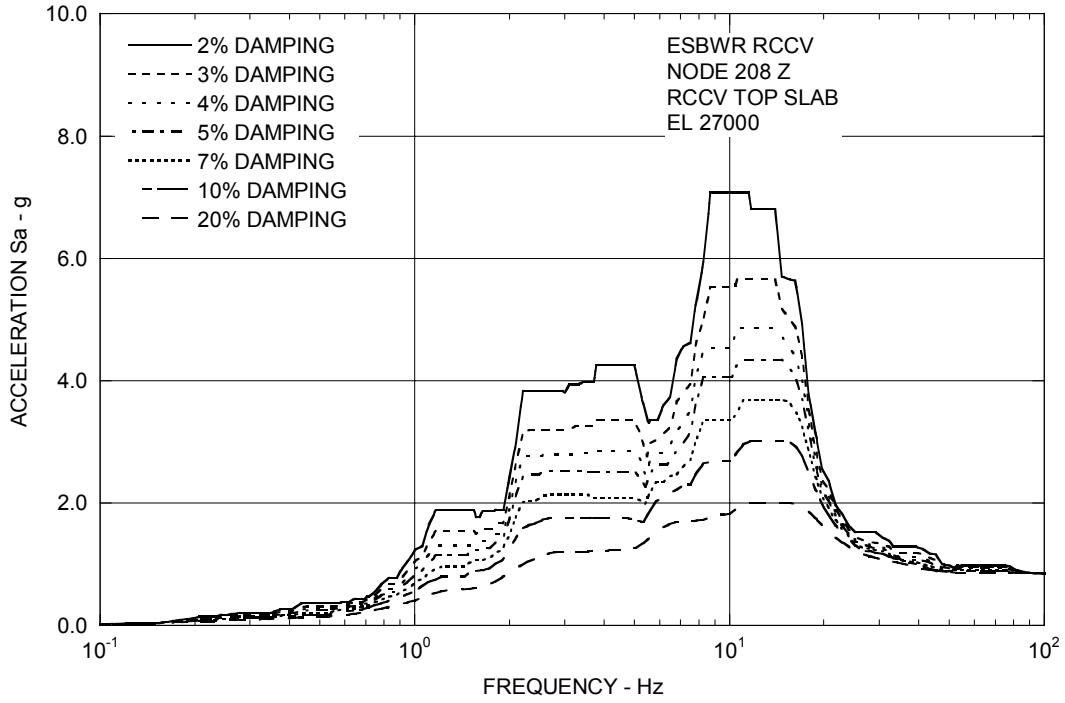

Figure 3A.9-3b. Enveloping Floor Response Spectra – RCCV Top Slab Z

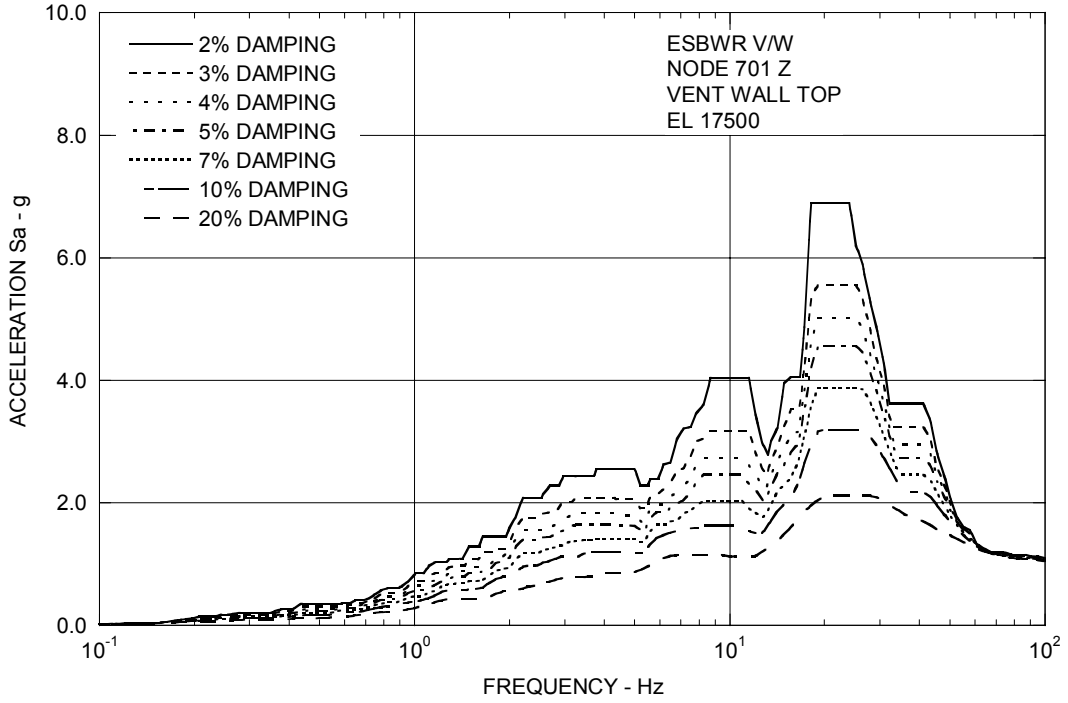

Figure 3A.9-3c. Enveloping Floor Response Spectra – Vent Wall Top Z

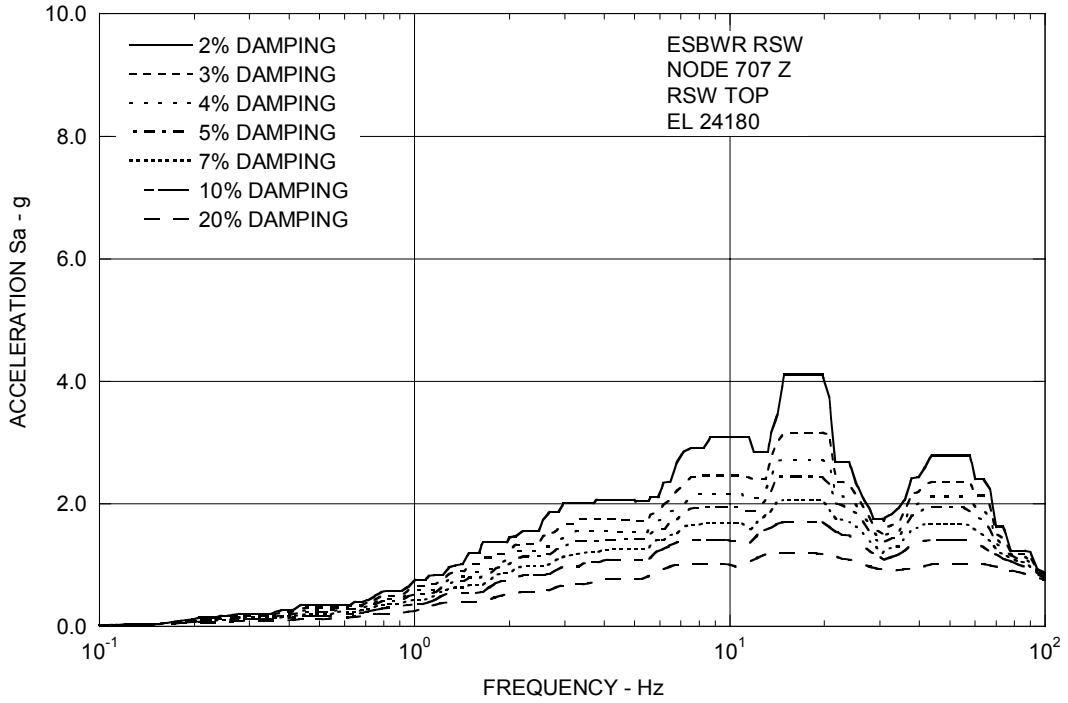

Figure 3A.9-3d. Enveloping Floor Response Spectra – RSW Top Z

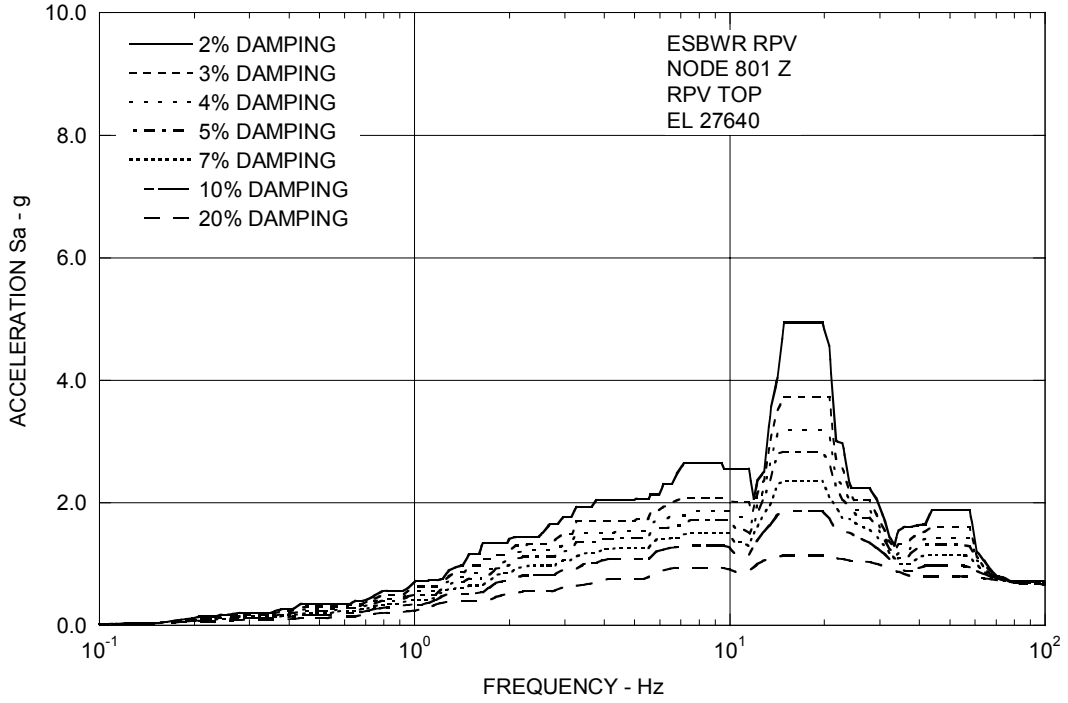

Figure 3A.9-3e. Enveloping Floor Response Spectra – RPV Top Z

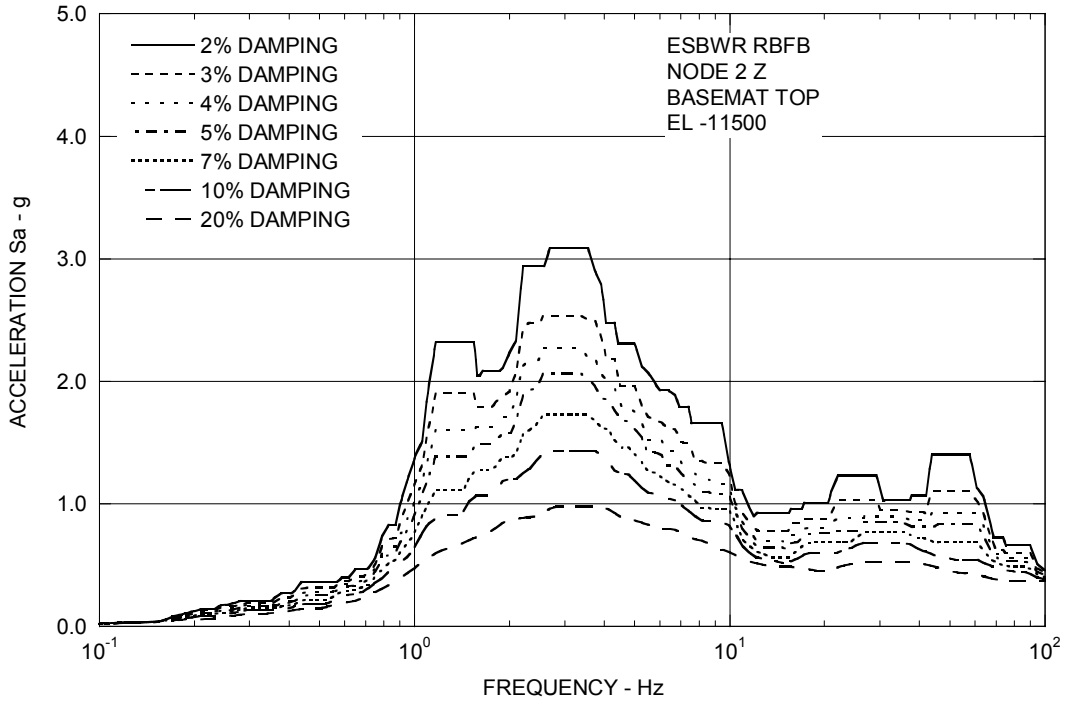

Figure 3A.9-3f. Enveloping Floor Response Spectra – RBFB Basemat Z

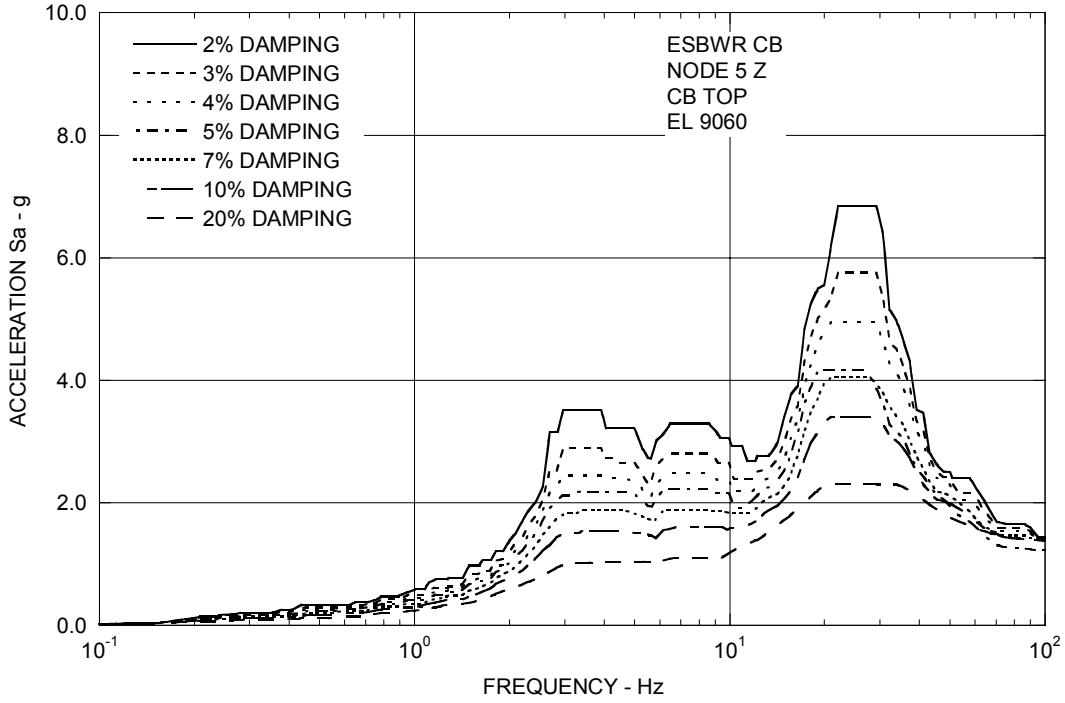

Figure 3A.9-3g. Enveloping Floor Response Spectra – CB Top Z

3B. CONTAINMENT HYDRODYNAMIC LOAD DEFINITIONS

This appendix provides the hydrodynamic loads applied in structural evaluations of the primary containment. The methodology used to develop these load definitions, and the justification for their applicability to ESBWR is given in Reference 3B-1.

3B.1 SAFETY RELIEF VALVE (SRV) LOADS

3B.1.1 Oscillating pressure load into the suppression pool from Safety Relief Valves (SRVs)

The distributions of SRV loads applied to structural evaluation of the boundary of the suppression pool are shown in Figure 3B-1.

3B.1.2 Pressure Time History

For acceleration response spectra generation, time histories of SRV are needed. Figure 3B-2 shows a typical pressure history applied to structural evaluation that is normalized to the maximum pressure value, with a frequency of 8 Hz. This pressure time history profile can be used in digitizing the pressure amplitude variation with time for other frequencies varying from 5 to 12 Hz. It should be noted that the bubble pressure decays to 1/3 Pmax with 5 cycles for any frequency between 5 and 12 Hz.

3B.2 ACCIDENT PRESSURE LOADS

During a LOCA, the suppression pool boundary is subjected to hydrodynamic loads, such as Pool Swell (PS), Condensation Oscillation (CO) and Chugging (CH) loads. These loads are not concurrent. The event-time relationship is shown in Figure 3B-3.

These pool swell boundary pressures shall be applied together with a drywell pressure of 345 kPag (50 psig). The pressure distribution is shown in Figure 3B-4.

The spatial distribution of CO and CH loads on the boundary of the suppression pool are shown in Figures 3B-5 and 3B-6, respectively. Dynamic load factors to convert the dynamic loads to static equivalent loads are also included in the RCCV and liner design.

For response spectra generation, pressure time histories of CO and CH are needed. There are five time histories of CO and eight time histories of CH required for the analysis. A typical pressure time history of CO and that of CH is shown in Figures 3B-7 and 3B-8, respectively.

For each chugging case, two sets of forcing frequencies shall be analyzed. The first forcing frequency is Figure 3B-8. The second forcing frequency is derived by adjusting the time scale of Figure 3B-8.

Each CO load is considered symmetric (in-phase for all vents). Each chugging load is considered symmetric (in-phase for all vents) and asymmetric (half of vents out-of-phase with other half).

In addition to CO and CH presented above, horizontal vent chugging and local CO loads are to be considered as follows:

A) Horizontal Vent Chugging

(1) Location: Each of top horizontal vents

(2) Loading: Triangular pulse in the upward direction as shown in Figure 3B-9 for global dynamic response analysis and Figure 3B-10 for vent pipe and pedestal design

(3) Phasing: Two cases, in-phase of all vents and half of vents 180 deg out-of phase with other half

(4) Combination with pool chugging: SRSS

B) Local Condensation Oscillation

(1) Location: Within 2 vent diameters for each of bottom horizontal vents

(2) Loading: Triangular pulses as shown in Figure 3B-11

(3) Phasing: In-phase of all vents

(4) Combination with pool CO: Absolute sum (ABS)

The CO and chugging load magnitudes are proprietary information. The values shown in Figure 3B-7, 8, 9, 10 and 11 are normalized values. The proprietary magnitudes used in Appendices 3F and 3G are given in Reference 3B-1.

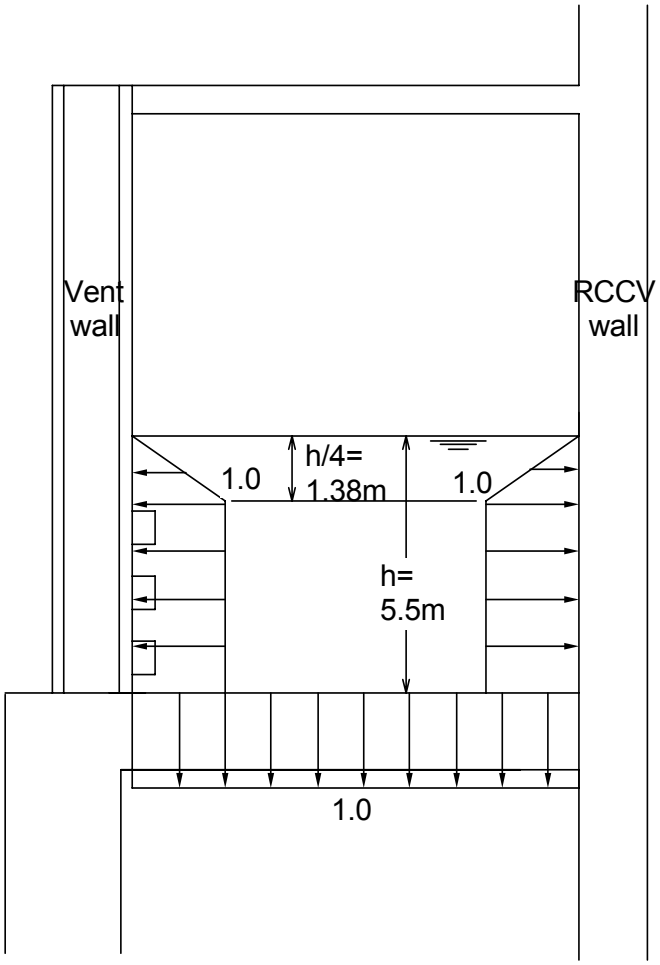

SRV Peak Positive Pressure = 152 kPag
SRV Peak Negative Pressure = -63 kPag
Dynamic Load Factor (DLF) = 2.0

Figure 3B-1. Safety Relief Valve (SRV) Pressure Loads

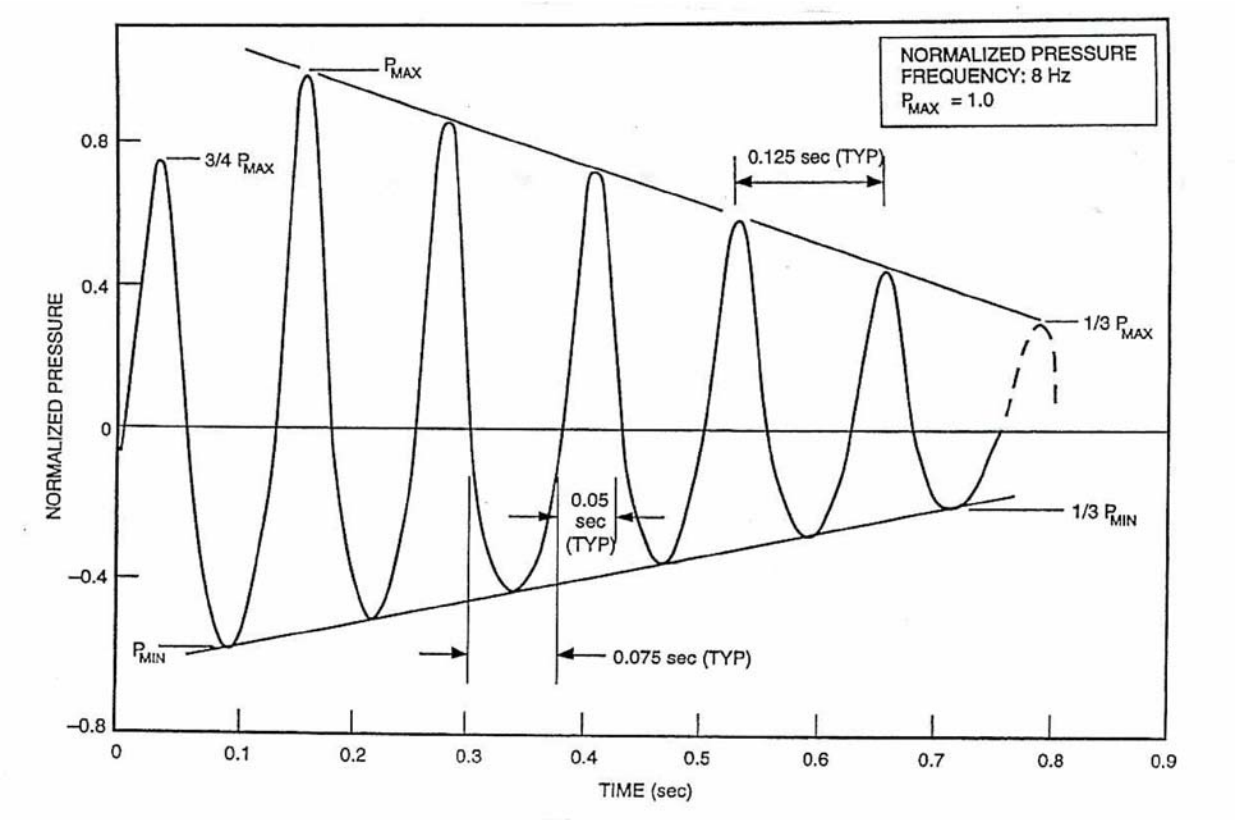

Figure 3B-2. Normalized SRV Pressure Time History (Idealized)

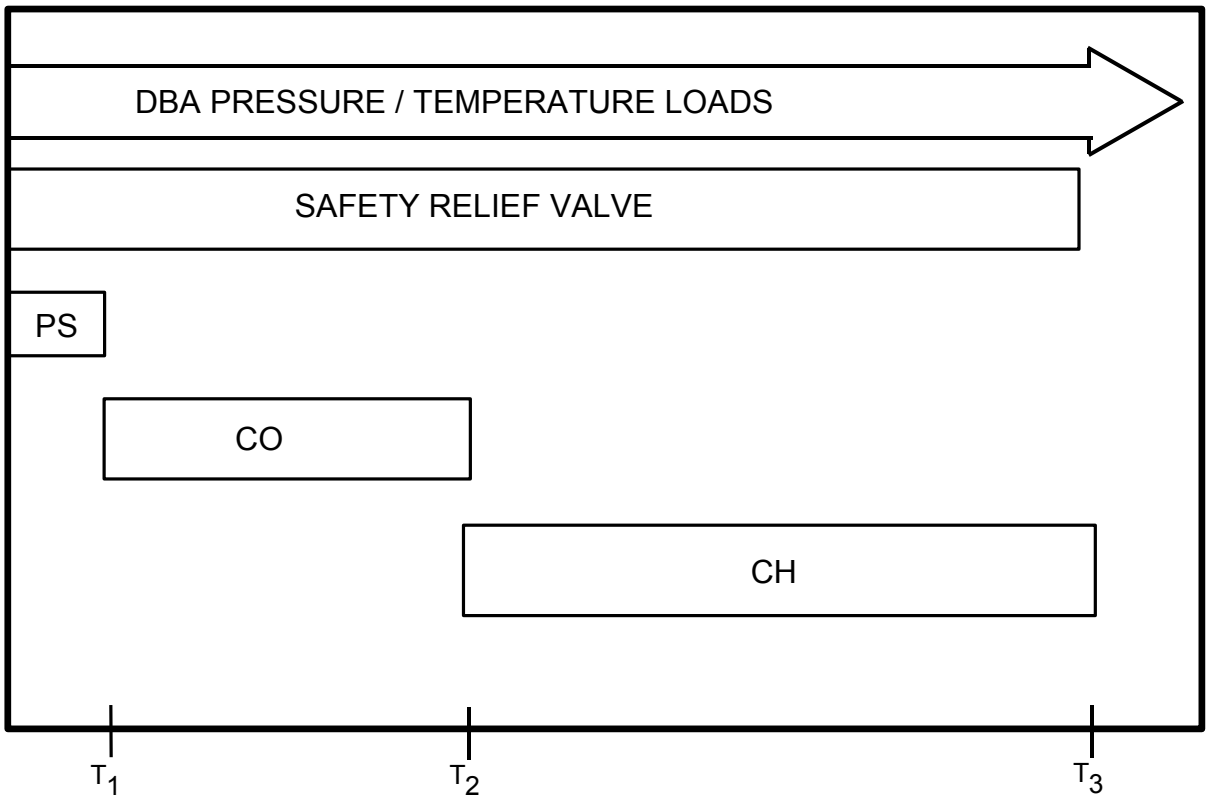

T_1 = 5 sec T_2 = 500 sec T_3 = 72 hr

PS = POOL SWELL

CO = CONDENSATION OSCILLATION

CH = CHUGGING

Figure 3B-3. Typical Event – Time Relationship for a DBA

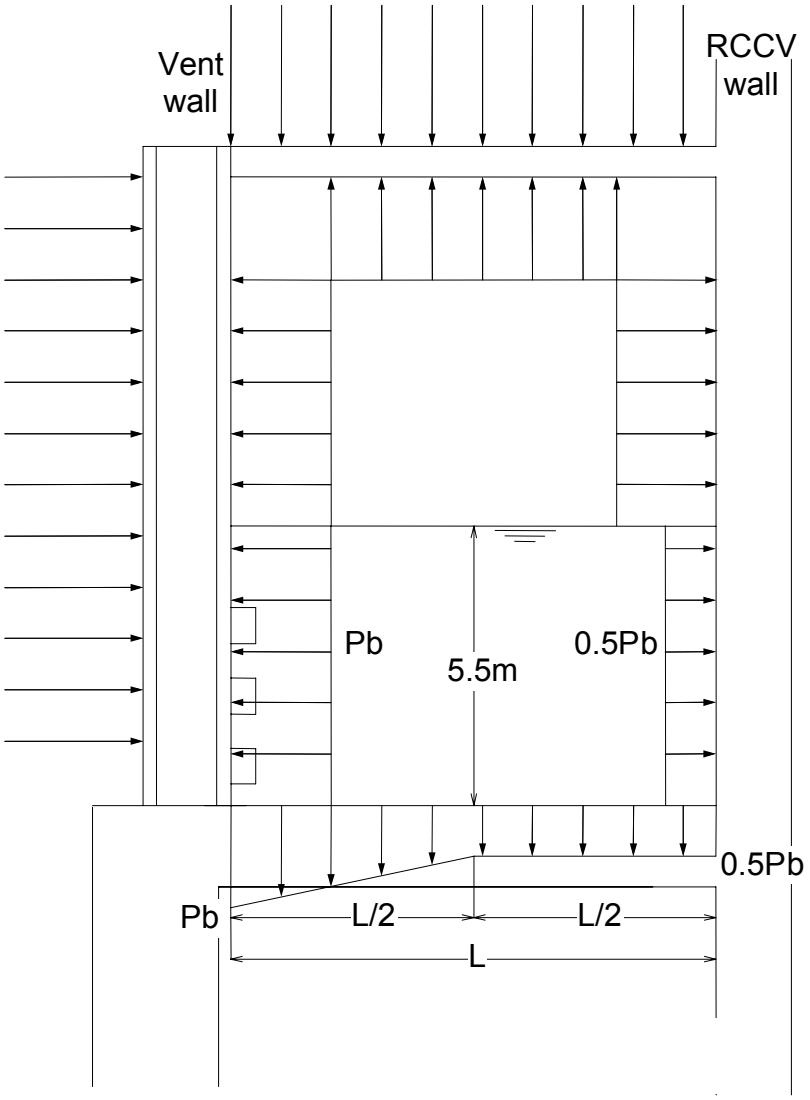

Note:Pb is the maximum pool swell boundary load. Pool swell height is 5.5 m. In addition to the gas space pressure, Pg, there is a linear variation pool swell boundary pressure above the S/P water surface. This additional pressure is not used for RCCV design but for platforms and objects in the S/P air space (catwalks, pipes, etc.).

Figure 3B-4. Pool Swell (PS) Pressure Loads

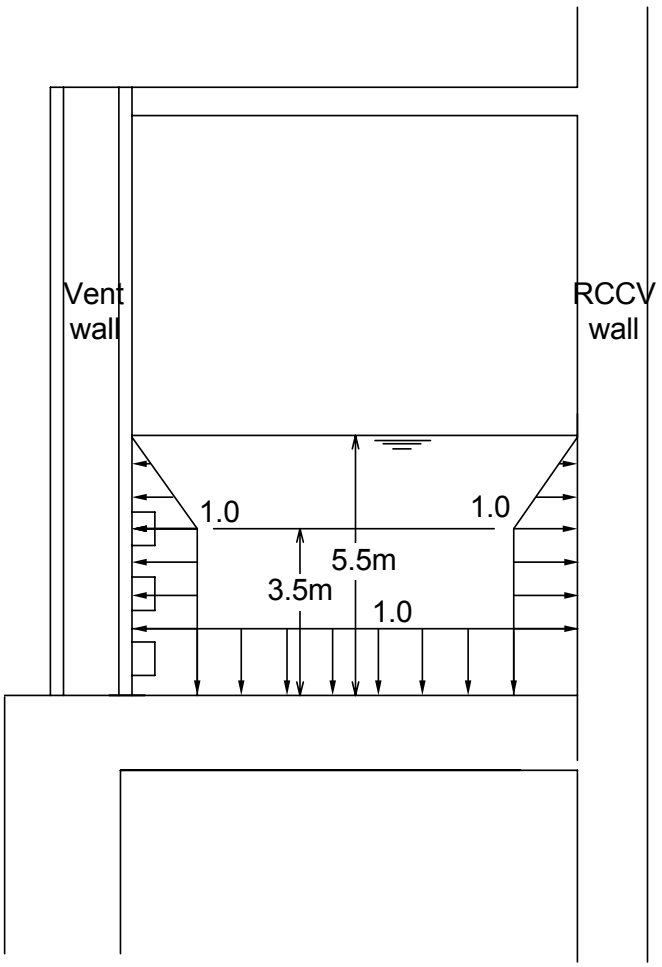

CO Peak Positive Pressure = 186 kPag
CO Peak Negative Pressure = -186 kPag
Dynamic Load Factor (DLF) = 2.0

Figure 3B-5. Condensation Oscillation (CO) Pressure Loads

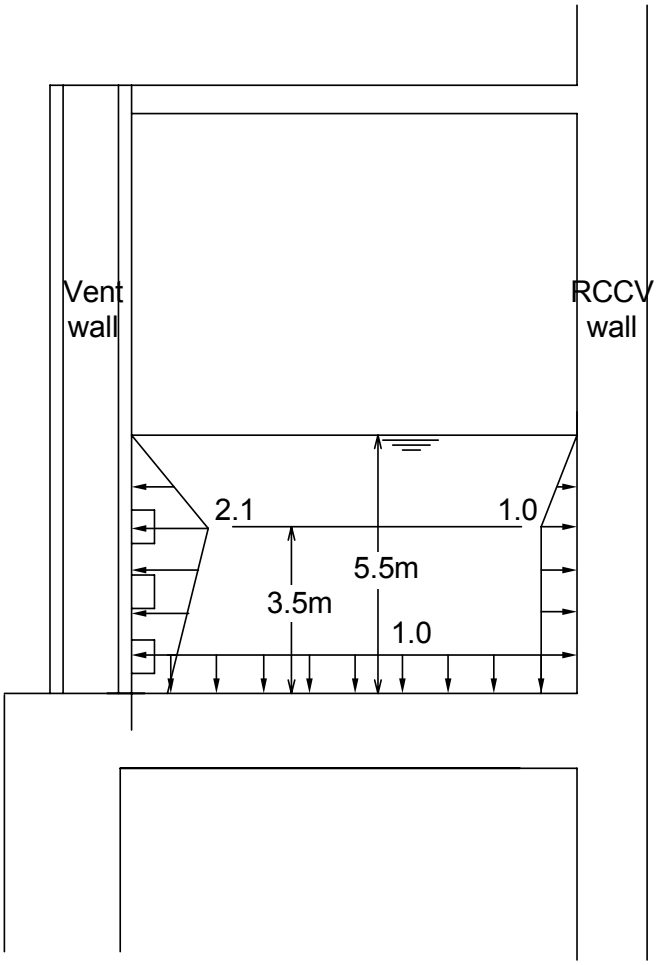

CHUG Peak Positive Pressure = 91 kPag
CHUG Peak Negative Pressure = -66 kPag
Dynamic Load Factor (DLF) = 2.0

Figure 3B-6. Chugging (CH) Load Spatial Distribution

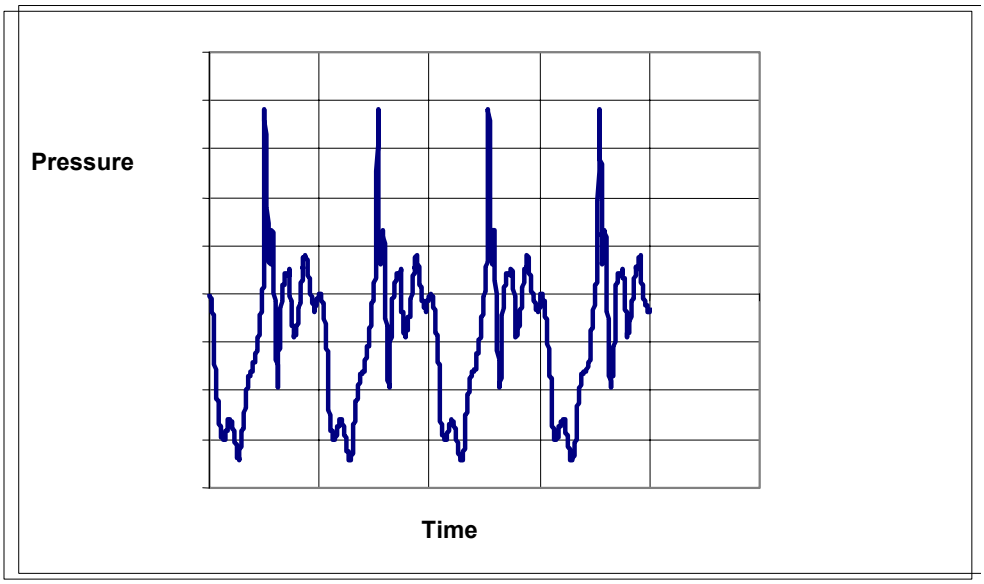

Figure 3B-7. A Typical Pressure Time History of CO

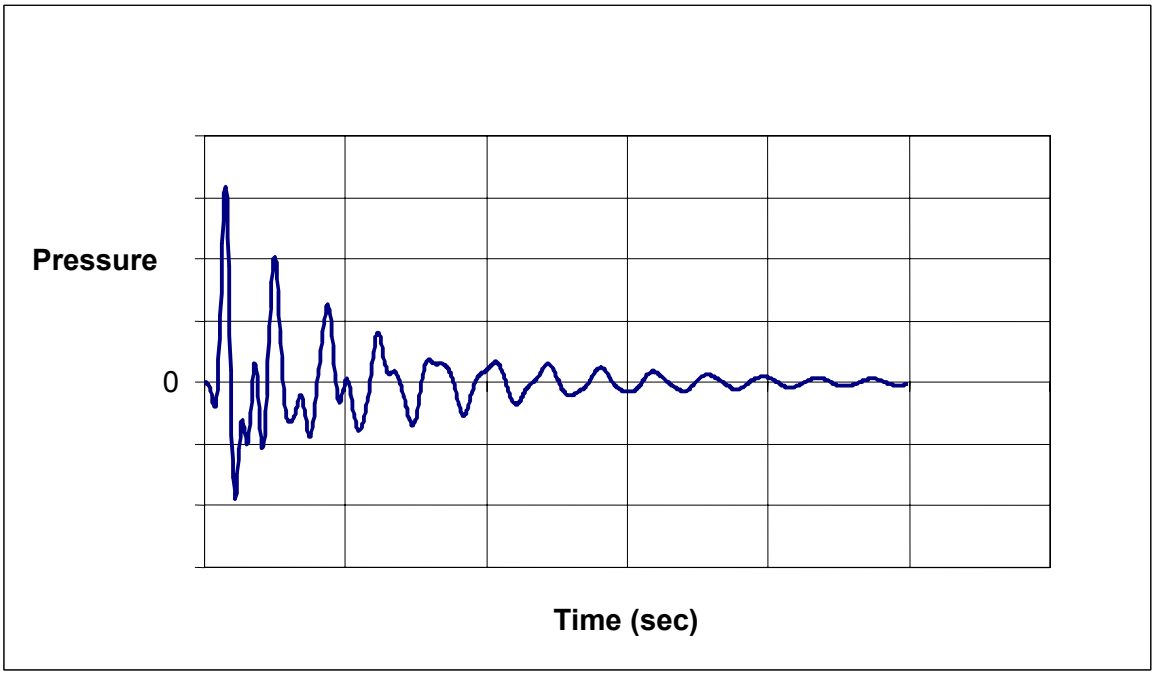

Figure 3B-8. A Typical Pressure Time History of CH

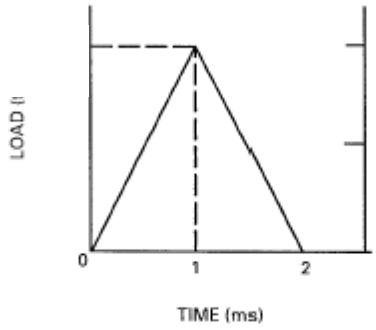

Figure 3B-9. Horizontal Vent Upward Loading for Structure Response Analysis

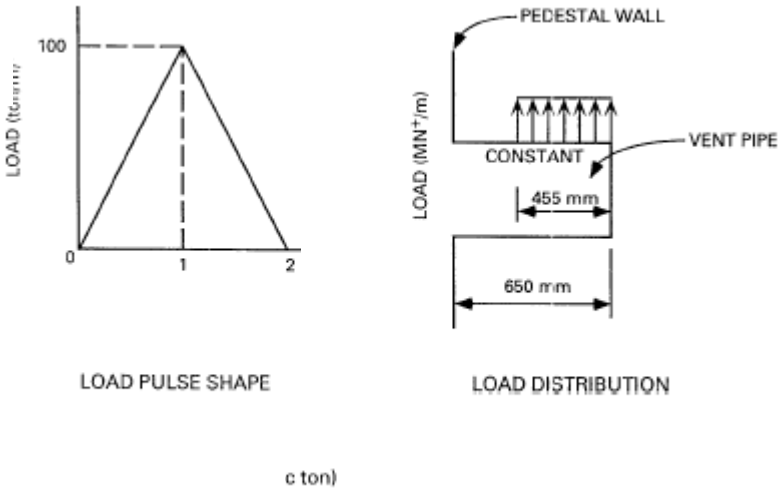

Figure 3B-10. Horizontal Vent Upward Loading for Vent Pipe and Pedestal

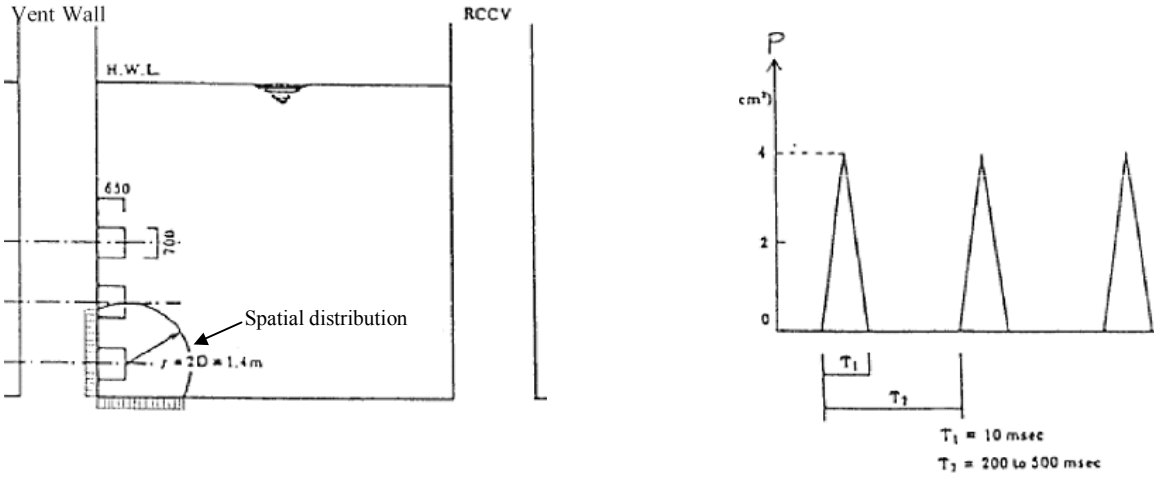

Figure 3B-11. Local CO Load

3B.3 REFERENCES

3B-1 General Electric Company, "ESBWR Containment Load Definition," NEDE-33261, Class III (proprietary), (To be issued).

3C. COMPUTER PROGRAMS USED IN THE DESIGN AND ANALYSIS OF SEISMIC CATEGORY I STRUCTURES

3C.1 INTRODUCTION

The following Seismic Category I structures and their foundations of the Nuclear Island are analyzed and/or designed using the computer programs described in this appendix:

(1) Concrete Containment Structure

(2) Reactor Building (RB)

(3) Fuel Building (FB)

(4) Control Building (CB)

3C.2 STATIC AND DYNAMIC STRUCTURAL ANALYSIS PROGRAM (NASTRAN)

3C.2.1 Description

NASTRAN is a general purpose computer program for finite element analysis; its capabilities include: static response to concentrated and distributed loads, to thermal expansion and to enforced displacements; dynamic response to transient loads, to steady-state sinusoidal loads, and to random excitation; and determination of eigenvalues for use in vibration analysis.

3C.2.2 Validation

The MSC_Software Corporation of Santa Ana, California developed NASTRAN. The program validation documentation is available at MSC Software Corporation.

3C.2.3 Extent of Application

This program is used for the static and eigenvalue analysis of the concrete containment, RB, FB, and CB. This program is also used for the static and dynamic analysis of the Drywell Head and containment internal structures.

3C.3 ABAQUS AND ANACAP-U

3C.3.1 Description

ABAQUS/Standard is a widely used, commercially available finite-element program that has a broad range of analysis capabilities. Implicit formulations for steady state and transient thermal solutions and for static stress analyses were employed using 3-dimensional models of continuum concrete elements, truss-type reinforcement sub-elements, and plate and membrane elements for liners and other steel components. Classical von Mises plasticity models, as well as strength degradation with elevated temperature, for the steel material are invoked for the nonlinear analyses. The ANACAP-U software is an advanced concrete constitutive model that is coupled to the ABAQUS software as a user subroutine. The ANACAP-U concrete material model provides formulations for concrete cracking under tensile and shear loads and post-cracking shear stiffness and shear capacity as a function of crack width and shear deformations, with yielding and strain softening (crushing) under large compressive loads. Degradation in modulus and strength with increasing temperatures is also included for the concrete model.

3C.3.2 Validation

ABAQUS is written and maintained by ABAQUS, Inc. of Providence R.I., (formerly Hibbitt, Karlssen, and Sorensen, Inc.). The program has an extensive library of example problems that are used for verification and validation testing. Additional descriptions and information on the

quality controls can be found on the ABAQUS web site, (www.abaqus.com). The ANACAP-U concrete material model for use with the ABAQUS program is written and maintained by ANATECH Corp, San Diego, CA. This software has been extensively verified with test problems and also validated against large-scale test results for the performance of reinforced concrete structures. ANACAP-U Program validation documentation is available at ANATECH Corp.

3C.3.3 Extent of Application

The ABAQUS/ANACAP-U software coupling is used for nonlinear analyses for the structural performance of the reinforced concrete containment under LOCA thermal conditions.

3C.4 CONCRETE ELEMENT CRACKING ANALYSIS PROGRAM (SSDP-2D)

3C.4.1 Description

SSDP-2D computes stresses in a thick concrete element under thermal and/or non-thermal (such as dead load, service loads) loads, considering effects of concrete cracking. The element represents a section of a concrete shell or slab, and may include two layers of orthogonal reinforcing. It does not include the effect of the liner.

SSDP-2D calculates the stresses considering two-dimensional equilibrium conditions of section forces with the existence of thermal loads and concrete cracking. It is assumed in the code that concrete has an anisotropic property and that cracked concrete does not carry tensile forces. Concrete is assumed to have no tensile strength.

3C.4.2 Validation

SSDP-2D is written and maintained by Shimizu Corporation of Tokyo, Japan. Program validation documentation is available at Shimizu Corporation.

3C.4.3 Extent of Application

This program is used for the analysis of the concrete containment, RB, FB, and CB.

3C.5 HEAT TRANSFER ANALYSIS PROGRAM (TEMCOM2)

3C.5.1 Description

TEMCOM2 solves a temperature distribution in a two-dimensional model based on a finite differential method. It performs analyses under the following conditions.

- Element: triangle and quadrilateral elements
- Surface heat transfer: convection and radiation
- Temperature condition: steady-state and transient temperature conditions

3C.5.2 Validation

TEMCOM2 is written and maintained by Shimizu Corporation of Tokyo, Japan. Program validation documentation is available at Shimizu Corporation.

3C.5.3 Extent of Application

This program is used for the transient heat transfer analysis of the concrete containment and RB.

3C.6 STATIC AND DYNAMIC STRUCTURAL ANALYSIS SYSTEMS: ANSYS

3C.6.1 Description

ANSYS is a large, finite element program for a broad range of analyses types. The structural analysis capabilities include material and geometric non-linear analysis, static analysis and a variety of dynamic analyses.

The element for a concrete cracking analysis allows a full non-linear analysis of reinforced concrete with cracking and crushing of concrete.

3C.6.2 Validation

ANSYS is maintained by ANSYS INC., located at 275 Technology Drive, Canonsburg, PA, 15317.

3C.6.3 Extent of Application

This program is used for the containment dynamic analysis of containment loads, for the containment ultimate capacity analyses and for containment seismic margin analysis.

3C.7 SOIL-STRUCTURE INTERACTION

3C.7.1 Dynamic Soil-Structure Interaction Analysis Program—DAC3N

3C.7.1.1 Description

DAC3N is a three-dimensional dynamic analysis program, which is used for the seismic response analysis of building considering soil-structure interaction. The response analysis is performed using the time history method solved by direct integration, Newmark's beta method. Eingenvalue analysis is performed using Subspace method.

In the DAC3N, soil-structure interaction system is modeled by the combination of soil spring and damping coefficient. Spring and damping coefficient are determined as frequency independent values, which fit the frequency dependent real and imaginary parts of soil spring obtained by the theoretical methods, such as vibration admittance theory based on three-dimensional wave propagation theory for uniform half space soil.

As mass elements, lumped mass and consistent mass are available. Structural elements, such as beam, truss, spring, damper, direct input matrix are available in this program.

This program also possesses nonlinear analysis functions.

3C.7.1.2 Validation

DAC3N is coded and maintained by Shimizu Corporation of Tokyo, Japan. Program validation documentation is available at Shimizu Corporation.

3C.7.1.3 Extent of Application

This program is used to perform the soil-structure interaction analysis required to obtain enveloped seismic design loads of the concrete containment, RB, FB and CB.

3D. COMPUTER PROGRAMS USED IN THE DESIGN OF COMPONENTS, EQUIPMENT AND STRUCTURES

3D.1 INTRODUCTION

As discussed in Subsection 3.9.1.2, this appendix describes the major computer programs used in the analysis of the safety-related components, equipment and structures. The quality of the programs and the computed results is controlled. The programs are verified for their application by appropriate methods, such as hand calculations, or comparison with results from similar programs, experimental tests, or published literature, including analytical results or numerical results to the benchmark problems.

3D.2 FINE MOTION CONTROL ROD DRIVE

3D.2.1 Fine Motion Control Rod Drive - FMCRD01

The FMCRD01A program is used to obtain scram performance data for various inputs to the fine motion control rod drive (FMCRD) stress analysis for both code and non-code parts. The use of this program is addressed in Subsection 3.9.1.3.2. Experimental data on pressure drops, friction factors, effects of fuel channel detection, etc., are used in the development and perfecting of this code. Internal drive pressures and temperatures used in the stress analysis are also determined during actual testing of the prototype FMCRD.

3D.2.2 Structural Analysis Programs

Structural analysis programs, such as NASTRO4V and ANSYS, that are mentioned in Subsections 3D.3 and 3D.4.9 are used in the analysis of the FMCRD.

3D.3 REACTOR PRESSURE VESSEL AND INTERNALS

Computer programs used in the analysis of the reactor pressure vessel, core support structures, and other safety class reactor internals are described in Subsection 4.1.4.

3D.4 PIPING

3D.4.1 Piping Analysis Program - PISYS

PISYS is a computer code for analyzing piping systems subjected to both static and dynamic piping loads. Finite element models of a piping system formed by assembling stiffness matrices represent standard piping components. The piping elements are connected to each other via nodes called pipe joints. It is through these joints that the model interacts with the environment, and loading of the piping system becomes possible. PISYS is based on the linear elastic analysis in which the resultant deformations, forces, moments and accelerations at each joint are proportional to the loading and the superposition of loading is valid.

PISYS has a full range of static dynamic load analysis options. Static analysis includes dead weight, uniformly distributed weight, thermal expansion, externally applied forces, moments, imposed displacements and differential support movement (pseudo-static load case). Dynamic analysis includes mode shape extraction, response spectrum analysis, and time-history analysis by modal combination or direct integration. In the response spectrum analysis [i.e., uniform support motion response spectrum analysis (USMA) or independent support motion response spectrum analysis (ISMA)], the user may request modal response combination in accordance with Regulatory Guide 1.92. In the ground motion (uniform motion) or independent support time history analysis, the normal mode solution procedure is selected. In analysis involving time varying nodal loads, the step-by-step direct integration method is used.

The PISYS program has been benchmarked against NRC piping models. The results are documented in Reference 3D-1 for mode shapes and USMA options. The ISMA option has been validated against NUREG/CR-1677 (Reference 3D-2).

3D.4.2 Component Analysis - ANSI7

ANSI7 is a computer code for calculating stresses and cumulative usage factors for Class 1, 2 and 3 piping components in accordance with articles NB, NC and ND-3650 of ASME Code Section III. ANSI7 is also used to combine loads and calculate combined service levels A, B, C and D loads on piping supports and pipe-mounted equipment.

3D.4.3 Area Reinforcement - NOZAR

The Nozzle Area Reinforcement (NOZAR) computer program performs an analysis of the required reinforcement area for openings. The calculations performed by NOZAR are in accordance with the rules of ASME Code Section III.

3D.4.4 Dynamic Forcing Functions

3D.4.4.1 Relief Valve Discharge Pipe Forces Computer Program - RVFOR

The relief valve discharge pipe connects the pressure-relief valve to the suppression pool. When the valve is opened, the transient fluid flow causes time-dependent forces to develop on the pipe wall. This computer program computes the transient fluid mechanics and the resultant pipe forces using the method of characteristics.

3D.4.4.2 Turbine Stop Valve Closure - TSFOR

The TSFOR program computes the time-history forcing function in the main steam piping due to turbine stop valve closure. The program utilizes the method of characteristics to compute fluid momentum and pressure loads at each change in pipe section or direction.

3D.4.4.3 Hydraulic Transients-RELAP5/Mod 3.3

The RELAP5 computer code is a light water reactor transient analysis code developed for the U.S. Nuclear Regulatory Commission for use in rulemaking, licensing audit calculations, evaluation of operator guidelines, and as a basis for nuclear plant analyses. Specific applications of this capability have included simulations of transients such as loss of feed-water, loss of offsite power, station blackout, and turbine trip. RELAP5 is a highly generic code that, in addition to calculating the behavior of a reactor coolant system during a transient, can be used for simulating a wide variety of hydraulic and thermal transients in both nuclear and non-nuclear systems involving mixtures of steam, water, non-condensables, and solutes.

The RELAP5 hydrodynamic model is a one-dimensional, transient, two-fluid model for flow of a two-phase steam-water mixture that can contain non-condensable components in the steam phase and/or a soluble component in the water phase.

The two-fluid equations of motion (mass, momentum, and energy conservation for each phase) that are used as the basis for the RELAP5 hydrodynamic model are formulated in terms of volume and time-averaged parameters of the flow. Phenomena that depend upon transverse gradients, such as friction and heat transfer, are formulated in terms of bulk properties using empirical transfer coefficient formulations.

On the basis of geometry input data, and thermohydraulic initial conditions (pressure, temperature, fluid), the code integrates fluid equations in order to calculate time-histories of pressure, temperature, forces in the different nodes and sections of the piping network.

3D.4.4.4 Subcompartment Pressurization - Contain

The CONTAIN 2.0 code is an analysis tool for predicting the physical, chemical, and radiological conditions inside the containment and connected buildings of a nuclear reactor in the event of an accident. CONTAIN 2.0 was developed at Sandia National Laboratories under the sponsorship of the US Nuclear Regulatory Commission (USNRC) for analyzing containment phenomena under severe accident and design basis accident conditions. It is designed and has capability to predict the thermal-hydraulic response inside the containment in the event of an accident.

CONTAIN 2.0 is a highly flexible and modular code that can run both everything from quite simple to highly complex problems.

3D.4.5 Integral Attachment - LUGST

The computer program LUGST evaluates the stress in the pipe wall that is produced by loads applied to the integral attachments. The program is based on Welding Research Council Bulletin 198.

3D.4.6 Response Spectra Generation

3D.4.6.1 ERSIN Computer Program

ERSIN is a computer code used to generate response spectra for pipe-mounted and floor-mounted equipment. ERSIN provides direct generation of local or global acceleration response spectra.

3D.4.6.2 RINEX Computer Program

RINEX is a computer code used to interpolate and extrapolate amplified response spectra used in the response spectrum method of dynamic analysis. RINEX is also used to generate response spectra with nonconstant model damping. The non-constant model damping analysis option can calculate spectral acceleration at the discrete eigenvalues of a dynamic system using either the strain energy weighted modal damping or the ASME Code Class N-411-1 damping values.

3D.4.6.3 CALESPW Computer Program

CALESPW is used to calculate the response spectra from time histories, for the degrees of freedom selected in a model. The program solves the second order differential equation through Nigam-Jennings method for an established set of frequencies.

3D.4.6.4 SFT Computer Program

SFT is a computer code used to calculate Fourier Transform and Power Density Spectrum (PDS) of an acceleration time history. The program also allows adjusting the input PDS to the PDS defined in Standard Review Plan (SRP 3.7.1) and calculating its corresponding time history.

3D.4.7 Piping Dynamic Analysis Program - PDA

PDA is used to determine the response of a pipe subjected to the thrust force occurring after a pipe break. It also is used to determine the pipe whip restraint design and capacity.

The program treats the situation in terms of generic pipe break configuration, which involves a straight, uniform pipe fixed (or pinned) at one end and subjected to a time-dependent thrust force at the other end. A typical restraint used to reduce the resulting deformation is also included at a location between the two ends. Nonlinear and time-independent stress-strain relations are used to model the pipe and the restraint. Using a plastic hinge concept, bending of the pipe is assumed to occur only at the fixed (or pinned) end and at the location supported by the restraint.

Effects of pipe shear deflection are considered negligible. The pipe-bending moment-deflection (or rotation) relation used for these locations is obtained from a static nonlinear cantilever beam analysis. Using moment angular rotation relations, nonlinear equations of motion are formulated using energy considerations, and the equations are numerically integrated in small time steps to yield the time-history of the pipe motion.

3D.4.8 Thermal Transient Program - LION

The LION program is used to compute radial and axial thermal gradients in piping. The program calculates a time-history of vT_1, vT_2, Ta, and Tb (defined in ASME Code Section III, Subsection NB) for uniform and tapered pipe wall thickness.

3D.4.9 Engineering Analysis System - ANSYS05

The ANSYS05 computer program is a finite element large-scale general-purpose program for the solution of several classes of engineering analysis problems. Analysis capabilities include static and dynamic, plastic, creep and swelling, small and large deflections, and other applications like thermal analysis, material non-linearities, contact analysis, etc.

This program is used to perform non-linear analysis of piping systems for time varying displacements and forces due to postulated pipe breaks. Also, this program is used to perform structural analysis of pressure retaining components and civil structures against the loads and events postulated in the design specifications.

3D.4.10 Piping Analysis Program - EZPYP

EZPYP links the ANSI-7 and PISYS program together. The EZPYP program can be used to run several PISYS cases by making user-specified changes to a basic PISYS pipe model. By controlling files and PISYS runs, the EZPYP program gives the analyst the capability to perform a complete piping analysis in one computer run.

3D.4.11 Differential Displacement Program - DISPL

The DISPL program provides differential movements at each piping attachment point based on building modal displacements.

3D.5 PUMPS AND MOTORS

Following are the computer programs used in the dynamic analysis to assure the structural and functional integrity of the ESBWR pump and motor assemblies.

3D.5.1 Structural Analysis Program - SAP4G07

SAP4G07 is used to analyze the structural and functional integrity of the pump/motor systems. This program is also identified in Subsections 4.1.4.1.2, 3D.3 and 3D.6. This is a general structural analysis program for static and dynamic analysis of linear elastic complex structures. The finite-element displacement method is used to solve the displacement and stresses of each element of the structure. The structure can be composed of unlimited number of three-

dimensional truss, beam, plate, shell, solid, plane strain-plane stress and spring elements that are axisymmetric. The program can treat thermal and various forms of mechanical loading. The dynamic analysis includes mode superposition, time-history, and response spectrum analysis. Seismic loading and time-dependent pressure can be treated. The program is versatile and efficient in analyzing large and complex structural systems. The output contains displacement of each nodal point as well as stresses at the surface of each element.

3D.5.2 Effects of Flange Joint Connections - FTFLG01

The flange joints connecting the pump bowl casings are analyzed using the FTFLG01 program. This program uses the local forces and moments determined by SAP4G07 to perform flat flange calculations in accordance with the rules set forth in the ASME Code, Section III, Appendices XI and L.

3D.6 HEAT EXCHANGERS

The following computer programs are used in dynamic and static analyses to determine the structural and functional integrity of ESBWR heat exchangers.

3D.6.1 Structural Analysis Program - SAP4G07

The structural integrity of the heat exchanger is evaluated using SAP4G07. This program is described in Subsection 3D.5.1.

3D.6.2 Calculation of Shell Attachment Parameters and Coefficients - BILDR01

BILDR01 is used to calculate the shell attachment parameters and coefficients used in the stress analysis of the support to shell junction. The method per Welding Research Council Bulletin 107 is implemented in BILDR01 to calculate local membrane stress due to the support reaction loads on the heat exchanger shell.

3D.7 REFERENCES

3D-1 General Electric Co., “PISYS Analysis of NRC Benchmark Problems,” NEDO-24210, August 1979.

3D-2 USNRC, “Piping Benchmark Problems Dynamic Analysis Independent Support Motion Response Spectrum Method,” NUREG/CR-1677, August 1985.

3E. GUIDELINES FOR LEAK BEFORE BREAK APPLICATION

3E.1 INTRODUCTION

As discussed in Subsection 3.6.3, this appendix provides detailed guidelines for addressing Leak Before Break (LBB) for specific piping systems. Also included in this appendix are the fracture mechanics properties of ESBWR piping materials and analysis methods, including the leak rate calculation methods.

Piping qualified by LBB is excluded from the non-mechanistic postulation requirements of a Double Ended Guillotine Break (DEGB) specified in Subsection 3.6.3. The LBB qualification means that the throughwall flaw lengths that are detectable by leakage monitoring systems (Subsection 5.2.5) are significantly smaller than the flaw lengths that could lead to pipe rupture or instability.

The fracture mechanics properties aspects required for evaluation in accordance with Subsection 3.6.3 are addressed in Section 3E.2. The fracture mechanics techniques and methods for the determination of critical flaw lengths and evaluation of flaw stability are described in Section 3E.3. The determination of flaw lengths for detectable leakages with margin is explained in Section 3E.4. A brief discussion on the leak detection capabilities is presented in Section 3E.5.

Material selection and the deterministic LBB evaluation procedure are discussed in this section.

3E.1.1 Material Selection Guidelines

The LBB approach is applicable to piping systems for which the materials meet the following criteria:

- low probability of failure from the effects of corrosion (e.g., intergranular stress corrosion cracking); and
- adequate margin before susceptibility to cleavage type fracture over the full range of systems operating temperatures where pipe rupture could have significant consequences.

The ESBWR plant design specifies use of austenitic stainless steel piping made of material (e.g., nuclear grade or low carbon type) that is recognized as resistant to Inter-Granular Stress Corrosion Cracking (IGSCC). The carbon steel or ferritic steels specified for the reactor pressure boundary are described in Subsection 3E.2.2. These steels are assured to have adequate toughness to preclude a fracture at operating temperatures. A COL applicant is expected to supply a detailed justification in the LBB evaluation report considering system temperature, fluid velocity and environmental conditions.

3E.1.2 Deterministic Evaluation Procedure

The following deterministic analysis and evaluation is performed as an NRC-approved method to justify applicability of the LBB concept.

- Use the fracture mechanics and the leak rate computational methods that are accepted by the NRC staff, or are demonstrated accurate with respect to other acceptable computational procedures or with experimental data.

- Identify the types of materials and materials specifications used for base metal, weldments and safe ends, and provide the materials properties including toughness and tensile data, long-term effects such as thermal aging, and other limitations.
- Specify the type and magnitude of the loads applied (forces, bending and torsional moments), their source(s) and method of combination. For each pipe size in the functional system, identify the location(s), which have the least favorable combination of stress and material properties for base metal, weldments and safe ends.
- Postulate a throughwall flaw at the location(s) specified above. The size of the flaw should be large enough so that the leakage is assured detection with sufficient margin using the installed leak detection capability when pipes are subjected to normal operating loads. If auxiliary leak detection systems are relied on, they should be described. For the estimation of leakage, the normal operating loads (i.e., deadweight, thermal expansion, and pressure) are to be combined based on the algebraic sum of individual values.

  Using fracture mechanics stability analysis or limit load analysis described below, and normal plus Safe Shutdown Earthquake (SSE) loads, determine the critical crack size for the postulated throughwall crack. Determine crack size margin by comparing the selected leakage detection size crack to the critical crack size. Demonstrate that there is a margin of 2 between the leakage detection and critical crack sizes. The same load combination method selected below is used to determine the critical crack size.
- Determine margin in terms of applied loads by a crack stability analysis. Demonstrate that the leakage detection size crack does not experience unstable crack growth if 1.4 times the normal plus SSE loads are applied. Demonstrate that crack growth is stable and the final crack is limited such that a double-ended pipe break should not occur. The deadweight, thermal expansion, pressure, SSE (inertial), and Seismic Anchor Motion (SAM) loads are combined based on the same method used for the primary stress evaluation by the ASME Code. The SSE (inertial) and SAM loads are combined by Square Root of the Sum of the Squares (SRSS) method.
- The piping material toughness (J-Resistance curves) and tensile (stress-strain curves) properties are determined at temperatures near the upper range of normal plant operation.
- The specimen used to generate J-Resistance (J-R) curves is assured large enough to provide crack extensions up to an amount consistent with J/T condition determined by analysis for the application. Because practical specimen size limitations exist, the ability to obtain the desired amount of experimental crack extension may be restricted. In this case, extrapolation techniques are used as described in NUREG-1061, Volume 3, or in NUREG/CR-4575. Other techniques can be used if adequately justified.
- The stress-strain curves are obtained over the range from the preoperational limit to maximum load.
- Preferably, the materials tests should be conducted using archival materials for the pipe being evaluated. If archival material is not available, plant specific or industry wide generic material databases are assembled and used to define the required material tensile and toughness properties. Test material includes base and weld metals.

- To provide an acceptable level of reliability, generic databases are reasonable lower bounds for compatible sets of material tensile and toughness properties associated with materials at the plant. To assure that the plant specific generic database is adequate, a determination is made to demonstrate that the generic database represents the range of plant materials to be evaluated. This determination is based on a comparison of the plant material properties identified above with those of the materials used to develop the generic database. The number of material heats and weld procedures tested are adequate to cover the strength and toughness range of the actual plant materials. Reasonable lower bound tensile and toughness properties from the plant specific generic database are to be used for the stability analysis of individual materials, unless otherwise justified.

  Industry generic data bases are reviewed to provide a reasonable lower bound for the population of material tensile and toughness properties associated with any individual specification (e.g., A106, Grade B), material type (e.g., austenitic steel) or welding procedures.

  The number of material heats and weld procedures tested should be adequate to cover the range of the strength and tensile properties expected for specific material specifications or types. Reasonable lower bound tensile and toughness properties from the industry generic database are used for the stability analysis of individual materials.

  If the data are being developed from an archival heat of material, three stress-strain curves and three J-Resistance curves from the one heat of material is sufficient. The tests should be conducted at temperatures near that upper range of normal plant operation. Tests should also be conducted at a lower temperature, which may represent a plant condition (e.g., hot standby) where pipe break would present safety concerns similar to normal operation. These tests are intended only to determine if there is any significant dependence of toughness on temperature over the temperature range of interest. The lower toughness should be used in the fracture mechanics evaluation. One J-R curve and one stress-strain curve for one base metal and weld metal are considered adequate to determine temperature dependence.

- There are certain limitations that currently preclude generic use of limit load analyses to evaluate leak-before-break conditions deterministically. However, a modified limit-load analysis can be used for austenitic stainless steel piping to demonstrate acceptable margins as described in Subsection 3E.3.3.

3E.2 MATERIAL FRACTURE TOUGHNESS CHARACTERIZATION

This Subsection describes the fracture toughness properties and flow stress evaluation for the ferritic and austenitic stainless steel materials used in ESBWR plant piping, as required for evaluation according to Subsection 3E.1.2.

3E.2.1 Fracture Toughness Characterization

When the Elastic-Plastic Fracture Mechanics (EPFM) methodology or the J-T methodology is used to evaluate the leak-before-break conditions with postulated throughwall flaws, the material toughness property is characterized in the form of J-integral Resistance curve (or J-R curve) (References 3E-1, 3E-2 and 3E-3). The J-R curve, schematically shown in Figure 3E-1, represents the material's resistance to crack extension. The onset of crack extension is assumed to occur at a critical value of J. Where the plane strain conditions are satisfied, initiation J is denoted by J_{IC}. Plane strain crack conditions, achieved in test specimen by side grooving, generally provide a lower bound behavior for material resistance to stable crack growth.

Once the crack begins to extend, the increase of J with crack growth is measured in terms of slope or the nondimensional tearing modulus, T, expressed as:

$$T = \frac{E}{(\sigma_f)^2} \cdot \frac{dJ}{da} \qquad \text{(3E-1)}$$

The flow stress, σ_f, is a function of the yield and ultimate strength, and E is the elastic modulus. Generally, σ_f is assumed as the average of the yield and ultimate strength. The slope of the material J-R curve is a function of crack extension Δa. Generally, the slope decreases with crack extension thereby giving a convex upward appearance to the material J-R curve in Figure 3E-1.

To evaluate the stability of crack growth, it is convenient to represent the material J-R curve in the J-T space as shown in Figure 3E-1. The resulting curve is labeled as J-T material. Crack instability is predicted at the intersection point of the J/T material and J/T applied curves.

The crack growth variably involves some elastic unloading and distinctly nonproportional plastic deformation near the crack tip. J-integral is based on the deformation theory of plasticity (References 3E-4 and 3E-5), which inadequately models both of these aspects of plastic behavior. In order to use J-integral to characterize crack growth (i.e., to assure J-controlled crack growth), the following sufficiency condition, in terms of a nondimensional parameter proposed by Hutchinson and Paris (Reference 3E-6), is used:

$$\omega = \frac{b}{j} \cdot \frac{dJ}{da} >> 1 \qquad \text{(3E-2)}$$

where b is the remaining ligament. Reference 3E-7 suggests that $\omega > 10$ would satisfy the J-controlled growth requirements. However, if the requirements of this criteria are strictly followed, the amount of crack growth allowed would be very small in most test specimen geometries. Use of such a material J-R curve in J/T evaluation would result in grossly underpredicting the instability loads for large diameter pipes where considerable stable crack growth is expected to occur before reaching the instability point. To overcome this difficulty, Ernst (Reference 3E-8) proposed a modified J-integral J_{mod}, which was shown to be effective even when limits on ω were grossly violated. The Ernst correction essentially factors in the

effect of crack extension in the calculated value of J. This correction can be determined experimentally by measuring the usual parameters: load, displacement, and crack length.

The definition of J_{mod} is

$$J_{mod} = J - \int_{a_0}^{a} \left| \frac{\partial}{\partial a}\left(J - G_e\right) \right| \frac{da}{\delta_{pl}} \tag{3E-3}$$

where:

J = is based on deformation theory of plasticity;
G_e = is the linear elastic Griffith energy release rate of elastic J, J_{el};
δ_{pl} = is the nonlinear part of the load-point displacement (or simply the total minus the elastic displacement); and
a_0, a = are the initial and current crack length, respectively.

For the particular case of the compact tension specimen geometry, the preceding equation and the corresponding rate take the form:

$$J_{mod} = J + \int_{a_0}^{a} \gamma \cdot \frac{J_{pl}}{b} \cdot da \tag{3E-4}$$

where J_{pl} is the nonlinear part of the deformation theory J, b is the remaining ligament and γ is

$$\gamma = \left(1 + 0.76\,\frac{b}{W}\right) \tag{3E-5}$$

Consequently, the modified material tearing modulus T_{mod} can be defined as:

$$T_{mod} = T_{mat} + \frac{E}{(\sigma_f)^2}\left(\frac{\gamma}{b} \cdot J_{pl}\right) \tag{3E-6}$$

Because in most of the test J-R curves the $\omega > 10$ limit was violated, all of the material J-T data were recalculated in the J_{mod}, T_{mod} format. The J_{mod}, T_{mod} calculations were performed up to crack extension of a = 10% of the original ligament in the test specimen. The J-T curves were then extrapolated to larger J values using the method recommended in NUREG 1061, Vol. 3 (Reference 3E-9). The J_{mod} - T_{mod} approach is used in this appendix for illustrative purposes. It should be adopted if justified based on its acceptability by the technical literature. A J_D – approach is another more justifiable approach.

For terminology see References 3E-1 through 3E-3 and 3E-9.

3E.2.2 Carbon Steels and Associated Welds

The carbon steels used in the ESBWR reactor coolant pressure boundary piping are SA 106 Gr. B, SA 333 Gr. 6, and SA 672 Gr. C70. The first specification covers seamless pipe and the second one pertains to both seamless and seam-welded pipe. The last one pertains to seam-welded pipe for which plate stock is specified as SA 516. Gr. 70. The corresponding material specifications used for carbon steel flanges, fittings and forgings are equivalent to the piping specifications.

While the chemical composition requirements for a pipe per SA 106 Gr. B and SA 333 Gr. 6 are identical, the latter is subjected to two additional requirements: (1) a normalizing heat treatment

which refines the grain structure and (2) a Charpy test at –45.6°C (-50°F) with a specified minimum absorbed energy of 85.5 Nm (13 ft-lb). The electrodes and filler metal requirements for welding carbon steel to carbon or low alloy steel are as specified in Table 3E-1.

A comprehensive test program was undertaken at GE to characterize the carbon steel base and weld material toughness properties. The next section describes the scope and the results of this program.

3E.2.2.1 Fracture Toughness Test Program

The test program consisted of generating true stress-true strain curves, J-Resistance curves and the Charpy V-notch tests. Two materials were selected: (1) SA333 Gr. 6, 16-in. diameter Schedule 80 pipe and (2) SA516, Gr. 70, 1-1/4 in. thickness plate. Table 3E-2 shows the chemical composition and mechanical property test information provided by the material supplier. The materials were purchased to the same specifications as those to be used in the ESBWR applications.

To produce a circumferential butt weld, the pipe was cut in two pieces along a circumferential plane and welded back using the shielded metal arc process. The weld prep was a single V design with a backing ring. The preheat temperature was 93.3°C (200°F).

The plate material was cut along the longitudinal axis and welded back using the submerged arc weld (SAW) process. The weld prep was of a single V type with one side as vertical and the other side at 45 degrees. A backing plate was used during the welding with a clearance of 0.64 cm (1/4 inch) at the bottom of the V. The interpass temperature was maintained at less than 260°C (500°F).

Both the plate and the pipe welds were x-rayed according to Code (Reference 3E-10) requirements and were found to be satisfactory.

It is well-known that carbon steel base materials show considerable anisotropy in fracture toughness properties. The toughness depends on the orientation and direction of propagation of the crack in relation to the principal direction of mechanical working or gain flow. Thus, the selection of proper orientation of Charpy and J-R curve test specimen is important. Figure 3E-2 shows the orientation code for rolled plate and pipe specimen as given in ASTM Standard E399 (Reference 3E-11). Because a throughwall circumferential crack configuration is of most interest from the Double Ended Guillotine Break (DEGB) point of view, the L-T specimen in a plate and the L-C specimen in a pipe provide the appropriate toughness properties for that case. On the other hand, T-L and C-L specimens are appropriate for the axial flaw case.

Charpy test data are reviewed first because they provide a qualitative measure of the fracture toughness.

Charpy Tests

The absorbed energy or its complement, the lateral expansion measured during a Charpy V-notch test provides a qualitative measure of the material toughness. For example, in the case of austenitic stainless steel flux weldments, the observed lower Charpy energy relative to the base metal was consistent with the similar trend observed in the J-Resistance curves. The Charpy tests in this program were used as preliminary indicators of relative toughness of welds, heat-affected zones (HAZs) and the base metal.

The carbon steel base materials exhibit considerable anisotropy in the Charpy energy as illustrated by Figure 3E-3 from Reference 3E-12. This anisotropy is associated with development of grain flow due to mechanical working. The Charpy orientation C in Figure 3E-3 (orientations LC and LT in Figure 3E-2) is the appropriate one for evaluating the fracture resistance to the extension of a throughwall circumferential flaw. The upper shelf Charpy energy associated with axial flaw extension (orientation A in Figure 3E-3) is considerably lower than that for the circumferential crack extension.

A similar trend in the base metal Charpy energies was also noted in this test program. Figure 3E-4 and Figure 3E-5 show the pipe and plate material Charpy energies for the two orientations as a function of temperature. The tests were conducted at six temperatures ranging from room temperature to 288°C (550°F). From the trend of the Charpy energies as a function of temperature in Figure 3E-4 and Figure 3E-5 it is clear that even at room temperature the upper shelf conditions have been reached for both the materials.

No such anisotropy is expected in the weld metal because it does not undergo any mechanical working after its deposition. This conclusion is also supported by the available data in the technical literature. The weld metal Charpy specimens in this test program were oriented the same way as the LC or LT orientations in Figure 3E-2. The Heat Affected Zone (HAZ) Charpy specimens were also oriented similarly.

Figure 3E-6 shows a comparison of the Charpy energies from the SA333 Gr. 6 base metal, the weld metal and the HAZ. In most cases two specimens were used. Considerable scatter in the weld and HAZ Charpy energy values is seen. Nevertheless, the average energies for the weld metal and the HAZ seem to fall at or above the average base metal values. This indicates that, unlike the stainless steel flux weldments, the fracture toughness of carbon steel weld and HAZ, as measured by the Charpy tests, is at least equal to the carbon steel base metal.

The preceding results and the results of the stress-strain tests discussed in the next section or other similar data are used as a basis to choose between the base and the weld metal properties for use in the J-T methodology evaluation.

Stress-Strain Tests

The stress-strain tests were performed at three temperatures: room temperature, 177°C (350°F), and 288°C (550°F). Base and weld metal from both the pipe and the plate were tested. The weld specimens were in the as-welded condition. The standard test data obtained from these tests are summarized in Table 3E-3.

An examination of Table 3E-3 shows that the measured yield strength of the weld metal, as expected, is considerably higher than that of the base metal. For example, the 288°C (550°F) yield strength of the weld metal in Table 3E-3 ranges from 358.6 MPa (52 ksi) to 406.8 MPa (59 ksi), whereas the base metal yield strength is only 234.5 MPa (34 ksi). The impact of this observation in the selection of appropriate material (J/T) curve is discussed in later sections.

Figure 3E-7 through Figure 3E-10 show the plots of the 288°C (550°F) and 177°C (350°F) stress-strain curves for both the pipe and the plate used in the test. As expected, the weld metal stress-strain curve in every case is higher than the corresponding base metal curve. The Ramberg-Osgood format characterization of these stress-strain curves is given in Subsection 3E.3.2 where appropriate values of α and n are also provided.

J-R Curve Tests

The test temperatures selected for the J-R curve tests were: room temperature, 177°C (350°F), and 288°C (550°F). Both the weld and the base metal were included. Due to the curvature, only the 1T plan compact tension (CT) specimens were obtained from the 0.41 m (16-in). diameter test pipe. Both 1T and 2T plan test specimens were prepared from the test plate. All of the CT specimens were side-grooved to produce plane strain conditions.

Table 3E-4 shows some details of the J-R curve tests performed in this test program. The J-R curve in the LC orientation of the pipe base metal and in the LT orientation of the plate base metal represent the material's resistance to crack extension in the circumferential direction. Thus, the test results of these orientations were used in the LBB evaluations. The orientation effects are not present in the weld metal. As an example of the J-R curve obtained in the test program, Figure 3E-11 shows the plot of J-R curve obtained from specimen OWLC-A.

3E.2.2.2 Material (J/T) Curve Selection

The normal operating temperatures for most of the carbon steel piping in the reactor coolant pressure boundary in the ESBWR generally fall into two categories: 274°C (528°F) to 288°C (550°F) and 216°C (420°F). The latter temperature corresponds to the operating temperature of the feedwater piping system. The selections of the appropriate material (J/T) curves for these two categories are discussed next.

Material J/T Curve for 288°C (550°F)

A review of the test matrix in Table 3E-4 shows that five tests were conducted at 288°C (550°F). Two tests were on the weld metal, two were on the base metal, and one was on the heat-affected zone. Figure 3E-12 shows the plot of material J_{mod}, T_{mod} values calculated from the J-Δa values obtained from the 288°C (550°F) tests. The value of flow stress, σ_f, used in the tearing modulus calculation (Equation 3E-1) was 358.5 MPa (52.0 ksi) based on data shown in Table 3E-3. To convert the deformation J and dJ/da values obtained from the J-R curve into J_{mod}, $T_{mod.}$ Equations 3E-4 and 3E-6 were used. Only the data from the pipe weld (Specimen ID OWLC-A) and the plate base metal (Specimen ID BMLI-12) are shown in Figure 3E-12. A few unreliable data points were obtained in the pipe base metal (Specimen ID OBLC-3) J-R curve test because of a malfunction in the instrumentation. Therefore, the data from this test were not included in the evaluation. The J-R curves from the other two 288°C (550°F) tests were evaluated as described in the next paragraph. For comparison purposes, Figure 3E-12 also shows the SA106 carbon steel J-T data obtained from the J-R curve reported by Gudas (Reference 3E-13). The curve also includes extrapolation to higher J values based on the method recommended in NUREG 1061, Vol. 3 (Reference 3E-9).

The J_{mod} - T_{mod} data for the plate weld metal and the plate HAZ were evaluated. A comparison shows that these data fall slightly below those for the plate base metal shown in Figure 3E-12. On the other hand, as noted in Subsection 3E.2.2.1, the yield strength of the weld metal and the HAZ is considerably higher than that of the base metal. The material stress-strain and J-T curves are the two key inputs in determining the instability load and flaw values by the (J/T) methodology. Calculations performed for representative throughwall flaw sizes showed that the higher yield strength of the weld metal more than compensates for the slightly lower J-R curve and, consequently, the instability load and flaw predictions based on base metal properties are

smaller (i.e., conservative). Accordingly, it was concluded that the material (J-T) curve shown in Figure 3E-12 is the appropriate one to use in the LBB evaluations for carbon steel piping at 288°C (550°F).

Material J/T Curve for 216°C (420°F)

Because the test temperature of 177°C (350°F) can be considered reasonably close to the 216°C (420°F), the test J-R curves for 177°C (350°F) were used in this case. A review of the test matrix in Table 3E-4 shows that three tests were conducted at 177°C (350°F). The J_{mod}, T_{mod} data for all three tests were reviewed. The flow stress value used in the tearing modulus calculation was 372.4 MPa (54 ksi) based on Table 3E-3. Also reviewed were the data on SA106 carbon steel at 300°F reported by Gudas (Reference 3E-13).

Consistent with the trend of the 288°C (550°F) data, the 177°C (350°F) weld metal (J-T) data fell below the plate and pipe base metal data. This probably reflects the slightly lower toughness of the SAW weld in the plate. The (J/T) data for the pipe base metal fell between the plate base metal and the plate weld metal. Based on the considerations similar to those presented in the previous section, the pipe base metal J-T data, although they may lie above the weld J-T data, were used for selecting the appropriate (J-T) curve. Accordingly, the curve shown in Figure 3E-13 was developed for using the (J-T) methodology in evaluations at 216°C (420°F).

3E.2.3 Stainless Steels and Associated Welds

The stainless steels used in the ESBWR reactor coolant pressure boundary piping are either nuclear grade or low carbon Type 304 or 316. These materials and the associated welds are highly ductile and, therefore, undergo considerable plastic deformation before failure can occur. Toughness properties of Type 304 and 316 stainless steels have been extensively reported in the open technical literature and are, thus, not discussed in detail in this section. Due to high ductility and toughness, modified limit load methods can be used to determine critical crack lengths and instability loads (Subsection 3E.3.3).

3E.3 FRACTURE MECHANICS METHODS

This Subsection deals with the fracture mechanics techniques and methods for the determination of critical flaw lengths and instability loads for materials used in ESBWR. These techniques and methods comply with criteria described in Subsection 3E.1.2.

3E.3.1 Elastic-Plastic Fracture Mechanics or (J/T) Methodology

Failure in ductile materials such as highly tough ferritic materials is characterized by considerable plastic deformation and significant amount of stable crack growth. The EPFM approach outlined in this Subsection considers these aspects. Two key concepts in this approach are (1) J-integral (References 3E-14 and 3E-15) which characterizes the intensity of the plastic stress-strain field surrounding the crack tip and (2) the tearing instability theory (References 3E-16 and 3E-17) which examines the stability of ductile crack growth. A key advantage of this approach is that the material fracture toughness characteristic is explicitly factored into the evaluation.

3E.3.1.1 Basic (J/T) Methodology

Figure 3E-14 schematically illustrates the J/T methodology for stability evaluation. The material (J/T) curve in Figure 3E-14 represents the material's resistance to ductile crack extension. Any value of J falling on the material R-curve is denoted as J_{mat} and is a function solely of the increase in crack length Δa. Also defined in Figure 3E-14 is the "applied" J, which for given stress-strain properties and overall component geometry, is a function of the applied load P and the current crack length, a. Hutchinson and Paris (Reference 3E-17) also define the following two nondimensional parameters:

$$T_{applied} = \frac{E}{(\sigma_f)^2} \cdot \frac{\partial J_{applied}}{\partial a}$$

$$T_{mat} = \frac{E}{(\sigma_f)^2} \cdot \frac{dJ_{mat}}{da} \qquad \text{(3E-7)}$$

where E is Young's modulus and σ_f is an appropriate flow stress.

Intersection point of the material and applied (J/T) curves denotes the instability point. This is mathematically stated as:

$$J_{applied}\left(a, P\right) = J_{mat}\left(a\right)\big) \qquad \text{(3E-8)}$$

$$T_{applied} < T_{mat}(\text{stable})$$

$$T_{applied} > T_{mat}(\text{unstable}) \qquad \text{(3E-9)}$$

The load at instability is determined from the J versus load plot also shown schematically in Figure 3E-14. Thus, the three key curves in the tearing stability evaluation are: $J_{applied}$ versus $T_{applied}$, J_{mat} versus T_{mat} and $J_{applied}$ versus load. The determination of appropriate J_{mat} versus T_{mat} or the material (J/T) curve has been already discussed in Subsection 3E.2.1. The $J_{applied} - T_{applied}$ or the (J/T) applied curve can be easily generated through perturbation in the crack length once the $J_{applied}$ versus load information is available for different crack lengths. Therefore, only the methodology for the generation of $J_{applied}$ versus load information is discussed in detail.

3E.3.1.2 J Estimation Scheme Procedure

The $J_{applied}$ or J as a function of load was calculated using the GE/EPRI estimation scheme procedure (References 3E-18 and 3E-19). The J in this scheme is obtained as sum of the elastic and fully plastic contributions:

$$J = J_e + J_p \tag{3E-10}$$

The material true stress-strain curve in the estimation scheme is assumed to be in the Ramberg-Osgood format:

$$\left(\frac{\varepsilon}{\varepsilon_0}\right) = \left(\frac{\sigma}{\sigma_0}\right) + \alpha\left(\frac{\sigma}{\sigma_0}\right)^n \tag{3E-11}$$

where σ_0 is the material yield stress, $\varepsilon_0 = \sigma/E_0$, and α and n are obtained by fitting the preceding equation to the material true stress-strain curve.

The estimation scheme formulas to evaluate the J-integral for a pipe with a throughwall circumferential flaw subjected to pure tension or pure bending are as follows:

Tension

$$J = f_1\left(a_e, \frac{R}{t}\right)\frac{P^2}{E} + \alpha\sigma_0\varepsilon_0 c\left(\frac{a}{b}\right)h_1\left(\frac{a}{b}, n, \frac{R}{t}\right)\left[\frac{P}{P_0}\right]^{n+1} \tag{3E-12}$$

where:

$$f_1\left(\frac{a}{b}, n, \frac{R}{t}\right) = \frac{aF^2\left(\frac{a}{b}, n, \frac{R}{t}\right)}{4\pi R^2 t^2}$$

$$P_0 = 2\sigma_0 Rt\left[\pi - \gamma - 2\,\text{asin}\left(\frac{1}{2}\sin\gamma\right)\right]$$

Bending

$$J = f_1\left(a_e, \frac{R}{t}\right)\frac{M^2}{E} + \alpha\sigma_0\varepsilon_0 c\left(\frac{a}{b}\right)h_1\left(\frac{a}{b}, n, \frac{R}{t}\right)\left[\frac{M}{M_0}\right]^{n+1} \tag{3E-13}$$

where:

$$f_1\left(\frac{a}{b}, n, \frac{R}{t}\right) = \pi a\left(\frac{R}{I}\right)^2 F^2\left(\frac{a}{b}, n, \frac{R}{t}\right)$$

$$M_0 = M_0\left[\cos\left(\frac{\gamma}{2}\right) - \frac{1}{2}\sin(\gamma)\right]$$

The non-dimensional functions f and h are given in Reference 3E-19.

While the calculation of J for given α, n, σ_0 and load type is reasonably straightforward, one issue that needs to be addressed is the tearing instability evaluation when the loading includes both the membrane and the bending stresses. The estimation scheme is capable of evaluating only one type of stress at a time.

This aspect is addressed next.

3E.3.1.3 Tearing Instability Evaluation Considering Both the Membrane and Bending Stresses

Based on the estimation scheme formulas and the tearing instability methodology just outlined, the instability bending and tension stresses can be calculated for various throughwall circumferential flaw lengths. Figure 3E-15 shows a schematic plot of the instability stresses as a function of flaw length. For the same stress level, the allowable flaw length for the bending is expected to be larger than the tension case.

When the applied stress is a combination of the tension and bending, a linear interaction rule is used to determine the instability stress or conversely the critical flaw length. The application of linear interaction rule is certainly conservative when the instability load is close to the limit load. The applicability of this proposed rule should be justified by providing a comparison of the predictions by the proposed approach (or an alternate approach) with those available for cases where the membrane and bending stresses are treated together.

The interaction formulas follow: (See Figure 3E-15)

Critical Flaw Length

$$a_c = \frac{(\sigma_t)}{\sigma_t + \sigma_b} a_{c,t} + \frac{(\sigma_b)}{\sigma_t + \sigma_b} a_{c,b} \qquad \text{(3E-14)}$$

where:

σ_t = applied membrane stress

σ_b = applied bending stress

$a_{c,t}$ = critical flaw length for a tension stress of $(\sigma_t + \sigma_b)$

$a_{c,b}$ = critical flaw length for a bending stress of $(\sigma_t + \sigma_b)$

Instability Bending Stress

$$S_b = \left(1 - \frac{\sigma_t}{\sigma'_t}\right)\sigma'_b \qquad \text{(3E-15)}$$

where:

S_b = instability bending stress for flaw length, a, in the presence of membrane stress, σ_t

σ_t = applied membrane stress

σ'_t = instability tension stress for flaw length, a

σ'_b = instability bending stress for flaw length, a

Once the instability bending stress, S_b, in the presence of membrane stress, σ_t, is determined, the instability load margin corresponding to the detectable leak-size crack (as required by LBB criterion in Subsection 3.6.3) can be calculated as follows:

$$\frac{\sigma_t + S_b}{\sigma_t + \sigma_b} \qquad (3E\text{-}16)$$

It is assumed in the preceding equation that the uncertainty in the calculated applied stress is essentially associated with the stress because of applied bending loads and that the membrane stress, which is generally due to the pressure loading, is known with greater certainty. This method of calculating the margin against loads is also consistent with the definition of load margin employed in Paragraph IWB-3640 of Section XI of Reference 3E-20.

3E.3.2 Application of (J/T) Methodology to Carbon Steel Piping

From Figure 3E-3, it is evident that carbon steels exhibit transition temperature behavior marked by three distinct stages: lower shelf, transition, and upper shelf. The carbon steels generally exhibit ductile failure mode at or above upper shelf temperatures. This would suggest that a net-section collapse approach may be feasible for the evaluation of postulated flaws in carbon steel piping. Such a suggestion was also made in a review report prepared by the Naval Research Lab (Reference 3E-21). Low temperature (i.e., less than 51.7ºC (125°F)) pipe tests conducted by GE (Reference 3E-22) and by Vassilaros (Reference 3E-23) which involved circumferentially cracked piping subjected to bending and/or pressure loading, also indicate that a limit load approach is feasible. However, test data at high temperatures, especially involving large diameter pipes, are currently not available. Therefore, a (J/T) based approach is used in the evaluation.

3E.3.2.1 Determination of Ramberg-Osgood Parameters for 288ºC (550°F) Evaluation

Figure 3E-7 shows the true stress-true strain curves for the carbon steels at 288ºC (550°F). The same data is plotted here in Figure 3E-16 in the Ramberg-Osgood format. It is seen that, unlike the stainless steel case, each set for stress-strain data (i.e., data derived from one stress-strain curve) follows approximately a single slope line. Based on the visual observation, a line representing $\alpha = 2$, $n = 5$ in Figure 3E-16 was drawn as representing a reasonable upper bound to the data shown.

The third parameter in the Ramberg-Osgood format stress-strain curve is σ_0, the yield stress. Based on the several internal GE data on carbon steels, such as SA 333 Gr. 6 and SA 106 Gr. B, a reasonable value of 288ºC (550°F) yield strength was judged as 238.6 MPa (34,600 psi). To summarize, the following values are used in this appendix for the (J/T) methodology evaluation of carbon steels at 288ºC (550°F):

α = 2.0

n = 5.0

σ_0 = 238.6 MPa (34,600 psi)

E = 1.79×10^5 MPa (26×10^6 psi)

3E.3.2.2 Determination of Ramberg-Osgood Parameters for 216ºC (420°F) Evaluation

Figure 3E-17 shows the Ramberg-Osgood (R-O) format plot of the 177ºC (350°F) true stress-strain data on the carbon steel base metal. Also shown in Figure 3E-17 are the CE data and SA 106 Gr. B at 204ºC (400°F). Because the difference between the ASME Code Specified minimum yield strength at 177ºC (350°F) and 216ºC (420°F) is small, the 177ºC (350°F) stress-

strain data were considered applicable in the determination of R-O parameters for evaluation at 216ºC (420°F).

A review of Figure 3E-17 indicates that the majority of the data associated with any one test can be approximated by one straight line.

It is seen that some of the data points associated with the yield point behavior fall along the y-axis. However, these data points at low strain level were not considered significant and, therefore, were not included in the R-O fit.

The 177ºC (350°F) yield stress for the base material is given in Table 3E-3 as 261.2 MPa (37.9 ksi). Because the difference between the ASME Code specified minimum yield strengths of pipe and plate carbon steels at 216ºC (420°F) and 177ºC (350°F) is roughly 6.18 MPa (0.9 ksi), the σ_o value for use at 216ºC (420°F) are chosen as 261.2–6.18 MPa (37.9–0.9 ksi) or 255.0 MPa (37 ksi). In summary, the following values of R-O parameters are used for evaluation of 216ºC (420°F):

σ_0 = 255.1 MPa (37,000 psi)

α = 5.0

n = 4.0

3E.3.3 Modified Limit Load Methodology for Austenitic Stainless Steel Piping

Reference 3E-24 describes a modified limit load methodology that may be used to calculate the critical flaw lengths and instability loads for austenitic stainless steel piping and associated welds. If appropriate, this or an equivalent methodology may be used in place of the (J/T) methodology described in Subsection 3E.3.1.

3E.3.4 Bimetallic Welds

For joining austenitic stainless steels to ferritic steels, the Ni-Cr-Fe Alloys 82 or 182 are generally used for weld metals. The procedures recommended in Section 3E.3.3 for the austenitic stainless steel welds are also applicable to these weld metals. This is justified based on the common procedures adopted for flaw acceptance in the ASME Code Section XI, Article IWB-3600 and Appendix C, for both types of the welds. If other types of bimetallic metals are used, proper procedures should be used with generally acceptable justifications.

3E.4 LEAK RATE CALCULATION METHODS

Leak rates of high pressure fluids through cracks in pipes are a complex function of crack geometry, crack surface roughness, applied stresses, and inlet fluid thermodynamic state. Analytical predictions of leak rates essentially consist of two separate tasks: calculation of the crack opening area, and the estimation of the fluid flow rate per unit area. The first task requires the fracture mechanics evaluations based on the piping system stress state. The second task involves the fluid mechanics considerations in addition to the crack geometry and its surface roughness information. Each of these tasks is now discussed separately considering the type of fluid state in ESBWR piping.

3E.4.1 Leak Rate Estimation for Pipes Carrying Water

EPRI-developed computer code PICEP (Reference 3E-25) may be used in the leak rate calculations. The basis for this code and comparison of its leak rate predictions with the experimental data is described in References 3E-26 and 3E-27. This code has been used in the successful application of LBB to primary piping system of a PWR. The basis for flow rate and crack opening area calculations in PICEP is briefly described first. A comparison with experimental data is shown next.

Other methods (e.g., Reference 3E-28) may be used for leak rate estimation at the discretion of the applicant.

3E.4.1.1 Description of Basis for Flow Rate Calculation

The thermodynamic model implemented in PICEP computer program assumes the leakage flow through pipe cracks to be isentropic and homogeneous, but it accounts for non-equilibrium "flashing" transfer process between the liquid and vapor phases.

Fluid friction-caused surface roughness of the walls and curved flow paths has been incorporated in the model. Flows through both parallel and convergent cracks can be treated. The model uses some approximations and empirical factors, which were confirmed by comparison against test data because of the complicated geometry within the flow path.

For given stagnation conditions and crack geometries, the leak rate and exit pressure are calculated using an iterative search for the exit pressure starting from the saturation pressure corresponding to the upstream temperature and allowing for friction, gravitational, acceleration and area change pressure drops. The initial flow calculation is performed when the critical pressure is lowered to the backpressure without finding a solution for the critical mass flux.

A conservative methodology was developed to handle the phase transformation into a two-phase mixture or superheated steam through a crack. To make the model continuous, a correction factor was applied to adjust the mass flow rate of a saturated mixture to be equal to that of a slightly sub-cooled liquid. Similarly, a correction factor was developed to ensure continuity as the steam became superheated. The superheated model was developed by applying thermodynamic principles to an isentropic expansion of the single phase steam.

The code can calculate flow rates through fatigue or IGSCC cracks and has been verified against data from both types. The crack surface roughness and the number of bends account for the difference in geometry of the two types of cracks. The guideline for predicting leak rates through IGSCCs when using this model was based on obtaining the number of turns that give the

best agreement for Battelle Phase II test data of Collier et al. (Reference 3E-29). For fatigue cracks, it is assumed that the crack path has no bends.

3E.4.1.2 Basic for Crack Opening Area Calculation

The crack opening area in PICEP code is calculated using the estimation scheme formulas. The plastic contribution to the displacement is computed by summing the contributions of bending and tension alone, a procedure that underestimates the displacement from combined tension and bending. However, the plastic contribution is expected to be insignificant because the applied stresses at normal operation are generally such that they do not produce significant plasticity at the cracked location.

3E.4.1.3 Comparison Verification with Experimental Data

Figure 3E-18 from Reference 3E-27 shows a comparison PICEP prediction with measured leak rate data. It is seen that PICEP predictions are virtually always conservative (i.e., the leak flow rate is under-predicted).

3E.4.2 Flow Rate Estimation for Saturated Steam

3E.4.2.1 Evaluation Method

The calculations for this case were based on the maximum two-phase flow model developed by Moody (Reference 3E-30). However, in an LBB-report, a justification should be provided by comparing the predictions of this method with the available experimental data, or a generally acceptable method, if available, should be used. The Moody model predicts the flow rate of steam-water mixtures in vessel blowdown from pipes (see Figure 3E-19). A key parameter that characterized the flow passage in the Moody analysis is fL/D_h, where f is the coefficient of friction, L, the length of the flow passage and D_h, the hydraulic diameter. The hydraulic diameter for the case of flow through a crack is 2δ where δ is the crack opening displacement and the length of the flow passage is t, the thickness of the pipe. Thus, the parameter fL/D_h in the Moody analysis was interpreted as $ft/2\delta$ for the purpose of this evaluation.

Figure 3E-20 shows the predicted mass flow rates by Moody for fL/D_h of 0 and 1. Similar plots are given in Reference 3E-30 for additional fL/D_h values of 2 through 100. Because the steam in the ESBWR main steam lines would be essentially saturated, the mass flow rate corresponding to the upper saturation envelope line is the appropriate one to use. Table 3E-5 shows the mass flow rates for a range of fL/D_h values for a stagnation pressure of 6.62 MPa (960 psi) which is roughly equal to the pressure in an ESBWR piping system carrying steam.

A major uncertainty in calculating the leakage rate is the value of f. This is discussed next.

3E.4.2.2 Selection of Appropriate Friction Factor

Typical relationships between Reynolds number and relative roughness ε/D_h, the ratio of effective surface protrusion height to hydraulic diameter, were relied upon in this case. Figure 3E-21, from Reference 3E-31, graphically shows such a relationship for pipes. The ε/D_h ratio for pipes generally ranges from 0 to 0.50. However, for a fatigue crack consisting of rough fracture surfaces represented by a few mils, the roughness height ε at some location may be almost as much as δ. In such cases, ε/D_h would seem to approach one-half. There are no data or any analytical model for such cases, but a crude estimate based on the extrapolation of the results

in Figure 3E-21 would indicate that f may be of the order of 0.1 to 0.2. For this evaluation an average value of 0.15 was used with the modification as discussed next.

For blowdown of saturated vapor, with no liquid present, Moody states that the friction factor should be modified according to

$$f_g = f_{GSP}\left(\frac{\upsilon_f}{\upsilon_g}\right)^{1/3} \quad \text{(3E-17)}$$

where:

f_g = modified friction factor

f_{GSP} = factor for single phase

$\frac{\upsilon_f}{\upsilon_g}$ = liquid/vapor specific volume ratio evaluated at an average static pressure in the flow path

This correction is necessary because the absence of a liquid film on the walls of the flow channel at high quality makes the two-phase flow model invalid as it stands. The average static pressure in the flow path is going to be something in excess of 3.31 MPa (480 psia) if the initial pressure is 6.62 MPa (960 psia); this depends on the amount of flow choking and can be determined from Reference 3E-30. However, a fair estimate of $(v_f/v_g)^{1/3}$ is 0.3, so the friction factor for saturated steam blowdown may be taken as 0.3 of that for mixed flow.

Based on this discussion, a coefficient of friction of 0.15 x 0.3 =0.45 was used in the flow rate estimation. Currently experimental data are unavailable to validate this assumed value of coefficient of friction.

3E.4.2.3 Crack Opening Area Formulation

The crack opening areas were calculated using LEFM procedures with the customary plastic zone correction. The loadings included in the crack opening area calculations were: pressure, weight, and thermal expansion.

The mathematical expressions given by Paris and Tada (Reference 3E-32) are used in this case. The crack opening areas for pressure (A_p) and bending stresses (A_b) were separately calculated and then added together to obtain the total area (A_c).

For simplicity, the calculated membrane stresses from weight and thermal expansion loads were combined with the axial membrane stress, σ_p, due to the pressure.

The formulas are summarized below:

$$A_p = \frac{\sigma_p}{E}(2\pi Rt)G_p(\gamma) \quad \text{(3E-18)}$$

where:

σ_p = axial membrane stress caused by pressure, weight and thermal expansion loads

E = Young's modulus

R = pipe radius

t = pipe thickness

λ = shell parameter = $\frac{a}{\sqrt{Rt}}$

a = half crack length

$$G_p(\lambda) = \lambda^2 + 0.16\lambda^4 (0 \le \lambda \le 1)$$
$$= 0.02 + 0.81\lambda^2 + 0.30\lambda^3 + 0.03\lambda^4 (1 \le \lambda \le 5) \quad \text{(3E-19)}$$

$$A_b = \frac{\sigma_b}{E} \cdot \pi \cdot R^2 \cdot \frac{(3 + \cos\theta)}{4} I_t(\theta) \quad \text{(3E-20)}$$

where:

σ_b = bending stress caused by weight and thermal expansion loads

θ = half crack angle

$$I_t(\theta) = 2\theta^2 \left[1 + \left(\frac{\theta}{\pi}\right)^{3/2} \left\{ 8.6 - 13.3\left(\frac{\theta}{\pi}\right) + 24\left(\frac{\theta}{\pi}\right)^2 \right\} + \left(\frac{\theta}{\pi}\right)^3 \right.$$
$$\left. \left\{ 22.5 - 75\left(\frac{\theta}{\pi}\right) + 205.7\left(\frac{\theta}{\pi}\right)^2 - 247.5\left(\frac{\theta}{\pi}\right)^3 + 242\left(\frac{\theta}{\pi}\right)^4 \right\} \right] (0 < \theta < 100^0) \quad \text{(3E-21)}$$

The plastic zone correction was incorporated by replacing a and θ in these formulas by a_{eff} and θ_{eff} which are given by

$$\theta_{eff} = \theta + \frac{(K_{total})^2}{(2\pi R\sigma_Y)^2}$$
$$a_{eff} = \theta_{eff} \cdot R \quad \text{(3E-22)}$$

The yield stress, σ_y, was conservatively assumed as the average of the code specified yield and ultimate strength. The stress intensity factor, K_{total}, includes contribution caused by both the membrane and bending stress and is determined as follows:

$$K_{total} = K_m + K_b \quad \text{(3E-23)}$$

where:

K_m = $\sigma_p \cdot \sqrt{a} \, . F_p(\lambda)$

$F_{p(\lambda)}$ = $\left(1 + 0.3225\,\lambda^2\right)^{1/2} (0 \le \lambda \le 1)$

$= 0.9 + 0.25\,\lambda \, (1 \le \lambda \le 5)$

K_b = $\sigma_b \cdot \sqrt{\pi a} \cdot F_b(\theta)$

$F_{b(\theta)}$ = $1 + 6.8\left(\frac{\theta}{\pi}\right)^{3/2} - 13.6\left(\frac{\theta}{\pi}\right)^{5/2} + 20\left(\frac{\theta}{\pi}\right)^{7/2} (0 \le \theta \le 100^0)$

The steam mass flow rate, M, shown in Table 3E-5 is a function of parameter, ft/2δ. Once the mass flow rate is determined corresponding to the calculated value of this parameter, the leak rate in gpm can then be calculated.

3E.5 LEAK DETECTION CAPABILITIES

A complete description of various leak detection systems is provided in Subsection 5.2.5. The leakage detection system gives separate considerations to: leakage within the drywell and leakage external to the drywell. The limits for reactor coolant leakage are described in Subsection 5.2.5.4.

The total leakage in the drywell consists of the identified leakage and the unidentified leakage. The identified leakage is that from pumps, valve stem packings, reactor vessel head seal and other seals, which all discharge to the equipment drain sump. The Technical Specifications (TS) limit on the identified leak rate is 114 Liters/min (25 gpm).

The unidentified leak rate in the drywell is the portion of the total leakage received in the drywell sumps that is not identified as previously described. As specified in subsection 5.2.5.2, the detection capability for unidentified leak rate is 3.8 Liters/min (1 gpm). To cover uncertainties in leak detection capability, although it meets Regulatory Guide 1.45 guidelines, a margin factor of 10 is required per Reference 3E-24 to determine a reference leak rate. A reduced margin factor may be used if accounts can be made of effects of sources of uncertainties such as plugging of the leakage crack with particulate material over time, leakage prediction, measurement techniques, personnel, and frequency of monitoring. For the piping in drywell, a reference leak rate of 37.85 L/min (10 gpm) may be used, unless a smaller rate can be justified.

The sensitivity and reliability of leakage detection systems used outside the drywell must be demonstrated to be equivalent to Regulatory Guide 1.45 systems. Methods that have been shown to be acceptable include local leak detection, for example, visual observation or instrumentation. Outside the drywell, the leakage rate detection and the margin factor depend upon the design of the leakage detection systems.

3E.6 REFERENCES

3E-1 P. C. Paris, H. Tada, A. Zahoor, and H. Ernst, "The Theory of Instability of the Tearing Mode of Elastic-Plastic Crack Growth, Elastic-Plastic Fracture," ASTM STP 668, J. D. Landes, J. A. Begley, and G. A. Clarke, Eds., American Society for Testing Materials, 1979, pp. 5-36.

3E-2 USNRC, "Resolution of the Task A-11 Reactor Vessel Materials Toughness Safety Issue," NUREG-0744, Rev. 1 October 1982.

3E-3 P. C. Paris, and R. E. Johnson, "A Method of Application of Elastic-Plastic Fracture Mechanics to Nuclear Vessel Analysis, Elastic-Plastic Fracture, Second Symposium, Volume II-Fracture Resistance Curves and Engineering Application," ASTM STP 803, C. F. Shih and J. P. Gudas, Eds., American Society for Testing and Materials, 1983, pp. 11-5 through 11-40.

3E-4 J. R. Rice, "A Path Independent Integral and the Approximate Analysis of Strain Concentration by Notches and Cracks," J. Appl. Mech., 35, 379–386 (1968).

3E-5 J. A. Begley, and J. D. Landes, "The J Integral as a Fracture Criterion, Fracture Toughness, Proceedings of the 1971 National Symposium on Fracture Mechanics," Part II, ASTM STP 514, American Society for Testing Materials, pp. 1-20 (1972).

3E-6 J. W. Hutchinson, and P. C. Paris, "Stability Analysis of J-Controlled Crack Growth, Elastic-Plastic Fracture," ASTM STP 668, J. D. Landes, J. A. Begley, and G. A. Clarke, Eds., American Society for Testing and Materials, 1979, pp. 37-64.

3E-7 Electric Power Research Institute, V. Kumar, M. D. German, and C. F. Shih, "An Engineering Approach for Elastic-Plastic Fracture Analysis," EPRI Topical Report NP-1831, July 1981.

3E-8 H. A. Ernst, "Material Resistance and Instability Beyond J-Controlled Crack Growth, Elastic-Plastic Fracture: Second Symposium, Volume I—Inelastic Crack Analysis," ASTM STP 803, C. F. Shih and J. P. Gudas, Eds., American Society for Testing and Materials, 1983, pp. I-191 through I-213.

3E-9 USNRC, "Report of the U.S. Nuclear Regulatory Commission Piping Review Committee," NUREG-1061, Vol. 3, November 1984.

3E-10 ASME, ASME Boiler & Pressure Vessel Code, Section III, Division 1, "Nuclear Power Plant Components.

3E-11 ASTM Standard E399, "Plane-Strain Fracture Toughness of Metallic Materials."

3E-12 AEC, M.B. Reynolds, "Failure Behavior in ASTM A106B Pipes Containing Axial Through-Wall Flaws," GEAP-5620, AEC Research and Development Report, April 1968.

3E-13 USNRC, J. P. Gudas, and D. R. Anderson, "JI-R Curve Characteristics of Piping Material and Welds," NUREG/CP-0024, Vol. 3, March 1982.

3E-14 J. R. Rice, "A Path Independent Integral and the Approximate Analysis of Strain Concentration," Notches and Cracks, J. Appl. Mech., 35, 379, 386 (1968).

3E-15 J. A. Begley, and J. D. Landes, "The J Integral as a Fracture Criterion, Fracture Toughness, Proceedings of the 1971 National Symposium on Fracture Mechanics," Part II, ASTM STP 514, American Society for Testing Materials, pp. 1-20 (1972).

3E-16 P.C. Paris, H. Tada, A. Zahoor, and H. Ernst, "The Theory of Instability of the Tearing Mode of Elastic-Plastic Crack Growth, Elastic-Plastic Fracture," ASTM STP 668, J.D. Landes, J. A. Begley, and G. A. Clarke, Eds., American Society for Testing Materials, 1979, pp. 5-36.

3E-17 J.W. Hutchinson, and P.C. Paris, "Stability Analysis of J-Controlled Crack Growth, Elastic-Plastic Fracture," ATSM STP 668, J. D. Landes, J. A. Begley, and G. A. Clarke, Eds., American Society for Testing and Materials, 1979, pp. 37-64.

3E-18 Electric Power Research Institute, V. Kumar, M. D. German, and C. F. Shih, "An Engineering Approach for Elastic-Plastic Fracture Analysis," EPRI Topical Report NP-1831, July 1981.

3E-19 Electric Power Research Institute, "Advances in Elastic-Plastic Fracture Analysis," EPRI Report No. NP-3607, August 1984.

3E-20 ASME, ASME Boiler and Pressure Vessel Code, Section XI, "Rules for In-Service Inspection of Nuclear Power Plant Components.

3E-21 USNRC, C. I. Chang, et. al., "Piping Inelastic Fracture Mechanics Analysis," NUREG/CR-1119, June 1980.

3E-22 USAEC, "Reactor Primary Coolant System Rupture Study Quarterly Progress Report No. 14," July-September, 1968, GEAP-5716, AEC Research and Development Report, December 1968.

3E-23 USNRC, M. G. Vassilaros, et al, "J-Integral Tearing Instability Analyses for 8-Inch Diameter ASTM A10.6 Steel Pipe," NUREG/CR-3740, April 1984.

3E-24 USNRC, "Standard Review Plan," Public Comments Solicited, Federal Register, Volume 52, No. 167, Notices, Pages 32626 to 32633, August 28, 1987.

3E-25 Electric Power Research Institute, D. Norris, B. Chexal, and T. Griesbach, "PICEP: Pipe Crack Evaluation Program," NP-3596-SR, Special Report, Revision 1, 1987.

3E-26 B. Chexal, and J. Horowitz, "A Critical Flow Model for Flow Through Cracks in Pipes," to be presented at the 24th ASME/AICHE National Heat Transfer Conference, Pittsburgh, PA, August 9-12, 1987.

3E-27 B. Chexal and J. Horowitz, "A Crack Flow Rate Model for Leak-Before-Break Applications," SMIRT-9 Transachoir Vol. G, pp. 281-285 (1987).

3E-28 USNRC, "Evaluation and Refinement of Leak Rate Estimation Models," NUREG/CR-5128, April 1991.

3E-29 Electric Power Research Institute, R. P. Collier, et. al., "Two Phase Flow Through Intergranular Stress Corrosion Cracks and Resulting Acoustic Emission," EPRI Report No. NP-3540-LD, April 1984.

3E-30 F. J. Moody, "Maximum Two-Phase Vessel Blowdown from Pipes," J. Heat Transfer, Vol. 88, No. 3, 1966, pp. 285-295.

3E-31 R. L. Daughterly, and J. B. Franzini, "Fluid Mechanics with Engineering Applications," McGraw-Hill Book Company, New York 1965.

3E-32 USNRC, P. C. Paris and H. Tada, "The Application of Fracture Proof Design Postulating Circumferential Through-Wall Cracks," U.S. Nuclear Regulatory Commission Report NUREG/CR-3464, Washington, D.C., April 1983.

3E-33 GE Nuclear Energy, "Investigation of Cause of Cracking in Austenitic Stainless Steel Piping, NEDO-21000 Volume 1 and 2, Class 1, Revision 0, July 1975.

3E-34 USNRC, "Investigation and Evaluation of Cracking in Austenitic Steel Piping of Boiling Water Reactor Plants," NUREG-75/067, October 1975.

Table 3E-1

Electrodes and Filler Metal Requirements for Carbon Steel Welds

Base Material	P-No.	Process	Electrode or Specification	Filler Metal Classification
Carbon Steel to Carbon Steel; or	P-1 to P-1, P-3	SMAW	SFA 5.1	E7018
Low Alloy Steel	P-4 or P-5	GTAW PAW	SFA 5.18	E70S-2, E70S-3
		GMAW	SFA 5.18 SFA 5.20	E70S-2, E70S-3, E70S-6 E70T-1
		SAW	SFA 5.17	F72EM12K, F72EL12

Table 3E-2

Supplier Provided Chemical Composition and Mechanical Properties Information

		Chemical Composition				Mechanical Property			
Material	**Product Form**	C	Ma	P	S	Si	Sy MPa (ksi)	Su MPa (ksi)	Elongation (%)
SA 333 Gr. 6 Heat #52339	16 in. Sch. 80 Pipe	0.12	1.18	0.01	0.026	0.27	303.4 (44.0)	465.4 (67.5)	42.0
SA 516 Gr. 70 Heat #E18767	1.0 in. Plate	0.18	0.98	0.017	0.0022	0.25	320.5 (46.5)	486.1 (70.5)	31.0

Notes:

(1) Pipe was normalized at 898.9°C (1650°F). Held for 2 hours and air-cooled.

(2) Plate was normalized at 926.7°C (1700°F) for one hour and air-cooled.

Table 3E-3

Standard Tension Test Data at Temperature

Specimen Number	**Material**	**Test Temperature**	**0.2% YS MPa** (ksi)	**UTS** (%)	**Elongation** (%)	**RA** (%)
OW1	Pipe Weld	RT	455.7 MPa (66.1)	81.6	32	77.2
OW2	Pipe Weld	288°C (550°F)	406.8 MPa (59.0)	93.9	24	56.7
ITWL2	Plate Weld	288°C (550°F)	365.4 MPa (53.0)	91.4	34	51.3
IBL1	Plate Base	RT	309.6 MPa (44.9)	73.7	38	51.3
IBL2	Plate Base	177°C (350°F)	261.3 MPa (37.9)	64.2	34	68.9
IBL3	Plate Base	288°C (550°F)	235.2 MPa (34.1)	69.9	29	59.4
OB1	Pipe Base	RT	300.9 MPa (43.6)	68.6	41	67.8
OB2	Pipe Base	177°C (350°F)	291.0 MPa (42.2)	74.9	21	55.4
OB3	Pipe Base	288°C (550°F)	238.6 MPa (34.6)	78.2	31	55.4

Table 3E-4

Summary of Carbon Steel J-R Curve Tests

Number	Specimen ID	Size	Description	Temperature
(1)	OWLC-A	1T	Pipe Weld	288°C (550°F)
(2)	OBCL-1	1T	Pipe Base C-L Orientation	RT
(3)	OBLC2	1T	Pipe Base L-C Orientation	288°C (550°F)
(4)	OBLC3-B	1T	Pipe Base L-C Orientation	177°C (350°F)
(5)	BML-4	1T	Plate Base Metal, L-T Orientation	RT
(6)	BML4-14	2T	Plate Base Metal, L-T Orientation	RT
(7)	BML2-6	2T	Plate Base Metal, L-T Orientation	177°C (350°F)
(8)	BML1-12	2T	Plate Base Metal, L-T Orientation	288°C (550°F)
(9)	WM3-9	2T	Plate Weld Metal	RT
(10)	XWM1-11	2T	Plate Weld Metal	177°C (350°F)
(11)	WM2-5	2T	Plate Weld Metal	288°C (550°F)
(12)	HAZ	(Non-standard) Width = 7.09 cm (2.793")	Heat-Affected Zone, Plate	RT
(13)	OWLC-7	1T	Pipe Weld	RT

Notes:

1. Pipe base metal, SA333 Gr. 6
2. Plate base metal, SA516 Gr. 70

Table 3E-5

Mass Flow Rate Versus fl/D_h Values

fl/D_h	Mass Flow Rate, kg/s m^2 (lbm/sec-ft^2 M)
0	18540 (3800)
1	10740 (2200)
2	7810 (1600)
3	5615 (1150)
4	4490 (920)
5	3904 (800)
10	2830 (580)
20	1950 (400)
50	1270 (260)
100	903 (185)

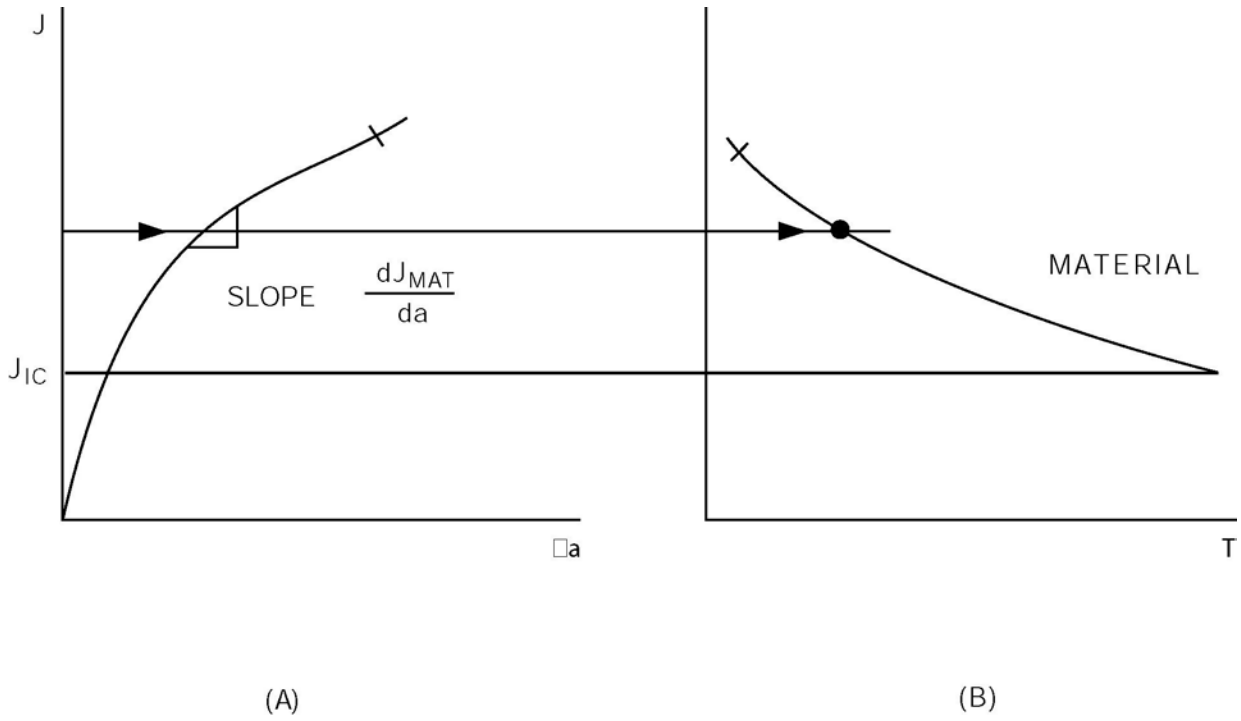

Figure 3E-1. Schematic Representation of Material J-Integral R and J-T Curves

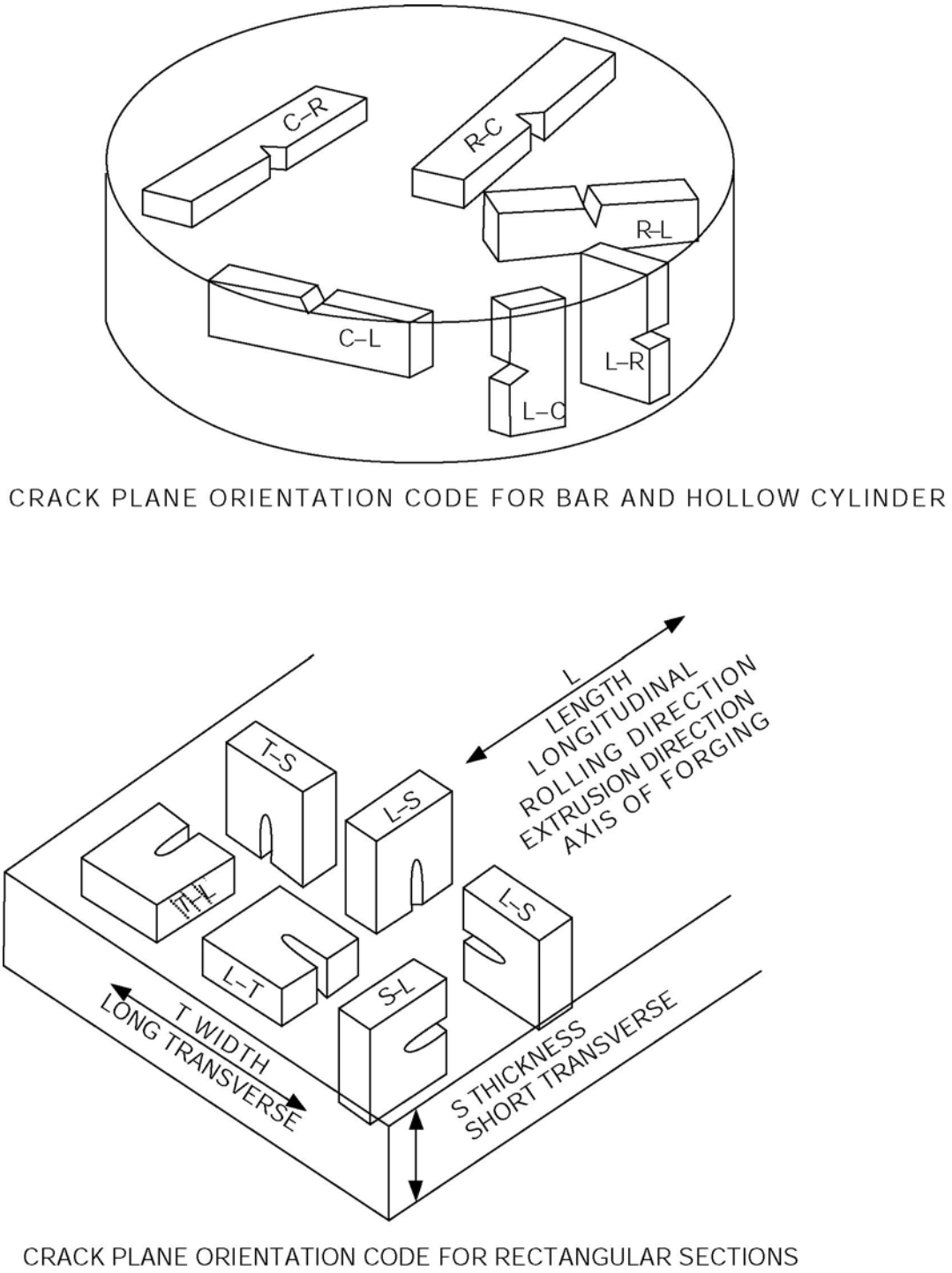

Figure 3E-2. Carbon Steel Test Specimen Orientation Code

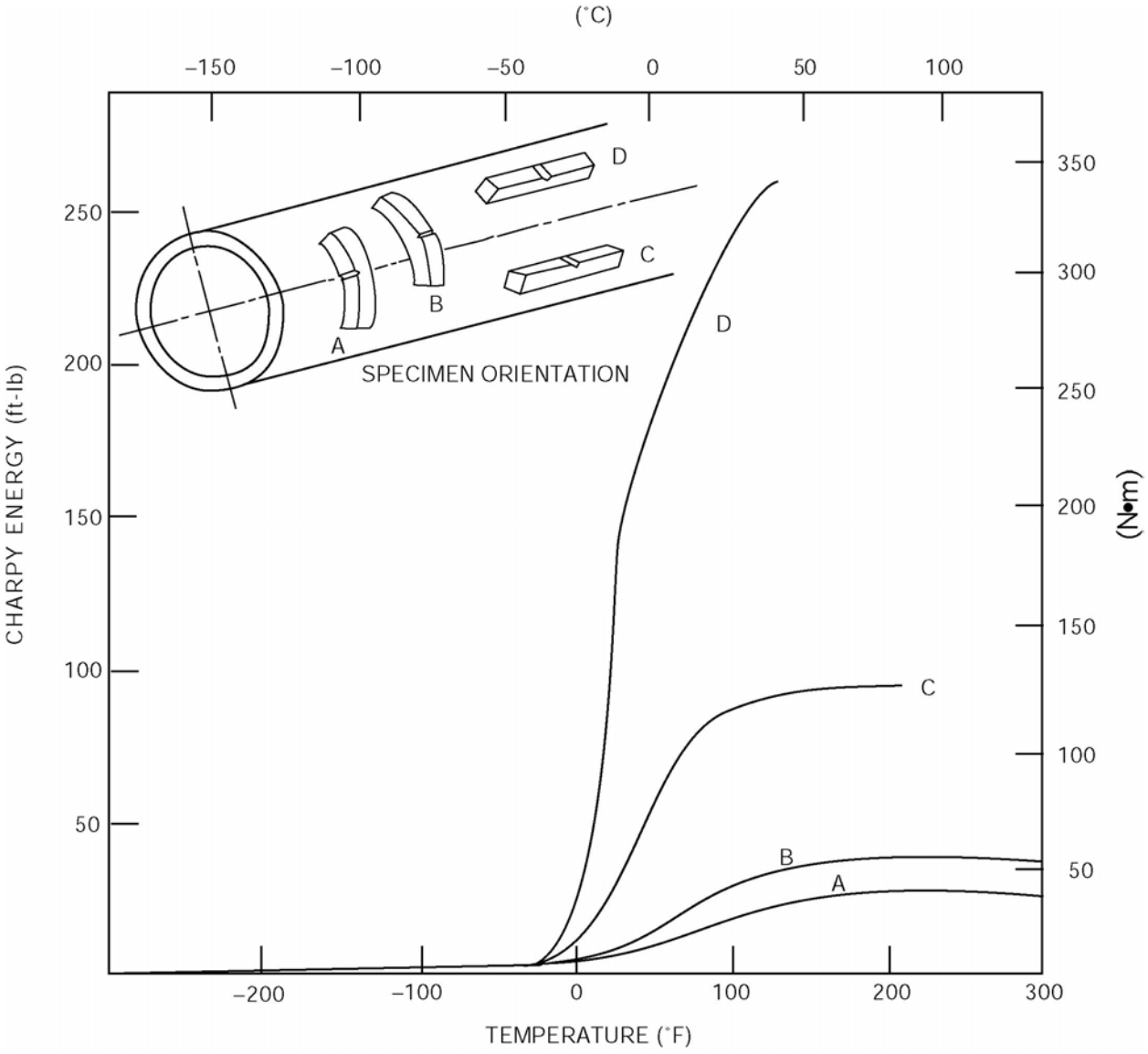

Figure 3E-3. Toughness Anisotropy of ASTM 106 Pipe (152 mm Sch. 80)

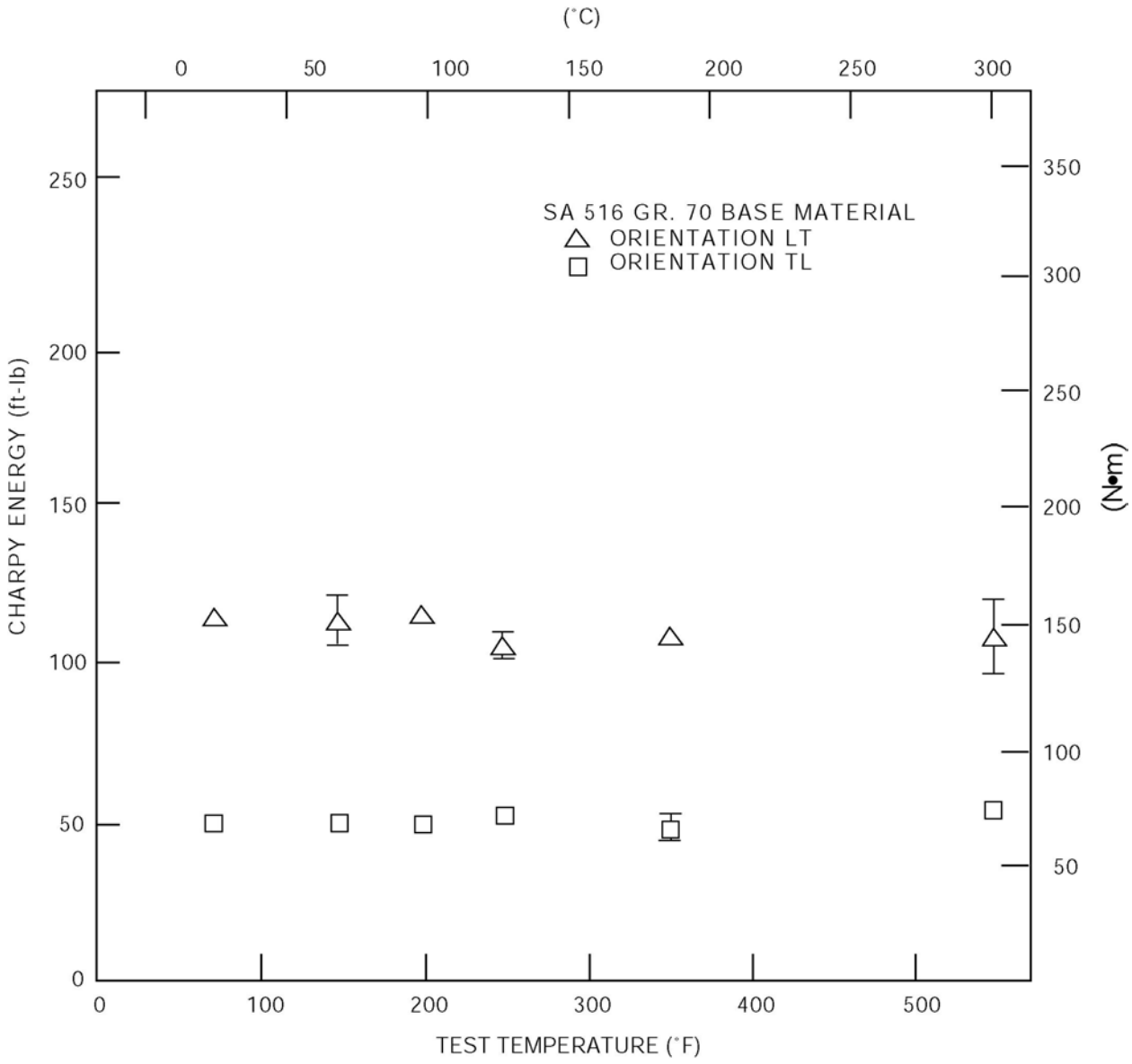

Figure 3E-4. Charpy Energies for Pipe Test Material as a Function of Orientation and Temperature

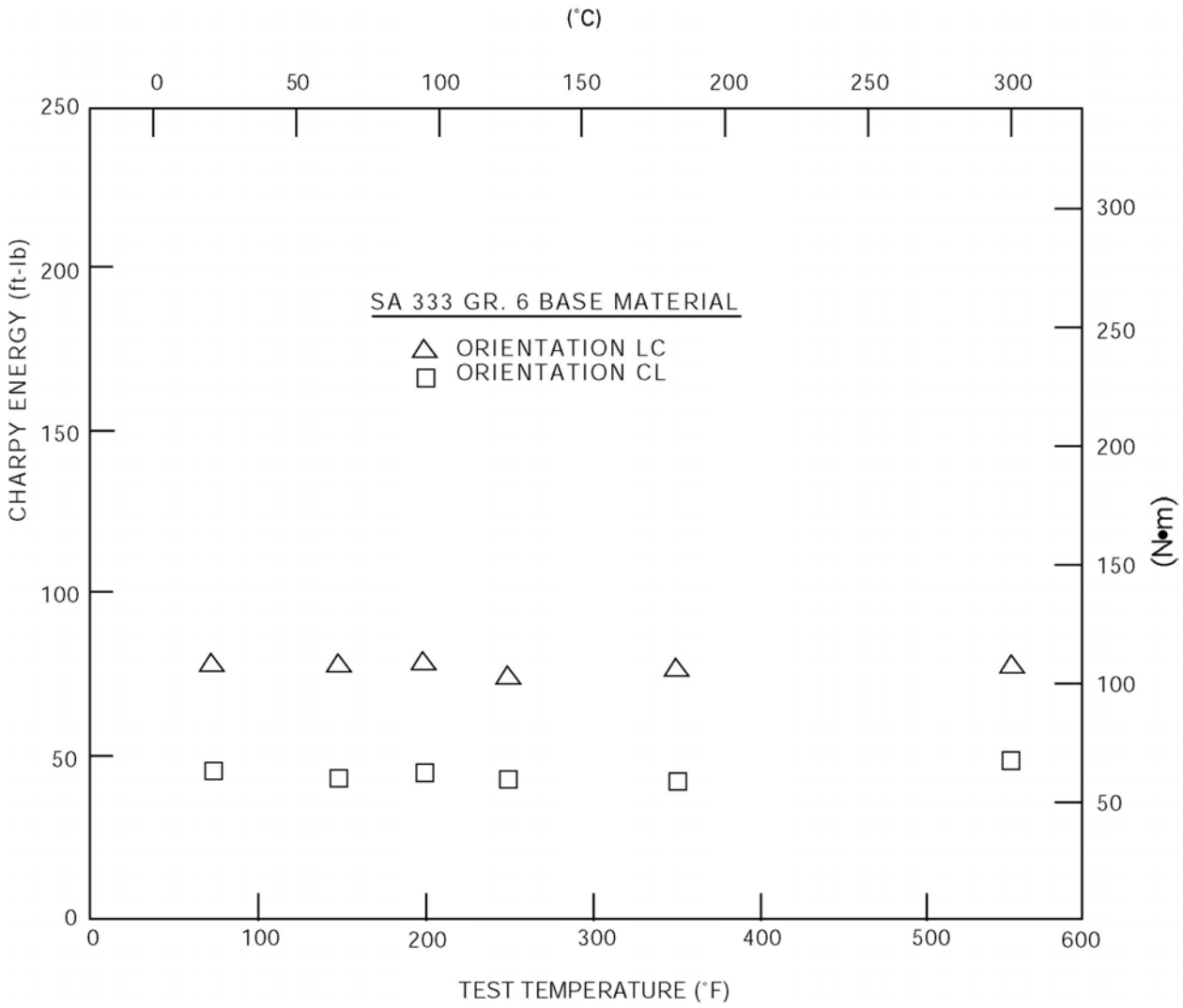

Figure 3E-5. Charpy Energies for Plate Test Material as a Function of Orientation and Temperature

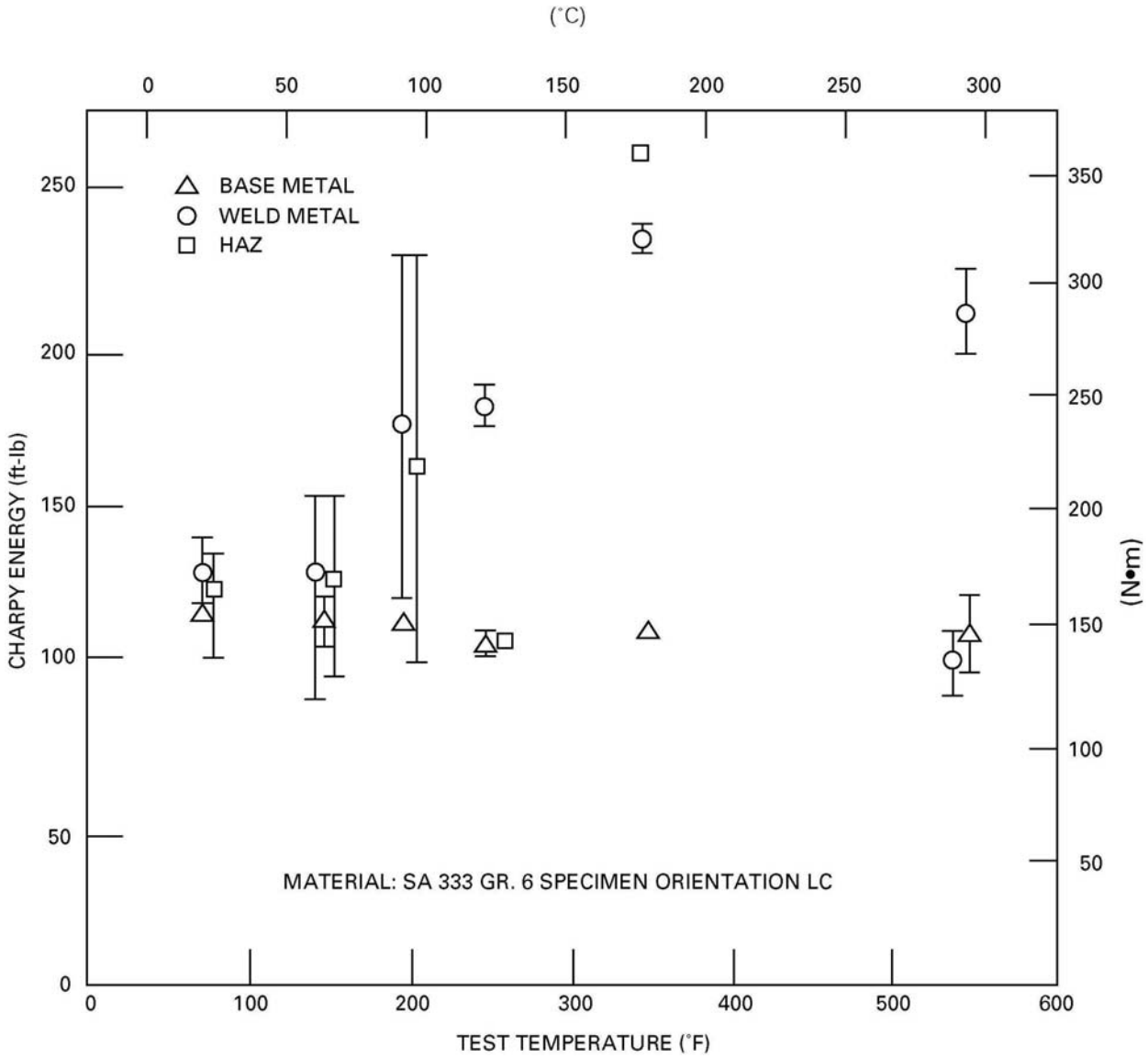

Figure 3E-6. Comparison of Base Metal, Weld and HAZ Charpy Energies for SA 333 Grade 6

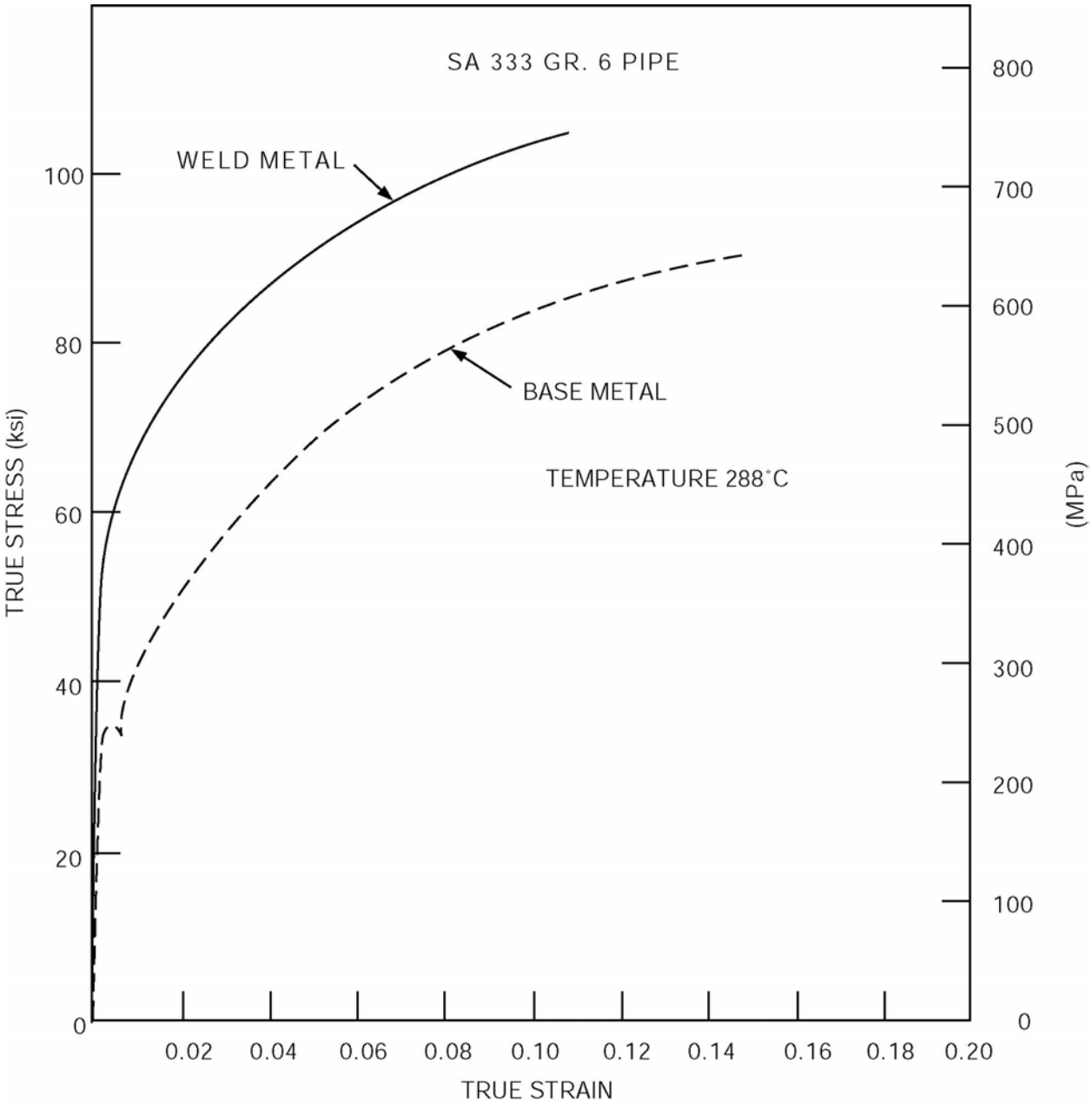

Figure 3E-7. Plot of 288ºC (550°F) True Stress-True Strain Curves for SA 333 Grade 6 Carbon Steel

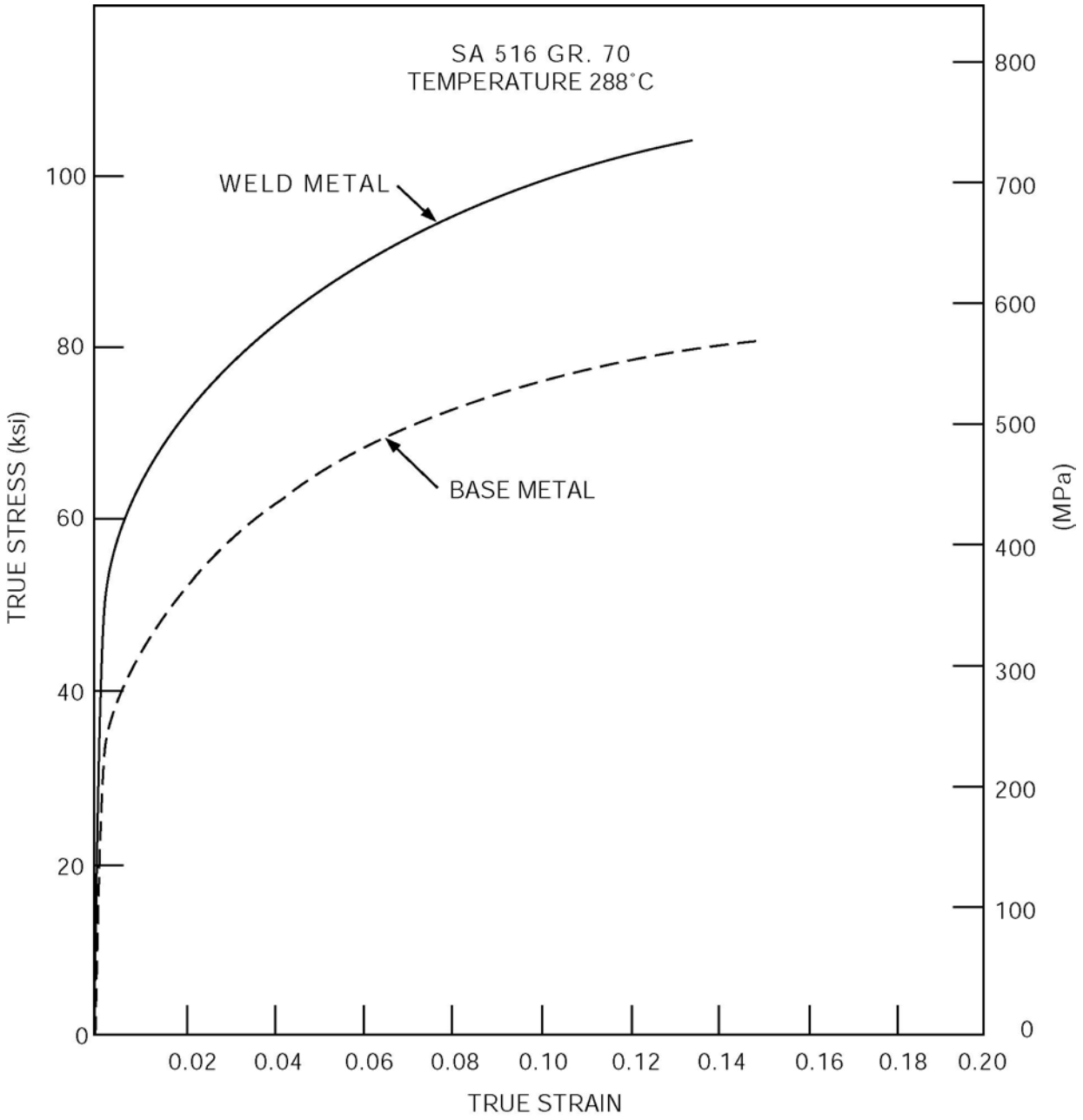

Figure 3E-8. Plot of 288ºC (550°F) True Stress-True Strain Curves for SA 516 Grade 70 Carbon Steel

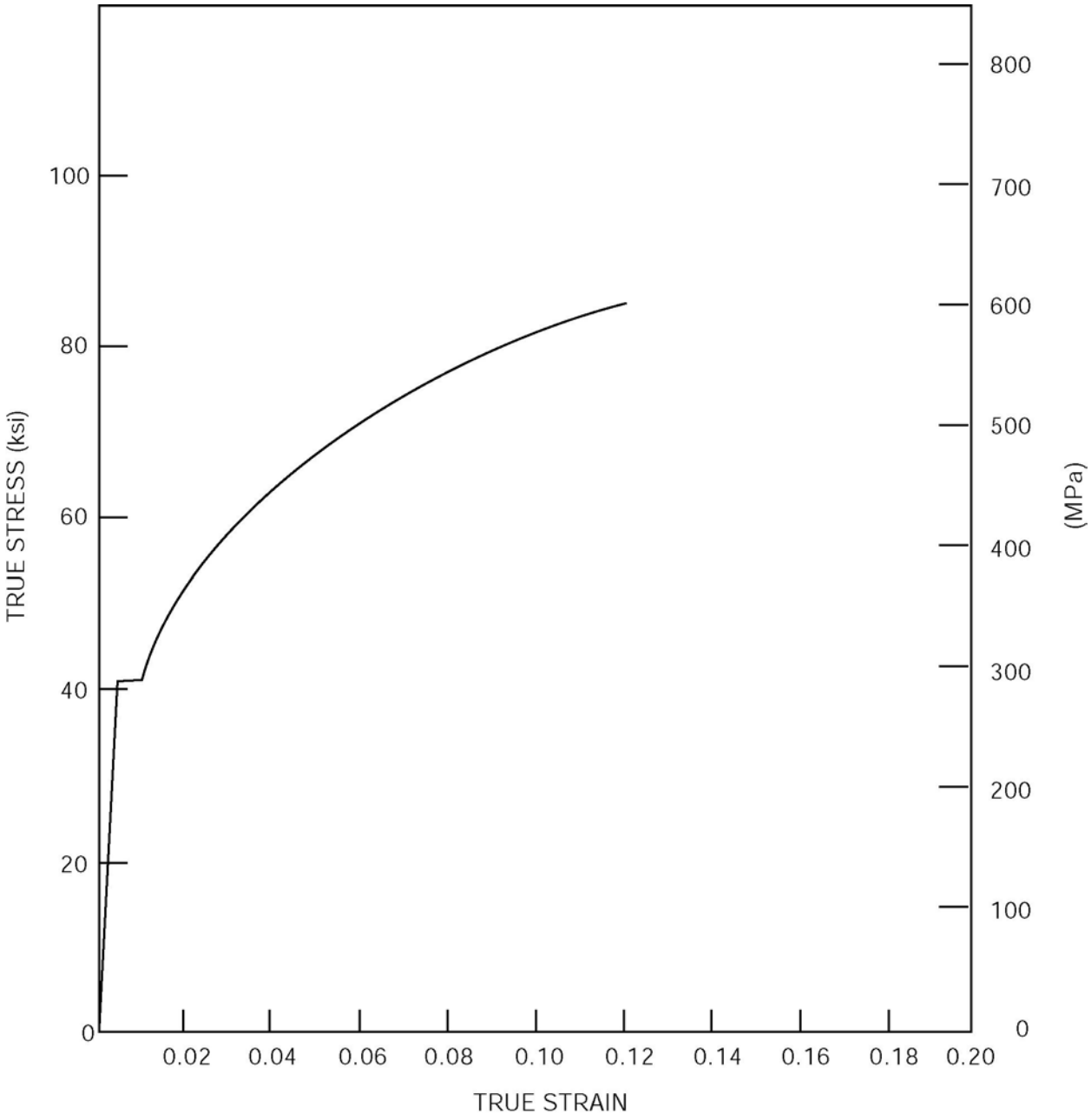

Figure 3E-9. Plot of 177ºC (350°F) True Stress-True Strain Curves for SA 333 Grade 6 Carbon Steel

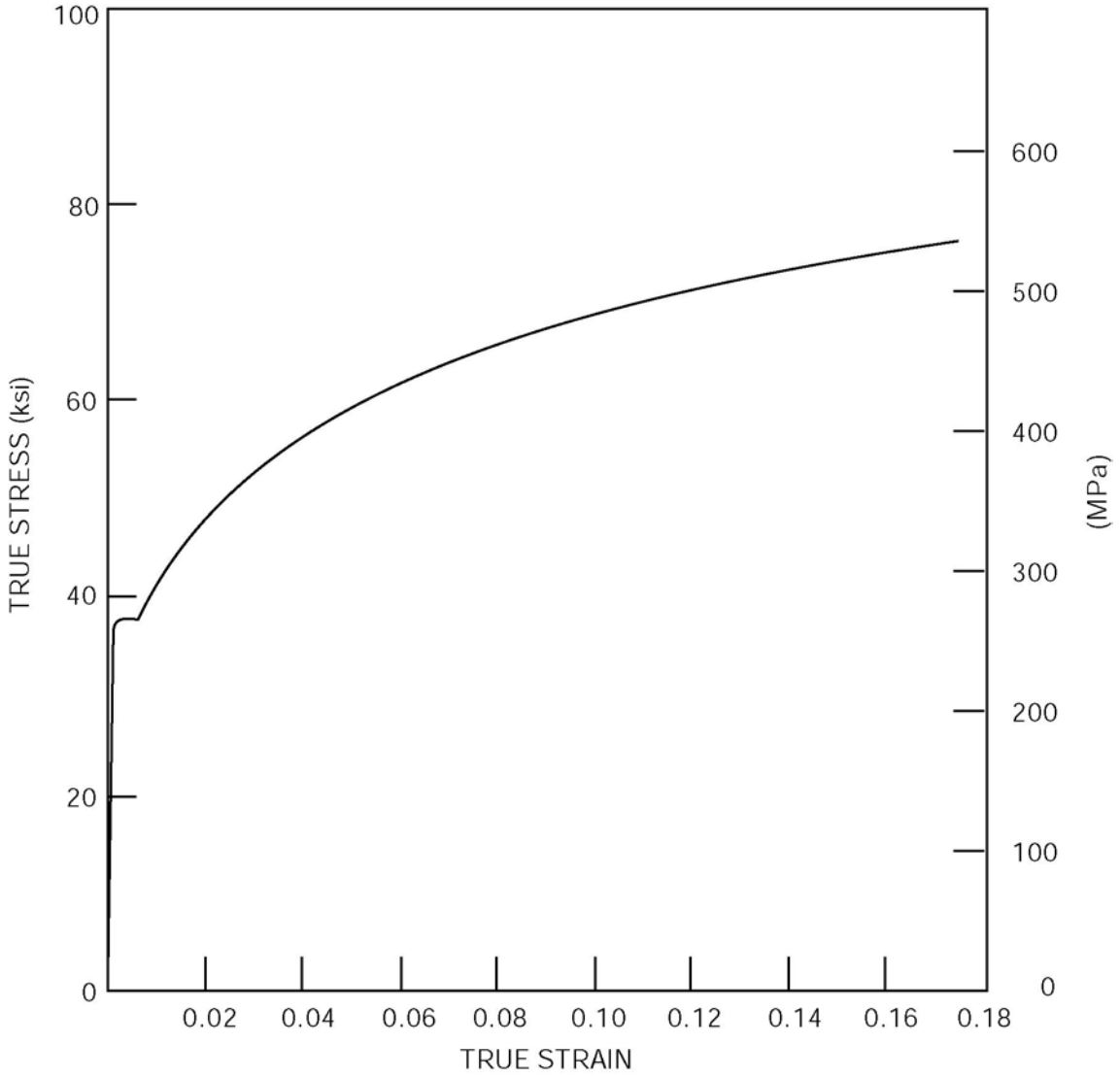

Figure 3E-10. Plot of 177ºC (350°F) True Stress-True Strain Curves for SA 516 Grade 70 Carbon Steel

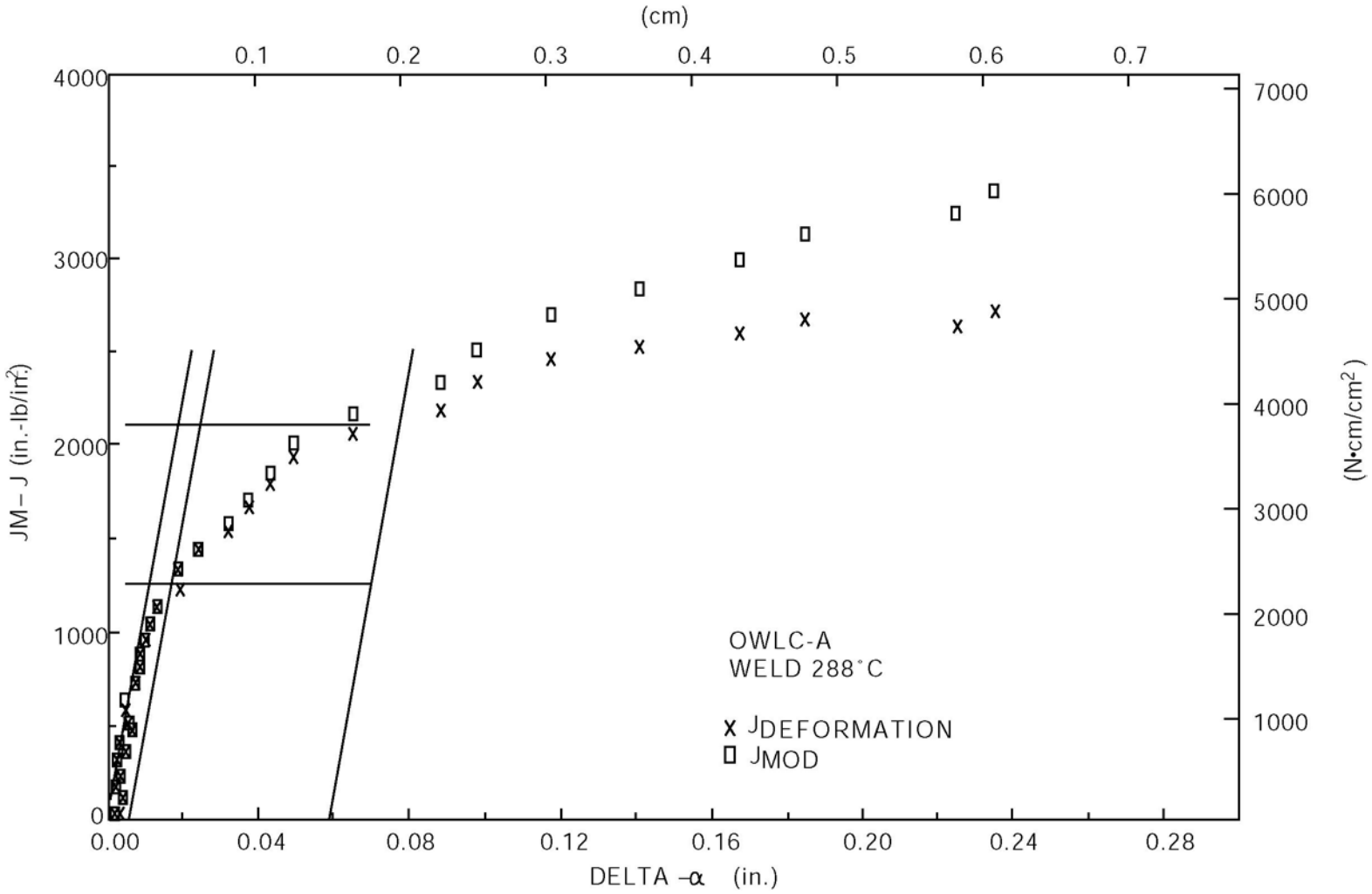

Figure 3E-11. Plot of 288ºC (550°F) Test J-R Curve for Pipe Weld

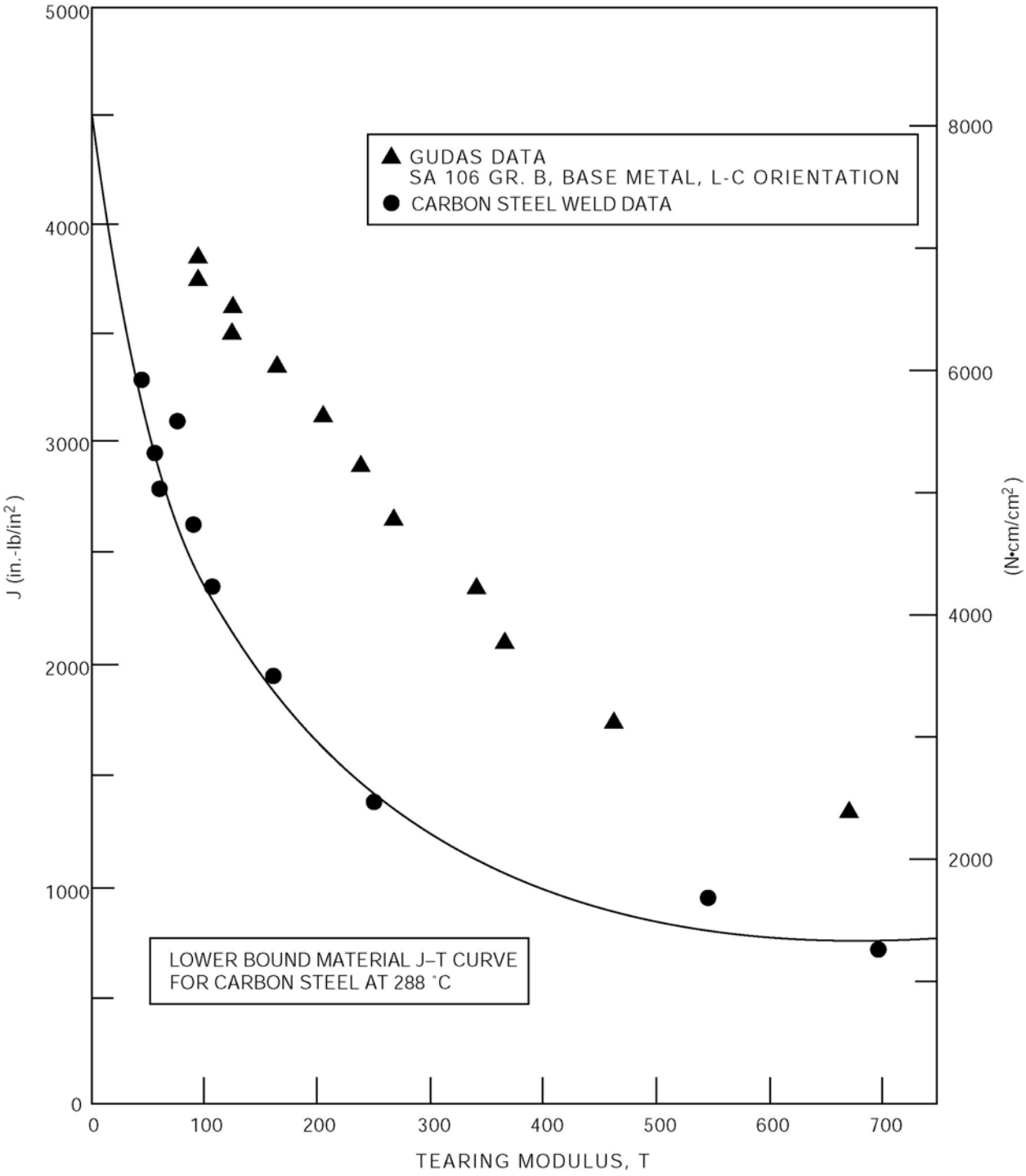

Figure 3E-12. Plot of 288ºC (550°F) J_{mod}, T_{mod} Data from Test J-R Curve

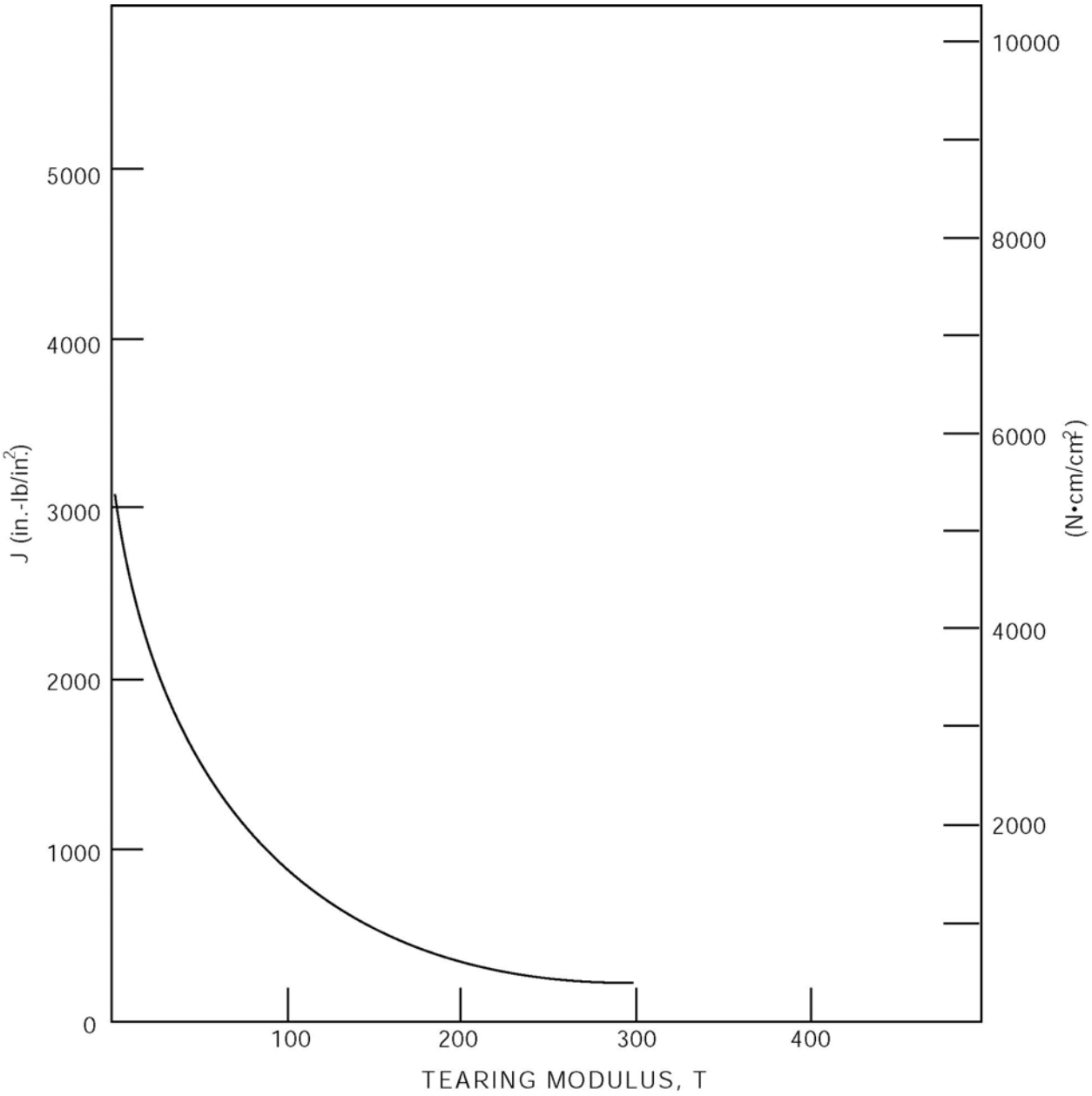

Figure 3E-13. Carbon Steel J-T Curve for 216ºC (420°F)

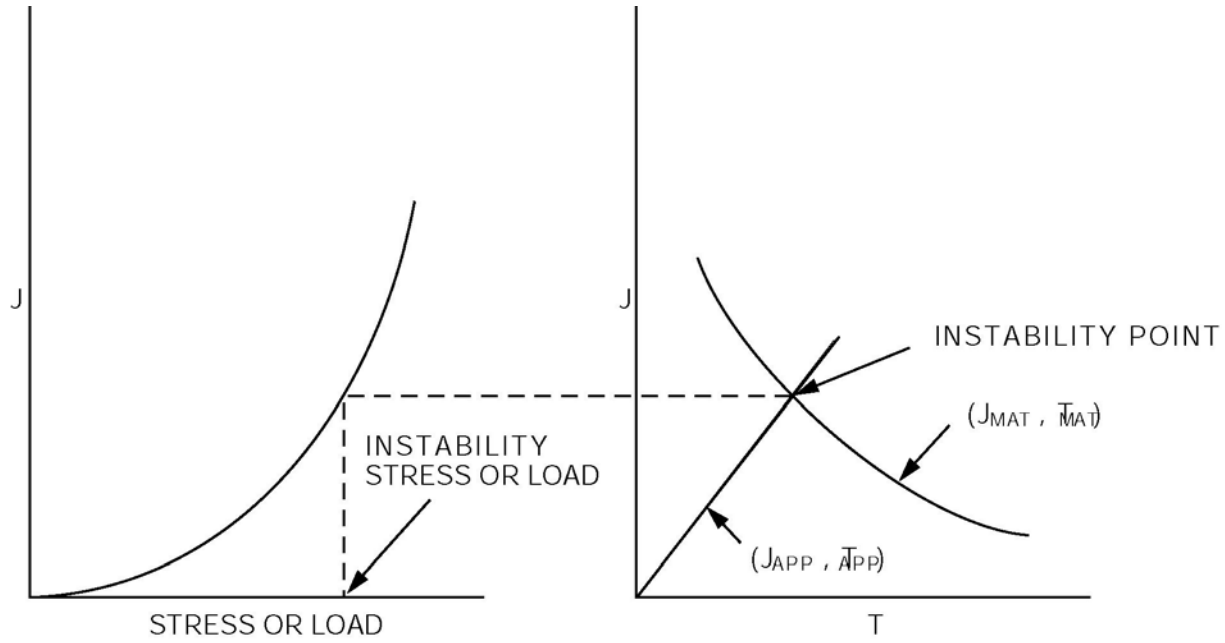

Figure 3E-14. Schematic Illustration of Tearing Stability Evaluation

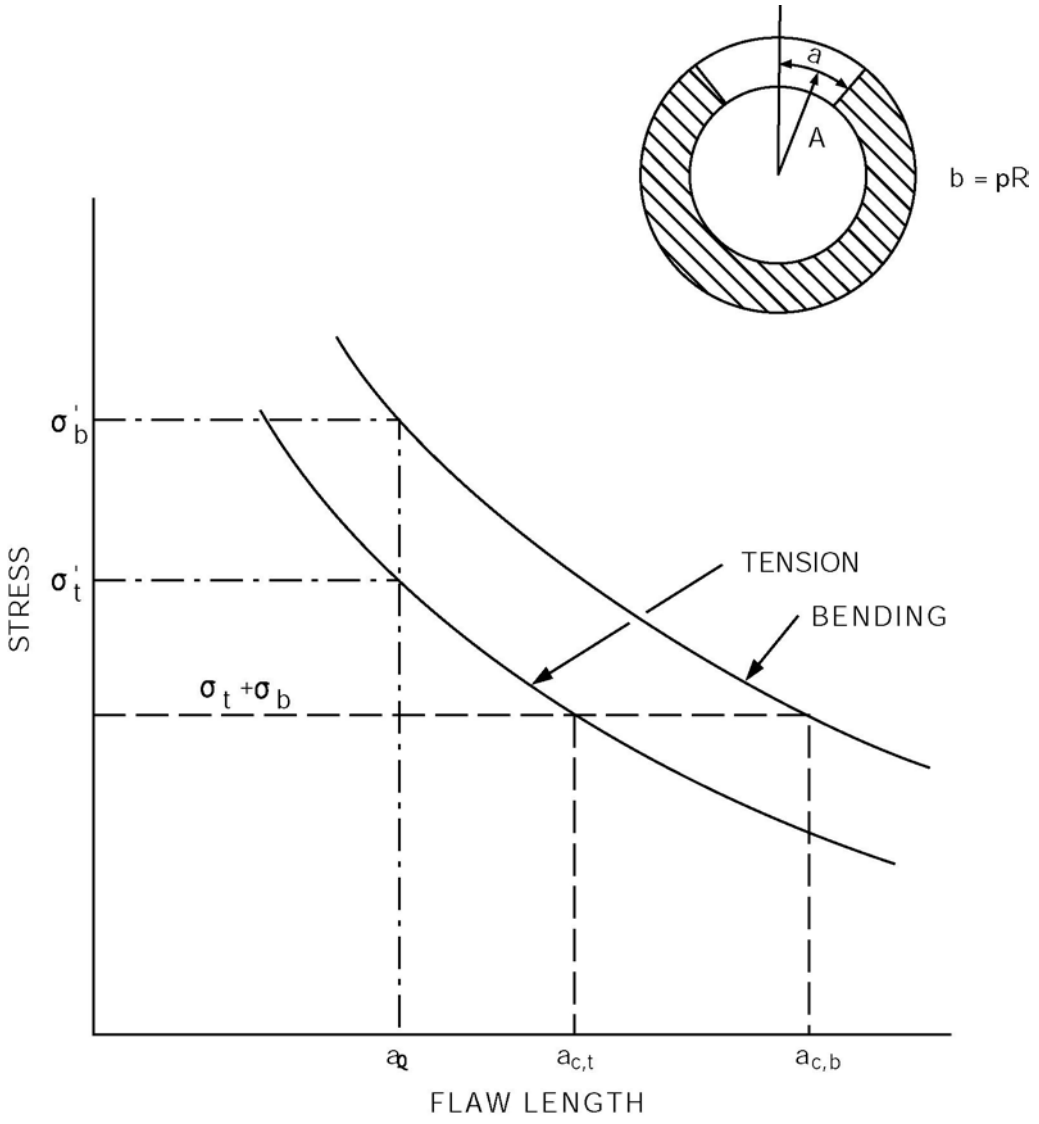

Figure 3E-15. Schematic Representation of Instability Tension and Bending Stresses as a Function of Flaw Strength

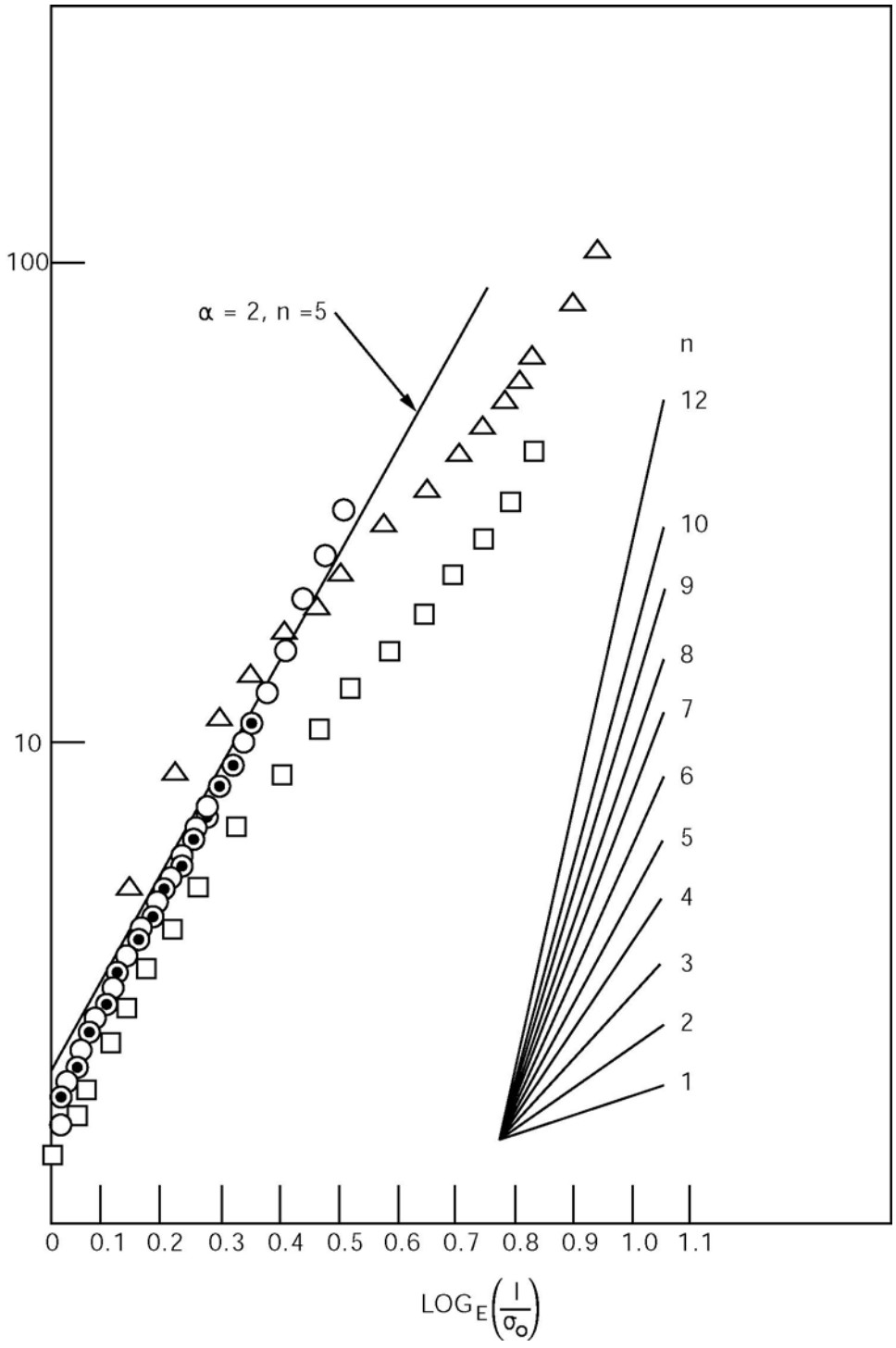

Figure 3E-16. SA 333 Grade 6 Stress-Strain Data at 288ºC (550°F) in the Ramberg-Osgood Format

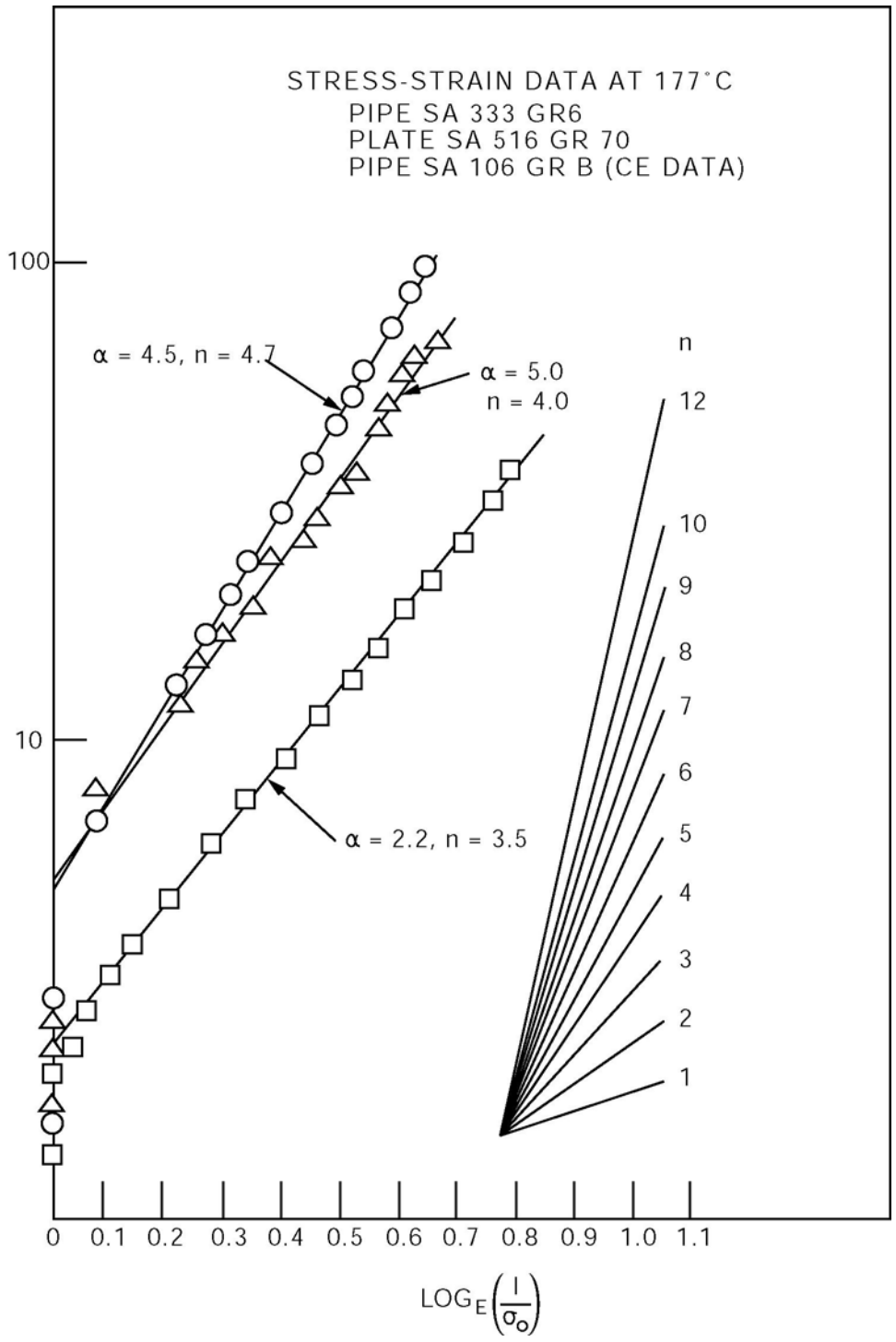

Figure 3E-17. Carbon Steel Stress-Strain Data at 177ºC (350°F) in the Ramberg-Osgood Format

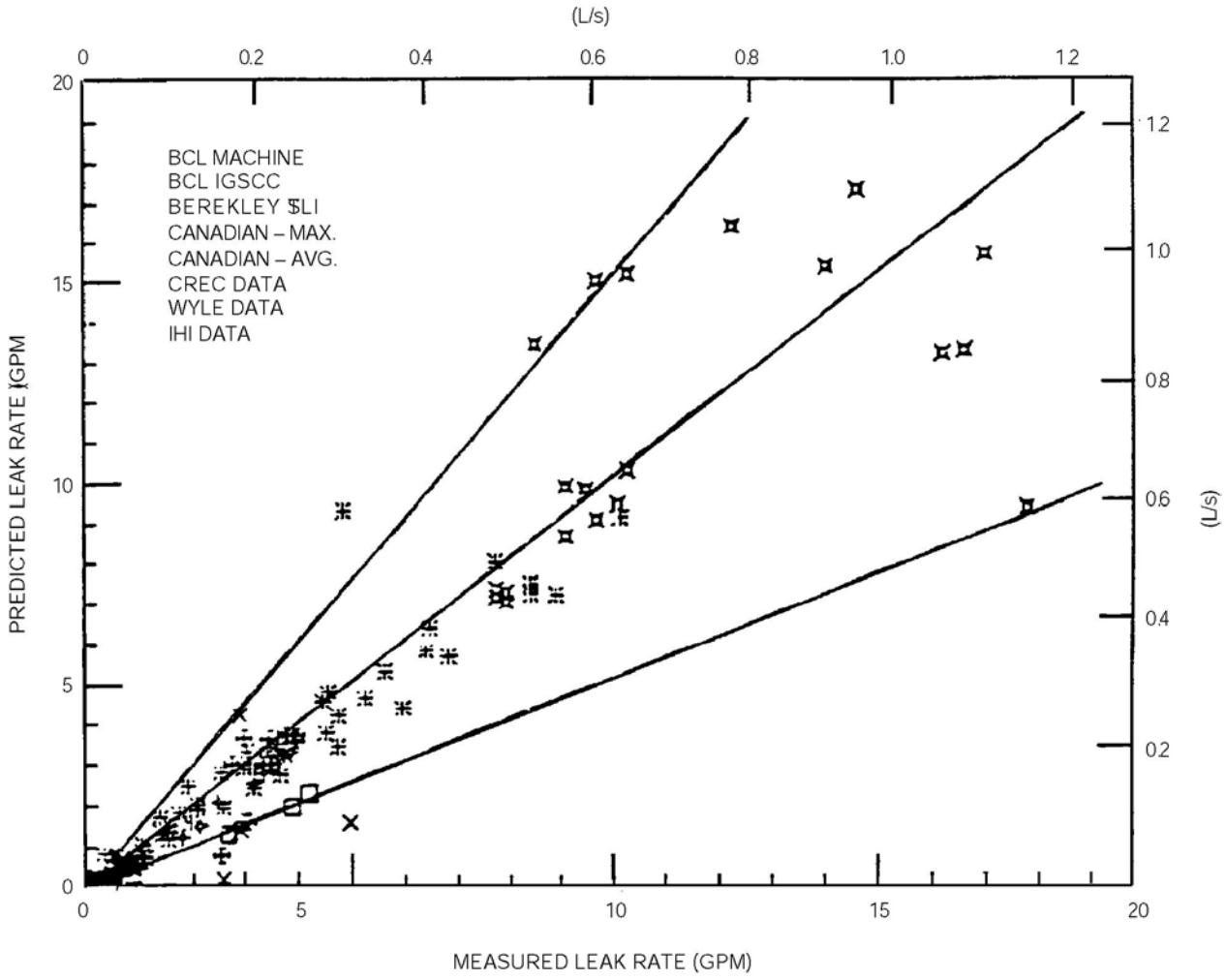

Figure 3E-18. Comparison of PICEP Predictions with Measured Leak Rates

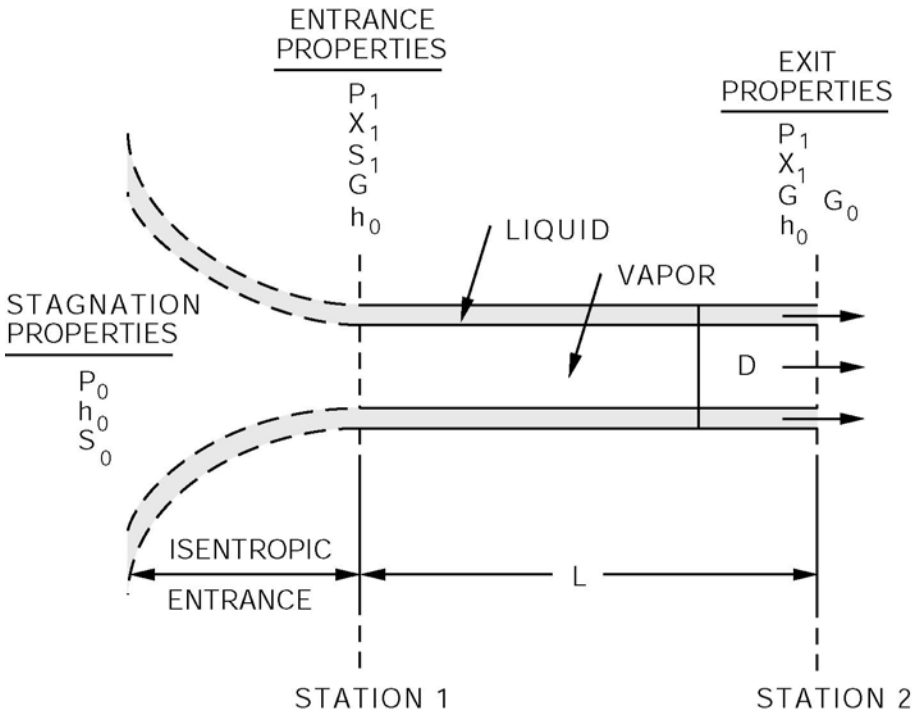

Figure 3E-19. Pipe Flow Model

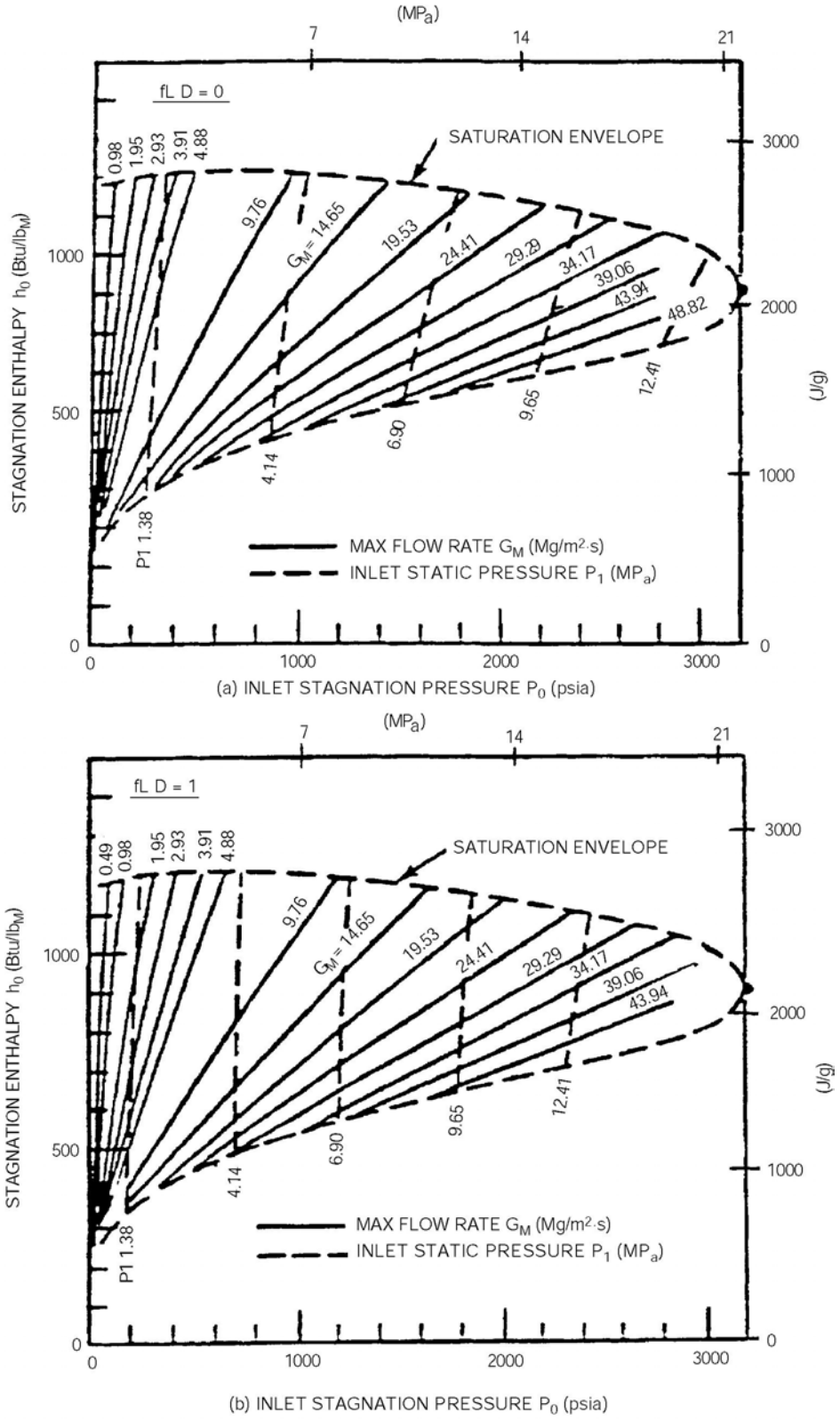

Figure 3E-20. Mass Flow Rates for Steam/Water Mixtures

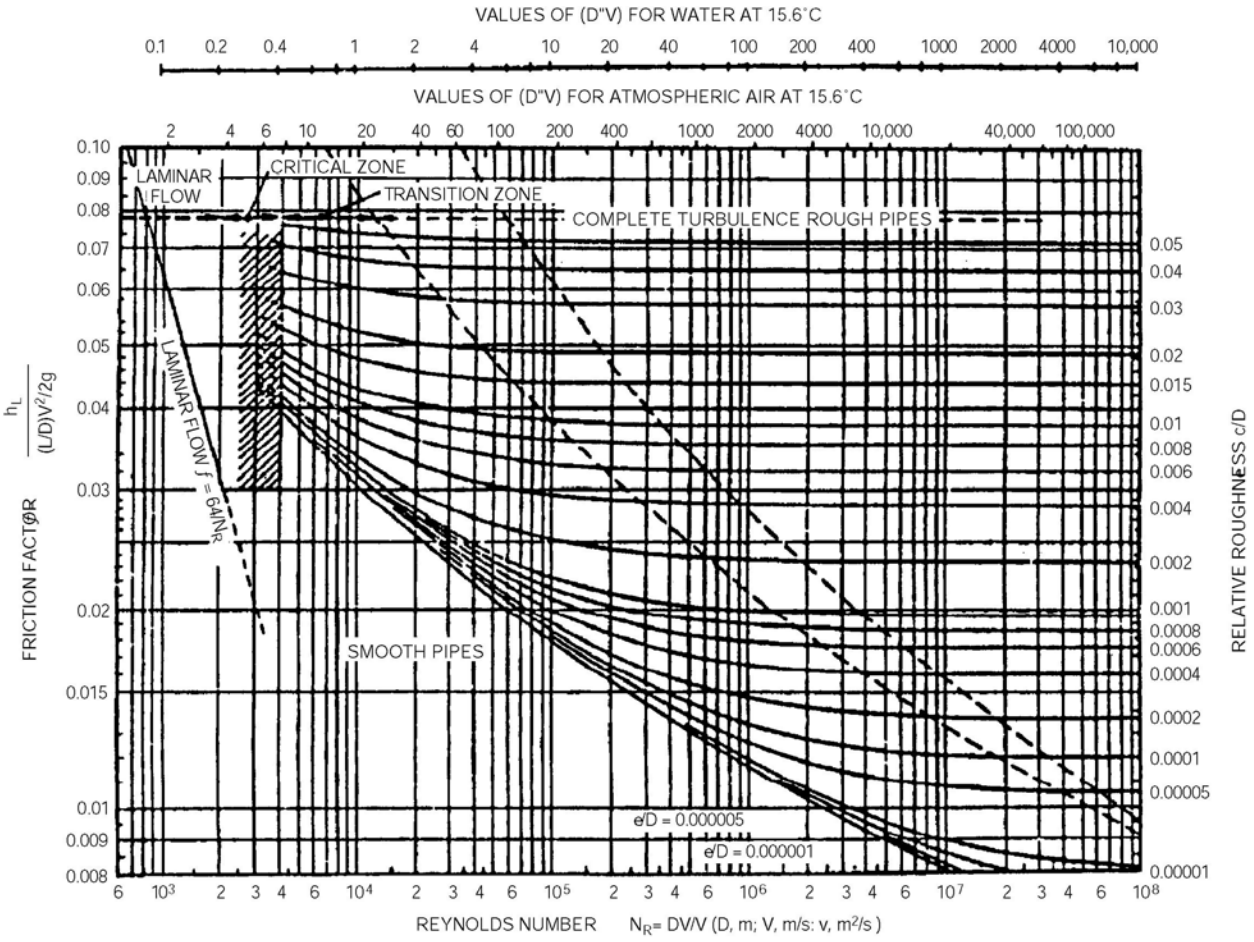

Figure 3E-21. Friction Factors for Pipes

3F. RESPONSE OF STRUCTURES TO CONTAINMENT LOADS

3F.1 SCOPE

This appendix specifies the design for safety-related structures, systems, and components as applicable due to dynamic excitations originating in the primary containment in the event of operational transients and LOCA. The input containment loads are described in Appendix 3B. The containment loads considered for structural dynamic response analysis are (1) Hydrodynamic Loads which are Condensation Oscillation (CO), Pool Chugging (CH), Horizontal Vent Chugging (HVL), Local Condensation Oscillation (LCO) and Safety Relief Valve discharge (SRV) in the Suppression Pool (SP), and (2) Pipe Break Loads which consist of Annulus Pressurization (AP) in the annulus between the Reactor Shield Wall (RSW) and Reactor Pressure Vessel (RPV), nozzle jet, jet impingement and pipe whip restraint loads.

3F.2 DYNAMIC RESPONSE

3F.2.1 Classification of Analytical Procedure

Analytical procedure of containment loads is classified into the following two groups:

(1) Hydrodynamic Loads in the SP: The loads included in this group are SRV loads and LOCA related loads such as CO, CH, HVL and LCO. Depending on the distribution of these loads in the pool, they can be further classified as:

- Symmetric loads in the suppression pool, or
- Asymmetric loads in the suppression pool

(2) Pipe break loads due to Main Steam (MS), Reactor Water Cleanup (RWCU) or Feedwater (FW) line break. The loads included in this group are pressure loads AP and concentrated loads, which are nozzle jet, jet impingement and pipe whip restraint loads.

3F.2.2 Analysis Models

(1) Analysis Model

The structural models used in the analyses represent a synthesis of the Reactor Building (RB) model and the RPV model. The beam model to be used for the pipe break load analysis is illustrated in Figure 3F-1. The hydrodynamic load analysis model of the building structure is illustrated in Figure 3F-2, which is coupled with the RPV model shown in Figure 3F-3. This coupled model is used for symmetric and asymmetric load cases.

(2) Structural Damping

Material damping values used for SRV and LOCA analyses are in accordance with Regulatory Guide 1.61.

3F.2.3 Load Application

(1) Pipe Break Nozzle Load

The AP pressures are converted to horizontal forces according to the following formula.

For RSW side:

$$Fj(t) = 2\sum_{i=1}^{8} Pij(t) \int_{\theta=ai}^{\theta=bi} R\cos(\theta)d\theta \quad (3F\text{-}1)$$

For RPV side:

$$Fj(t) = -2\sum_{i=1}^{8} Pij(t) \int_{\theta=ai}^{\theta=bi} r\cos(\theta)d\theta \quad (3F\text{-}2)$$

where :

Fj(t)	=	Force per unit height each level
Pij(t)	=	Pressure each level and angle
i	=	Cell No.
j	=	Level No.
R	=	RSW Inner Radius
r	=	RPV Outer Radius
θ	=	Angle (180°)
ai,bi	=	Extreme angles of the arc on which the load is applied

Jet reaction, jet impingement, and pipe whip reaction forces are considered as constant forces with a finite rise time of one millisecond. Pipe whip load is included as a transient load ending with a steady load.

(2) SRV Load

Symmetric SRV (all) response analysis is covered by n=0 harmonic. Asymmetric case of SRV (all) actuation is covered by n=1 harmonic that corresponds to overturning moment. The SRV air bubble frequencies are expected to be within a range of 5 to 12 Hz. Ways of selecting minimum number of bubble frequencies for dynamic analysis are selected as follows.

Frequency range of SRV Loads: $f_1 \leq f \leq f_2$ (f_1 = 5 Hz, f_2 = 12 Hz)

For vertical structural frequencies $(fs)_v$ (n=0):

a. If $(fs)_v > f_2$ then use f_2

b. If $f_1 < (fs)_v < f_2$ then use $(fs)_v$

c. If $f_1 > (fs)_v$ then use f_1

For horizontal structural frequencies $(fs)_h$ (n=1):

a. If $(fs)_h > f_2$ then use f_2

b. If $f_1 < (fs)_h < f_2$ then use $(fs)_h$

c. If $f_1 > (fs)_h$ then use f_1

In symmetric load case, three vertical frequencies of 5 Hz (SRV-V1), 6.06 Hz (SRV-V2) and 12 Hz (SRV-V3) are selected. In asymmetric load case, 3 horizontal frequencies, 5 Hz (SRV-H1), 8.83 Hz (SRV-H2) and 12 Hz (SRV-H3), of the structure satisfying the above selection criteria are adopted as bubble frequencies.

(3) HVL Load

Both symmetric and non-symmetric upward loads are considered on the ventwall structure due to chugging in the top horizontal vents.

(4) Chugging, Condensation Oscillation Loads

From a comparison of the natural frequencies of the structure and the frequency contents in the Fourier spectra of the time histories of CH and CO loads, 7 critical pressure time histories out of 16 for CH and 5 out of 5 for CO, are selected for dynamic analysis. Furthermore, one local spike load is added in CO response study.

3F.2.4 Analysis Method

(1) Pipe Break Load Analysis

For these analyses, multi-input excitation time history analyses are performed using a full transient analysis. The α mass matrix and β stiffness matrix multipliers are used for the damping matrix.

(2) Symmetric Load Analysis

For the dynamic response analyses of SRV and LOCA cases, the full harmonic analysis solution method is used. The input time history is first transformed into harmonic loads. Each harmonic loading is analyzed individually for Fourier n=0 spatial distribution in the frequency domain. Responses to each harmonic loading are transformed back to the time domain and then superimposed, on a time consistent basis, to obtain the total responses. The constant (frequency-independent) stiffness for each material is used. The damping matrix is obtained as follows:

$$[C] = \sum_{j=1}^{Nm} \frac{2}{\Omega} \beta_j [K_j] \qquad \text{(3F-3)}$$

where:

N_m = Number of materials

Ω = circular excitation frequency

$[K_j]$ = structural stiffness matrix

$[C]$ = structural damping matrix

β_j = constant damping stiffness matrix coefficient

(3) Asymmetric Load Analysis

The same analysis approach as symmetric loads is used except that Fourier n=1 spatial distribution is considered.

3F.3 CONTAINMENT LOADS ANALYSIS RESULTS

The acceleration response spectra at selected locations for each loading event are presented in Figures 3F-4 through 3F-22. The maximum displacements and accelerations at selected locations for each loading event are presented Tables 3F-1 through 3F-4.

The input excitation of suppression pool boundary horizontal loads (SRV, CH, and HVL) is considered unidirectional which can be set at any direction in the horizontal plane, and the AP analysis is performed assuming that pipe break can be associated with any one of the vessel nozzles for each of the postulated line breaks.

The resulting response of structures considered in the analyses is thus unidirectional applicable to any azimuth angle for suppression pool loads and to the horizontal direction corresponding to the break direction for AP loads.

For subsystem analyses using floor response spectra and, if applicable, building displacement data, the input direction of the horizontal load is selected to result in the worst subsystem response.

As an alternate approach, the horizontal input to the subsystem may be taken to be the same in the two orthogonal horizontal directions.

Table 3F-1

Maximum Accelerations for AP Loadings (g)

Location	Node	MS	RWCU	FW
Top of Vent wall	701	0.0036	0.0097	0.0063
Top of pedestal	706	0.0014	0.0053	0.0033
Upper pool slab	208	0.0018	0.0058	0.0034

Table 3F-2

Maximum Accelerations for Hydrodynamic Loads (g)

Location	Direction	Node	SRV	HVL	CH	CO
Top of vent wall	Horizontal Vertical	1104 1104	0.11 0.19	0.007 0.142	0.229 0.0408	 0.88
SP Floor	Horizontal Vertical	1254 1254	0.14 0.31	0.000 0.036	0.14 1.325	1.97
RCCV Top slab side	Horizontal Vertical	1119 1119	0.08 0.09	0.000 0.000	0.051 0.113	0.25
RCCV Top slab center	Horizontal Vertical	1159 1159	0.08 0.13	0.000 0.000	0.070 0.067	0.43

Table 3F-3

Maximum Displacements for AP Loadings (mm)

Location	Node	MS	RWCU	FW
VW Top	701	0.0075	0.0063	0.0068
Top of Pedestal	706	0.0047	0.0053	0.0050
Upper pool slab	208	0.0080	0.0060	0.0065

Table 3F-4

Maximum Displacements for Hydrodynamic Loads (mm)

Location	Direction	Node	SRV	HV	CH	CO
VW Top	Horizontal Vertical	1104 1104	0.18 1.57	0.0 0.005	0.054 0.073	8.48
SP Floor	Horizontal Vertical	1254 1254	0.27 1.11	0.0 0.004	0.039 0.229	7.86
RCCV Top slab side	Horizontal Vertical	1119 1119	0.21 0.94	0.0 0.004	0.050 0.033	7.45
RCCV Top slab center	Horizontal Vertical	1159 1159	0.21 1.37	0.0 0.006	0.050 0.045	8.72

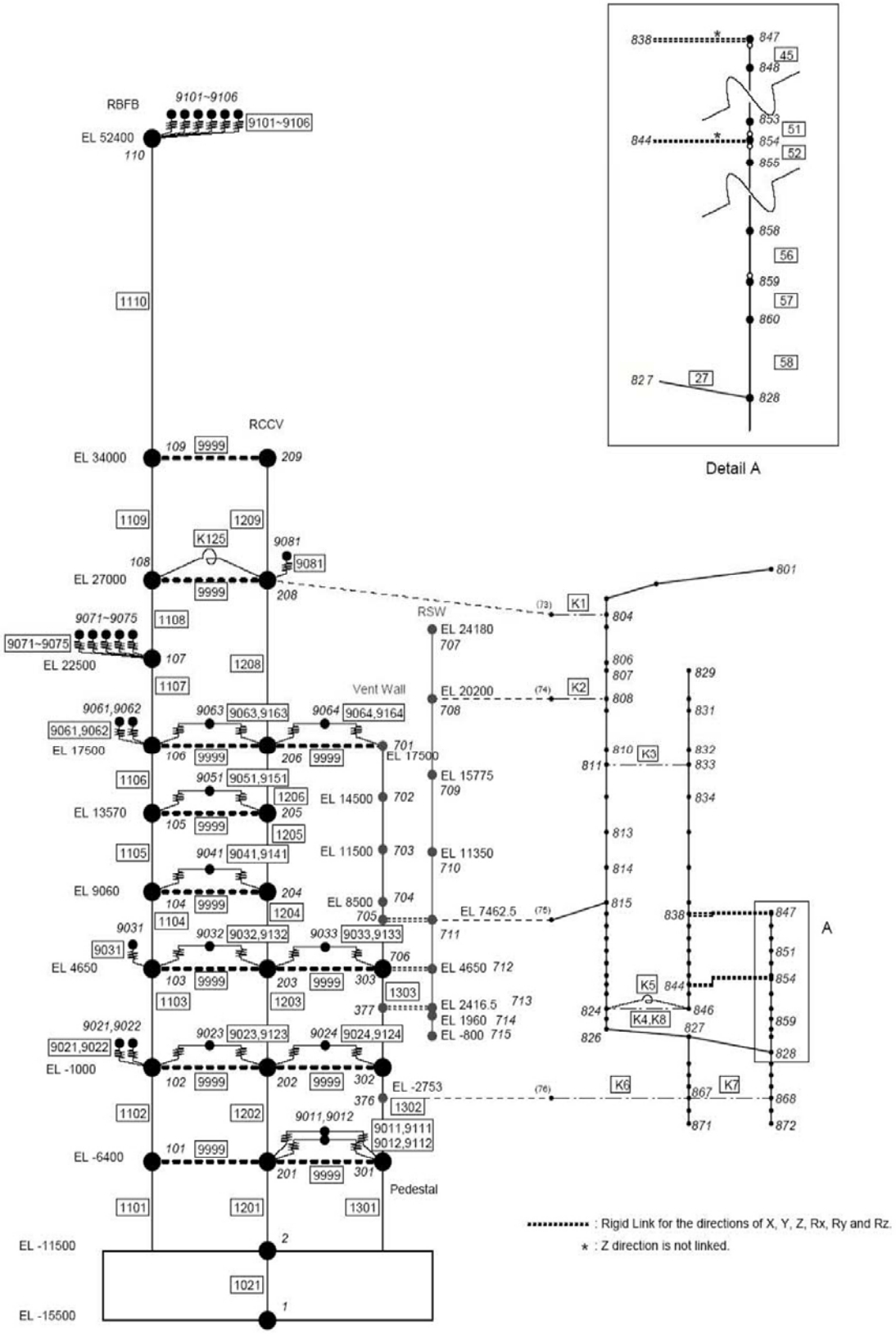

Figure 3F-1. Beam Model for AP Load

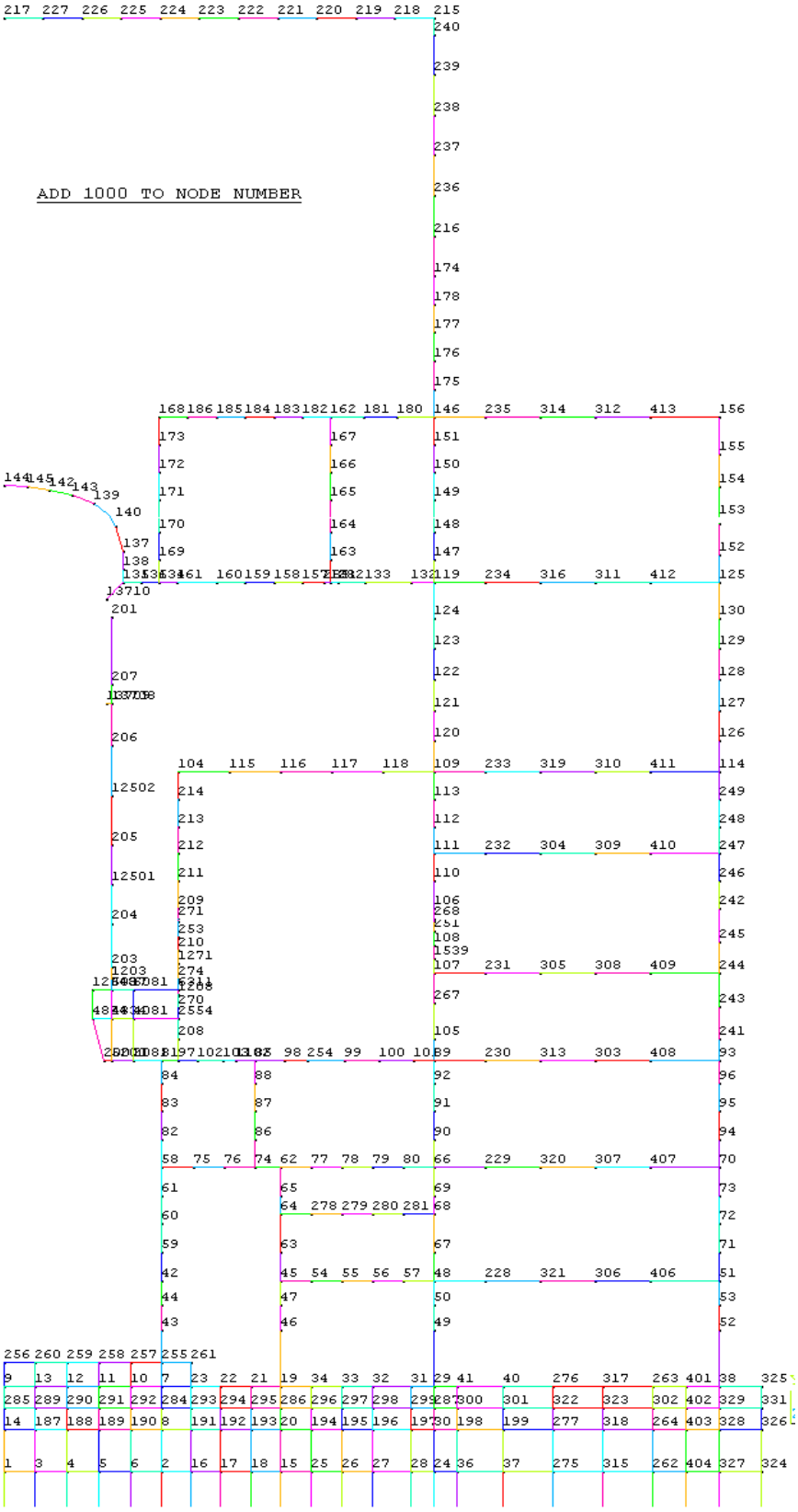

Figure 3F-2. Building Shell Model

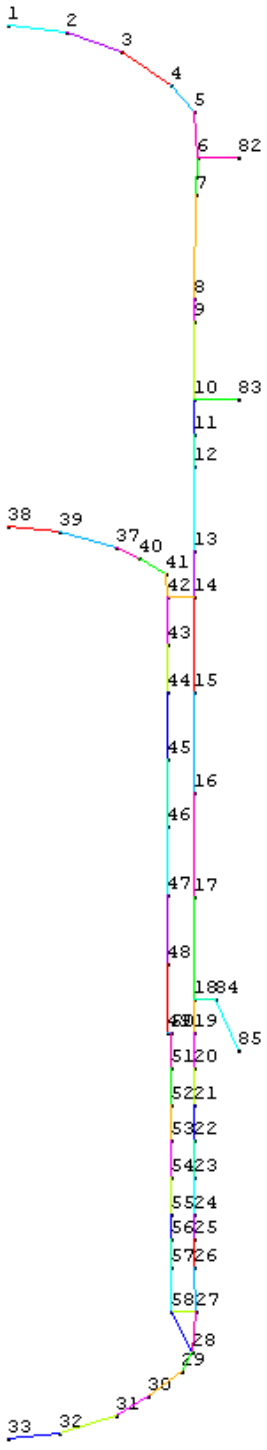

Figure 3F-3. RPV Shell Model

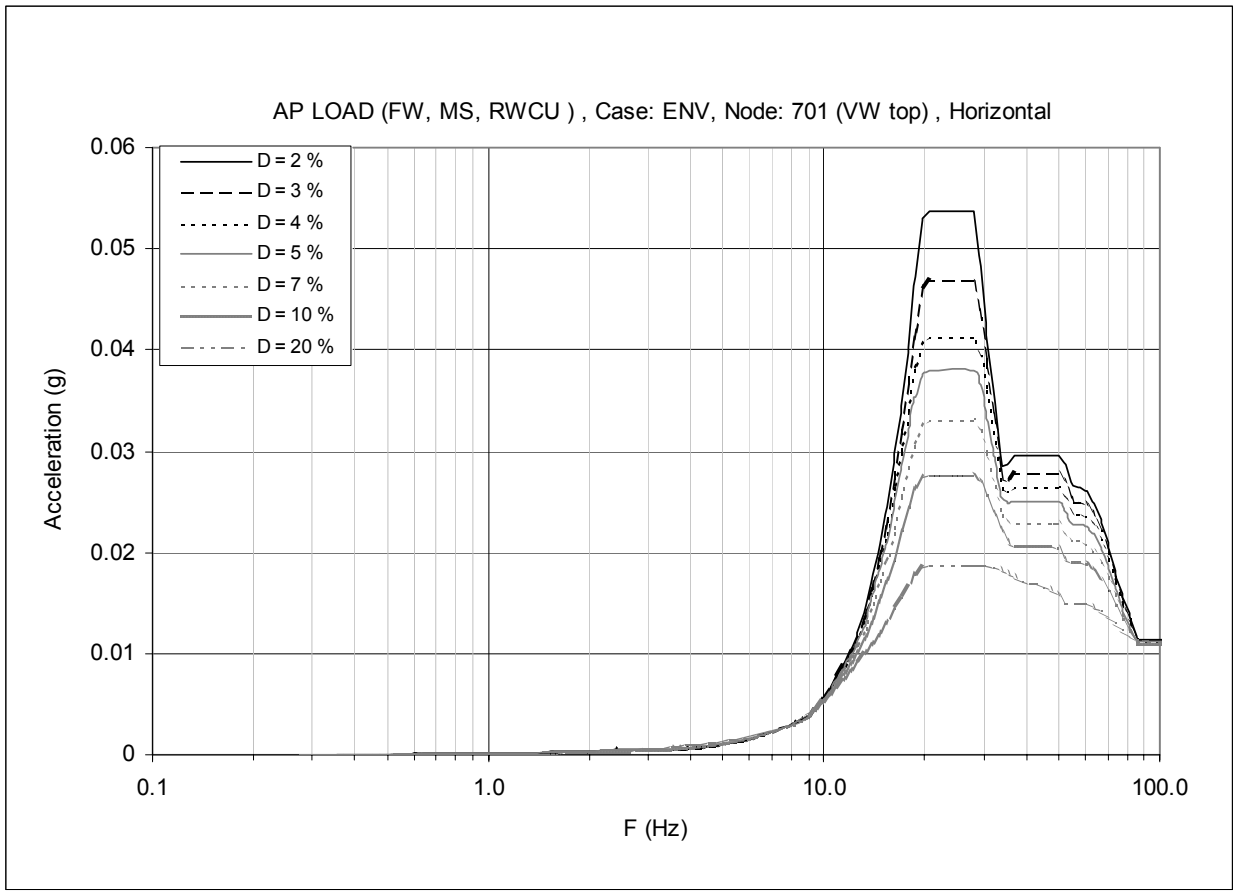

Figure 3F-4. Floor Response Spectrum—AP Envelope, Node: 701, Horizontal

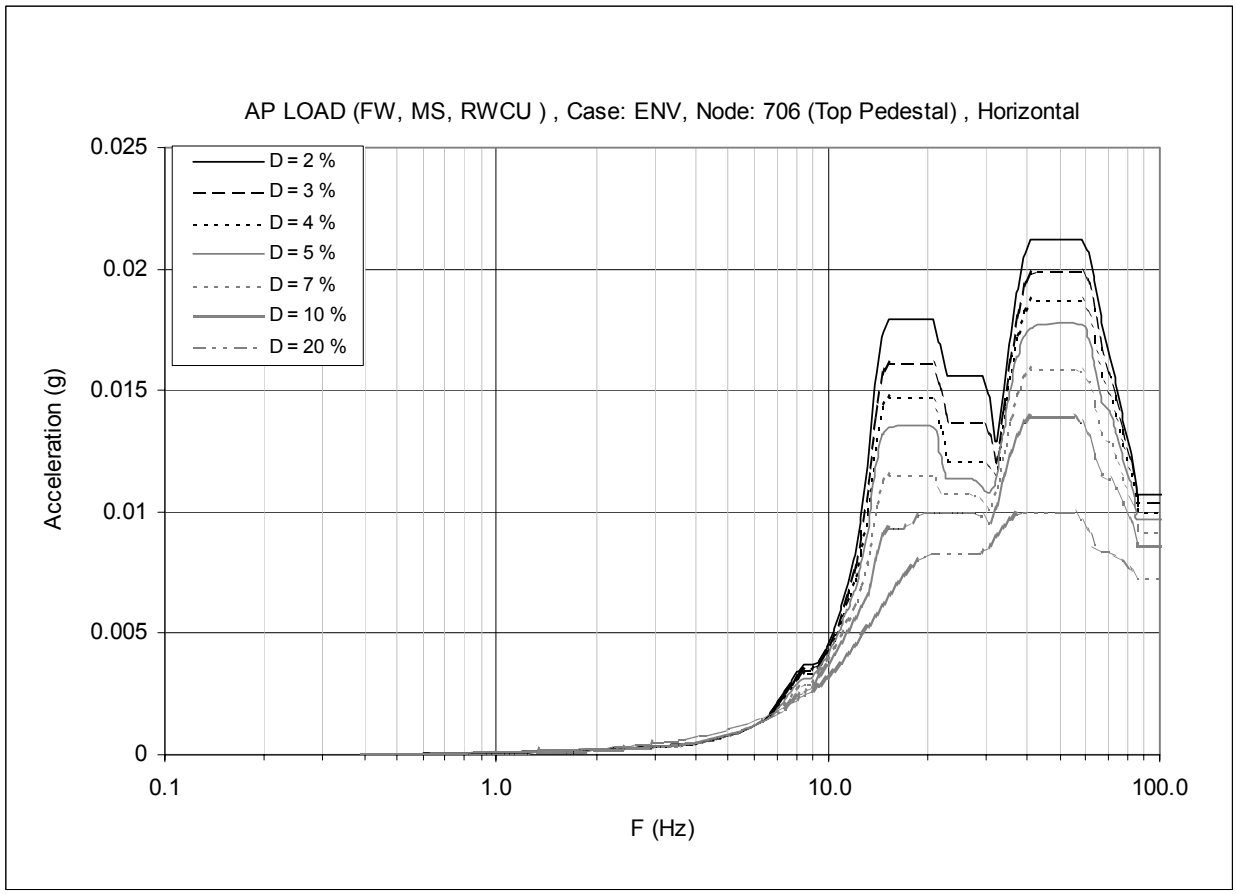

Figure 3F-5. Floor Response Spectrum—AP Envelope, Node: 706, Horizontal

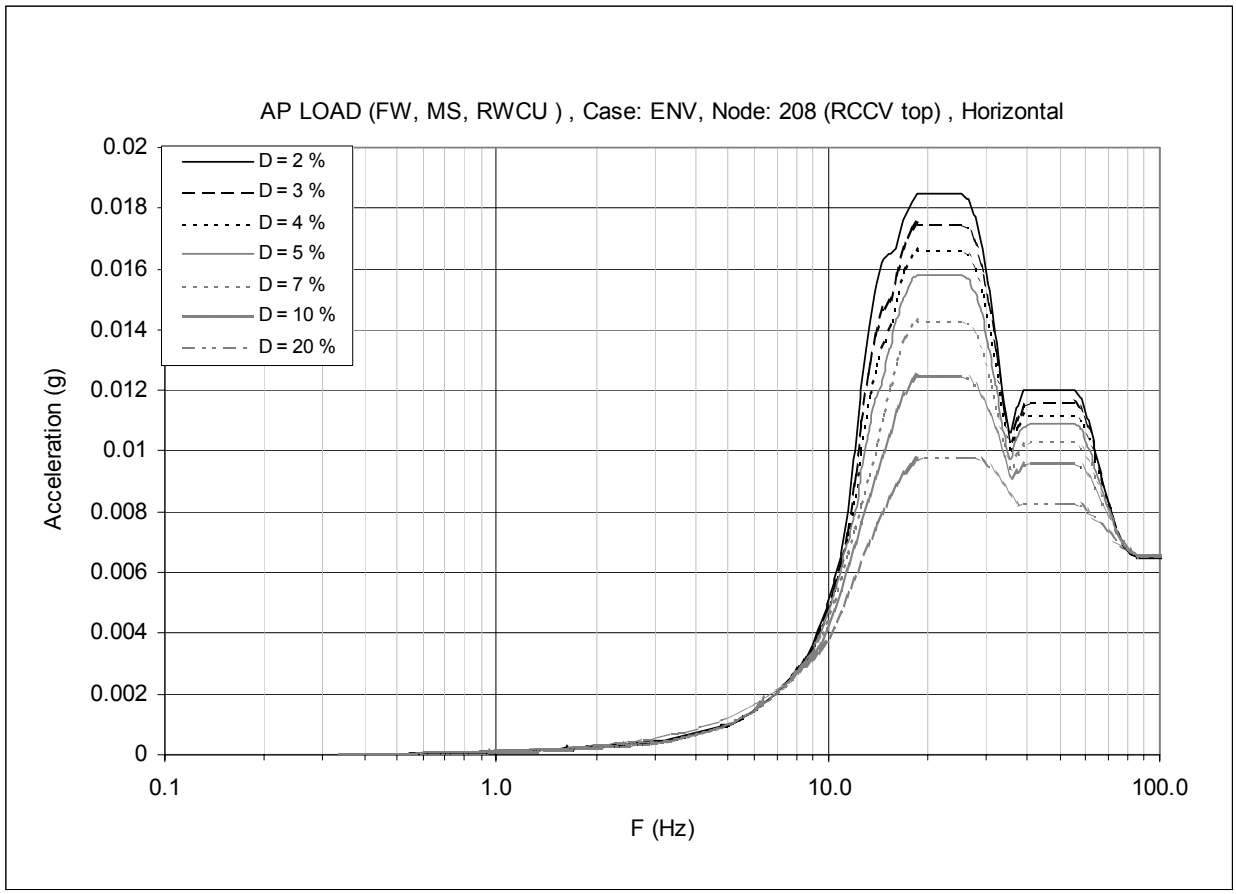

Figure 3F-6. Floor Response Spectrum—AP Envelope, Node: 208, Horizontal

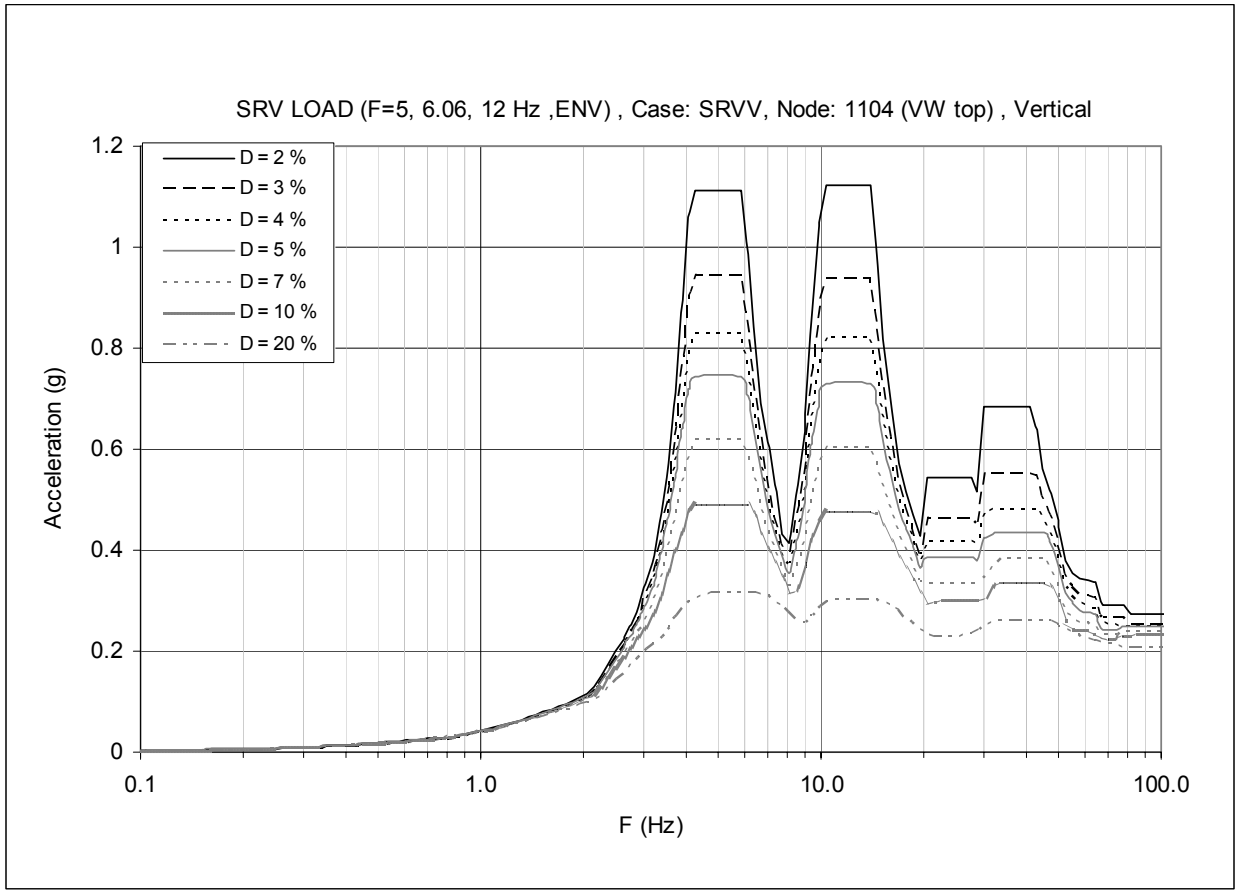

Figure 3F-7. Floor Response Spectrum—SRV Envelope, Node: 1104, Vertical

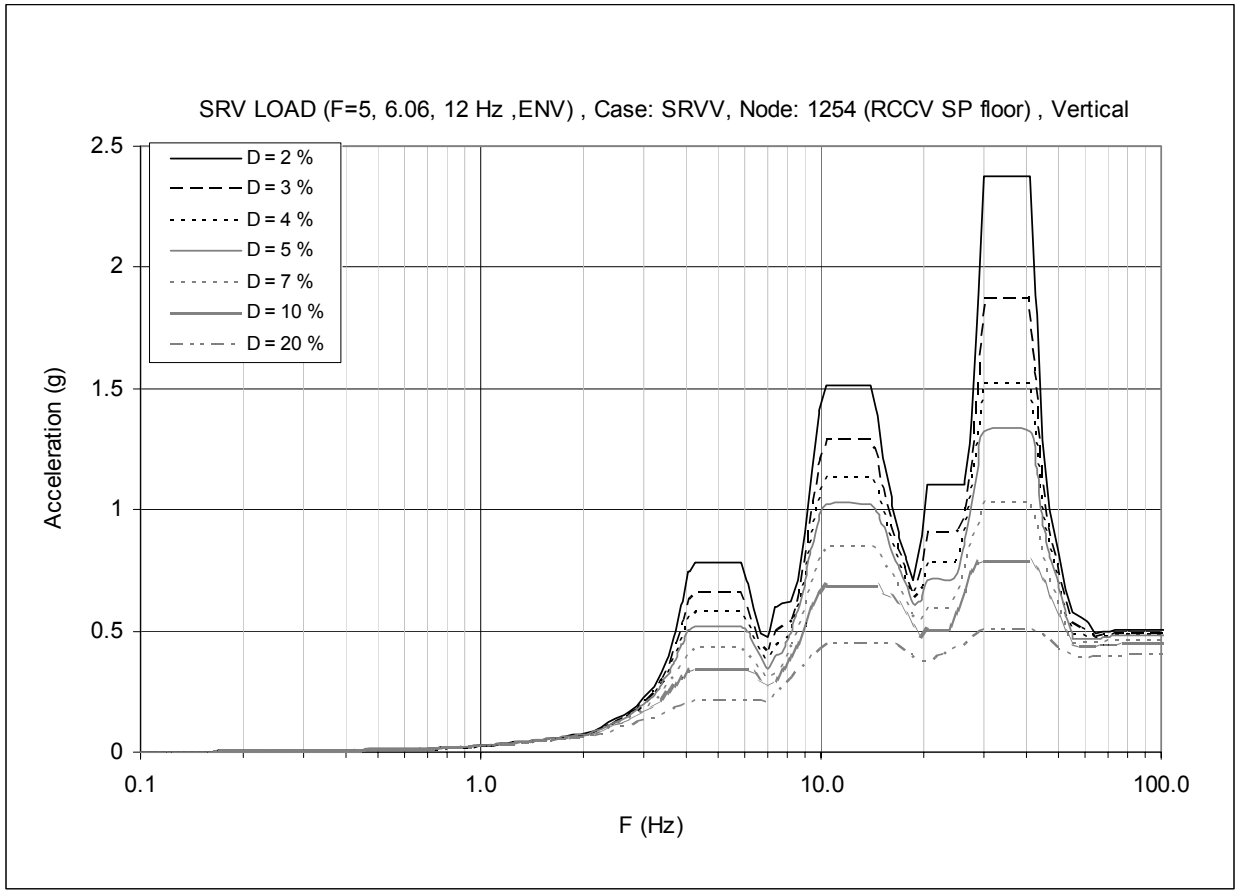

Figure 3F-8. Floor Response Spectrum—SRV Envelope, Node: 1254, Vertical

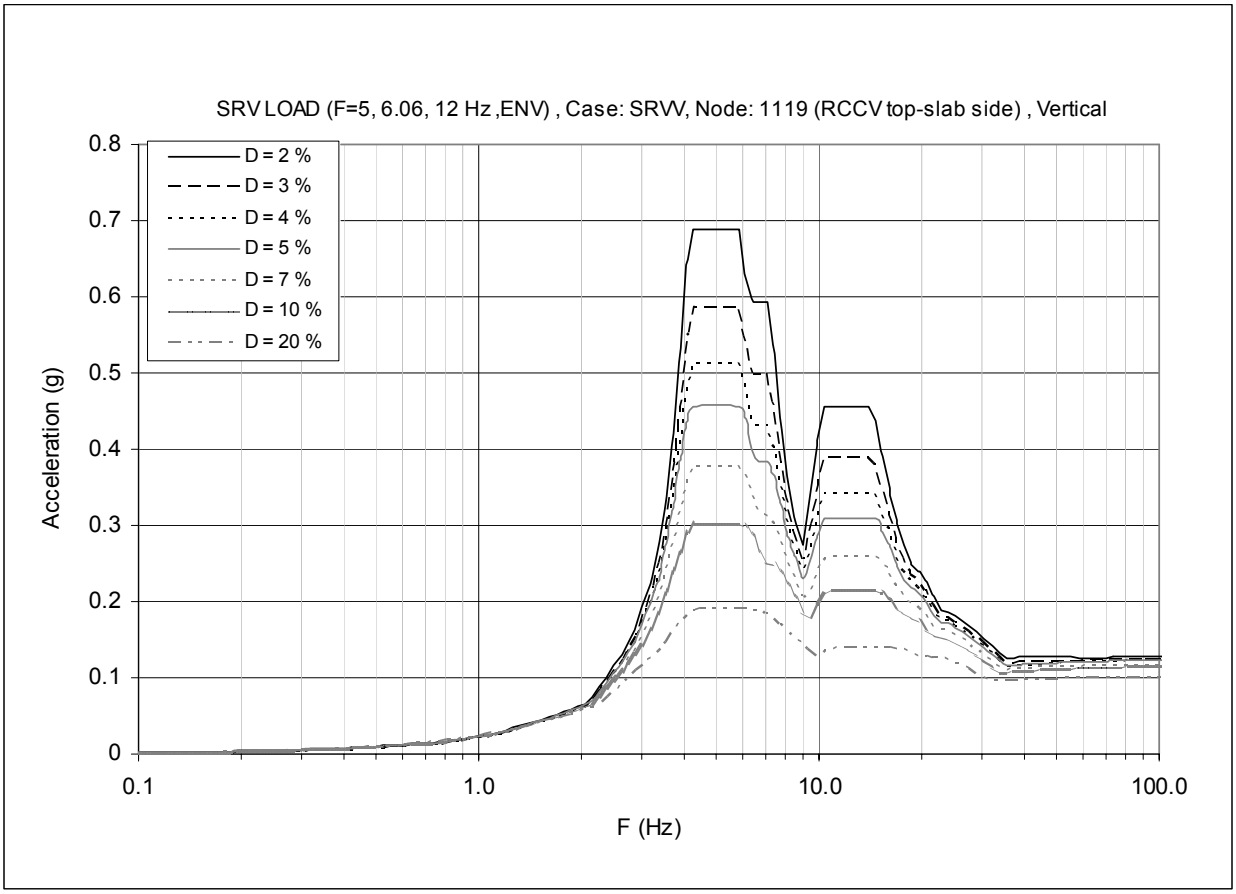

Figure 3F-9. Floor Response Spectrum—SRV Envelope, Node: 1119, Vertical

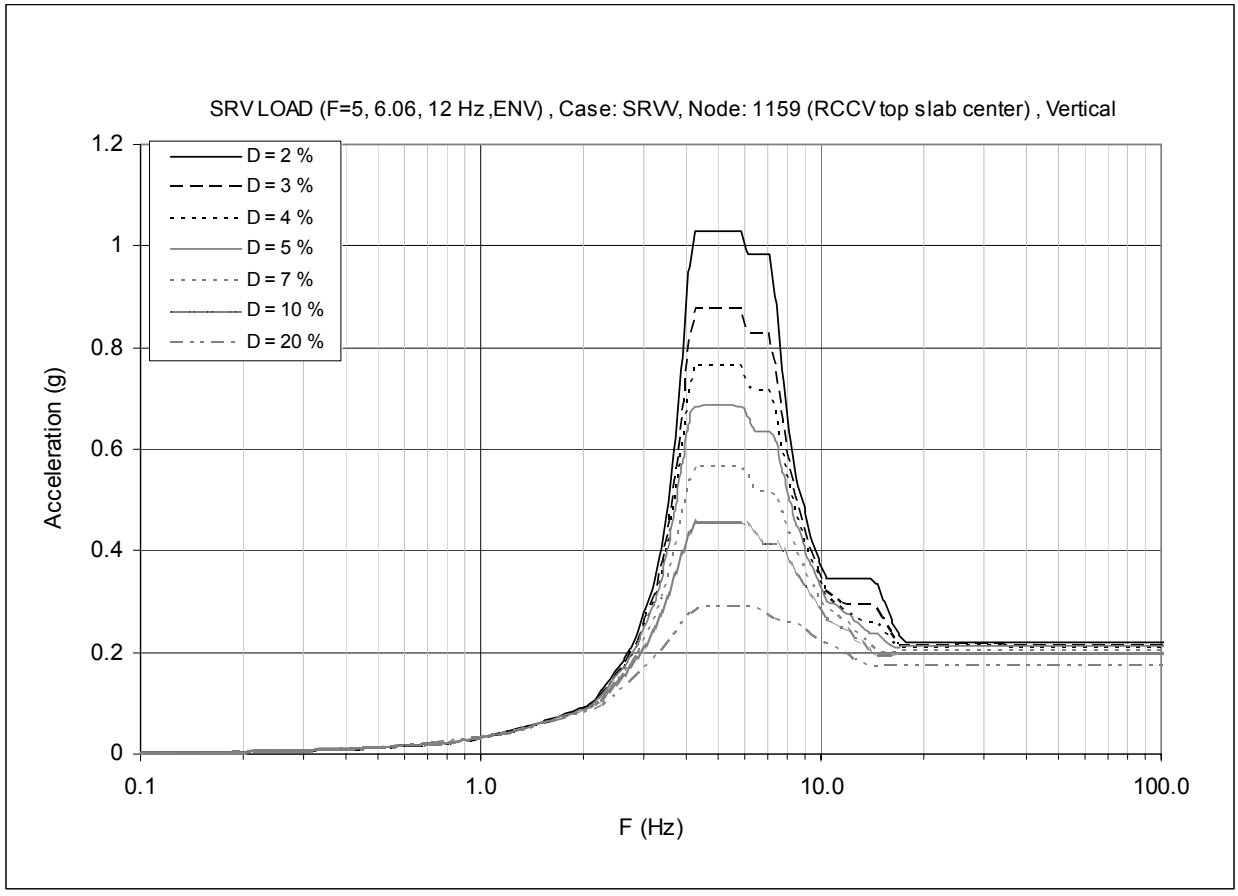

Figure 3F-10. Floor Response Spectrum—SRV Envelope, Node: 1159, Vertical

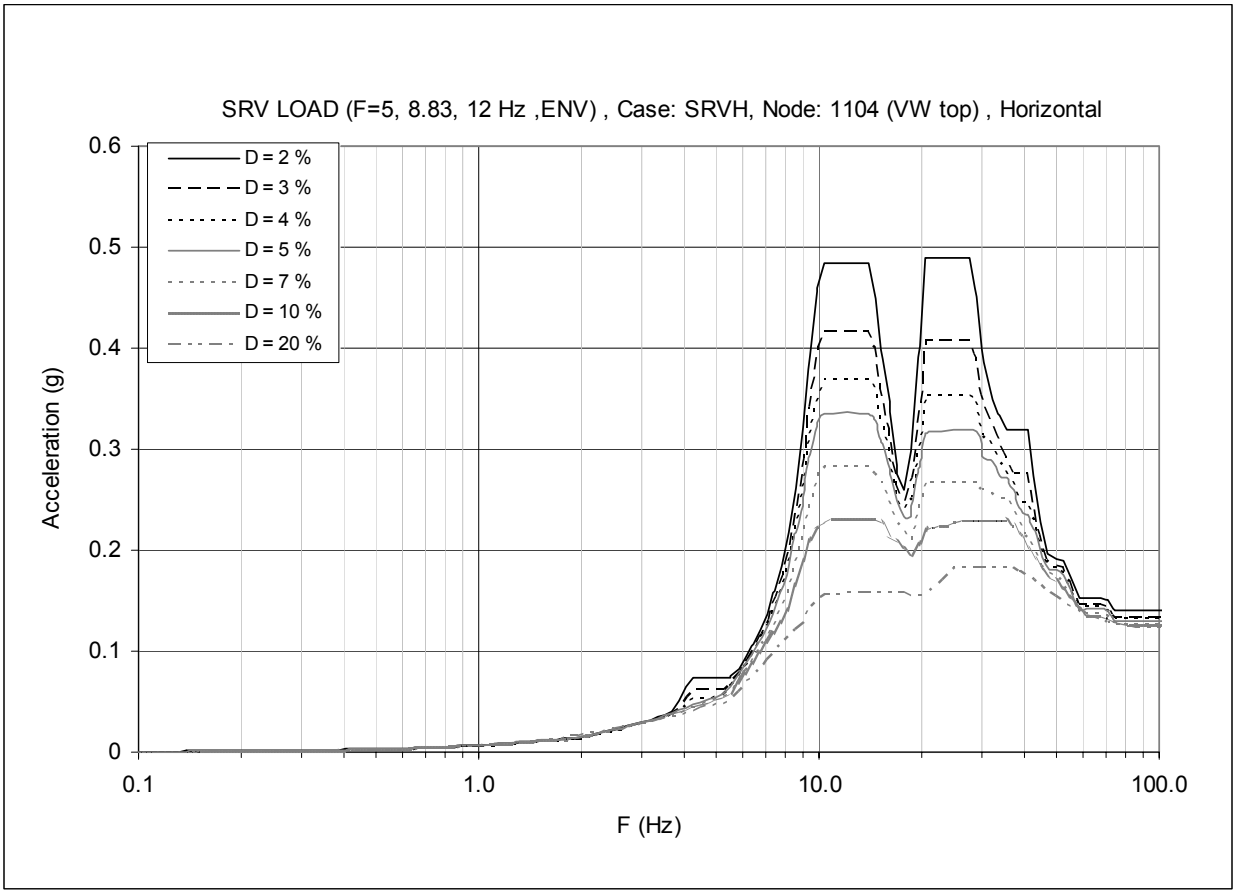

Figure 3F-11. Floor Response Spectrum—SRV Envelope, Node: 1104, Horizontal

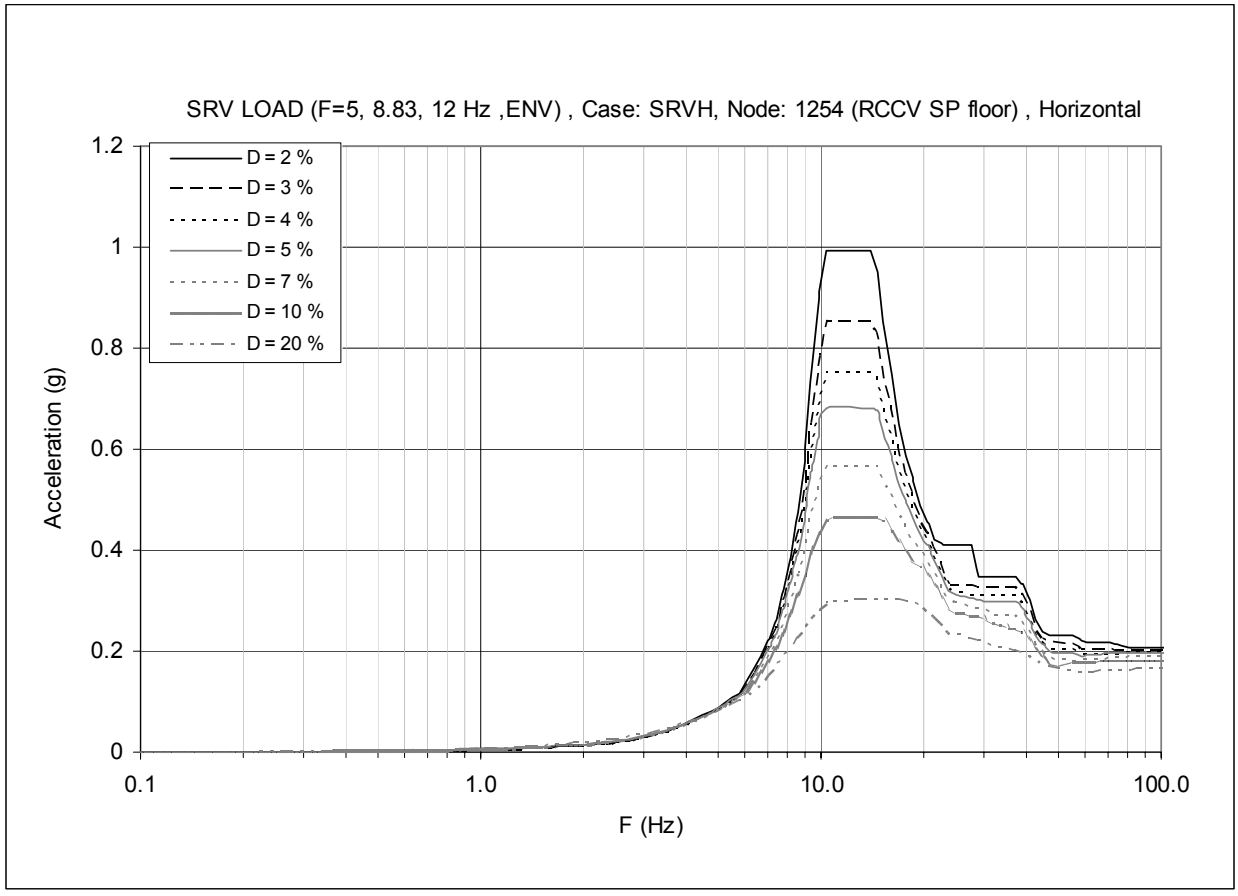

Figure 3F-12. Floor Response Spectrum—SRV Envelope, Node: 1254, Horizontal

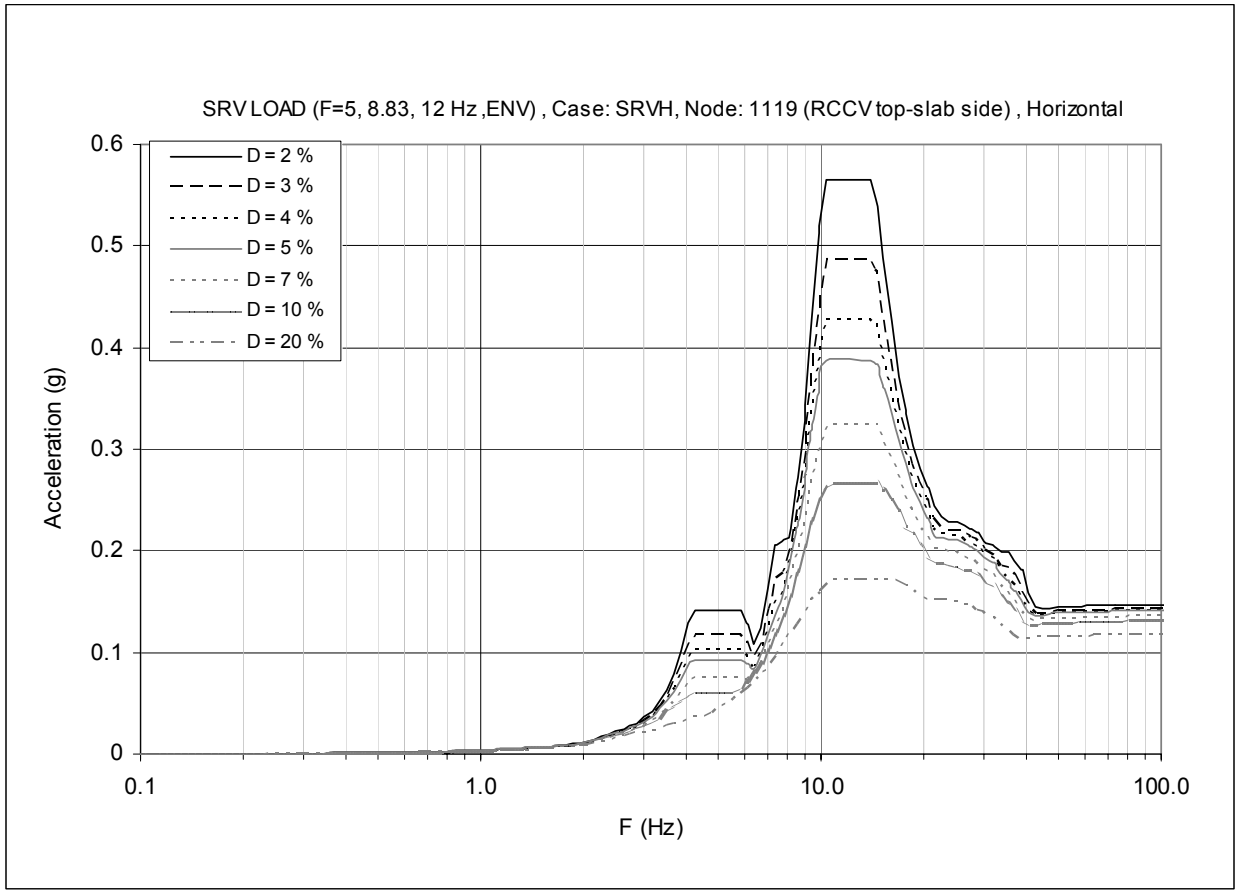

Figure 3F-13. Floor Response Spectrum—SRV Envelope, Node: 1119, Horizontal

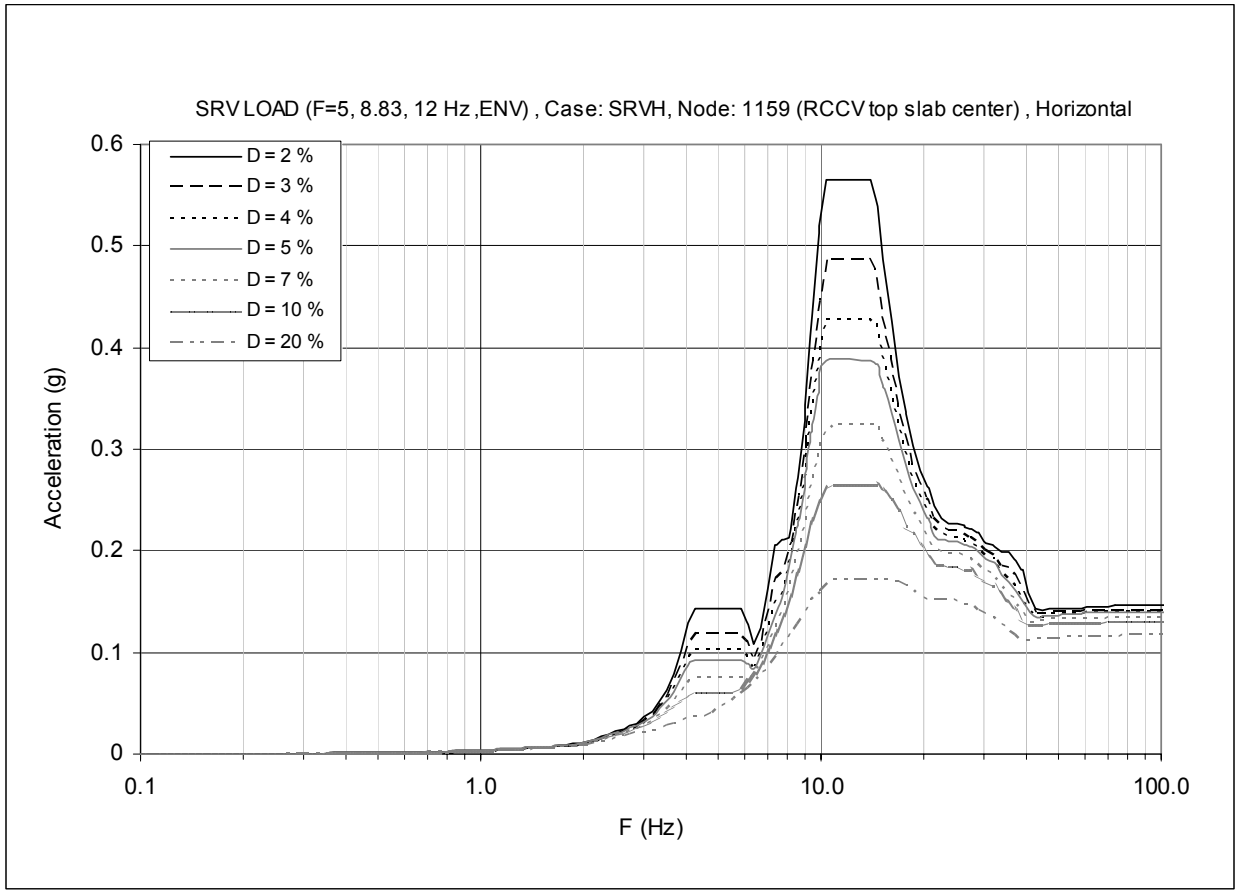

Figure 3F-14. Floor Response Spectrum—SRV Envelope, Node: 1159, Horizontal

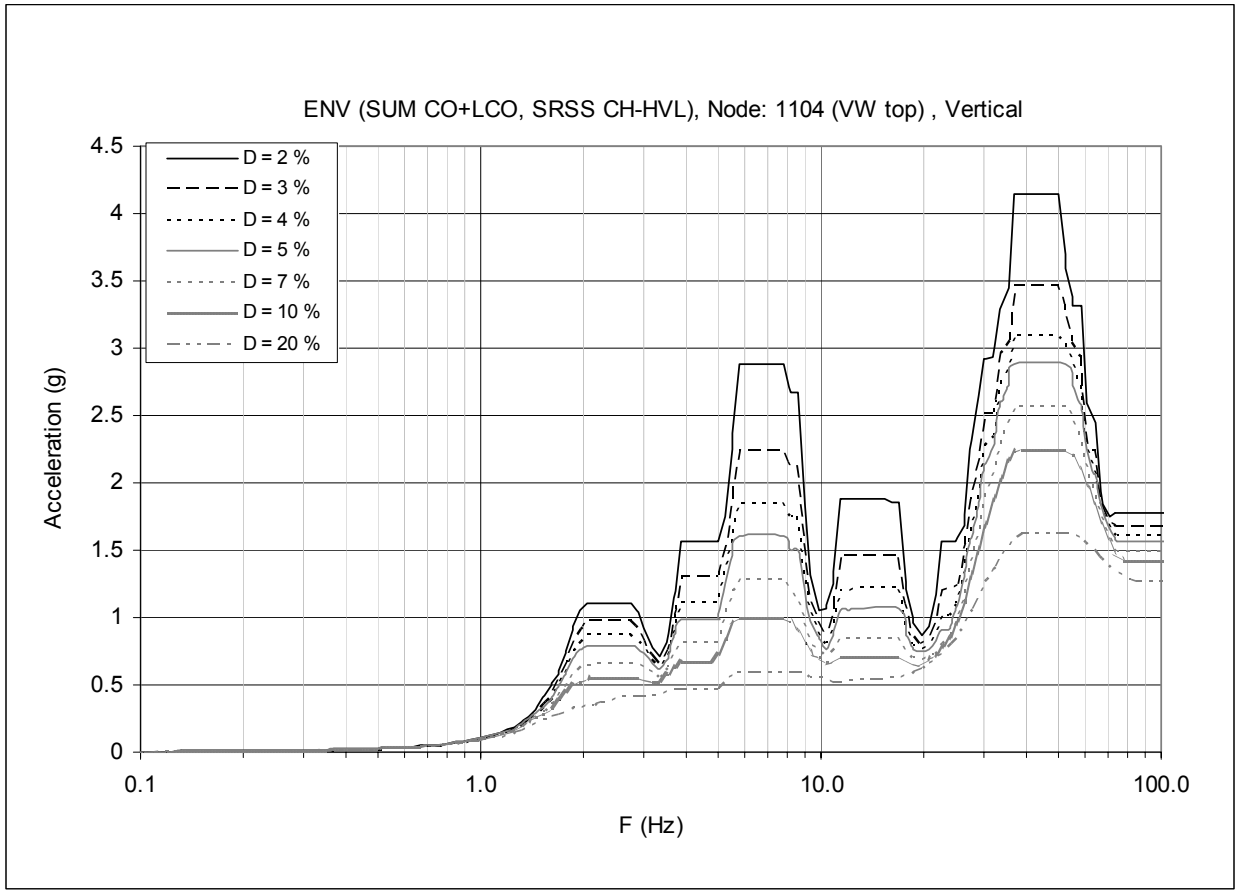

Figure 3F-15. Floor Response Spectrum—CH & CO Envelope, Node: 1104, Vertical

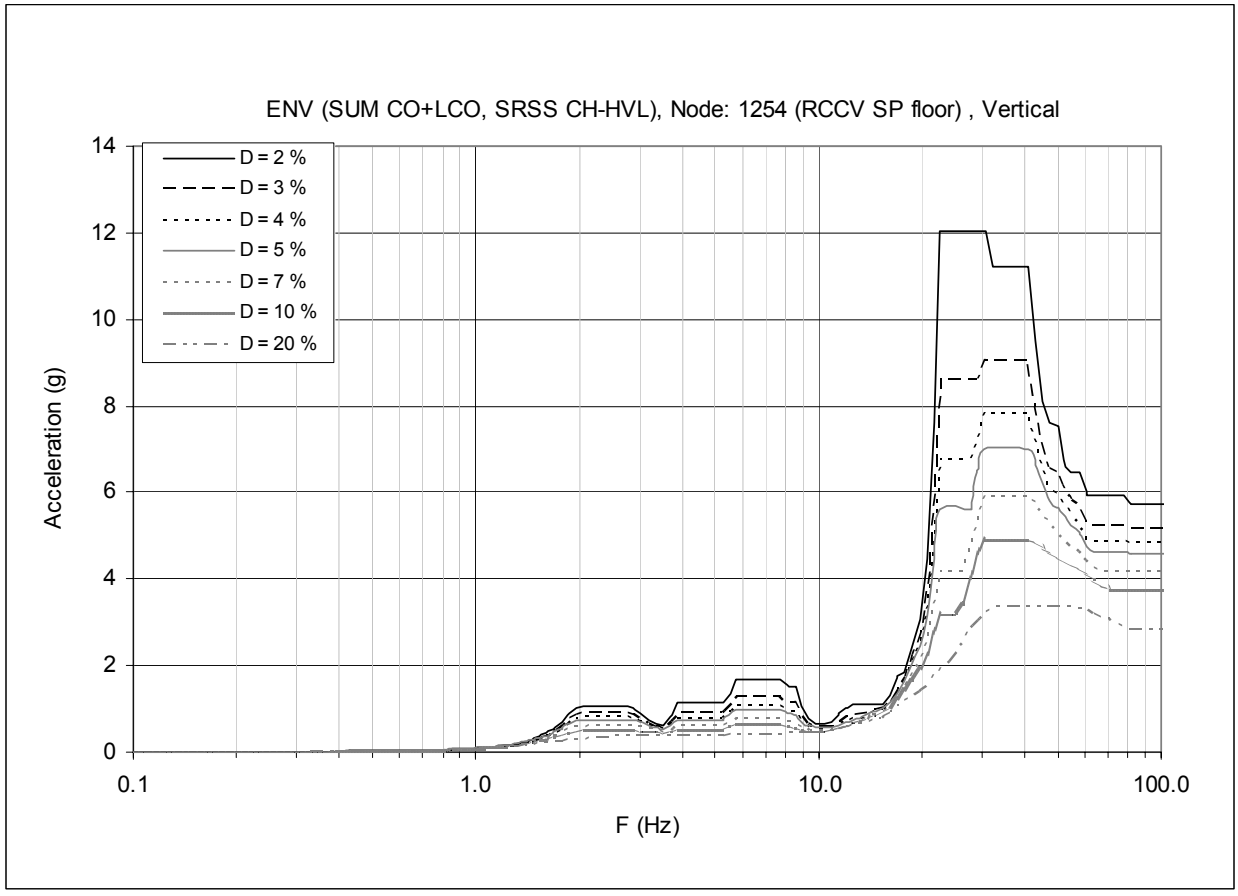

Figure 3F-16. Floor Response Spectrum—CH & CO Envelope, Node: 1254, Vertical

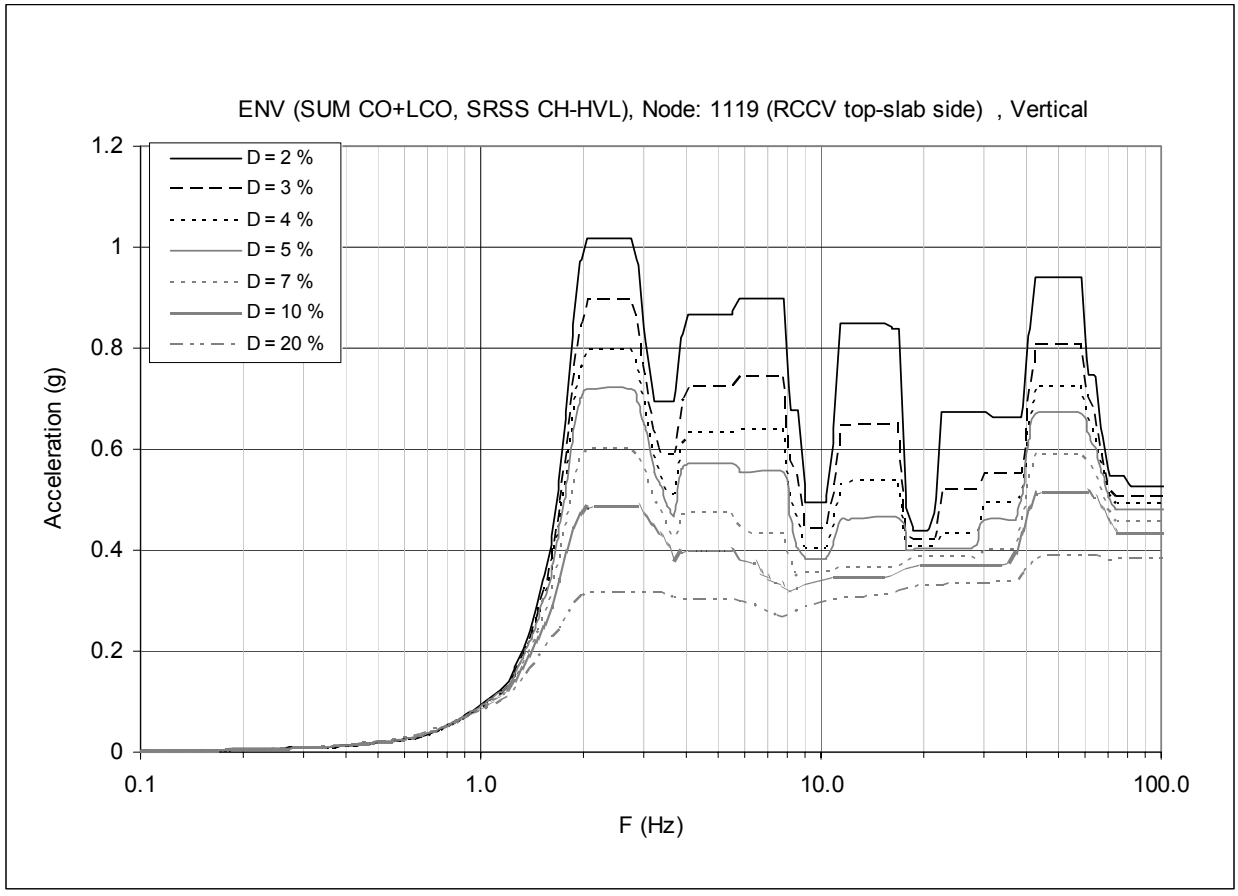

Figure 3F-17. Floor Response Spectrum—CH & CO Envelope, Node: 1119, Vertical

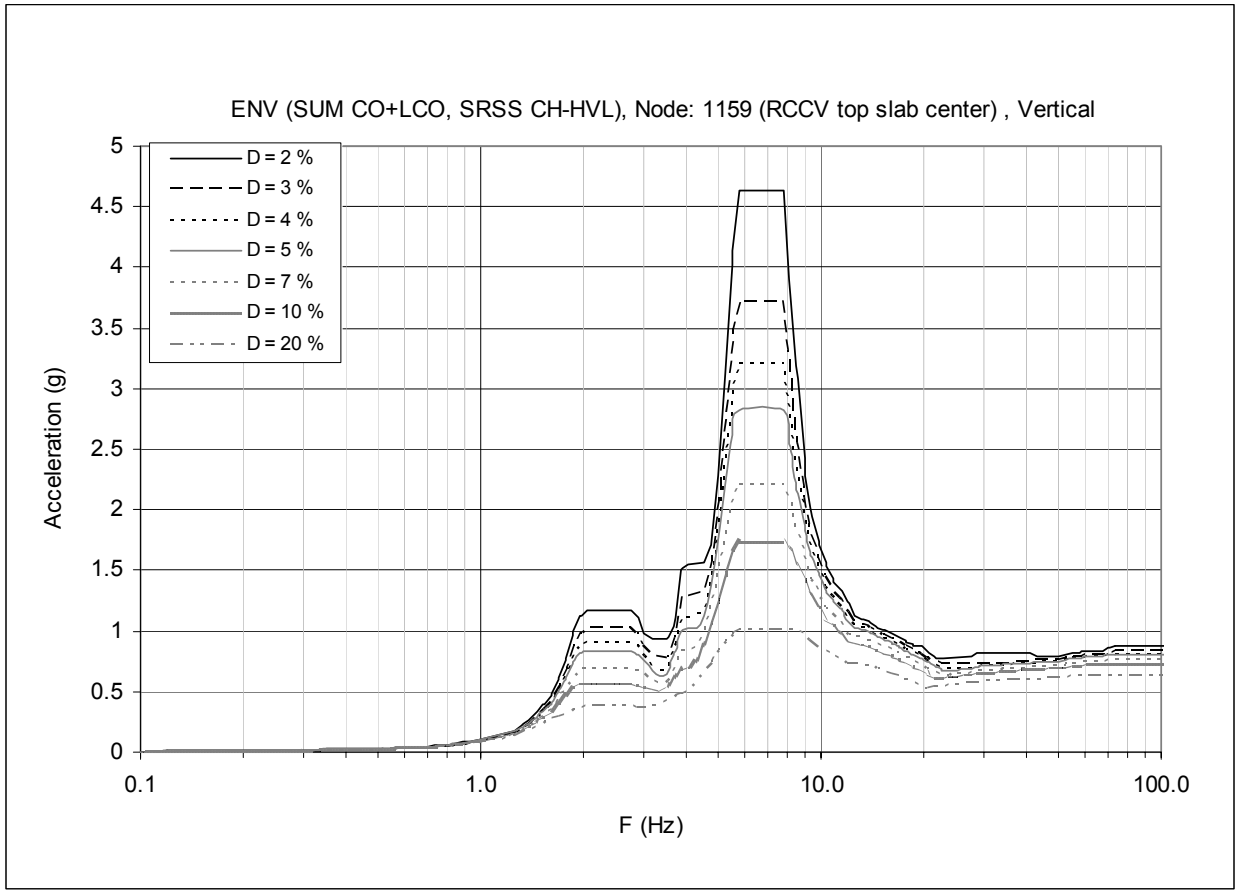

Figure 3F-18. Floor Response Spectrum—CH & CO Envelope, Node: 1159, Vertical

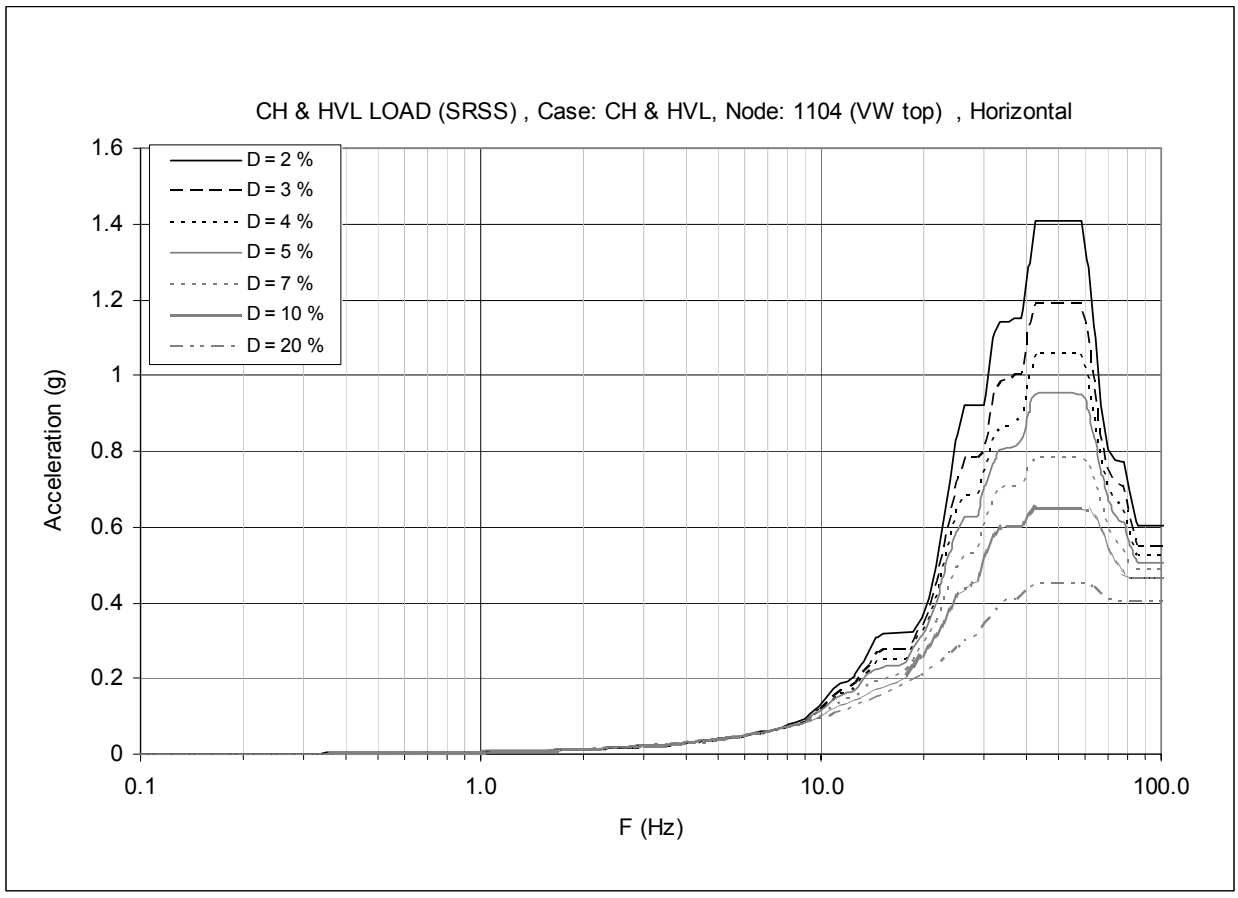

Figure 3F-19. Floor Response Spectrum—CH Envelope, Node: 1104, Horizontal

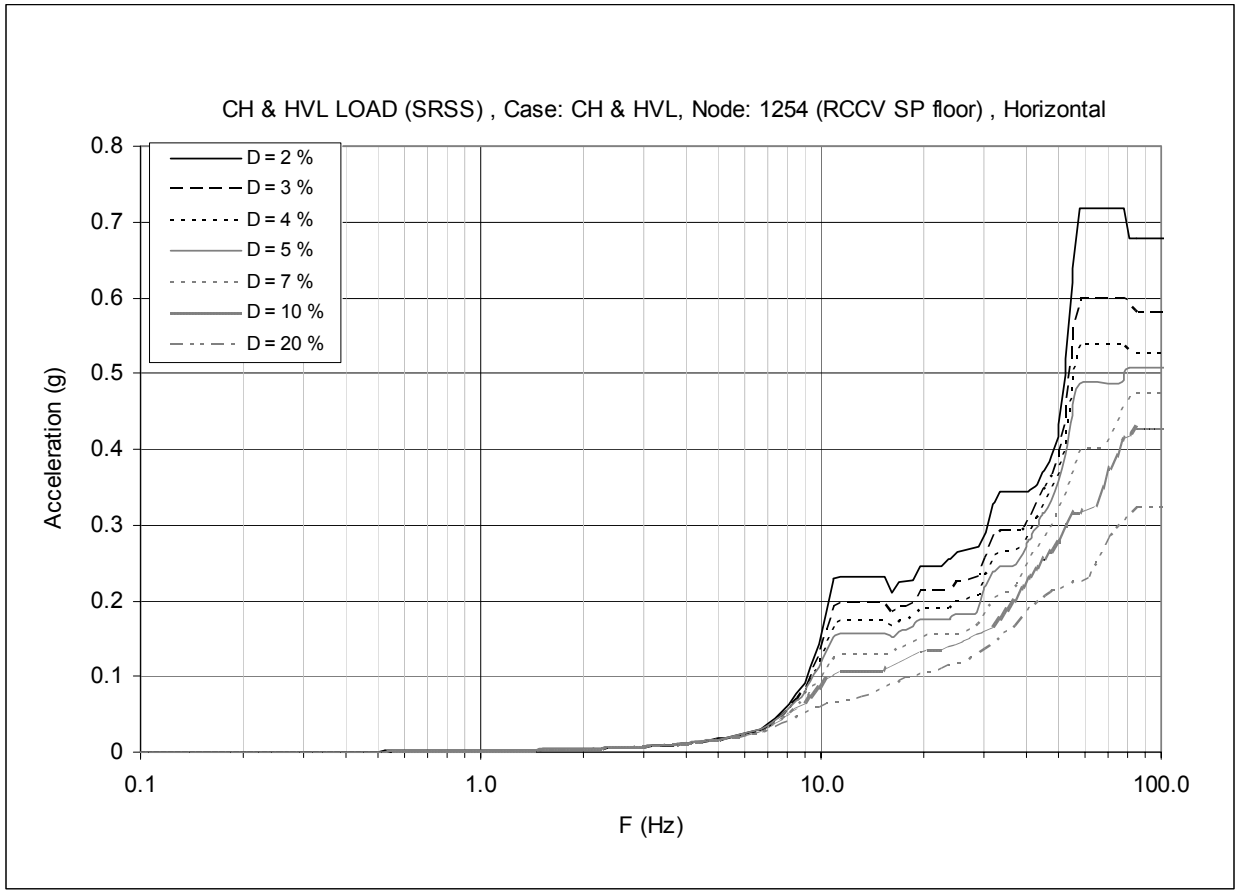

Figure 3F-20. Floor Response Spectrum—CH Envelope, Node: 1254, Horizontal

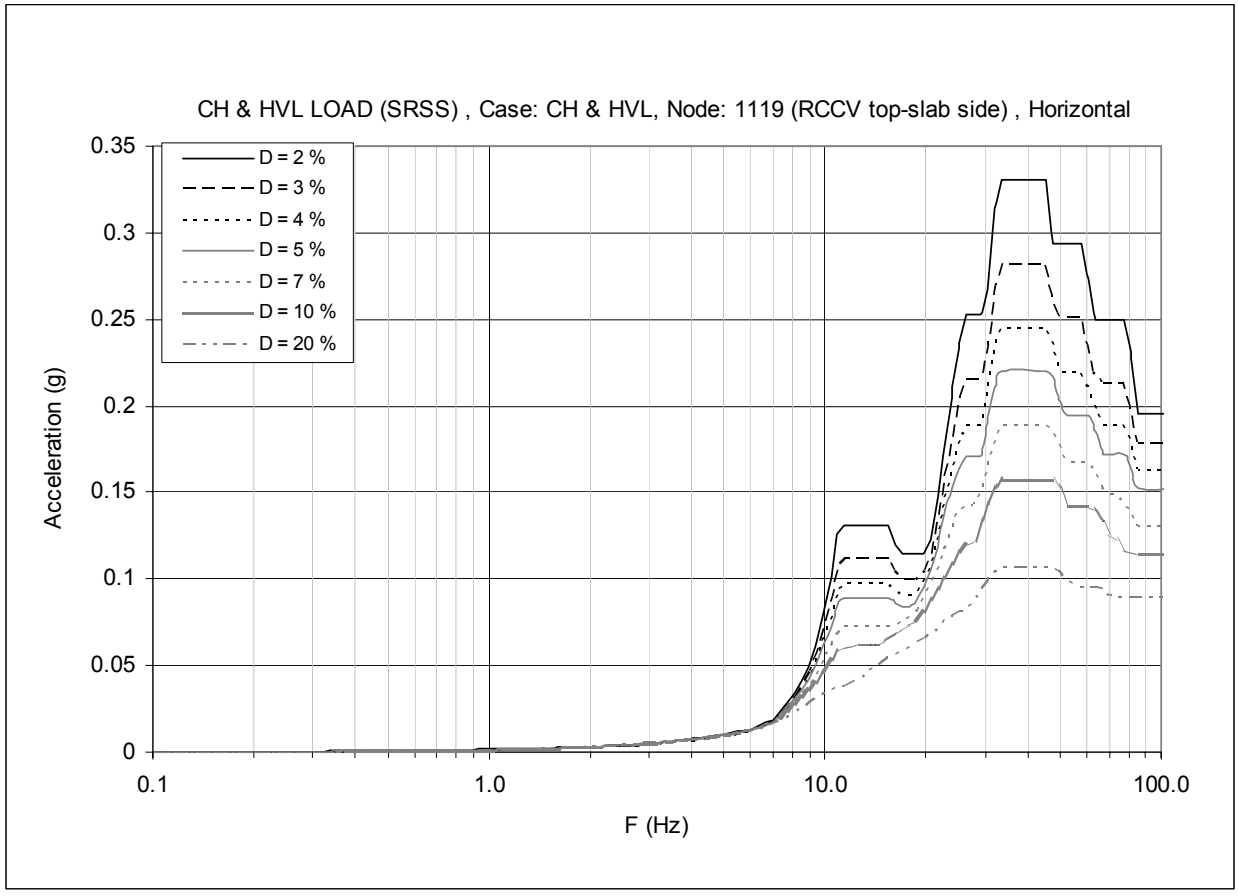

Figure 3F-21. Floor Response Spectrum—CH Envelope, Node: 1119, Horizontal

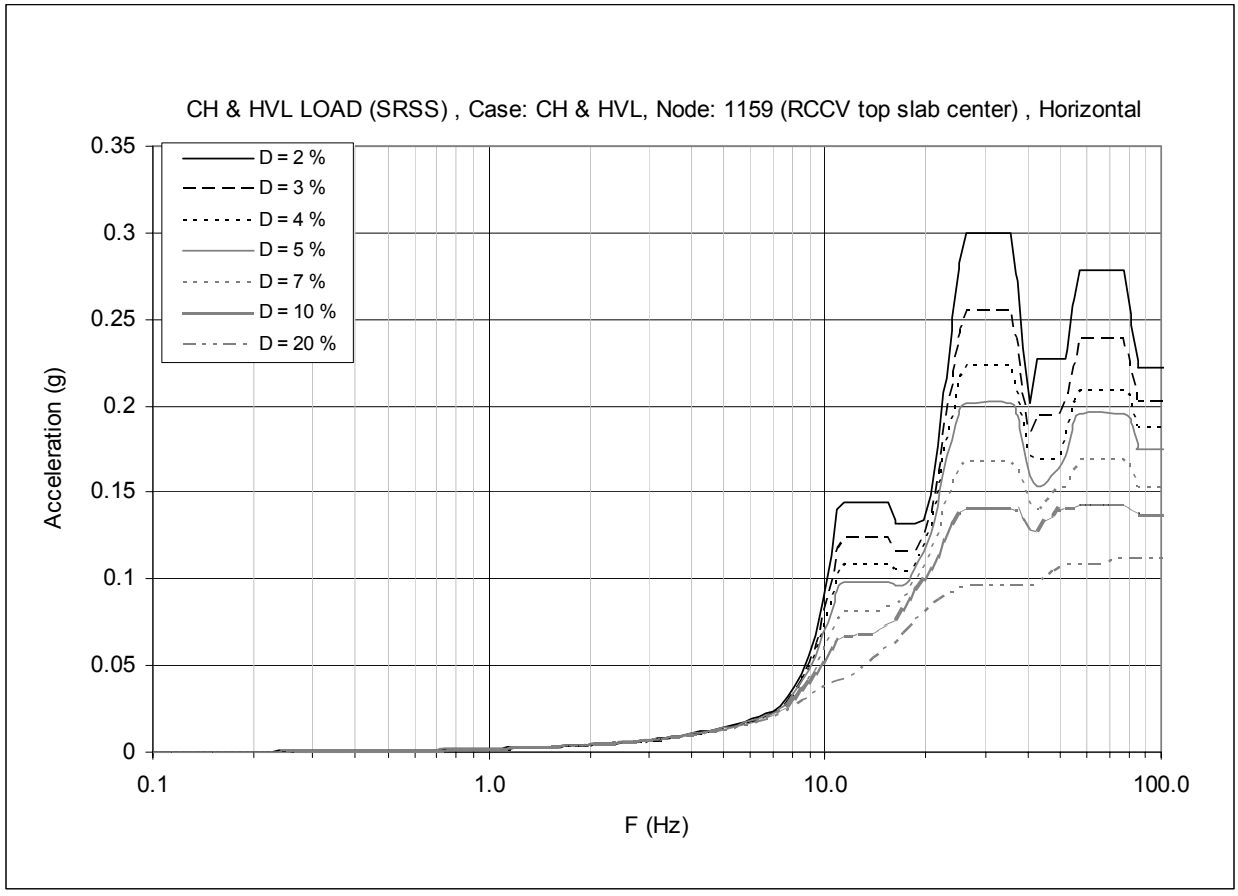

Figure 3F-22. Floor Response Spectrum—CH Envelope, Node: 1159, Horizontal